CONTROL FOR FUSION THERMAL STABILITY

BY

ISAAC MAYA

A DISSERTATION PRESENTED TO THE GRADUATE SCHOOL
OF THE UNIVERSITY OF FLORIDA IN
PARTIAL FULFILLMENT OF THE REQUIREMENTS
FOR THE DEGREE OF DOCTOR OF PHILOSOPHY

UNIVERSITY OF FLORIDA

1983

To my wife Debbie, without whom •••

With Love,

ACKNOWLEDGEMENTS

I would like to express my deep sense of gratitude to Dr. Hugh D. Campbell for his counsel, guidance, dedication, and ubiquitous encouragement throughout my graduate career and the preparation of this work. Through the many uncertain situations encountered in the completion of this research, I was always secure in the knowledge that he is a man that can be counted upon. His forethought in his suggestion of the topic for this dissertation is also truely appreciated.

I would like to express my love and appreciation to my wife Debbie for the many sacrifices which she suffered and endured in support of this cause. Her unshakeable determination served as a fresh and replenishable source of strength for me. Her tremendous drive and encouragement were indeed key factors in maintaining continual progress toward the goal. This accomplishment is just as much hers as mine.

I would like to thank Dr. Kenneth R. Schultz, whose gentle persistence played a highly significant part in ensuring that progress was maintained toward completion of this dissertation. I am forever sincerely grateful. I also thank him for removing the wooden splints from underneath my fingernails. Between Ken at work and Debbie at home, I really had all the "encouragement" I needed.

I would like to thank Dr. Edward T. Dugan, whose careful review and many helpful comments and suggestions resulted in a tremendously improved written text. Thanks are also extended to Drs. Edward E. Carroll, Thomas E. Bullock, and Francis E. Dunnam for their review of the dissertation, and their participation on the supervisory committee and final examination.

I would also like to acknowledge my parents Roberto and Graciela Maya and Leonard and Anne Eichenbaum, and my brothers and sisters Elias, Jaime, Naomi, and Joseph Maya and Lee Eichenbaum, each of whom demonstrated in their own way their encouragement and desire for me to attain this achievement.

The cooperation and financial assistance of the Department of Nuclear Engineering and the Graduate School of the University of Florida are also sincerely appreciated.

TABLE OF CONTENTS

ACKNOWLEDGEMENTS iii

ABSTRACT vi

1. INTRODUCTION 1
   1.1 Motivation 1
   1.2 Previous Work 4
   1.3 Control for Fusion Thermal Stability 6

2. PLASMA MODEL AND TRANSFER FUNCTION DEVELOPMENT 10
   2.1 Model Assumptions 10
   2.2 Open- and Closed-Loop Plasma Transfer Function 17

3. CLASSICAL OPEN-LOOP ANALYSIS OF PLASMA MODEL 24
   3.1 Open-Loop Plasma Transfer Function Characteristics 24
   3.2 Open-Loop System Performance 59
   3.3 Summary 70

4. CLASSICAL CLOSED-LOOP ANALYSIS OF PLASMA MODEL 77
   4.1 Closed-Loop Plasma Transfer Function Characteristics . . . 78
   4.2 Closed-Loop System Performance 117
   4.3 Summary 186

5. PROPORTIONAL-INTEGRAL-DERIVATIVE CONTROL 187

6. CONCLUSIONS 202

APPENDIX A. INTRODUCTION TO FUSION AND REVIEW OF THE LITERATURE ON THERMAL STABILITY 206

APPENDIX B. CONTROL THEORY REVIEW 225

APPENDIX C. DERIVATION OF SPECIFICATIONS FOR A STABLE CLASSICAL SECOND-ORDER SYSTEM WITH A FINITE ZERO 246

REFERENCES 256

BIOGRAPHICAL SKETCH 260

Abstract of Dissertation Presented to the Graduate Council
of the University of Florida in Partial Fulfillment of the
Requirements for the Degree of Doctor of Philosophy

CONTROL FOR FUSION THERMAL STABILITY

By

Isaac Maya

April, 1983

Chairman: Hugh D. Campbell
Major Department: Nuclear Engineering Sciences

This work represents an analysis of the thermal balance of a fusioning plasma from a control system perspective. By applying the techniques of classical control theory, the requirements for stability and the response characteristics of the thermal balance have been evaluated. The results show that open-loop equilibria are characterized by restrictively narrow stable operating temperature regimes and generally poor system performance. The results also show that closed-loop proportional feedback using fuel feedrate and injection energy can be used to extend the stable operating temperature regime and significantly improve the system response. Additional improvement is available using proportional-integral-derivative (PID) control.

The stabilized temperature regime is a function of the governing confinement law, the injection energy of incoming fuel, and the feedback coefficients. A broad range of feedback fractions is

available with which to stabilize the fusion power balance. The feedback can thus be chosen so as to improve the system response. With constant confinement, sluggish open-loop performance with no injection energy can be moderately improved, and the high overshoots present with 75 kev injection energy can be significantly reduced. These improvements are possible only at temperatures above 20 keV and require high feedback fractions. With Bohm confinement, high open-loop overshoots present with zero injection energy can be reduced to acceptable levels at temperatures as low as 20 keV, with a simultaneous decrease in settling times to under 30 seconds. With 75 keV injection energy, acceptable overshoot can be obtained at temperatures as low as 10 keV, with the time-to-peak below 20 seconds and settling times less than 30 seconds. Even with Bohm confinement, it is still difficult to simultaneously satisfy overshoot and speed of response requirements at low temperatures and low feedback fractions.

Though the system response is significantly improved with only proportional feedback, additional improvement is desirable. Preliminary indications of the benefits of PID control are that more efficient control is possible while simultaneously improving system response.

CHAPTER 1
INTRODUCTION

1.1. Motivation

The magnetic confinement of a plasma is presently the leading approach to achieving the conditions necessary to sustain thermonuclear fusion reactions. The confined plasma, consisting of ionized deuterium and tritium fuel, is heated to a sufficiently high temperature that fusion events occur, releasing energy in the form of neutrons and charged particles. Though the scientific feasibility of fusion, i.e., that the energy released is greater than the energy used in initiating the fusion events, has yet to be demonstrated, there is strong belief in the scientific community that this proof will come within the next two years at the Tokamak Fusion Test Reactor (TFTR) presently in its final year of construction at Princeton, New Jersey.

Beyond scientific proof-of-principle, fusion will become a practical energy source when the engineering and economic issues of producing net energy from magnetic-confinement fusion are resolved. Foremost among the issues of scientific feasibility is the question of plasma stability. A magnetically confined plasma is out of thermodynamic equilibrium, but attempts to relax toward equilibrium via Coulomb collisions and collective plasma instabilities. If Coulomb collisions were the only equilibration mechanism, viable reactor

designs would be possible. However, plasma instabilities associated with magnetic confinement represent sufficiently enhanced energy loss modes as well as mechanisms for undesirable system behavior that control is essential in order to demonstrate the engineering feasibility of fusion.

Plasma instabilities can be categorized into three groups: macroinstability, microinstability, and thermal instability. The macroinstabilities are often referred to as MHD instabilities because they are derivable from magnetohydrodynamic (MHD) fluid models of the plasma. The MHD instabilities result in gross movement of the plasma and rapid loss of confinement on the microsecond time scale. These instabilities have received major theoretical treatment and fortunately can be controlled by proper design of the magnetic field topology, machine configuration, plasma positioning circuitry, and by proper selection of the machine operating parameters. Present theory predicts the existence of magnetic configurations of the Tokamak type, with operating parameters permitting an attractive reactor, that are absolutely stable to all the important macroinstabilities [1].

The microinstabilities are not detrimental to overall plasma confinement as is the case with the macroinstabilities. Instead, these instabilities represent rapid, small-scale plasma transport processes which lead to losses which are in excess of classical predictions. Despite the abundance of measured data and sophisticated diagnostic and analysis tools, the mechanism for many of these enhanced diffusive losses remains unexplained. The resultant diffusion is thus generally referred to as "anomalous transport." The net effect of microinstabilities is a degradation of plasma confinement, increasing

the difficulty of achieving engineering break-even. Much of the present experimental effort in fusion plasma physics is devoted to resolving the issues arising from the microinstabilities.

The subject of this dissertation is the control of the thermal instability. This instability is associated with considerations relating to the behavior of the global power balance as determined by plasma mass and energy conservation considerations. In particular, the thermal instability refers to the proclivity of the plasma temperature to either rise uncontrollably to a high temperature, or extinguish the fusion burn, at the onset of perturbations from the desired operating conditions which may arise from system and component disturbances.

The temperature above which the plasma energy balance is naturally stable to perturbations in the parameters governing the thermal equilibrium, i.e., above which it does not require external control, is defined as the critical temperature. Control of the energy balance to ensure thermal stability is of importance to the field of thermonuclear fusion because the operating temperature range which would result in peak power density in the plasma has been found to be unstable, i.e., it is below the critical temperature. Operation at or near peak power density is desirable because fusion is expected to be a highly capital cost intensive energy source with a significant sensitivity of the plant cost to the plasma power density. In addition to the economic penalty, operation at high temperatures introduces engineering feasibility issues. High operating temperatures require materials and components operating at or beyond the limits of present day or even near term technology. In addition to the economic and engineering issues, control over the thermal balance is required to accommodate

load changes, input and system perturbations, and component malfunctions.

1.2. Previous Work

In contrast to the macroinstabilities, which have been studied since the 1950's, and the microinstabilities, which have been studied since the 1960's, the thermal instability was not recognized until the 1970's. The first considerations of the thermal instability and its control were provided by Mills [2,3], and Ohta et al. [4]. Using dynamic computer simulations of the mass and energy conservation equations, Mills' early papers demonstrated that if the equilibrium plasma temperature was below a certain value, later termed the critical temperature by Ohta et al. [4], perturbations in the parameters governing the power balance would lead to a thermal runaway in which the plasma temperature would either decrease and extinguish the reaction rate, or increase to a higher, thermally stable but undesirable value.

This behavior can be explained as follows. The steady state of the thermal balance is determined by the careful balance of the energy production rate via fusion and the energy loss mechanisms of optical radiation, conduction, and diffusion (convection). In the case of thermally unstable equilibria, a perturbation resulting in an increase in the plasma temperature results in an increase in the energy production rate which is greater than the increase in the energy loss rates, which in turn results in a further increase in the temperature,

etc. As the temperature continues to rise, fusion power production eventually decreases, whereas the sum of the loss terms, particularly radiation, increases, until a new, stable equilibrium is established at a temperature much higher that the original. An analogous scenario for an initial decrease in the plasma temperature can be constructed wherein the final temperature extinguishes the plasma burn.

To obtain thermal stability, Mills suggested several methods by which control might permit operation below the critical temperature. Though not completely satisfactory, these early analyses were very useful, and provided a platform for the work of Ohta et al. [4] In their work, Ohta et al. [4] supplemented dynamic simulations with a perturbation analysis of the nonlinear particle and energy balance equations to analytically predict and verify the stability of an equilibrium. They quantified the critical temperature for a number of confinement laws and were the first to suggest feedback stabilization for operation in the unstable temperature regime. Their work still continues to serve as a standard against which improved analyses are compared.

After the work of Mills [3] and Ohta et al. [4], the thrust of research was directed at improving the representative models of the plasma processes and extending the analyses to additional control mechanisms. Further details, and representative models for the plasma processes and terms contributing to the energy balance are presented in Chapter 2, and an extensive review of the literature on thermal stability is presented in Appendix A.

1.3. Control for Fusion Thermal Stability

As the literature review of Appendix A shows, a number of control mechanisms have been proposed, implemented and analyzed for the fusion thermal balance that have permitted operation in otherwise unstable temperature regimes. By the nature of the methods used to obtain them, the types of mechanisms explored have been hit-or-miss in character, have left gaps in the system analysis, and although some have achieved the goal of stabilizing the thermal balance, none has adequately addressed the issues of overall system response. Certainly stability is a necessary condition for operation, but perturbations in component parts and systems disturbances will additionally require that the integrated system possess certain desirable characteristics and properties, such as acceptable overshoot, adequate speed of response, etc. A control systems approach to the problem of thermal stability is necessary, and a knowledge of the system behavior is required in order to effect suitable control.

The work described herein is the first formal classical control theory formulation of the thermal stability problem which extends the application of control theory beyond a simple eigenvalue or roots of the characteristic equation analysis. The present formulation is able to duplicate nearly all previous work regarding the determination of the critical temperature for the onset of the thermal instability, with generally good agreement. In addition to determining the stability of the system, the extended analysis performed on the plasma model has resulted in the first evaluation of the response characteristics of the thermal balance of a fusioning plasma. Thus, the expected temporal

behavior of the plasma following both normal system changes and external disturbances can be assessed and compared to reference systems using standard inputs and accepted weighting criteria.

A model of the fusioning plasma thermal balance was developed which incorporates improvements over many of the models found in the literature while still permitting physical interpretation of the results. Included were the major processes of fusion burnup and energy production, bremsstrahlung radiation emission, and particle and energy diffusion. Processes which would be present in a fusioning plasma but not expected to contribute to the question of thermal stability, such as finite energy transfer mechanisms among particle species, impurity radiation and synchrotron radiation were not included.

The selected plasma model was cast in the form of a classical second order system with a finite zero, and analytical expressions for the system characteristics and specifications were derived in terms of the plasma conditions. Physical associations were drawn between the processes present in a fusioning plasma and the system characteristics and transfer function coefficients. Expressions were derived for the system characteristics of gain, the finite zero, the damped and undamped natural frequencies, the damping ratio, and the damping factor. Expressions were derived for the impulse and step response, as well as the system specifications of time-to-peak, peak overshoot, settling time, bandwidth, resonance frequency, resonance peak, and phase margin. These were evaluated for the cases of zero and 75 keV injection energy, assuming both constant and Bohm confinement laws. The injection energy case was examined because this is currently the leading form of plasma heating [1]. Bohm confinement was evaluated

because the particle and energy transport in the reactor regime is expected to exhibit a Bohm-type of dependence [5]. The analytical expressions so derived were used to provide the initial evaluation of the system characteristics and specifications of the open-loop plasma thermal balance. Similarly, expressions for the closed-loop transfer function using proportional feedback were derived and evaluated. The results were used to determine the feedback fractions necessary to guarantee stability and acceptable system performance. Feedback using advanced control techniques was also investigated.

The format of this study on the control of a fusioning plasma to achieve thermal stability and acceptable system response proceeds in a straightforward manner. The next chapter presents the assumptions made in modeling the plasma thermal balance and describes the range of applicability. It also develops the system transfer functions that are used in the open- and closed-loop analysis of Chapters 3 and 4. Open-loop characteristics, such as natural frequency and damping, and the system specifications, such as peak overshoot and settling time, of the fusioning plasma are presented in Chapter 3. The analogous closed-loop behavior is presented in Chapter 4. Chapter 5 uses the analyses and results of the previous chapters to develop criteria for the desired plasma behavior and implements advanced control techniques to further improve the system response. The conclusions of this study and the recommendations for future work are also presented in Chapter 5. The background information on the major topics of this dissertation is contained in the Appendices. Appendix A presents an introduction to the aspects of fusion which are central to the issues of the thermal instability. It also presents a comprehensive literature review of the

field of plasma thermal stability. Appendix B presents a review of control theory. And Appendix C derives analytical expressions for the system specifications of the transfer function describing the plasma thermal balance.

CHAPTER 2
PLASMA MODEL AND TRANSFER FUNCTION DEVELOPMENT

2.1. Model Assumptions

The governing dynamics of the thermal balance of a magnetically confined fusioning plasma are aptly described by a zero-dimensional formulation of the particle and energy conservation equations. The application of certain simplifying assumptions to these nonlinear differential equations transforms them from a complex collection of mathematical terms into a workable set of equations. The usefulness of the latter rests on their simplicity, permitting their analysis and optimization via classical control methods. In addition, after linearization these streamlined equations yield plasma transfer functions whose coefficients have explicit physical associations. Temporal response characteristics can then be directly attributed to the various plasma parameters. The equations are now presented and the simplifying assumptions described. The development of the plasma transfer functions then follows.

The equations of particle and energy conservation for a fusioning plasma are given by

$$\frac{dn}{dt} = S + K_s(kT_o - kT) - \frac{n^2}{2}\langle DT\rangle - \frac{n}{\tau_n} \qquad 2.1$$

and

$$\frac{d3nkT}{dt} = [S + K_S(kT_o - kT)][T_S + K_{T_S}(kT_o - kT)]$$

$$+ Q_\alpha \frac{n^2}{4}\langle DT\rangle - b_B n^2 (kT)^{1/2} - \frac{3nkT}{\tau_E} \qquad 2.2$$

where

n = fuel particle density [cm^{-3}]

kT = plasma temperature [keV]

kT_o = desired operating temperature [keV]

$\langle DT\rangle$ = reactivity for the deuterium-tritium reaction [$cm^3 sec^{-1}$]

S = fuel injection rate [$cm^{-3} sec^{-1}$]

K_S = fuel injection rate feedback gain

T_S = fuel injection energy [keV]

K_{T_S} = fuel injection energy feedback gain

τ_n = particle confinement time [sec]

τ_E = energy confinement time [sec]

Q_α = alpha particle energy = 3520 keV, and

b_B = bremsstrahlung emission constant = 3.36×10^{-15} $cm^3 keV^{1/2} sec^{-1}$

The terms on the right-hand-side of equation 2.1 represent (in order) particle injection from an external source, feedback injection from an external source, fuel ion consumption via fusion reactions, and diffusion leakage. In equation 2.2, the right-hand terms represent power input to the plasma from external particle injection (including the feedback contributions), power gain from fusion reactions, bremsstrahlung radiation power loss, and lastly, power loss through

diffusion.

The diffusion of particles from a magnetically confined plasma remains the largest source of uncertainty in current fusion research. The basic mechanism for particle loss in a linear magnetic confinement system is classical diffusion. Classical diffusion losses are the result of binary Coulomb collisions. Collisions cause particles to step their way across magnetic field lines with a characteristic step size given by the particle orbits' gyroradii. In a toroidal device, the characteristic step size is modified by the spatial variation of the magnetic configuration. The resulting diffusion is called neoclassical. Experimental results, however, have demonstrated that particle transport in toroidal machines is dominated by microinstabilities. These experimentally-determined transport laws have been labeled pseudoclassical diffusion. Anomalous behavior still predominates and for this reason, confinement in this analysis is modeled with general expressions of the form

$$\tau_E = \tau_c n^{\ell} (kT)^m \qquad 2.3$$

and

$$\tau_n = R\tau_E \qquad 2.4$$

where τ_c, ℓ, m, and R are confinement constants characterizing the desired confinement scheme. The schemes investigated herein include constant (ℓ = m = 0) and Bohm (ℓ = 0 m = -1) confinement.

These four equations comprise the plasma model used in the initial analysis and design procedures. Implicit in their formulation is a set of assumptions. These are first listed and subsequently discussed.

1. The D + T → He^4(3.52 MeV) + n(14.06 MeV) reaction is the dominant fusion reaction.
2. The ion density is maintained at 50% - 50% D-T.
3. The plasma is homogeneous.
4. All particles are at the same Maxwell-Boltzman temperature kT.
5. Particles above kT instantaneously slow down to kT.
6. Beam fusion events are neglected.
7. Synchrotron, recombination and line radiation are negligible.

The validity of the first assumption is quickly established through a comparison of the D-T reactivity with those of all other fusion reactions. It is seen to be two orders of magnitude larger, up to a temperature of 70 keV, and no less than one and one-half orders of magnitude larger from 70 to 100 keV, than the reactivities of competing reactions. Having thus established the dominance of the D-T reaction, the fusion reaction rate, given by $n_D n_T \langle DT \rangle$, is maximized, under the constraint of constant total number of particles, for $n_D = n_T = n/2$, $\underline{n}$ denoting in this case the total fuel ion density. Since each D-T reaction removes one deuterium and one tritium, the ratio of the two will be maintained. One additional consideration, the fractional buildup concentration of product alpha particles, given by $n\langle DT \rangle/4$, can be shown to be less than 10% for total ion densities less than $10^{15}/cm^3$ at 20 keV. The first two assumptions given above are then seen to be valid and self-consistent.

In order to obtain the spatial distribution of density and temperature in a plasma, it is necessary to solve the macroscopic equations obtained by taking moments of the Boltzmann transport equation with a Fokker-Plank collision term and then averaging over

magnetic surfaces. Workers in the field who have performed such analyses have obtained profiles which are basically parabolic in nature [6], with the exact shape factors depending strongly on the transport mechanisms and boundary conditions assumed. Alternately, profiles obtained by solving the set of equations consisting of the electron and power balance equations with radial heat conduction, Faraday's law, Ampere's law, Ohm's law, and charge neutrality also show extreme sensitivity to the scaling laws used [7]. The inclusion of spatial effects, with the attendant complexities, would quickly dispose of one of our initial objectives for this model, that of explicit physical interpretation of the ensuing mathematical terms. This analysis will therefore assume plasma homogeneity and contend with global, volume-averaged parameters.

In the presence of a multispecies plasma, a proper treatment of the slowing down behavior of a fast particle as it undergoes Coulomb scattering involves the solution of a Fokker-Plank-type equation [8], requiring lengthy numerical computations. Similar results can be obtained using closed expressions for the time behavior of the mean energy of these fast particles as determined by Butler and Buckingham [9] and Houlberg [10]. Using the latter's expressions, O'Farrill and Campbell [11] and Hoxie [12] computed slowing down times for product alphas and injected deuterium ions. Typical times required to slow down to 20 keV in a 10 keV background plasma of density $10^{14}/cm^3$ are 0.4 seconds for a fusion alpha and 0.05 seconds for a 75 keV injected deuteron. These are quite small when compared with plasma thermal motion periods of the order of 10's of seconds.

As these fast particles slow down, they will initially impart their energy preferentially to the electrons. As an example, a 3.02 MeV proton in a 10 keV plasma will initially lose energy to the electrons at a rate 170 times greater than to the ions. Not until the particle's velocity has reached approximately one-fourteenth the electron thermal velocity will the rate of energy loss be equivalent to both species [9]. The electrons and ions will therefore have different kinetic temperatures, resulting in an interchange of energy with an equipartition time given by Spitzer [13]. For a 10 keV deuterium plasma with a 20 keV electron component this time constant is on the order of 3×10^{-3} seconds, again quite small when compared to the thermal stability time constants.

Fast particles will not just serve to impart energy to the background plasma. Fast fuel ions, whether produced in secondary fusion reactions or beam-injected, will also induce fusion reactions. Beam reactions can provide a major contribution to the fusion power density due to the resonance peak in the D-T cross section at about 100 keV. (In fact, this effect will be employed to advantage in TFTR, the Tokamak Fusion Test Reactor currently under construction.) The fraction of beam particles, w, that will be investigated here is small enough ($w < 0.07$) so that equilibrium conditions will not be appreciably different except at the very low temperatures (below 6 keV) [14]. In addition, for injection energies below 60-75 keV, the beam fusion contribution to the energy balance is also negligible [15]. These two factors combine to warrant the exclusion of the beam interaction from this analysis.

The isotopes of hydrogen are essentially 100% ionized above 50 eV. Therefore the only sources of recombination and line radiation would arise from impurity ions present in the plasma. The greatest source of impurity ions is the first wall as a result of its bombardment by neutrons, energetic charged particles and radiation. Typical impurities may be carbon, silicon, oxygen, beryllium, and aluminum, with their expected concentrations varying widely, depending on the impurity removal system considered. If the impurity concentration can be kept below 0.1%, say with a divertor of modest efficiency, then the power radiated away by, for example, silicon, will be less than one-fifth of the hydrogenic bremsstrahlung. Therefore, recombination and line radiation will be neglected.

The accurate estimation of synchrotron radiation is not very straightforward. Synchrotron radiation is emitted in a series of harmonics, with the intensity of the radiation decreasing with increasing harmonics. But the plasma is opaque to radiation of frequencies lower than the plasma frequency; therefore the bulk of the synchrotron radiation will be reabsorbed by the plasma. In addition, the entire synchrotron radiation spectrum is of such frequency that it will be reflected by metallic surfaces, resulting in the reentry into the plasma of the radiation that was not initially absorbed. Notwithstanding, the ratio of synchrotron to bremsstrahlung radiation as given by simple expressions, for 95% reflecting walls in a machine of aspect ratio of 5 and toroidal magnetic field strength of 4 Tesla at a temperature of 10 keV, is approximately one-tenth. The small magnitude and the uncertainty associated with synchrotron radiation therefore warrants its exclusion from further consideration in the

present model.

Having established the range of validity of the model, the next step in the analysis is to obtain the plasma transfer functions for this two-input system. This can be done by expanding the nonlinear equations in a first-order Taylor series about an equilibrium point. The resulting time-invariant linear differential equations describing the time response of the perturbation variables yield the desired transfer functions. The derivation of the system transfer functions follows.

2.2. Open- and Closed-Loop Plasma Transfer Functions

In the steady-state, the time derivatives in equations 2.1 and 2.2 are zero, resulting in the following equations:

$$S_o - \frac{n_o^2}{2}\langle DT\rangle_o - \frac{n_o}{\tau_{n_o}} = 0 \qquad 2.5$$

$$S_o T_{s_o} + Q_\alpha \frac{n_o^2}{4}\langle DT\rangle_o - b_B n_o^2 (kT_o)^{1/2} - \frac{3n_o kT_o}{\tau_{E_o}} = 0 \qquad 2.6$$

$$\tau_{E_o} = \tau_c n_o^{\ell} (kT_o)^m \qquad 2.7$$

$$\tau_{n_o} = R\tau_{E_o} \qquad 2.8$$

The subscript zero denotes each variable's value at steady-state.

Performing a perturbation expansion of equations 2.1 - 2.4 about the equilibrium conditions dictated by equations 2.5 - 2.8 results in the desired linearized equations. Therefore, into equations 2.1 - 2.4, substitute the following:

$$n = n_o + n'$$

$$kT = kT_o + kT'$$

$$S = S_o + S'$$

$$T_s = T_{s_o} + T_s'$$

$$\langle DT \rangle = \langle DT \rangle_o + \frac{\partial \langle DT \rangle}{\partial kT}\Big]_o kT' \equiv \langle DT \rangle_o + \langle DT \rangle_\partial kT'$$

$$\tau_E^{-1} = \tau_{E_o}^{-1} + \frac{\partial \tau_E^{-1}}{\partial n}\Big]_o n' + \frac{\partial \tau_E^{-1}}{\partial kT}\Big]_o kT' \equiv \tau_{E_o}^{-1} + \tau_{E\partial n} n' + \tau_{E\partial kT} kT'$$

$$\tau_n^{-1} = \tau_{n_o}^{-1} + \frac{\partial \tau_n^{-1}}{\partial n}\Big]_o n' + \frac{\partial \tau_n^{-1}}{\partial kT}\Big]_o kT' \equiv \tau_{n_o}^{-1} + \tau_{n\partial n} n' + \tau_{n\partial kT} kT'$$

where the following definitions and expansions apply:

$$(kT_o + kT')^{1/2} = (kT_o)^{1/2}(1 + \frac{kT'}{kT_o})^{1/2} = (kT_o)^{1/2} + \frac{kT'}{2(kT_o)^{1/2}}$$

$$\tau_{E\partial n} \equiv \frac{\partial \tau_E^{-1}}{\partial n}\Big]_o = -\ell \tau_c n_o^{-\ell-1} (kT_o)^{-m} = -\frac{\ell}{n_o \tau_{n_o}}$$

$$\tau_{E\partial kT} \equiv \frac{\partial \tau_E^{-1}}{\partial kT}\Big]_o = -m \tau_c n_o^{-\ell} (kT_o)^{-m-1} = -\frac{m}{kT_o \tau(kT_o)}$$

$$\tau_{n\partial n} \equiv \frac{\partial \tau_n^{-1}}{\partial n}\Big]_o = \frac{1}{R}\frac{\partial \tau_E^{-1}}{\partial n}\Big]_o = -\frac{\ell}{Rn_o\tau_{E_o}} = -\frac{\ell}{n_o\tau_{n_o}}$$

$$\tau_{n\partial kT} \equiv \frac{\partial \tau_n^{-1}}{\partial kT}\Big]_o = \frac{1}{R}\frac{\partial \tau_E^{-1}}{\partial kT}\Big]_o = -\frac{m}{RkT_o\tau_{E_o}} = -\frac{m}{kT_o\tau_{n_o}}$$

The resulting equations are

$$\frac{dn'}{dt} = S' + \left(\frac{\ell - 1}{\tau_{n_o}} - n_o\langle DT\rangle_o\right)n' + \left(\frac{mn_o}{RkT_o\tau_{E_o}} - \frac{n_o^2}{2}\langle DT\rangle_\partial - K_s\right)kT' \qquad 2.9$$

$$\frac{dkT'}{dt} = \left(\frac{T_{s_o} - 3kT_o}{3n_o}\right)S' + \frac{S_o}{3n_o}T_s'$$

$$+ \left[\left(\frac{Q_\alpha + 6kT_o}{6}\right)\langle DT\rangle_o - \frac{2}{3}b_B(kT_o)^{1/2} + (\ell - 1)\left(\frac{R - 1}{Rn_o\tau_{E_o}}\right)kT_o\right]n'$$

$$+ \left[\left(\frac{Q_\alpha + 6kT_o}{12}\right)n_o\langle DT\rangle_\partial - \frac{b_Bn_o}{6(kT_o)^{1/2}} + \frac{m(R - 1) - R}{R\tau_{E_o}}\right.$$

$$\left. - K_s\left(\frac{T_{s_o} - 3kT_o}{3n_o}\right) - K_{T_s}\frac{S_o}{3n_o}\right]kT' \qquad 2.10$$

For convenience rewrite equations 2.9 and 2.10 as

$$\frac{dn'}{dt} = S' + an' + bkT' \qquad 2.11$$

$$\frac{dkT'}{dt} = g_1S' + g_2T_s' + cn' + dkT' \qquad 2.12$$

with

$$a = \frac{\ell - 1}{\tau_{n_o}} - n_o \langle DT \rangle_o \qquad 2.12a$$

$$b = \frac{mn_o}{RkT_o\tau_{E_o}} - \frac{n_o^2}{2}\langle DT \rangle_\partial - K_s \qquad 2.12b$$

$$c = \left(\frac{Q_\alpha + 6kT_o}{6}\right)\langle DT \rangle_o - \frac{2}{3}b_B(kT_o)^{1/2} + (\ell - 1)\left(\frac{R - 1}{Rn_o\tau_{E_o}}\right)kT_o \qquad 2.12c$$

$$d = \left(\frac{Q_\alpha + 6kT_o}{12}\right)n_o\langle DT \rangle_\partial - \frac{b_B n_o}{6(kT_o)^{1/2}} + \frac{m(R - 1) - R}{R\tau_{E_o}}$$

$$- g_1K_s - g_2K_{T_s} \qquad 2.12d$$

$$g_1 = \frac{T_{s_o} - 3kT_o}{3n_o} \qquad 2.12e$$

$$g_2 = \frac{S_o}{3n_o} \qquad 2.12f$$

Taking the Laplace transform of equations 2.11 and 2.12 gives

$$sN(s) = S(s) + aN(s) + bT(s)$$

$$sT(s) = g_1S(s) + g_2T_s(s) + cN(s) + dT(s),$$

where now N, T, S, and T_s are functions of the Laplace transform variable s; they represent the Laplace transforms of the perturbation

variables n', kT', S', and T_s' respectively, and are not to be confused with any of the function-of-time variables of equations 2.1 to 2.4.

The desired transfer functions can now be determined. The open-loop transfer functions (i.e., $K_s = K_{T_s} = 0$ in coefficients b and d above and denoted as b^* and d^*) are given by

$$G_1(s) \equiv \frac{T(s)}{S(s)} = \frac{g_1(s - a + c/g_1)}{s^2 + (-a - d^*)s + (ad^* - cb^*)} \qquad 2.13$$

$$G_2(s) \equiv \frac{T(s)}{T_s(s)} = \frac{g_2(s - a)}{s^2 + (-a - d^*)s + (ad^* - cb^*)} \qquad 2.14$$

and are presented in functional block diagram form in Figure 2-1. As a consequence of the principle of superposition of linear systems, the temperature perturbation can be computed independently for each of the two system inputs and the results added to yield the total plasma temperature deviation.

The closed-loop plasma system is given in block diagram form in Figure 2-2. Manipulations of the block diagram equations can be used to yield an expression for T(s) given by (dropping the function-of-s notation),

$$T = \frac{SG_1 + T_sG_2}{1 + G_1H_1 + G_2H_2}$$

Once again, transfer functions can be obtained for each of the inputs individually, and the principle of superposition can then be used to obtain the total plasma temperature variation. For simple proportional

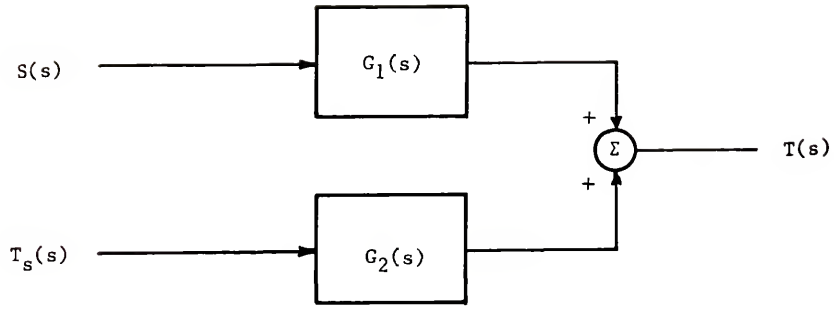

Figure 2-1. Open-loop plasma system block diagram representation.

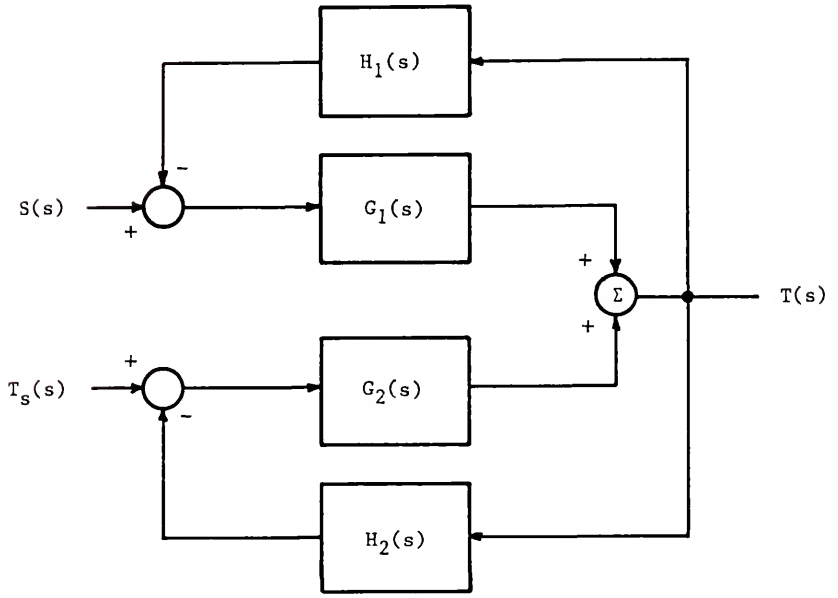

Figure 2-2. Closed-loop plasma system block diagram representation.

feedback, i.e., $H_1 = K_s$ and $H_2 = K_{T_s}$, the closed-loop transfer functions are given by

$$J_1 \equiv \frac{T}{S} = \frac{G_1}{1 + G_1H_1 + G_2H_2} = \frac{g_1(s - a + c/g_1)}{s^2 + (-a - d)s + (ad - cb)} \quad 2.15$$

$$J_2 \equiv \frac{T}{T_s} = \frac{G_2}{1 + G_1H_1 + G_2H_2} = \frac{g_2(s - a)}{s^2 + (-a - d)s + (ad - cb)} \quad 2.16$$

The effect of proportional-integral-derivative feedback control is evaluated and discussed in Chapter 5.

The working model and transfer functions described in this chapter provide the necessary basis for the analysis of a fusioning plasma as a control system and the design of a suitable controller. The open-loop analysis is presented in Chapter 3, followed by the classical closed-loop analysis in Chapter 4.

CHAPTER 3
CLASSICAL OPEN-LOOP ANALYSIS OF PLASMA MODEL

The transfer functions obtained in the previous chapter are of the form of a classical second-order system with a finite zero. This lends them handily to analysis via classical methods, e.g., root locus, Bode and Nyquist plots, etc., and to characterization via classical specifications, e.g., peak overshoot, settling time, bandwidth, resonance peak and frequency, etc. In fact, analytical expressions can be found for the classical specifications for the model at hand and these are derived in Appendix C. Due to the premium placed on computer time, and the desire to explore the broadest parameter range possible, the analytical expressions were used in the calculations performed in the analyses of this chapter. In the first section of this chapter, the coefficients of the open-loop plasma transfer functions are associated with physical processes present in a fusioning plasma. The system performance is then presented. These sections are followed by a summary of the open-loop results.

3.1. Open-Loop Plasma Transfer Function Characteristics

The open-loop plasma transfer functions correspond to equations 2.13 and 2.14 with $K_s = K_{T_s} = 0$. These are now repeated.

$$G_1(s) \equiv \frac{T(s)}{S(s)} = \frac{g_1(s - a + c/g_1)}{s^2 + (-a - d^*)s + (ad^* - cb^*)} \qquad 3.1$$

$$G_2(s) \equiv \frac{T(s)}{T_s(s)} = \frac{g_2(s - a)}{s^2 + (-a - d^*)s + (ad^* - cb^*)} \qquad 3.2$$

The supporting equations 2.12a-f with $K_s = K_{T_s} = 0$ reduce to the following:

$$a = \frac{\ell - 1}{\tau_{n_o}} - n_o\langle DT\rangle_o \qquad 3.2a$$

$$b^* = \frac{mn_o}{RkT_o\tau_{E_o}} - \frac{n_o^2}{2}\langle DT\rangle_\partial \qquad 3.2b$$

$$c = \left(\frac{Q_\alpha + 6kT_o}{6}\right)\langle DT\rangle_o - \frac{2}{3}b_B(kT_o)^{1/2} + (\ell - 1)\left(\frac{R - 1}{Rn_o\tau_{E_o}}\right)kT_o \qquad 3.2c$$

$$d^* = \left(\frac{Q_\alpha + 6kT_o}{12}\right)n_o\langle DT\rangle_\partial - \frac{b_B n_o}{6(kT_o)^{1/2}} + \frac{m(R - 1) - R}{R\tau_{E_o}} \qquad 3.2d$$

$$g_1 = \frac{T_{s_o} - 3kT_o}{3n_o} \qquad 3.2e$$

$$g_2 = \frac{S_o}{3n_o} \qquad 3.2f$$

These are in a form that can be compared to that of the classical second-order system with a finite zero given by

$$G_i(s) = \frac{g_i(s + z_i)}{s^2 + 2\xi\omega_n s + \omega_n^2} = \frac{g_i(s + z_i)}{(s + \sigma)^2 + \omega_d^2} \qquad 3.3$$

where

g_i = gain of $i^{\underline{th}}$ transfer function, $i = 1,2$

$-z_i$ = location of zero of $i^{\underline{th}}$ transfer function

$-\sigma \pm j\omega_d$ = location of poles

ξ = damping ratio

ω_n = undamped natural frequency

$\sigma = \xi\omega_n$ = damping factor ($0 < \xi < 1$), and

$\omega_d = \omega_n\sqrt{1 - \xi^2}$ = damped natural frequency.

A comparison of equations 3.1 and 3.2 with 3.3 can be used to equate

$$g_1 = \frac{T_{s_o}/3 - kT_o}{n_o} \qquad 3.4$$

$$g_2 = \frac{S_o}{3n_o} \qquad 3.5$$

$$z_1 = -a + c/g_1 = \frac{(Q_\alpha + 2T_{s_o})}{2(T_{s_o} - 3kT_o)} n_o \langle DT \rangle_o - \frac{2b_B n_o (kT_o)^{1/2}}{T_{s_o} - 3kT_o}$$

$$- \frac{(\ell - 1)(T_{s_o} - 3RkT_o)}{R\tau_E(T_{s_o} - 3kT_o)} \qquad 3.6$$

$$z_2 = -a = n_o\langle DT\rangle_o - \frac{\ell - 1}{R\tau_{E_o}} \qquad 3.7$$

$$\omega_n^2 = ad^* - cb^* = \frac{b_B n_o^2}{6(kT_o)^{1/2}}(\langle DT\rangle_o - 2kT_o\langle DT\rangle_\partial)$$

$$+ \{[2(1 - m)\langle DT\rangle_o + (\ell - 1)kT_o\langle DT\rangle_\partial][\frac{(Q_\alpha + 6RkT_o)n_o}{12R\tau_{E_o}kT_o}]$$

$$- \frac{Q_\alpha n_o\langle DT\rangle_o}{6R\tau_{E_o}kT_o}\} + \frac{b_B n_o(4m - \ell + 1)}{6R\tau_{E_o}(kT_o)^{1/2}} - \frac{\ell - 1}{R\tau_{E_o}^2} \qquad 3.8$$

$$\xi = \frac{-a - d^*}{2\omega_n} = \frac{1}{2\omega_n}[n_o\langle DT\rangle_o - (\frac{Q_\alpha + 6kT_o}{12})n_o\langle DT\rangle_\partial + \frac{b_B n_o}{6(kT_o)^{1/2}}$$

$$+ \frac{1 - \ell + m + R - mR}{R\tau_{E_o}}] \qquad 3.9$$

Equations 3.4 to 3.9 provide the means by which physical associations can be attached to the control system terminology.

3.1.1. Open-Loop Gains

The expression for g_1 is discussed first. A Maxwellian plasma of total density n_t at temperature kT has on the average $\frac{3}{2}n_t kT$ of kinetic energy. Assuming the ions and electrons to be at the same temperature and the plasma to be electrically neutral and hydrogenic, the average kinetic energy in terms of the ion density is 3nkT. A unidirectional beam of ions at temperature kT, however, has average kinetic energy of only nkT. Therefore a beam of particles with injection energy $T_s = 3kT$

injected into a plasma at temperature kT would have no effect on the plasma temperature, regardless of its intensity. It follows then, that the beam could either cool or heat the plasma, depending on whether its injection energy is below or above 3kT, kT being the temperature of the plasma. This is the statement made by equation 3.4 for g_1, that the gain of the feedrate transfer function is proportional to the difference in energy between the injected beam and the background plasma.

The expression for g_2, equation 3.5, also permits straightforward physical interpretation. It is seen to be the ratio of injected ion density to plasma ion density. Therefore, the magnitude of the effect of injection energy will be proportional to this ratio of densities.

Figure 3-1 plots the gains g_1 and g_2 as a function of plasma temperature for 0 and 75 keV injection energy, normalized by the value of the corresponding input function. As was shown in Section 2.2, the closed-loop transfer functions are proportional to the gains g_1 and g_2. Since the total response of the plasma is the sum of the feedrate and injection energy transfer functions, the plots in Figure 3-1 show that considerable flexibility is available for affecting the closed-loop plasma performance.

3.1.2. Zeroes

In this section, the physical basis of each zero found in the plasma transfer functions is presented. The effect of a zero in the response characteristics of a second-order system can be determined from the derivations provided in Appendix C. The effect is noted where appropriate within the discussions of the classical specifications.

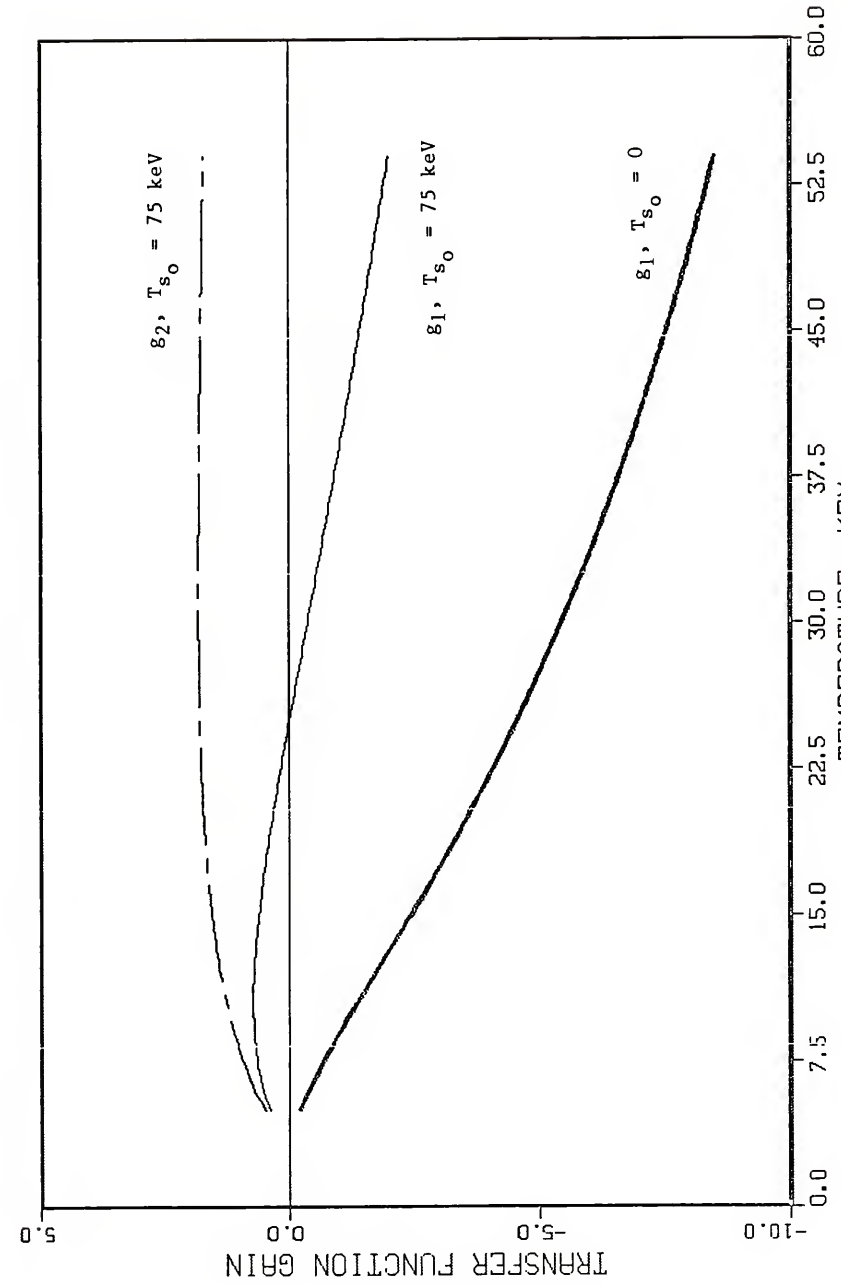

Figure 3-1. The gains g_1 and g_2 as a function of plasma temperature, for 0 and 75 keV injection energy.

With $T_s = 0$, the expression for z_1 reduces to

$$z_1 = -\frac{Q_\alpha n_o \langle DT \rangle_o}{6kT_o} + \frac{2b_B n_o}{3(kT_o)^{1/2}} - \frac{\ell - 1}{\tau_{E_o}} \qquad 3.10$$

The three terms on the right-hand-side (RHS) of this equation can be associated with the thermonuclear fusion power, bremsstrahlung radiation power, and energy confinement (loss rate), respectively. Figure 3-2 is a plot of these terms and their sum, as a function of plasma temperature. It can be seen that following an initial singularity corresponding to the ignition temperature, the zero is a smooth, slowly-varying function of temperature. Throughout the range of temperature under investigation, the bremsstrahlung contribution to the zero is negligible, while the fusion power term is approximately twice that of the confinement term and of opposite sign. The terms combine to produce a left-hand-plane (LHP) zero of magnitude on the order of 0.1 - 0.2 sec^{-1}. With T_s = 75 kev, equation 3.6 for z_1 applies and its terms are plotted in Figure 3-3. The presence of the $T_{s_o} - 3kT_o$ term in the denominator accounts for the appearance of the singular point in Figure 3-3. The zero approaches positive infinity as kT_o approaches $T_{s_o}/3$ and reappears at negative infinity as kT_o becomes slightly greater than $T_{s_o}/3$. The reason why the associated transfer function does not similarly "blow up" is that its gain contains the same $T_{s_o} - 3kT_o$ term in the numerator and therefore approaches zero at the same rate. As mentioned previously, the implications of a zero on the system response will receive further discussion under the appropriate system specifications.

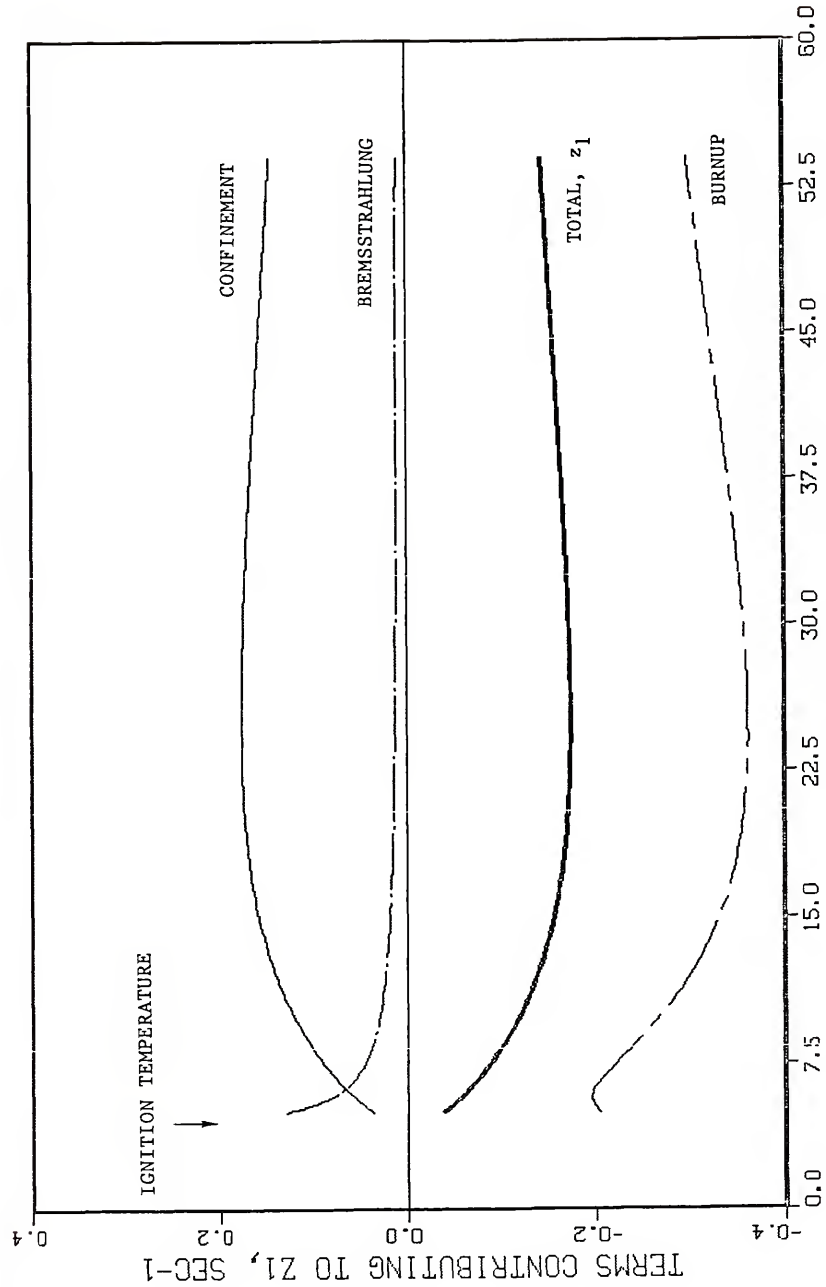

Figure 3-2. Temperature dependence of the terms contributing to z_1. No injection energy, constant or Bohm confinement.

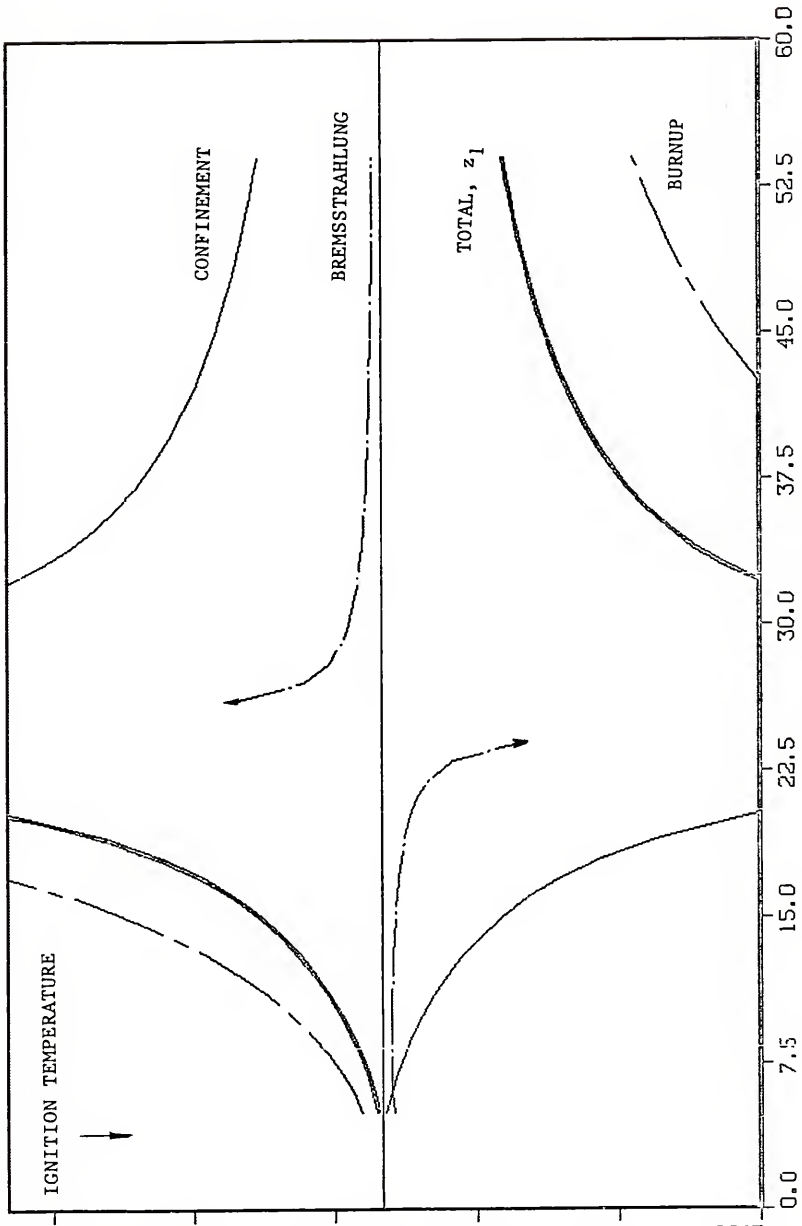

Figure 3-3. Temperature dependence of the terms contributing to z_1. T_{s_o} = 75 keV, constant or Bohm confinement.

With or without injection energy, the expression for z_2 is given by equation 3.7. This zero is comprised of a fuel burnup term and a particle confinement term. For zero injection energy, confinement effects dominate by an order of magnitude throughout nearly the entire range of temperature. The result, shown in Figure 3-4, is a fairly slowly-varying RHP zero of magnitude 0.1 - 0.2 sec^{-1}. With 75 keV injection energy, due to lower $n\tau$ requirements, both the burnup and confinement terms are lower in magnitude than for zero injection energy. However, as the temperature is lowered,, the reduction in τ_E is greater than the reduction in n, which coupled to the $1/\tau_E$ dependence of the confinement term allows confinement effects to dominate the magnitude of the zero only below 30 keV. This zero is of magnitude 0.05 - 0.1 sec^{-1} in the RHP and is shown in Figure 3-5.

3.1.3. Undamped Natural Frequency, Damping Ratio, and the Poles of the Open-Loop Plasma Transfer Function

Examination of the expression for the square of the undamped natural frequency, equation 3.8, reveals four terms corresponding to the mathematical coupling of the competing physical processes. The terms are expressed below for easy reference.

$$\frac{b_B n_o^2}{6(kT_o)^{1/2}}(\langle DT\rangle_o - 2kT_o\langle DT\rangle_\partial) \qquad 3.11$$

$$[2(1-m)\langle DT\rangle_o + (\ell - 1)kT_o\langle DT\rangle_\partial]\left[\frac{(Q_\alpha + 6RkT_o)n_o}{12R\tau_{E_o}kT_o}\right] - \frac{Q_\alpha n_o\langle DT\rangle_o}{6R\tau_{E_o}kT_o} \qquad 3.12$$

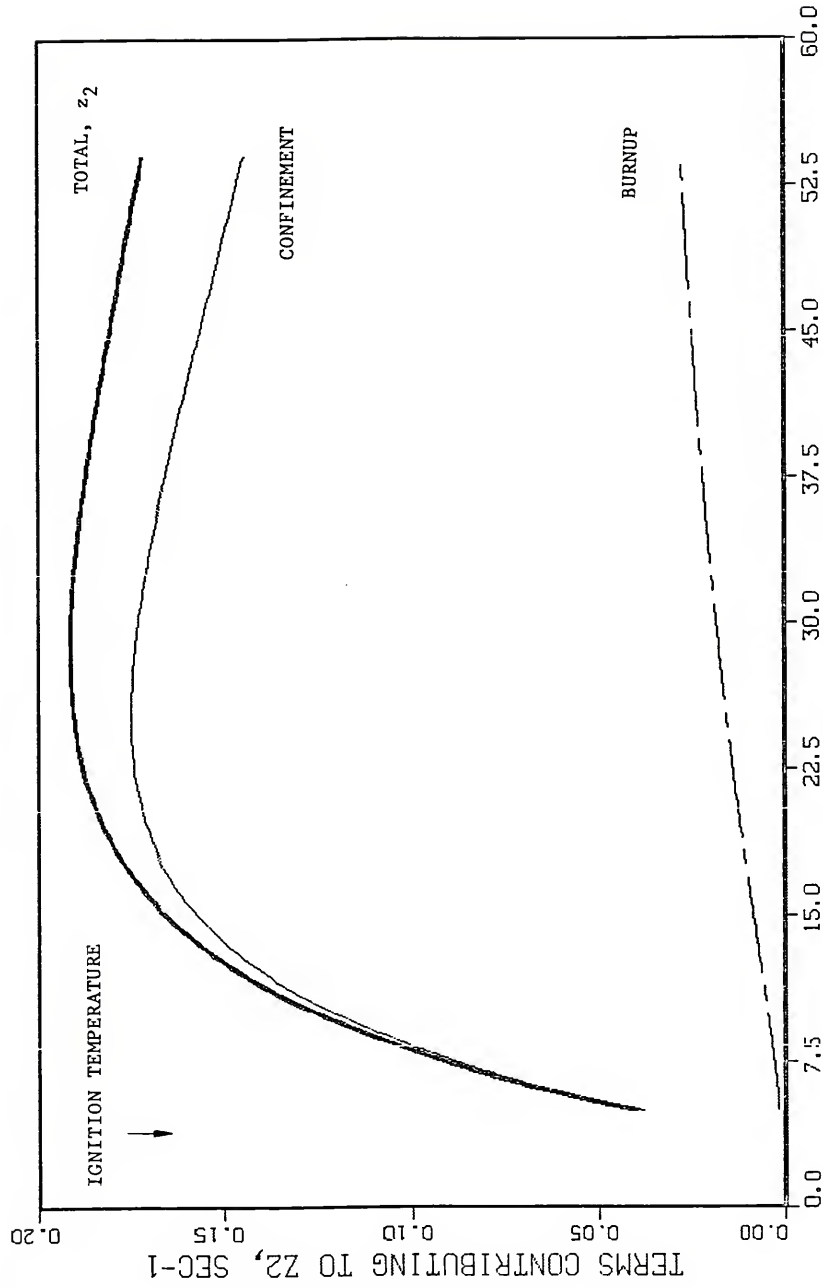

Figure 3-4. Temperature dependence of the terms contributing to z_2. No injection energy, constant or Bohm confinement.

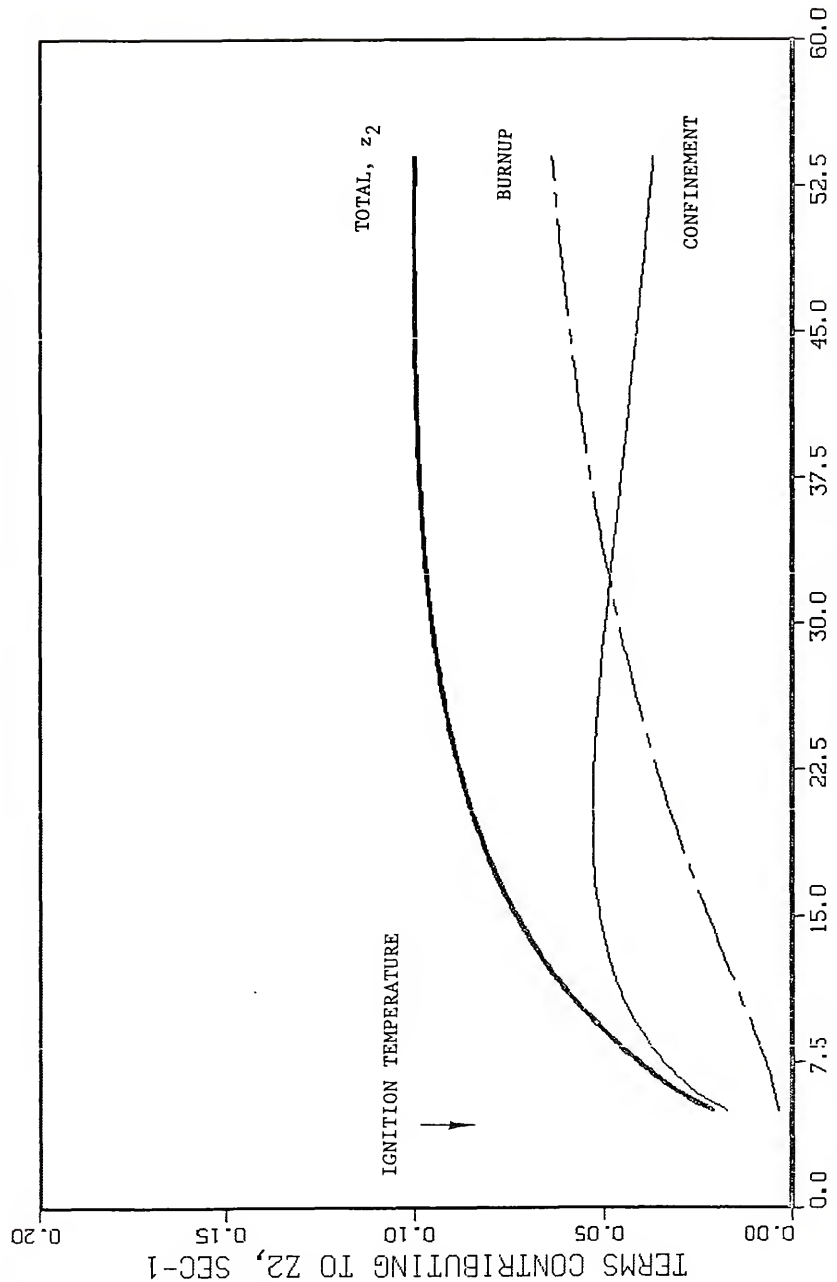

Figure 3-5. Temperature dependence of the terms contributing to z_2. T_{s_o} = 75 keV, constant or Bohm confinement.

$$\frac{b_B n_o (4m - \ell + 1)}{6R\tau_{E_o}(kT_o)^{1/2}} \qquad 3.13$$

$$-\frac{\ell - 1}{R\tau_{E_o}^{\,2}} \qquad 3.14$$

The four terms can be identified with the coupling of fusion processes and bremsstrahlung, expression 3.11; fusion processes and confinement, expression 3.12; bremsstrahlung and confinement, expression 3.13; and lastly, of particle and energy confinement, expression 3.14. These are displayed as a function of plasma temperature in Figures 3-6 through 3-9, covering the cases of 0 and 75 keV injection energy, with constant and Bohm confinement. The reason for plotting the square of the natural frequency becomes apparent upon inspection of the figures, as the sum of the terms is found to be negative below the critical temperature. This is sufficient to indicate thermal instability. Note however, that for stability, both the natural frequency and the damping ratio must be greater than zero.

One of the characteristics of the four figures which comes to the foreground immediately is the small magnitude of the contribution of bremsstrahlung radiation to the natural frequency oscillation of the thermal balance. This can be attributed to the assumption of a hydrogenic plasma, i.e., free of impurities. Noting the Z^2 dependence of bremsstrahlung emission suggests the use of the impurity concentration as a potential control mechanism; indeed, this has recently been proposed for the latest Tokamak reactor design [16].

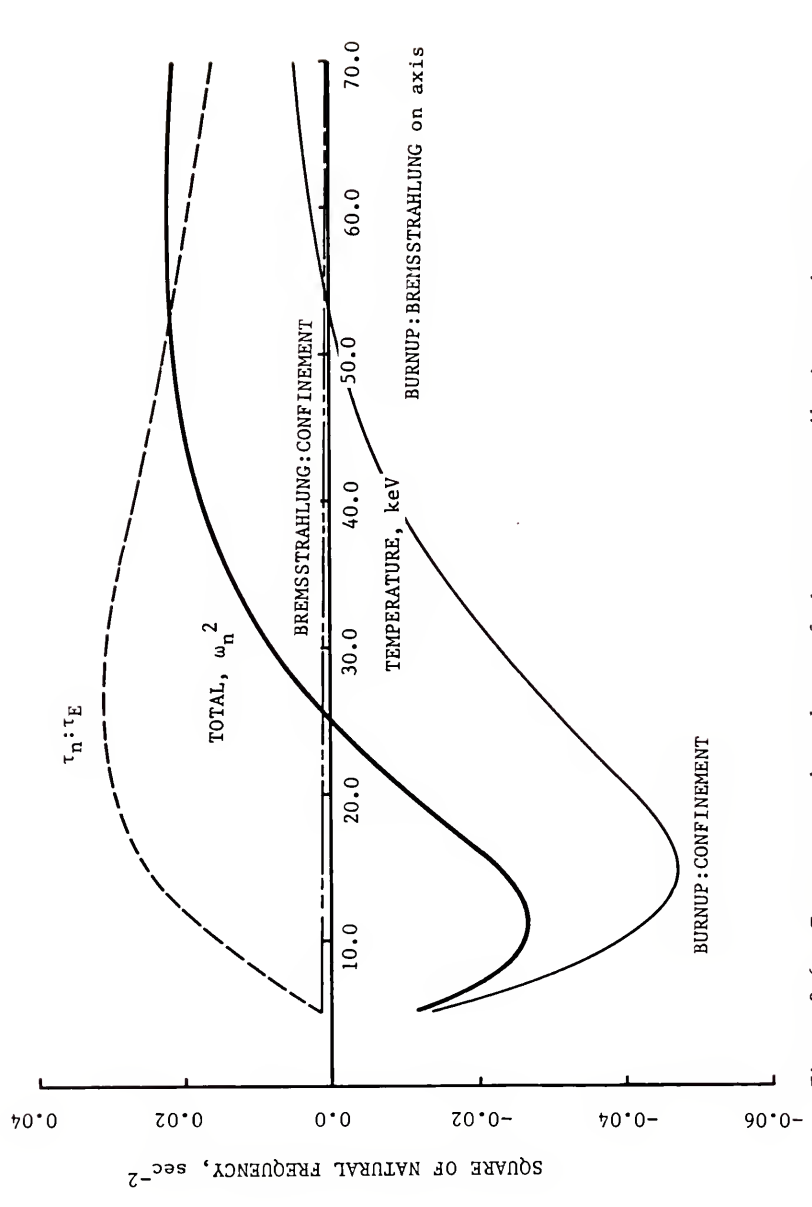

Figure 3-6. Temperature dependence of the terms contributing to the square of the natural frequency. No injection energy, constant confinement.

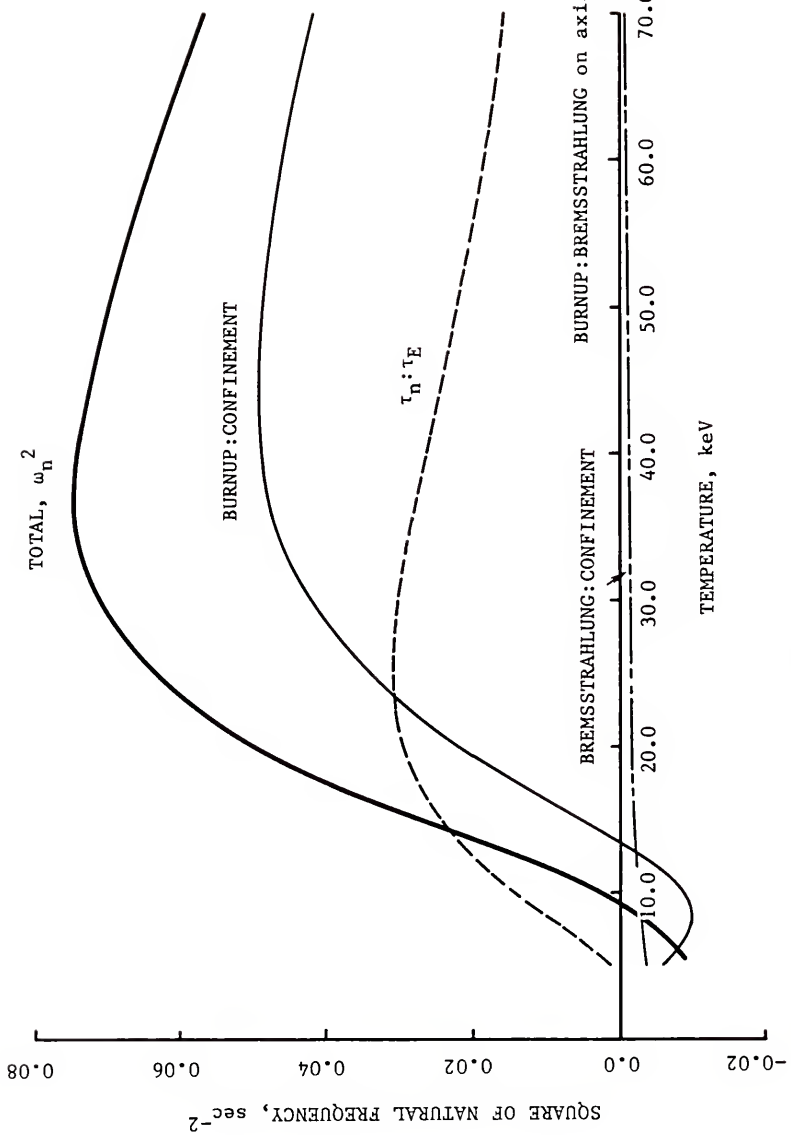

Figure 3-7. Temperature dependence of the terms contributing to the square of the natural frequency. No injection energy, Bohm confinement.

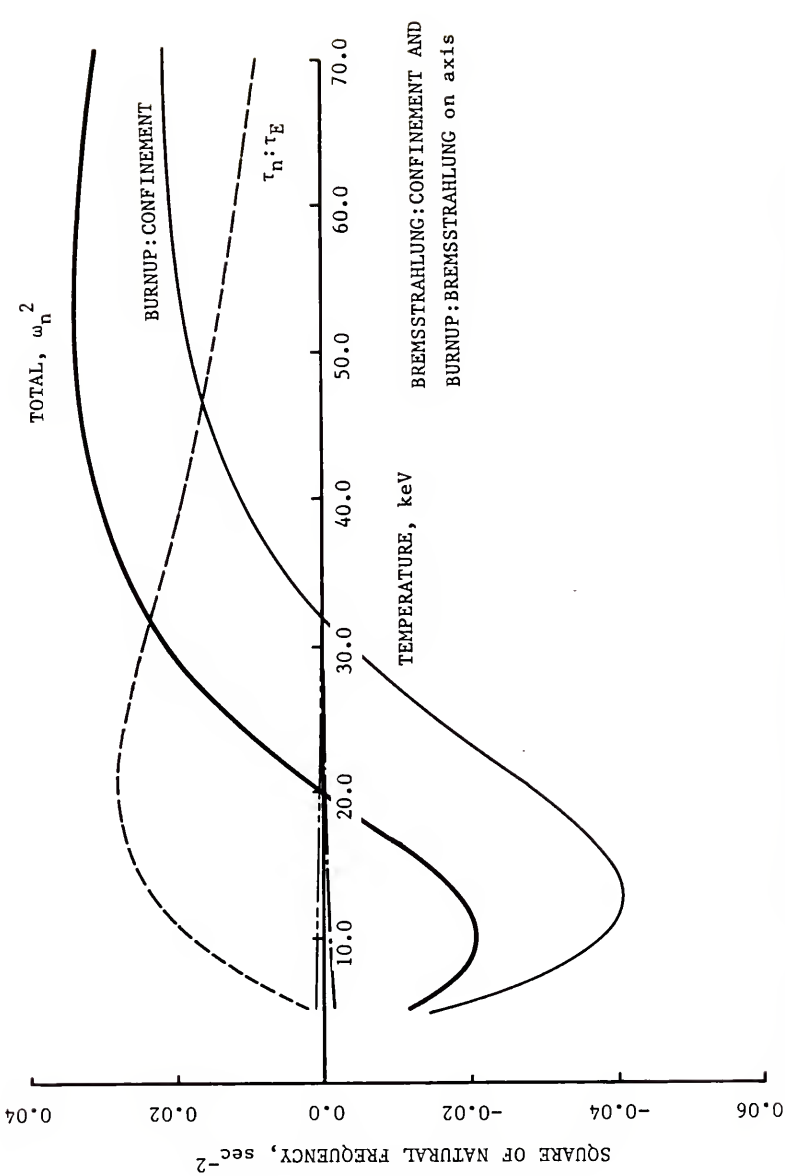

Figure 3-8. Temperature dependence of the terms contributing to the square of the natural frequency. T_{s_o} = 75 keV, constant confinement.

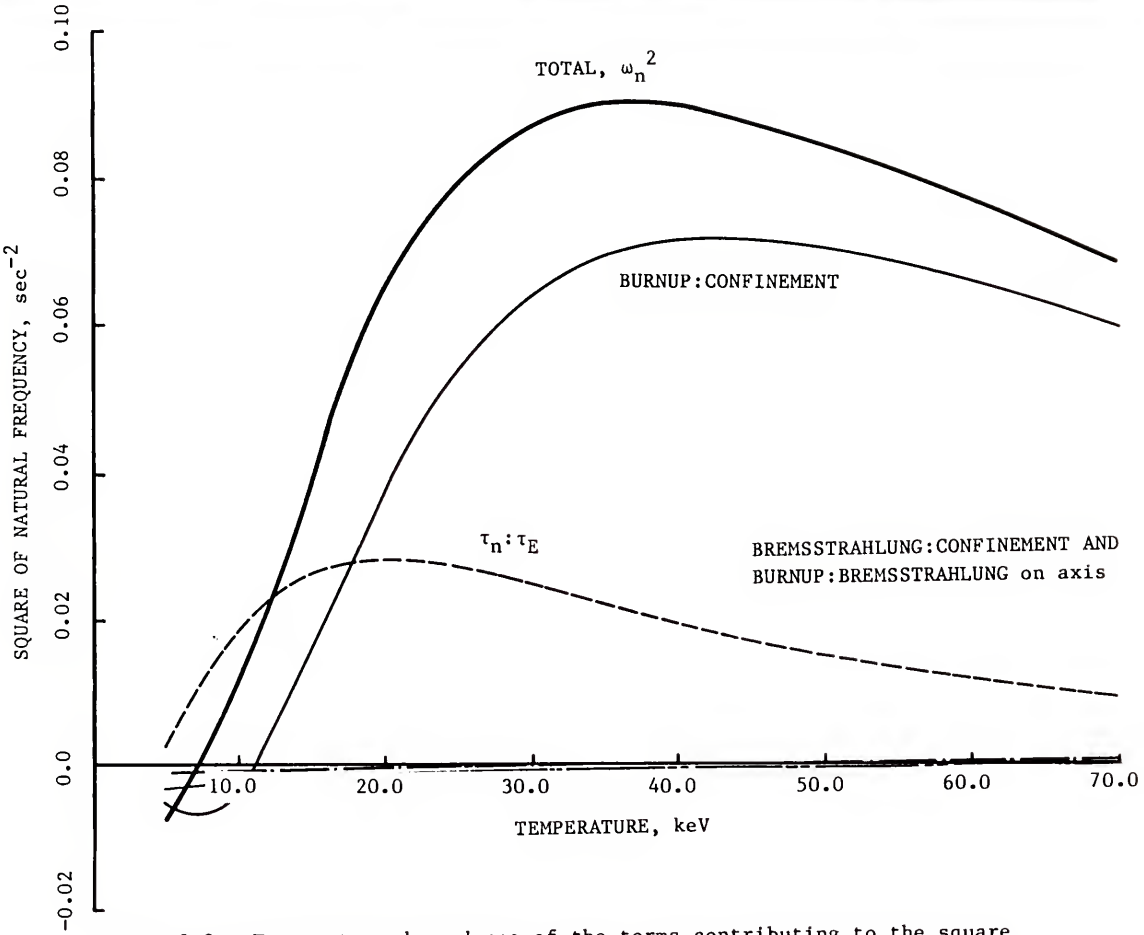

Figure 3-9. Temperature dependence of the terms contributing to the square of the natural frequency. T_{s_o} = 75 keV, Bohm confinement.

The dominating terms influencing the natural frequency are the fusion processes-particle and energy confinement cross-product, expression 3.12, and the particle confinement-energy confinement cross-product, expression 3.14. The latter is seen to be fairly independent of the injection energies and confinement schemes considered. Its variation with temperature can be attributed directly to the required $n\tau$ condition for steady state operation and is fairly constant. To a great extent then, the former term (i.e., the term given by 3.12) contains the determining characteristics responsible for the variations of the natural frequency with plasma temperature.

Rearrangement and closer inspection of expression 3.12 for the fusion processes-confinement term reveals it to be composed of a particle burnup-energy confinement term and an energy production-particle confinement term. These are given respectively by

$$\frac{n_o}{2\tau_{E_o}}[2(1 - m)\langle DT\rangle_o + (\ell - 1)kT_o\langle DT\rangle_\partial] \qquad 3.15$$

and

$$\frac{Q_\alpha n_o}{12R\tau_{E_o} kT_o}[-m\langle DT\rangle_o + (\ell - 1)kT_o\langle DT\rangle_\partial] \qquad 3.16$$

The fractions outside the brackets are very slowly varying functions of temperature; therefore the main contributions to the variations in natural frequency can be further localized to the terms inside the brackets, i.e., the functional dependence of the confinement scheme, and the reactivity function and its derivative. For both constant and

Bohm confinement, in the low temperature region, a change in temperature due to a perturbation induces a change in the reactivity of a magnitude large enough to perpetuate the perturbation in its original direction. As the temperature increases, the incremental increase in the reactivity decreases in magnitude such that at the critical temperature the accompanying changes in the confinement characteristics have compensated for the change in reactivity, initiating the natural oscillations of the thermal balance.

The stabilizing influence of the inverse temperature dependence of Bohm confinement can be seen by comparing Figure 3-6 with 3-7, and Figure 3-8 with 3-9. Note that the figures all have the same abscissa scale, but different stability ranges. The plasma can begin stable natural oscillations at a temperature that is 11 keV lower with Bohm confinement than with constant confinement with either zero or 75 keV injection energy. The effect of 75 keV injection energy is a 4 keV lowering of the temperature required for stable natural oscillations, mainly due to the different equilibrium conditions required for steady state.

The actual frequency of oscillation will depend on the presence of damping modes in the plasma energy balance. Equation 3.9 is the analytical expression for the damping ratio in terms of its constituents. Figures 3-10 through 3-17 depict the relative magnitudes of these terms as they combine to produce the system damping. Throughout the range of temperatures and conditions under consideration, the strong damping effect of diffusion is delicately balanced by an opposing force from the fusion reactivity. Bremsstrahlung provides a small but positive contribution to the

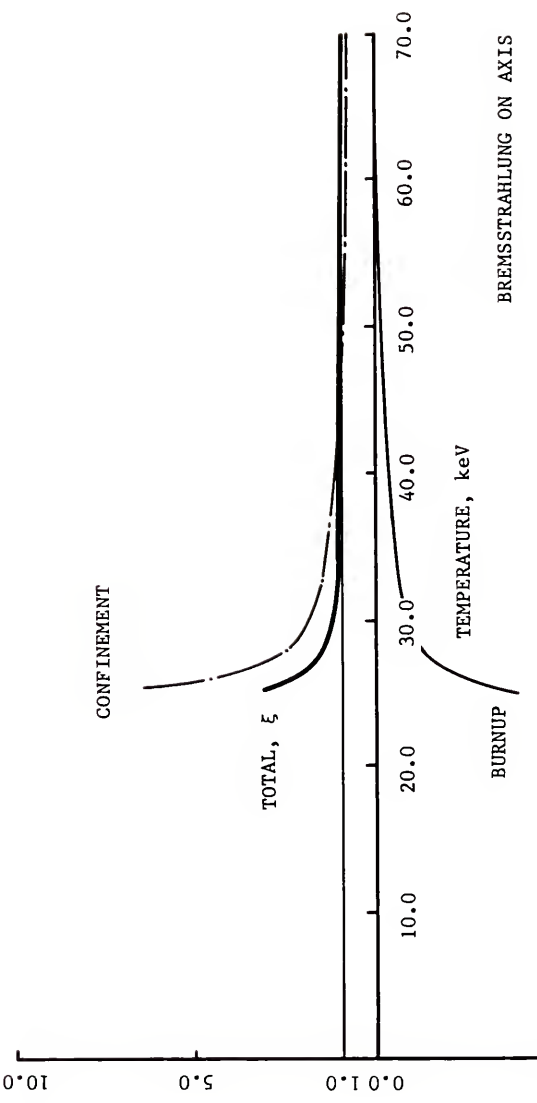

Figure 3-10. Temperature dependence of the terms contributing to the system damping. No injection energy, constant confinement.

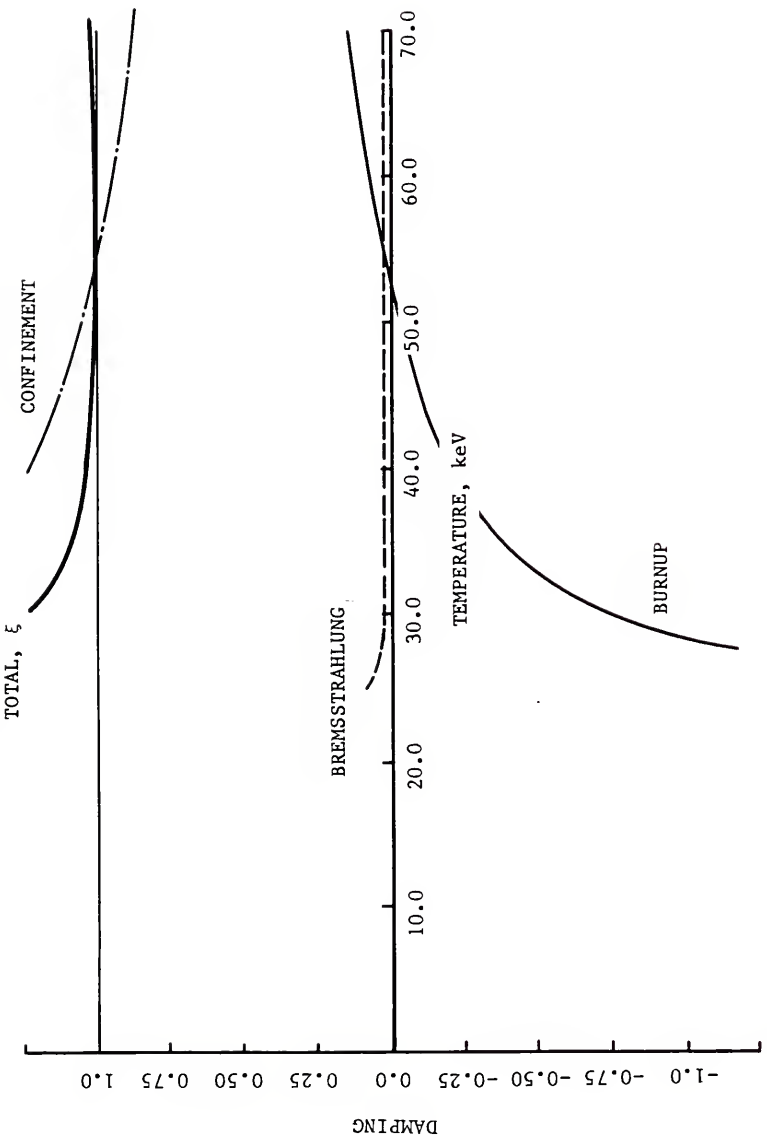

Figure 3-11. Change of scale for data of Figure 3-10.
No injection energy, constant confinement.

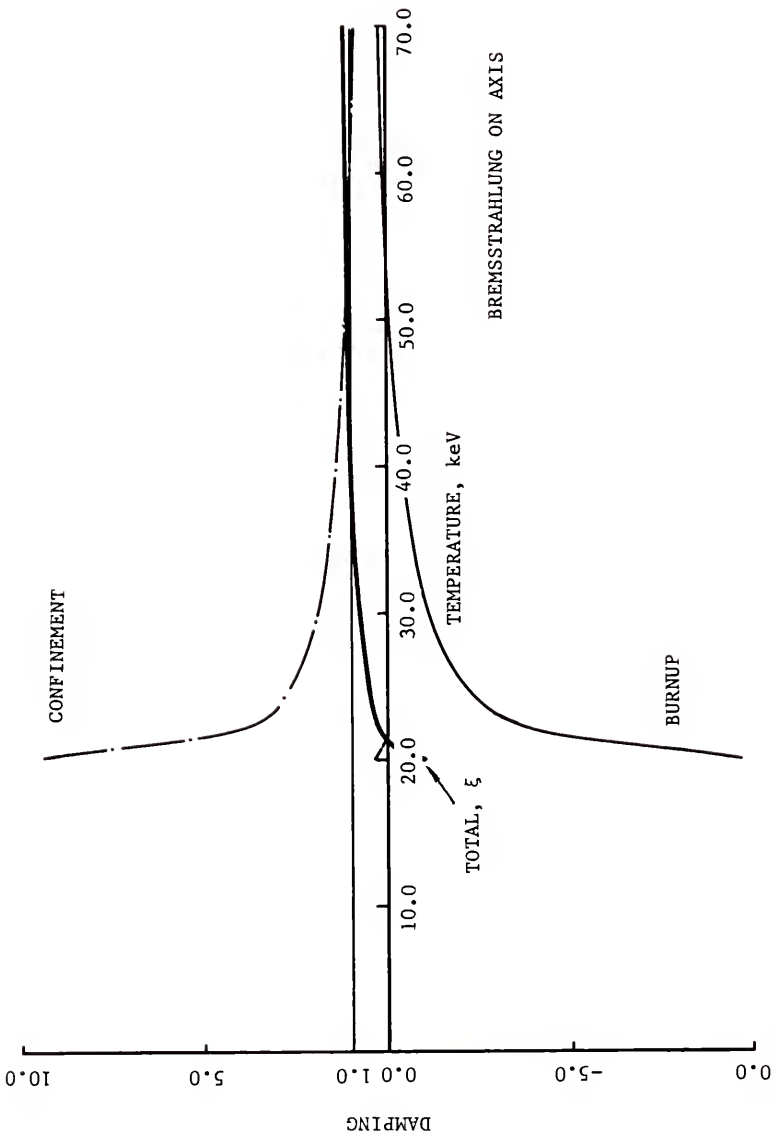

Figure 3-12. Temperature dependence of the terms contributing to the system damping. T_{s_o} = 75 keV, constant confinement.

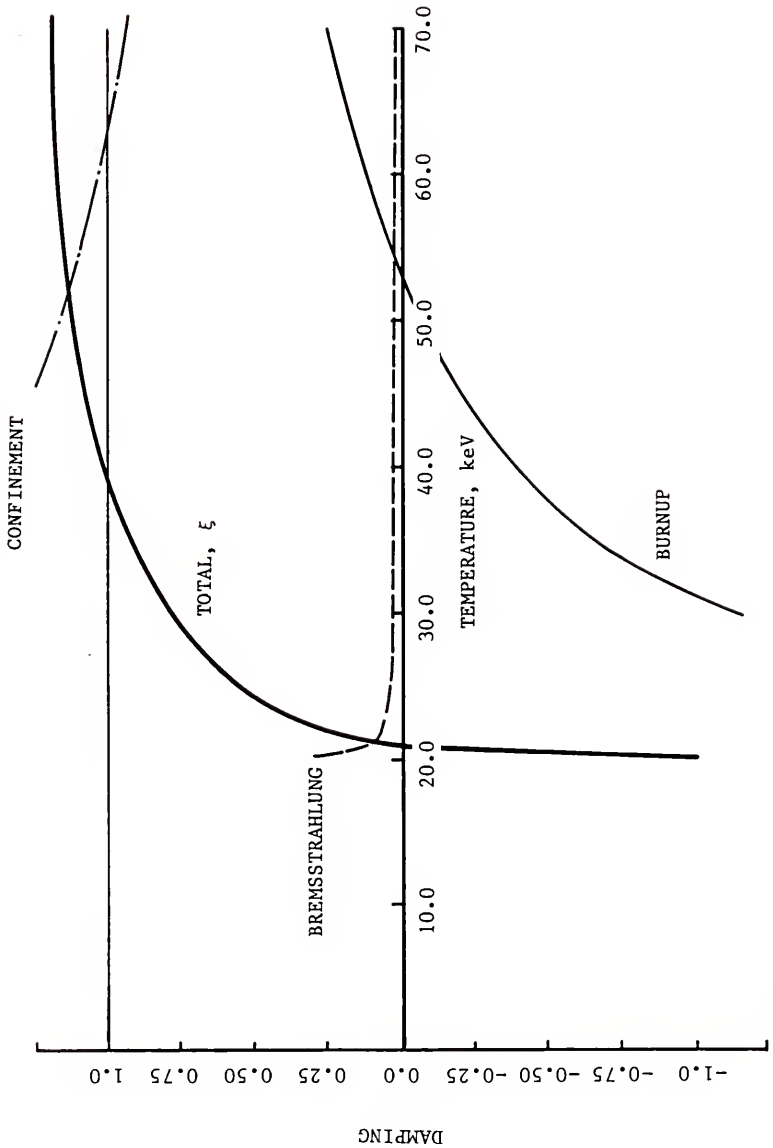

Figure 3-13. Change of scale for data of Figure 3-12. T_{s_o} = 75 keV, constant confinement.

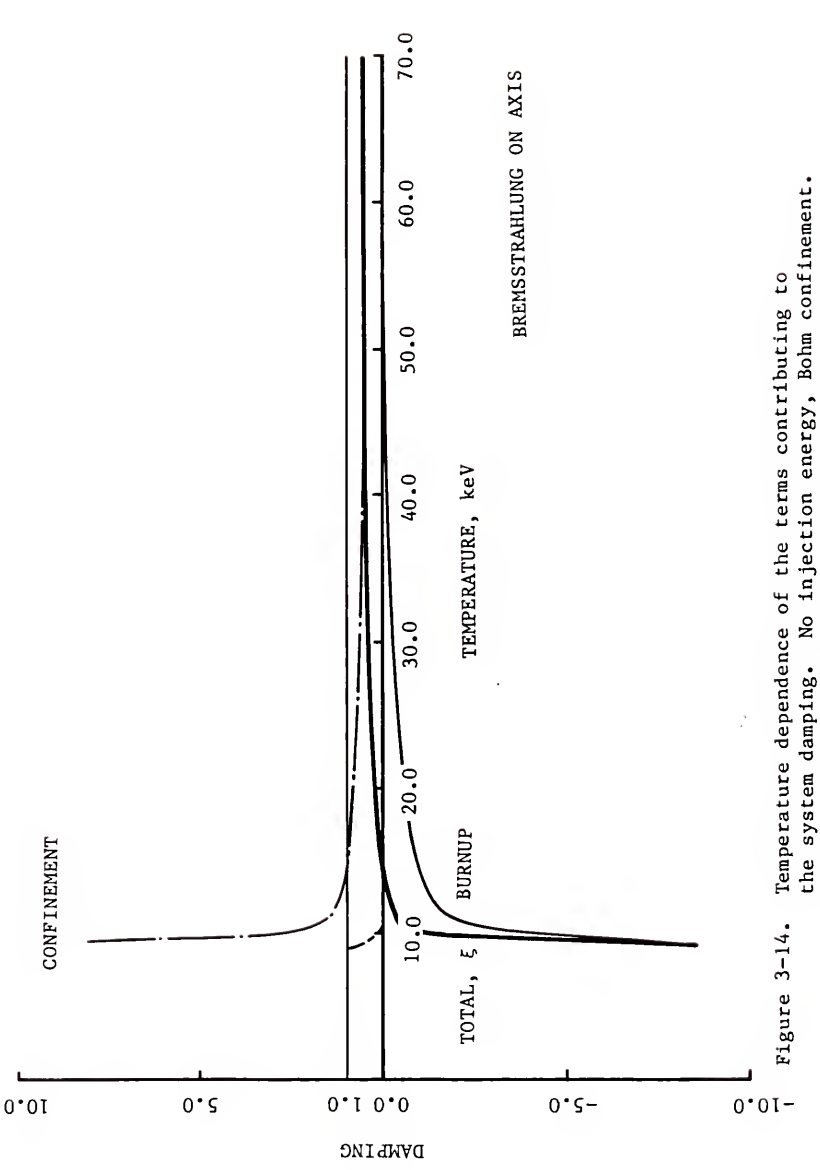

Figure 3-14. Temperature dependence of the terms contributing to the system damping. No injection energy, Bohm confinement.

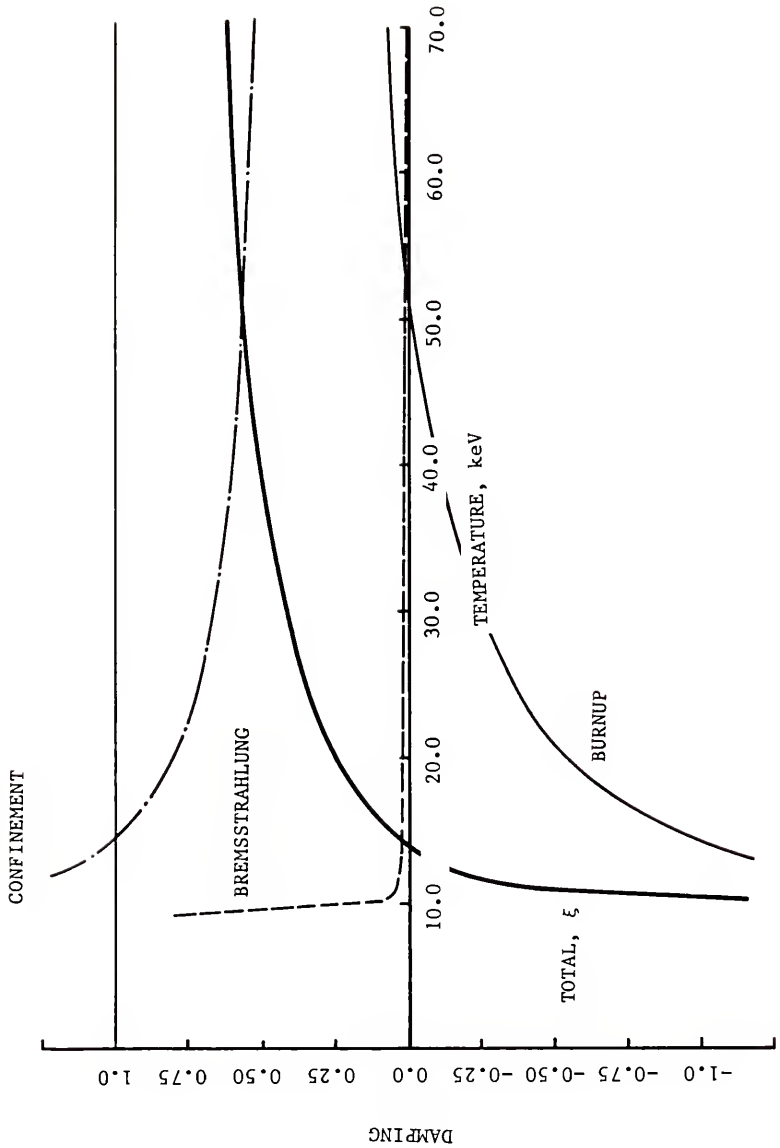

Figure 3-15. Change of scale for data of Figure 3-14. No injection energy, Bohm confinement.

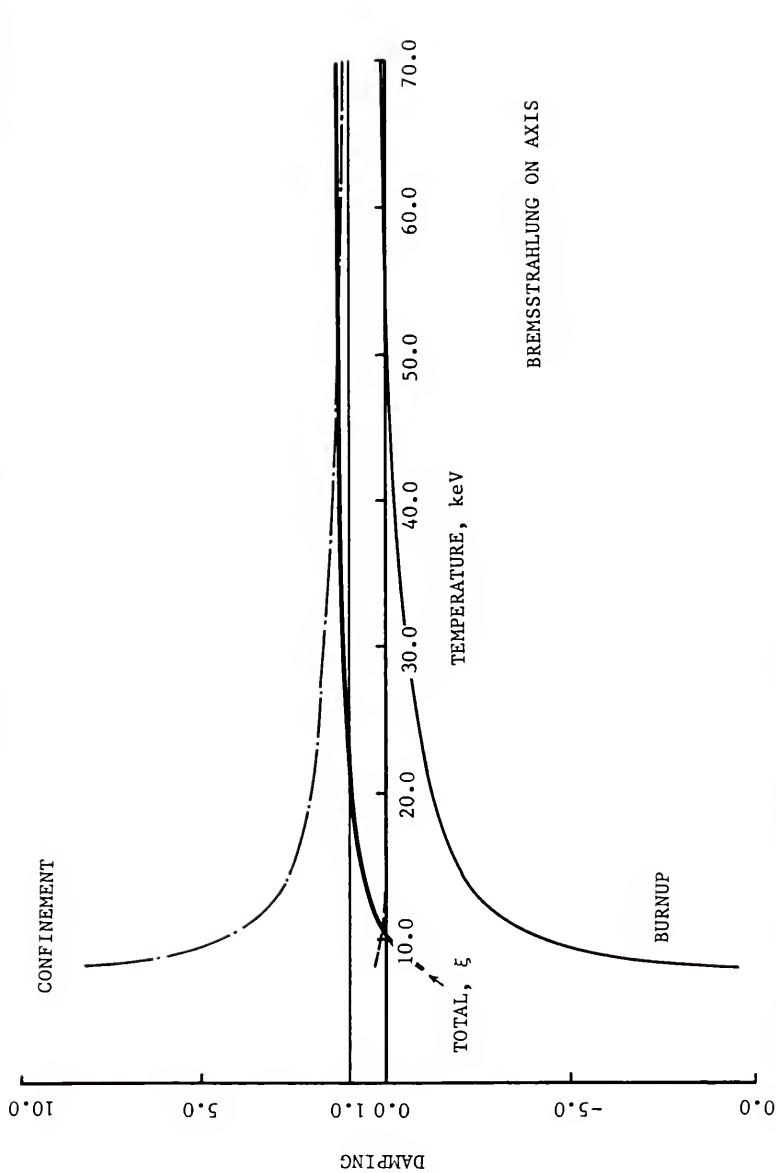

Figure 3-16. Temperature dependence of the terms contributing to the system damping. T_{s_o} = 75 keV, Bohm confinement.

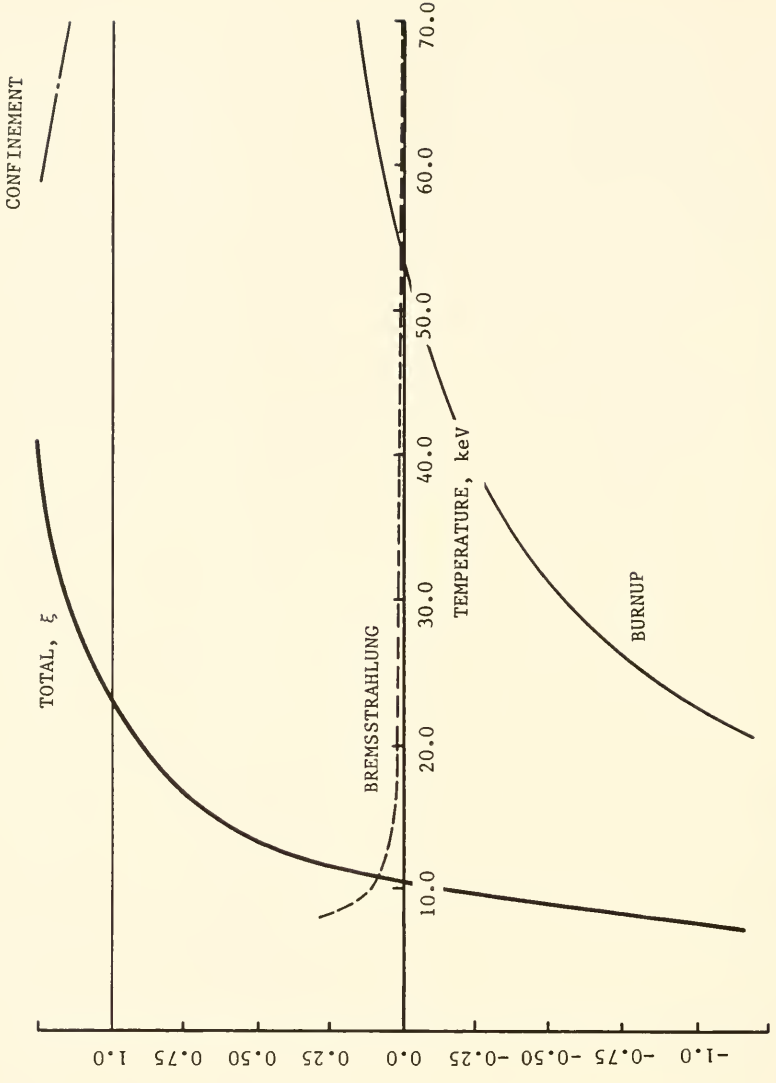

Figure 3-17. Change of scale for data of Figure 3-16. T_{s_o} = 75 keV, Bohm confinement.

overall damping of the system. For constant confinement and no energy injection, the system is overdamped except for a narrow band in the 50 to 60 keV range. The addition of injection energy energy lowers the critical temperature and the required $n\tau$ condition. This shifts the damping balance in favor of the fusion reactivity and the system is now underdamped from the critical temperature up to approximately 40 keV. For Bohm confinement, the situation is reversed. For zero injection, Bohm diffusion is not as strongly damping as constant diffusion, and the system is underdamped throughout the temperature range. With 75 keV injection, diffusion damping increases and the system becomes overdamped above 20 keV.

Figures 3-18 and 3-19 show the undamped and damped natural frequencies for 0 and 75 keV injection and constant and Bohm confinement. For temperatures approximately 5 keV higher than the critical temperature, the undamped natural frequency is found to be 0.1 to 0.2 sec^{-1} for constant confinement and 0.2 to 0.3 sec^{-1} for Bohm confinement. The damped natural frequency is found in the underdamped temperature bands previously identified and is, of course, always smaller than the undamped frequency. These figures summarize the discussion in the preceding paragraphs and serve as stepping stones to the presentation of the system poles.

The poles of the open loop transfer function are shown in root contour form in Figures 3-20 and 3-21 with temperature as the varying parameter along the curves. Both figures have the same scale and range. The real part of the poles is plotted as a function of temperature in Figures 3-22 and 3-23. Complex poles are found for the temperature ranges corresponding to the presence of the damped natural

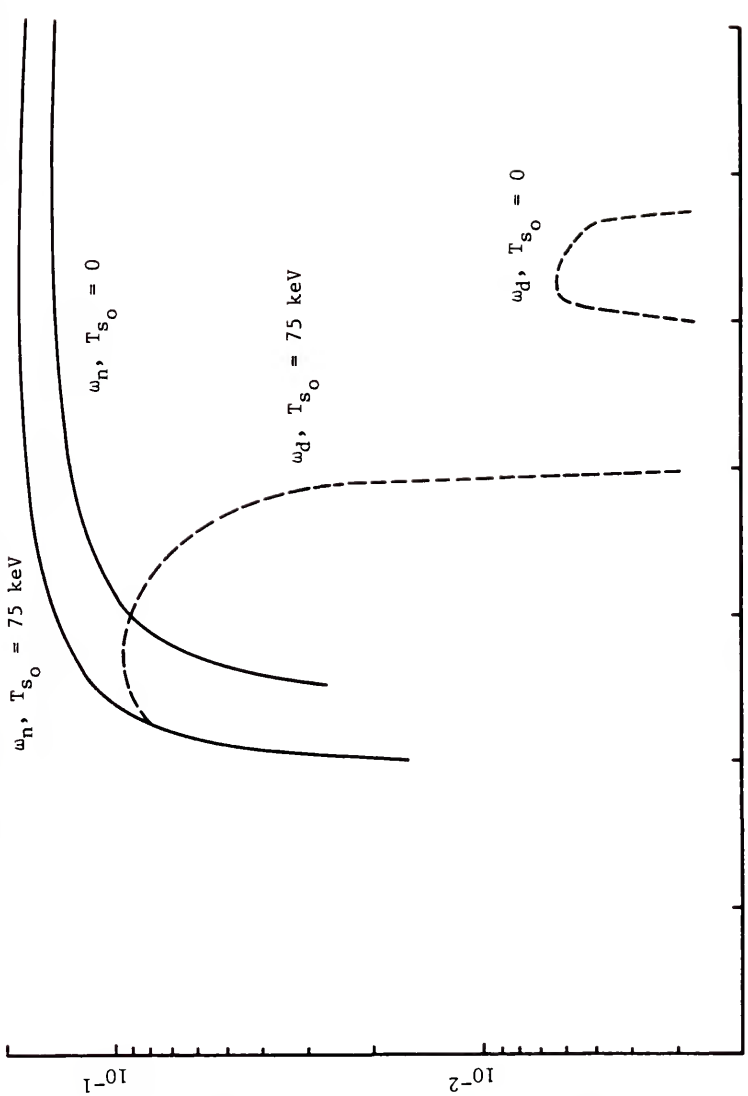

Figure 3-18. Temperature dependence of the undamped and damped natural frequencies. T_{s_o} = 0 and 75 keV, constant confinement.

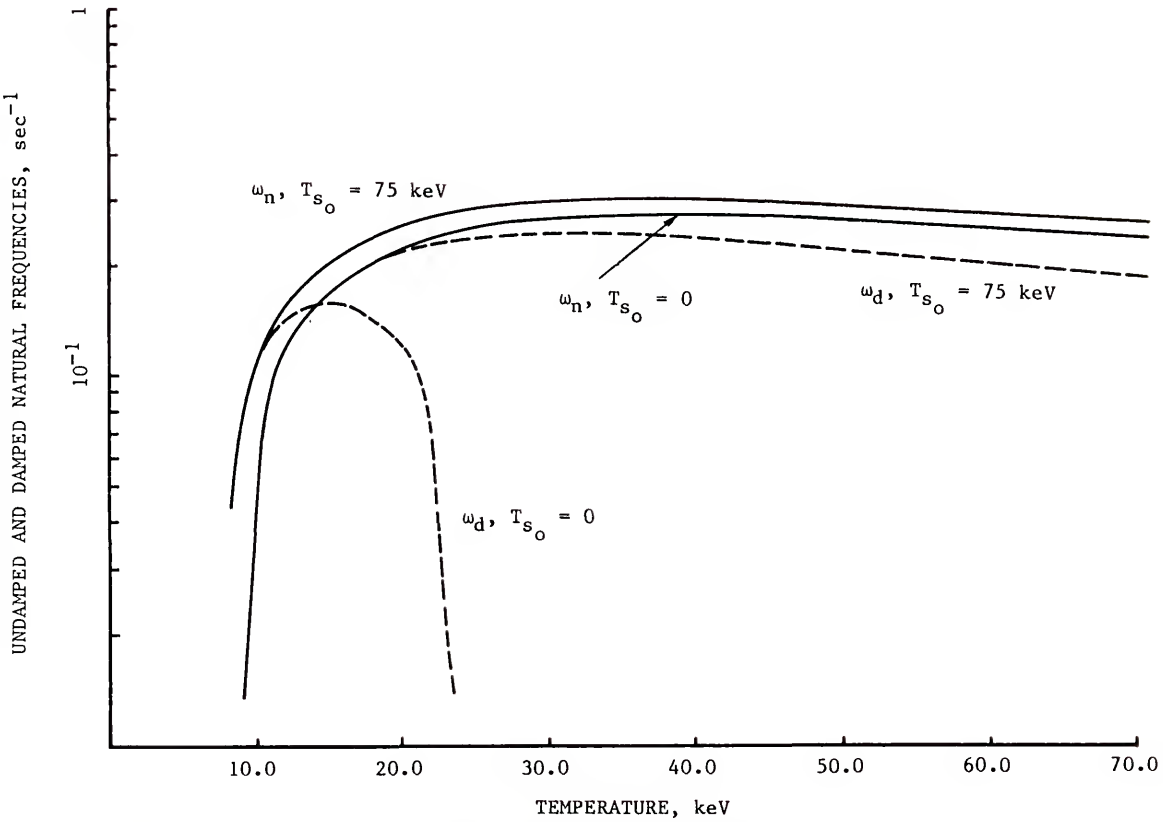

Figure 3-19. Temperature dependence of the undamped and damped natural frequencies. T_{s_o} = 0 and 75 keV, Bohm confinement.

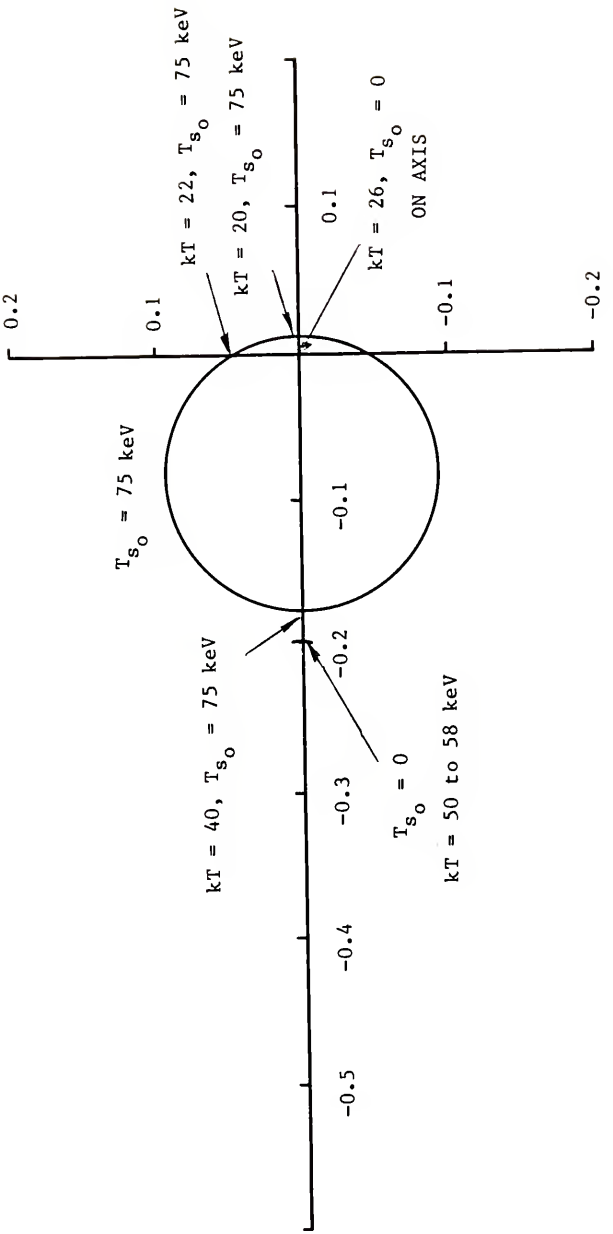

Figure 3-20. Root contour of the open-loop poles with the plasma temperature as the parameter of variation. T_{s_o} = 0 and 75 keV, constant confinement.

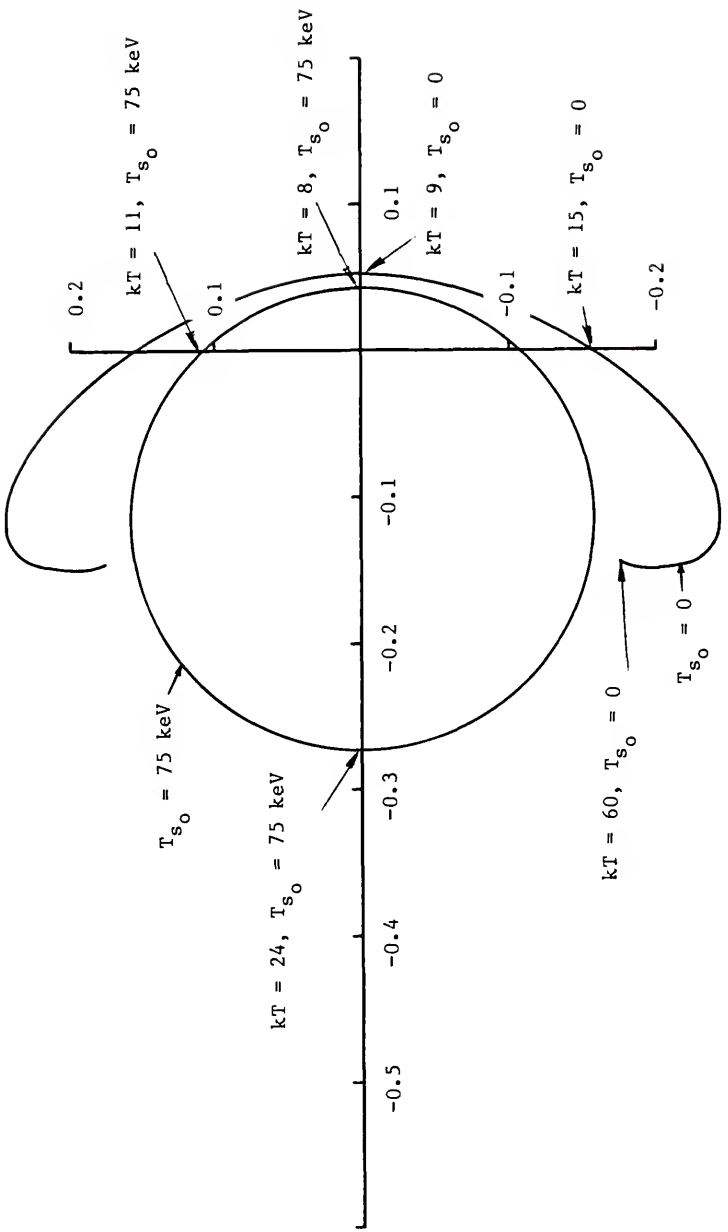

Figure 3-21. Root contour of the open-loop poles with the plasma temperature as the parameter of variation. T_{s_o} = 0 and 75 keV, Bohm confinement.

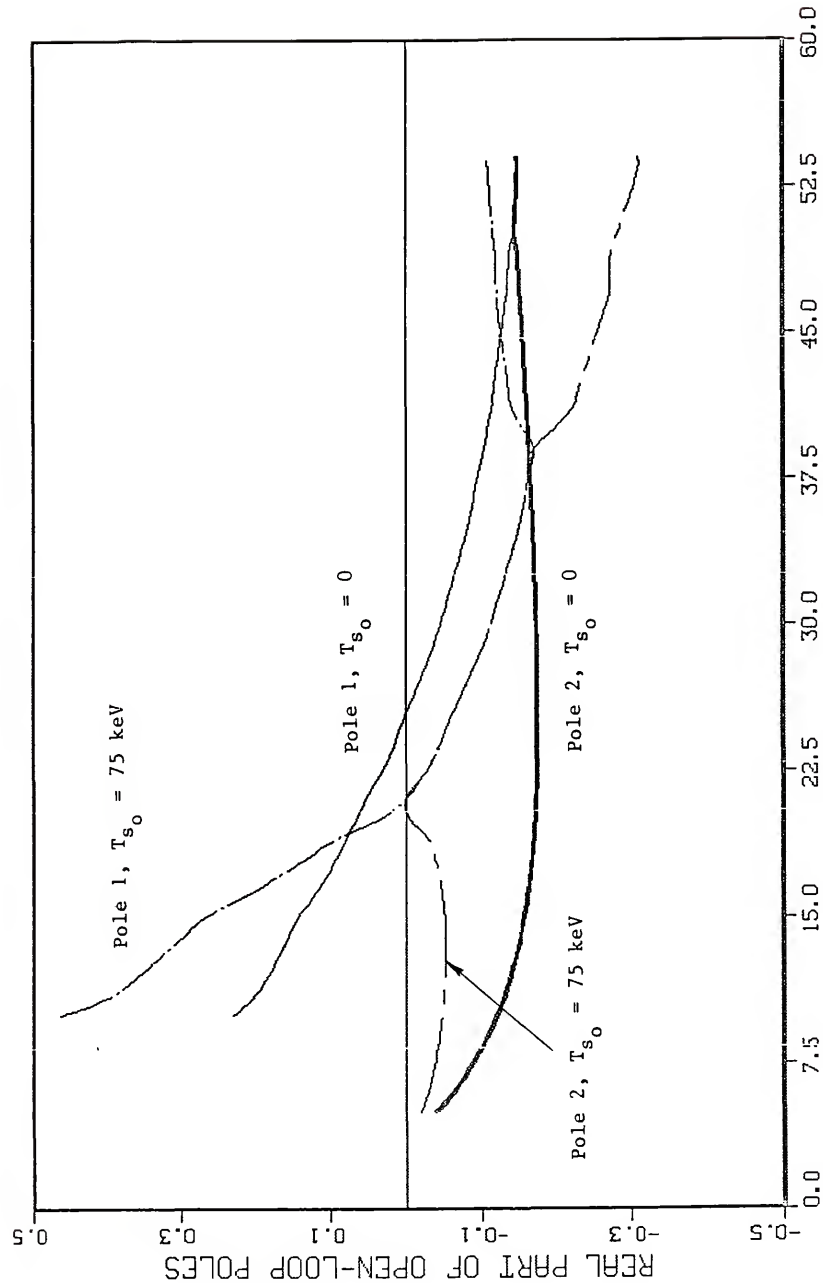

Figure 3-22. Temperature dependence of the real parts of the open-loop system poles. T_{s_o} = 0 and 75 keV, constant confinement.

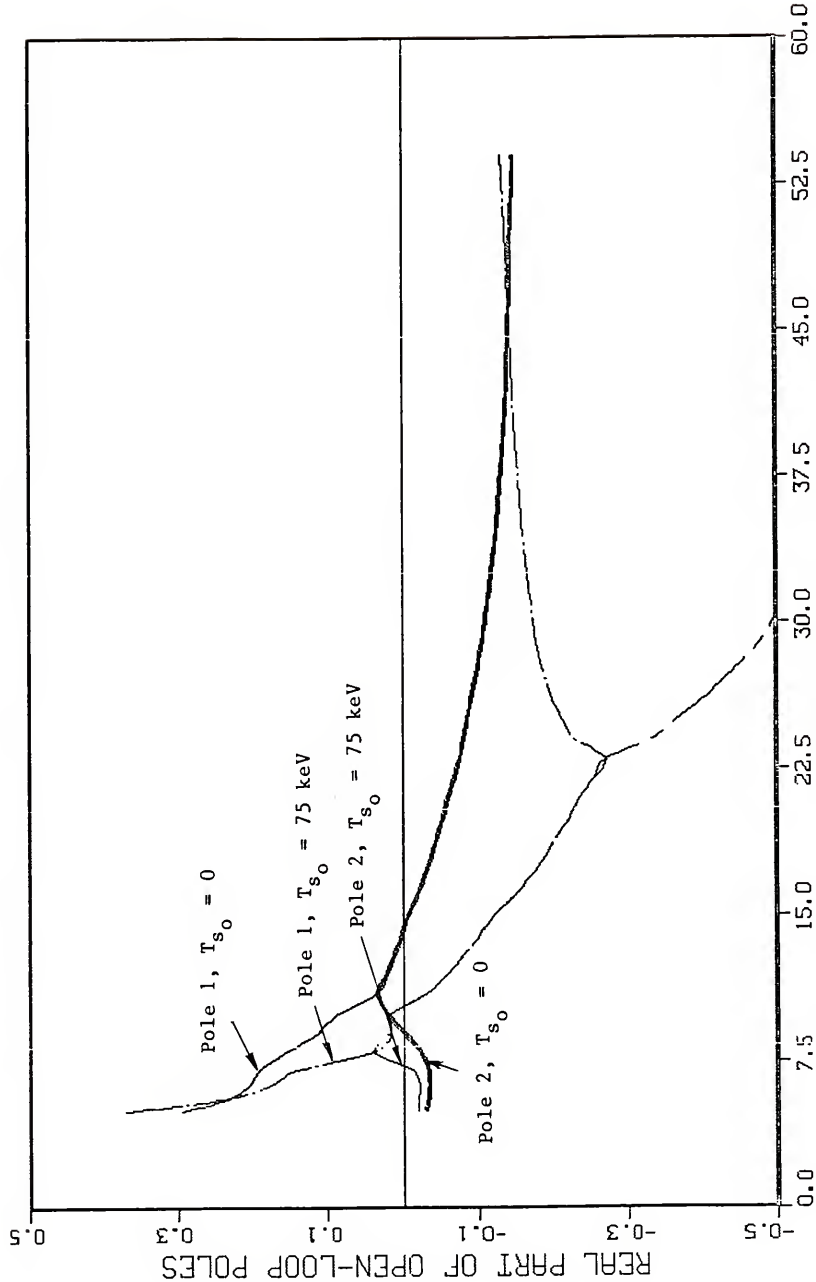

Figure 3-23. Temperature dependence of the real parts of the open-loop system poles. T_{s_o} = 0 and 75 keV, Bohm confinement.

frequencies of Figures 3-18 and 3-19. These in turn correspond to the damping ratio being in the range of 0 to 1. With the exception of the zero injection energy, constant confinement case, the system poles are complex in the vicinity of the critical temperature. The complex part of the pole is given by the damped natural frequency. The real part of the pole, that portion which governs the stability of the system, is given by the damping factor, $\sigma = \xi\omega_n$, which in terms of system parameters, can be expressed as

$$\sigma = \frac{1}{2}\left[n_o\langle DT\rangle_o - \left(\frac{Q_\alpha + 6kT_o}{12}\right)n_o\langle DT\rangle_\partial + \frac{b_B n_o}{6(kT_o)^{1/2}} + \frac{1 - \ell + m + R - mR}{R\tau_{E_o}}\right] \qquad 3.17$$

This factor must be positive, i.e., the real part of the poles must be in the left-hand s-plane, for the system to be stable.

Equation 3.17 is equation 3.9 multiplied by ω_n. Therefore the relative magnitudes of the terms in equation 3.17 can be extracted from Figures 3-10 through 3-17. By inspecting the figures, it can be seen that the culprit in causing the thermal instability at low temperatures is the magnitude of the slope of the fusion reactivity in this temperature region. Stability is achieved by the natural increase in magnitude of the reactivity and the decrease in magnitude of its slope with increasing temperature. Bremsstrahlung and diffusion losses contribute to the stability of the system throughout the temperature range. The contribution of diffusion to stability diminishes with increasing temperature as a result of the longer confinement times

required for equilibrium.

The parameters of this section completely define the characteristics of the open-loop plasma behavior. The resulting system response is presented in the next section.

3.2. Open-Loop System Performance

The design of a closed-loop control system begins with a given set of performance specifications in the time and/or frequency domain. This demands that these specifications be compatible and realistic. In order to obtain a "ball park" feel for what the system response should be for a fusioning plasma operating in a closed-loop, feedback-stabilized thermal equilibrium, the open-loop system specifications are presented in this section and examined in light of the parameters discussed in the previous section.

The time domain specifications for the plasma thermal balance are presented in Figures 3-24 through 3-27. These figures show relative temperature change, peak overshoot, M_p, time-to-peak, t_p, and settling time, t_s. Results are presented for 0 and 75 keV, with constant and Bohm confinement, for step inputs in feedrate and injection energy. The frequency domain specifications of bandwidth, resonance peak and resonance frequency are presented in Figures 3-28 through 3-30.

The transfer functions of the plasma thermal balance involve input functions that may differ by many orders of magnitude over a broad range of equilibrium conditions. To provide a normalized basis for

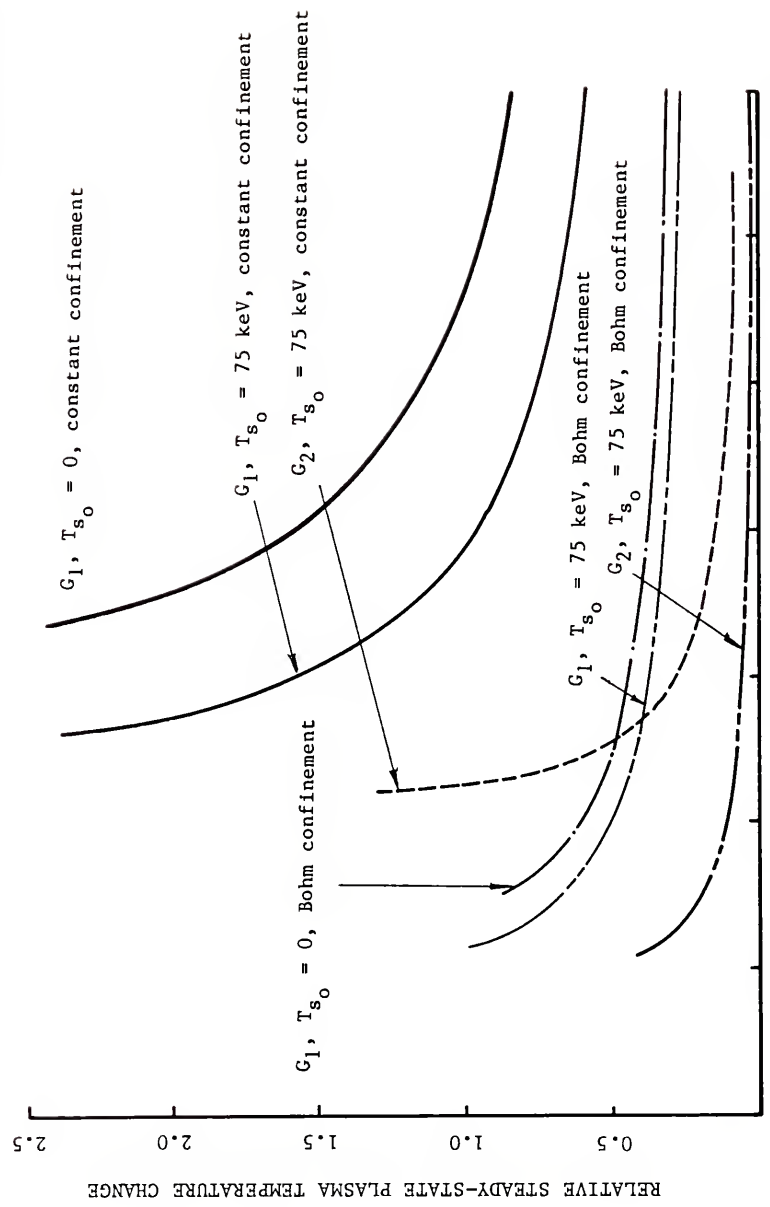

Figure 3-24. Relative temperature change of the open-loop system transfer functions, following a step input. T_{s_o} = 0 and 75 keV, constant and Bohm confinement.

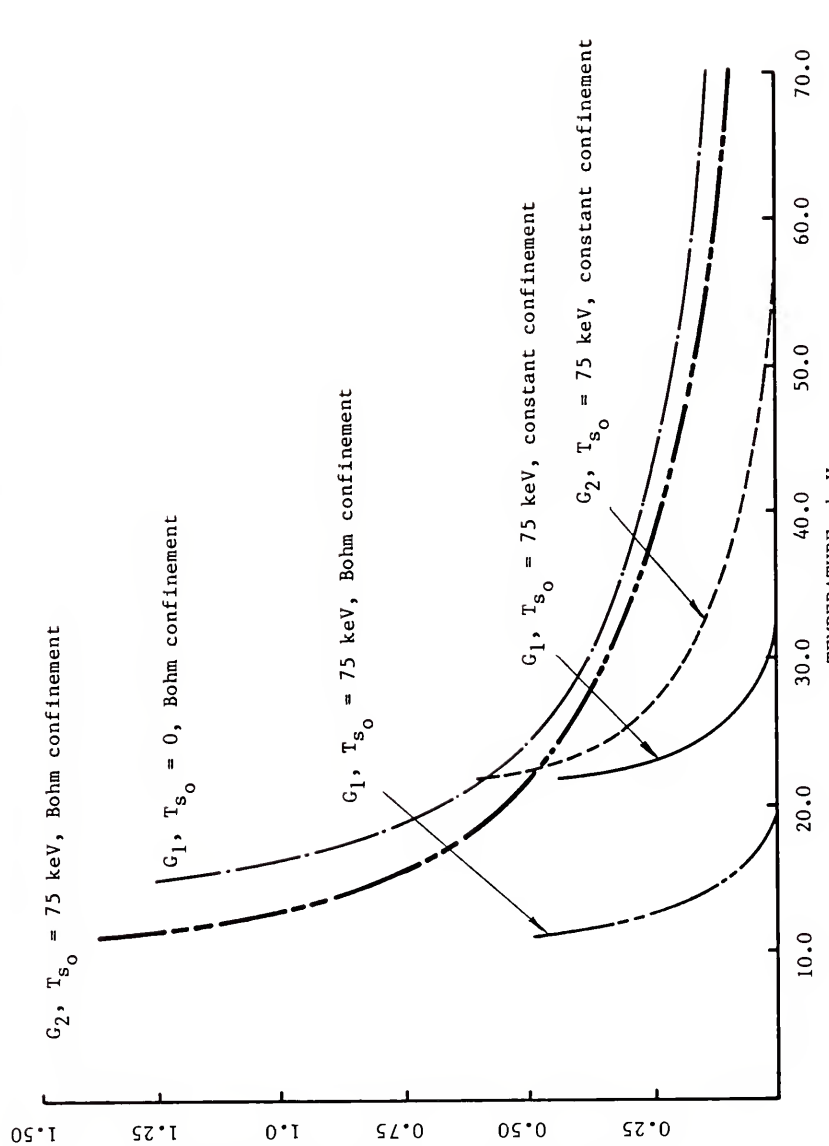

Figure 3-25. Peak overshoot of the open-loop system transfer functions, following a step input. T_{s_o} = 0 and 75 keV, constant and Bohm confinement.

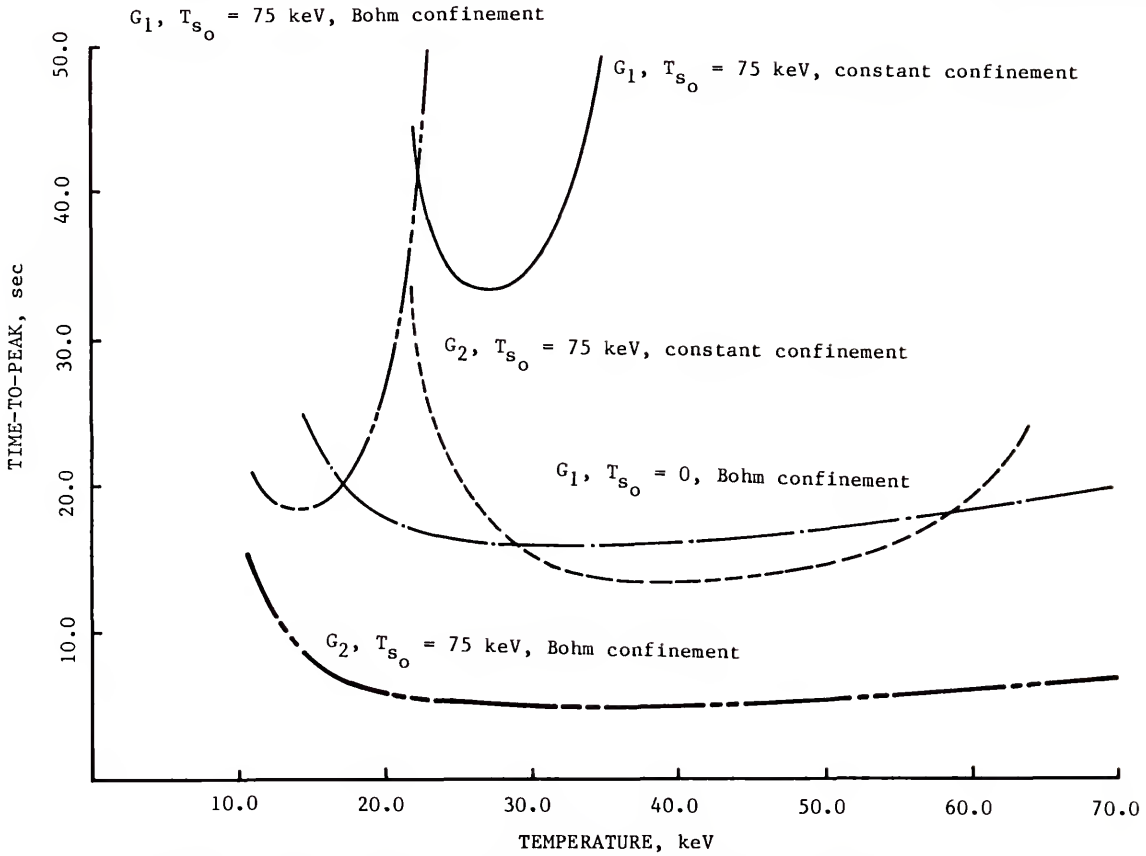

Figure 3-26. Time-to-peak of the open-loop system transfer functions, following a step input. T_{s_o} = 0 and 75 keV, constant and Bohm confinement.

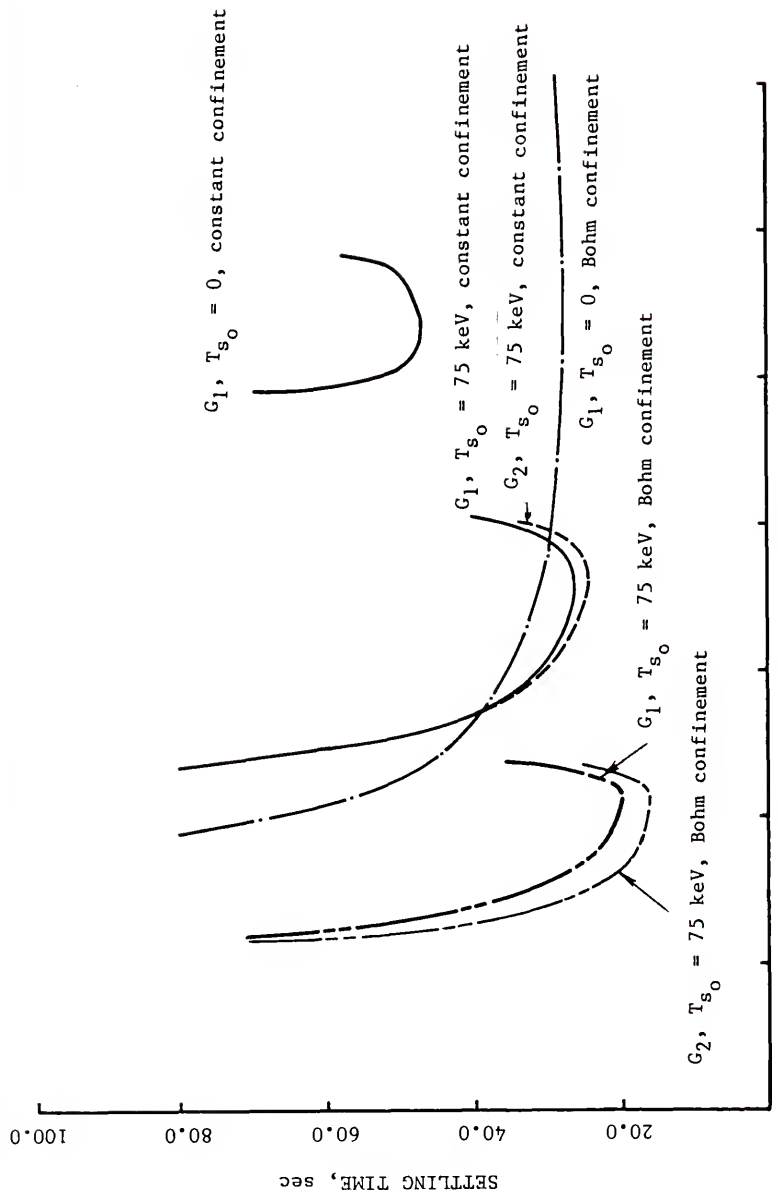

Figure 3-27. Settling time of the open-loop system transfer functions, following a step input. T_{s_o} = 0 and 75 keV, constant and Bohm confinement.

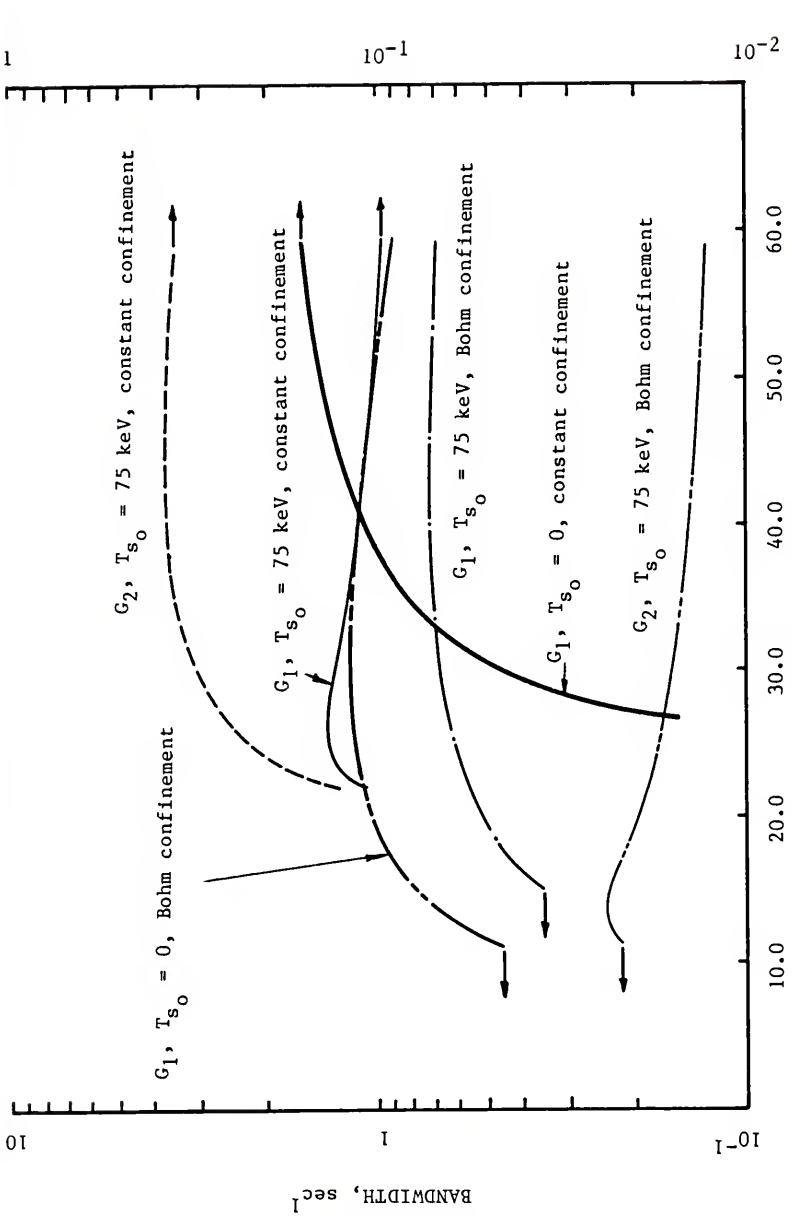

Figure 3-28. Bandwidth of the open-loop system transfer functions, following a step input. T_{s_o} = 0 and 75 keV, constant and Bohm confinement.

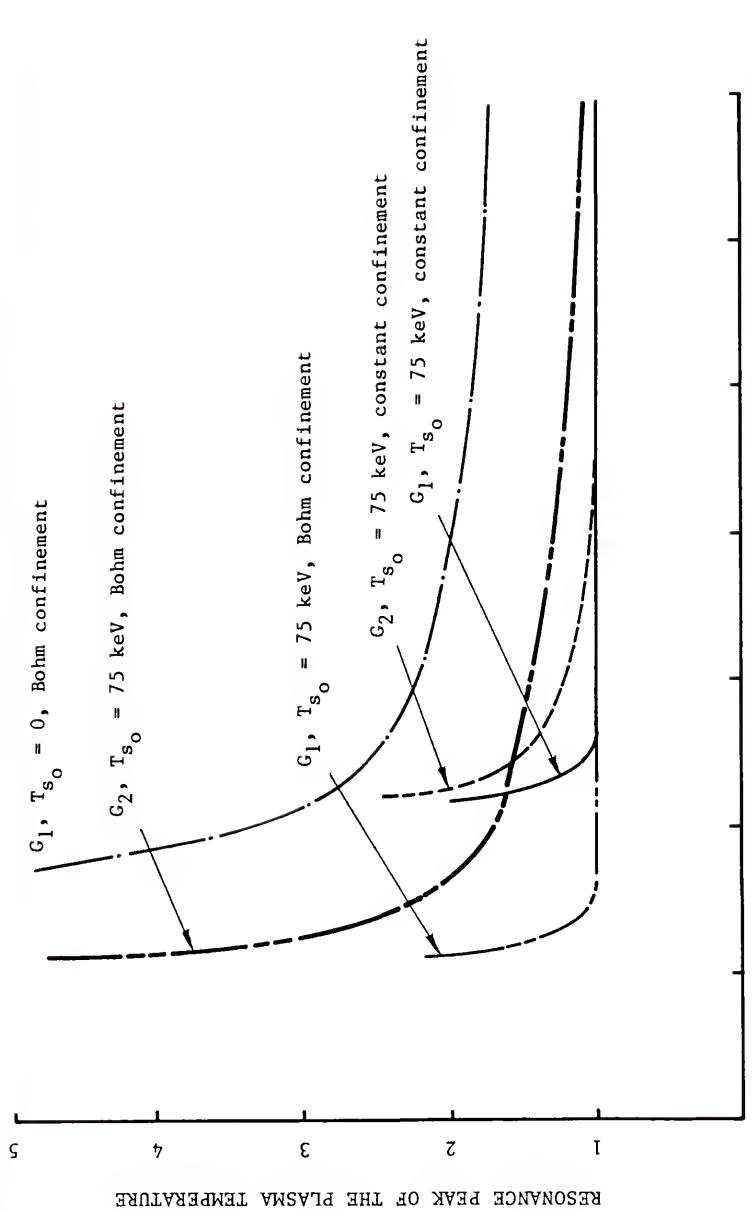

Figure 3-29. Resonance peak of the open-loop system transfer functions, following a step input. T_{s_o} = 0 and 75 keV, constant and Bohm confinement.

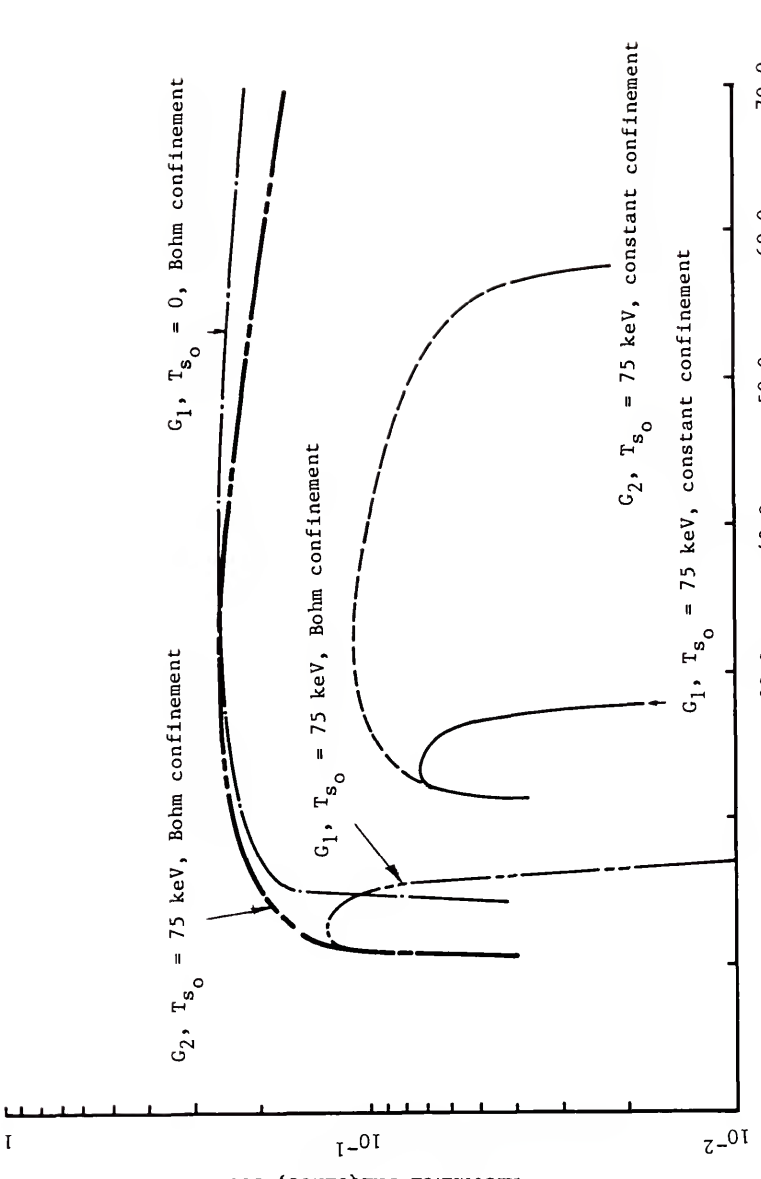

Figure 3-30. Resonance frequency of the open-loop system transfer functions, following a step input. T_{s_o} = 0 and 75 keV, constant and Bohm confinement

comparing the system responses from such diverse conditions, the Final Value Theorem was used to provide weighting factors. The weighting factors were obtained from the final value of the transfer functions assuming step inputs of a magnitude equal to the steady state value of the input functions. The resultant weighting factors, shown in Figure 3-24, can then be used in conjuction with the specifications of Figures 3-25 through 3-30, which are presented for unit step inputs, in relative comparisons of system performance.

In general, Figure 3-24 indicates that the transfer function with respect to feedrate responds to a step input with changes in steady state temperature that are 3 and 8 times larger than those of the transfer function with respect to injection energy for constant and Bohm confinement, respectively. This implies that the magnitude of the plasma response is more sensitive to changes in feedrate. Physically, this can be explained as follows. An increase in S results in an increase in n, which in turn increases kT by the square of the increase in n due to the enhanced reaction rate. An increase in T_s, however, produces only a proportional increase in kT. This behavior will be more fully exploited in Chapter 4.

In addition to the permanent temperature change caused by a step change in the input, the plasma temperature will experience an initial transient component. The magnitude of this initial transient is characterized by its peak overshoot (M_p). The time behavior of this component is described by the time required to reach its peak (t_p), and the time required for its magnitude to settle to 5% of its final value (t_s). These three specifications are shown in Figures 3-25 through 3-27.

Peak overshoot values above 25 to 30 per cent are seldom allowable in control engineering applications. Inspection of Figure 3-25 quickly shows that in most cases, plasma behavior is unacceptable below the temperature range of 20 to 30 keV. The large overshoots were to be expected, as peak overshoot is strongly dependent on the system damping, and as presented earlier, damping is very low below this temperature range. An interesting point to note is the presence of overshoot in overdamped regions of Figure 3-25. In a simple classical second order system, overshoot does not occur for overdamped conditions. However, due to the presence of a finite zero in the plasma transfer functions, overshoot can occur in an overdamped case if the condition is met that the zero not be located between the poles, as derived in Appendix C. This is not a sufficient condition, only a necessary one. This condition is satisfied for the 75 keV injection cases for both constant and Bohm confinement.

The overshoot problem in both the underdamped and overdamped cases is less severe for constant confinement than for Bohm confinement due to the smaller pole-zero separation in the former case. This can be seen with the aid of equations C.11 and C.12 and Figures 3-5, 3-22, and 3-23. As with the final steady-state temperature changes (Figure 3-24), the maximum overshoot is also more sensitive to changes in feedrate than in injection energy.

Along with the overshoot problem, Figures 3-26 and 3-27 show the plasma to have very poor speed of response. In the vicinity of the critical temperature (when the damping is generally small), and at other temperatures where the damping is high, settling times can rapidly become greater than 100 seconds. Present conceptual

designs[17] project pseudo-steady-state burn times on the order of 500 seconds for Tokamak reactors. If this were indeed the case, approximately one-fifth of the power production phase of operation would be required to arrive at the desired steady-state operating conditions. Control is clearly suggested.

In the frequency domain, bandwidth, resonance peak and resonance frequency are shown in Figures 3-28 through 3-30. The system bandwidth and resonance frequency are seen to increase very rapidly in the vicinity of the critical temperature. Somewhat above the critical temperature, the bandwidth remains essentially constant with temperature. The resonance frequency bears a functional relationship to the damping ratio and decreases as the system becomes overdamped. Thus, no resonance frequency is found for G_1 with $T_{S_o} = 0$ and constant confinement. Damping in this case is greater than or nearly equal to 1 at all temperatures. The variation of the resonance frequency of the transfer functions for the other cases can similarly be related to the variation in the damping ratio. Lastly, the resonance peak is seen to be unacceptable in most temperature regions of interest, exceeding the 1.1 to 1.5 design range of practical control systems. These characteristics correlate very well with the speed of response noted above from time domain considerations.

This section has presented the classical specifications for the open-loop plasma system. In most cases, these have been shown to be unacceptable. This can be attributed to the extreme sensitivity of the plasma in the vicinity of the critical temperature resulting from the rapid change of plasma parameters in this temperature region. In the next chapter, the system is closed using proportional feedback and the

effect on the system characteristics and specifications is noted. Derivative and integral feedback considerations are presented in Chapter 5.

3.3. Summary

In this section the selected plasma model was cast in the form of a classical second order system with a finite zero, and analytical expressions for the system characteristics and specifications were derived in terms of the plasma conditions. Expressions were derived for the system characteristics of gain, the finite zero, the damped and undamped natural frequencies, the damping ratio, and the damping factor. Expressions were derived for the impulse and step response, as well as the system specifications of time-to-peak, peak overshoot, settling time, bandwidth, resonance frequency, resonance peak, and phase margin. These were evaluated for the cases of zero and 75 keV injection energy, assuming both constant and Bohm confinement laws. The injection energy case was examined because this is the currently preferred form of plasma heating. Bohm confinement was evaluated because the transport expected in the reactor regime is expected to exhibit a Bohm-type of dependence.

Physical associations were drawn between the processes present in a fusioning plasma and the system characteristics and transfer function coefficients. The gain of the plasma system with respect to the fuel injection rate was found to be proportional to the difference between the beam energy and the temperature of the background plasma. With

respect to the injection energy input, the gain of the plasma system was determined to be proportional to the ratio of the fuel ion density in the beam to the fuel ion density on the background plasma.

The dominant processes influencing the natural frequency of the plasma where found to be the functional dependence of the confinement scheme, and the magnitude of the reactivity function and its derivative. At low temperatures such as between the ignition and critical temperatures, a perturbation which induces a change in the energy balance perpetuates itself in the original direction and induces unstable behavior. Above the critical temperature, the change in the fusion energy production rate caused by a perturbation is accompanied by an opposing change in the diffusion rate. These opposing effects result in the natural frequency of oscillation of the plasma.

The actual frequency of oscillation depends on the presence of damping modes in the energy balance. Throughout the range of temperatures and conditions studied, diffusion exerts a strong damping influence on the thermal balance. The fusion reactivity on the other hand has a strong disruptive effect on the thermal balance, up to high temperatures in the range of 50 to 60 keV. In this temperature range, the slope of the reactivity function begins to decrease in magnitude, ultimately reversing in sign. Above the temperature at which it reverses in sign, the reactivity also adds to the system damping.

An additional zero in a second order system generally decreases the time to peak and increases the overshoot. The zero in the present transfer function arises from the need for two independent differential equations to aptly describe the plasma thermal balance. The location of the zero is determined from the relative magnitudes of terms

associated with the rates of energy production from fusion and energy loss via diffusion. The contribution of bremsstrahlung radiation emission to the location of the transfer function zero and the other system characteristics of natural frequency, damping ratio, and the damping factor was determined to be minor. For the specific case of complex poles, the damping factor, i.e., the real part of the poles, is the product of the damping ratio and the natural frequency, and the above discussion of these system characteristics applies. When both of these are greater than zero, the system is stable.

The present analysis provided an assessment of the relative magnitude of the contributions of each of the processes present in the plasma to the overall thermal response. The open-loop system analysis provided an initial evaluation of the system characteristics and specifications. Thus, the natural frequency of the thermal balance was determined to be in the range of 0.05 to 0.3 sec^{-1} for temperatures greater than a few keV above the critical temperature. This corresponds to a time scale for the thermal response on the order of 3 to 20 seconds. This time scale verifies the assumption made in Chapter 2 of the exclusion from the analysis model of effects which occur on more rapid time scales, such as the slowing down of alpha particles and beam-injected fuel ions.

The damping ratio of the open-loop thermal balance was found to be highly sensitive to the plasma parameters. For the case of no injection energy and a constant confinement law, the damping ratio is much greater than 1 in the vicinity of the critical temperature, decreasing to approximately 1 at the higher temperatures. With no injection energy and the Bohm confinement law, the system is

underdamped in the vicinity of the critical temperature, increases with increasing temperature, and levels off at ~ 0.5 to 0.6. With injection energy and either constant or Bohm confinement, the system is underdamped in the vicinity of the critical temperature, increases with temperature, and then levels off in the overdamped range of 1.0 to 1.25. These considerations play an important role in the selection of the plasma and reactor operating conditions and the design of the control system.

The manifestation of the system characteristics on the performance of the open-loop thermal balance was evaluated via the system specifications of peak overshoot, time-to-peak, settling time(5%), bandwidth, resonance peak, and resonance frequency. This work is the first evaluation of the response characteristics of the plasma thermal balance. Such an evaluation is a required first step in determining the type of control best suited for this application. The results of this phase of this study are summarized in Table 3-1 and described below.

- Zero injection energy, constant confinement. This system is overdamped in the entire temperature range of applicability of the model. It therefore does not exhibit overshoot. This condition is accompanied by very poor speed of response, with settling times greater than 100 seconds at temperatures below 30 keV. In agreement with the time domain specifications, the system bandwidth is 0.01 sec^{-1} slightly above the critical temperature and remains very low, less than 0.2 sec^{-1} at temperatures above 30 keV, with no resonance peak.

TABLE 3-1
SUMMARY OF OPEN-LOOP SYSTEM RESPONSE

	M_p	t_p	t_s	ω_B	M_m	ω_m
Zero injection energy, constant confinement kT_c = 25 keV	No overshoot, 25 to 50 keV	∞, 25 to 50 keV	>100 sec, 25 to 30 keV; 100 to 30, 30 to 40 keV; 30 to 20, 40 to 50 keV	<0.1 sec^{-1}, 25 to 35 keV; 0.1 to 0.2 sec 35 to 50 keV	No resonance peak, 25 to 50 keV	No resonance frequency, 25 to 50 keV
Zero injection energy, Bohm confinement kT_c = 14 keV	>0.25, 15 to 50 keV	15 to 25 sec, 15 to 50 keV	>40 sec, 15 to 25 keV; 40 to 30 sec, 25 to 30 keV; 30 to 20 sec, 30 to 50 keV	<0.5 sec^{-1}, 15 to 20 keV; 0.5 to 0.7 sec^{-1}, 20 to 50 keV	>2, 15 to 40 keV; 2 to 1.8, 40 to 50 keV	<0.2 sec^{-1}, 15 to 20 keV; 0.2 to 0.3 sec^{-1}, 20 to 50 keV
75 keV injection energy, constant confinement kT_c = 21 keV	>0.25, 20 to 25 keV; 0.25 to 0, 25 to 35 keV; No overshoot, 35 to 50 keV	>50 sec, 20 to 25 keV; 30 to 50 sec, 25 to 35 keV; ∞, 35 to 50 keV	>50 sec, 20 to 25 keV; 50 to 30 sec, 25 to 30 keV; 30 to 20 sec, 30 to 50 keV	<0.1 sec^{-1}, 20 to 25 keV; 0.1 to 0.3 sec^{-1} 25 to 50 keV	>2, 20 to 25 keV; 2 to 1, 25 to 35 keV; 1, 35 to 50 keV	<0.08 sec^{-1}, 20 to 25 keV; 0.08 to 0.1 sec^{-1}, 25 to 50 keV
75 keV injection energy, Bohm confinement kT_c = 10 keV	>0.25, 10 to 15 keV; 5 .25 to 0, 15 to 20 keV; No overshoot, 20 to 50 keV	20 sec, 10 to 15 keV; 20 to 50 sec, 15 to 20 keV; ∞, 20 to 50 keV	>30 sec, 10 to 15 keV; 30 to 15 sec, 15 to 20 keV; 20 to 10 sec, 20 to 50 keV	<0.9 sec^{-1}, 10 to 15 keV; 0.9 to 1.5 sec^{-1}, 15 to 50 keV	>2, 10 to 15 keV; 2 to 1, 15 to 50 keV	<0.2 sec^{-1} 10 to 15 keV; 0.2 to 0.3 sec^{-1}, 15 to 50 keV

kT_c = critical temperature

• Zero injection energy, Bohm confinement. The strong effect of the confinement law on the sytem response is evident from a comparison of the specifications of this case with those of the constant confinement case. With Bohm confinement, the system exhibits unacceptably high overshoot, greater than 25% below 40 keV, and a resonance peak greater than 2 throughout the applicable temperature range. Its speed of response is improved over the constant confinement case in that the time-to-peak is 15 to 25 seconds, and the settling time is on the order of 30 to 60 seconds above 25 keV. The bandwidth is also increased to $\sim 0.4 - 0.7$ sec^{-1} at temperatures above 15 keV. A resonance peak of magnitude greater than 2 is found in the 0.2 to 0.3 sec^{-1} frequency range below 30 keV.

• 75 keV injection energy, constant confinement. The introduction of injection energy into the plasma balance serves to initiate plasma oscillations below 35 keV. Peak overshoot is unacceptably high up to 25 - 30 kev, and decreases rapidly between 25 and 35 kev. There is no significant overshoot above 35 kev. In general, the speed of response is improved over the no injection case, though it is still not as good as with Bohm confinement and zero injection energy at temperatures below 25 keV. Time-to-peak and the settling time are both greater than 1 minute at temperatures below 20 - 25 keV, decreasing to 30 seconds at 30 keV. The bandwidth is not affected greatly by the 75 keV injection energy. Between 20 and 25 keV, a resonance peak of magnitude greater than 2 appears in the frequency range of 0.01 to 0.1 sec^{-1}.

• 75 keV injection energy, Bohm confinement. This combination of input and plasma parameters demonstrates the most favorable open-loop system response. Its stable operating temperature range is the widest,

starting as low as 10 keV. Acceptable overshoot is found starting at 15 keV. In addition, reasonable settling times of less than 30 seconds are also attained at temperatures greater than 15 keV, and the system bandwidth is in the 1 sec^{-1} range. The magnitude of the resonance peak is reduced significantly with 75 keV injection energy. The resonance frequency is in the range of 0.1 - 0.3 sec^{-1} above 10 keV.

This brief summary demonstrates the broad range of system response that results from open-loop operation. Though the system response is improved via the use of injection energy and as a result of the Bohm confinement law, the response can be further improved through the use of closed-loop feedback control.

CHAPTER 4
CLASSICAL CLOSED-LOOP ANALYSIS OF PLASMA MODEL

Analysis of the thermal balance in the previous chapter showed that open-loop operation of a fusioning plasma requires undesirably high temperatures for stability. It was also demonstrated that even at the elevated temperatures, the open-loop system possesses poor performance characteristics, including excessive overshoot and slow speed of response. The open-loop plasma system can be transformed into a closed-loop system through the addition of feedback, i.e., by modifying the input variables in accordance with the behavior of the system variables. The closed-loop plasma system may then be able to sustain stable performance at lower temperatures which would be open-loop unstable. The closed-loop system may also be able to improve the system response at temperatures which would be open-loop stable, but would possess poor response characteristics.

The effect of closing the loop on the stability and system response of the plasma thermal balance is presented in this chapter. In the first section, the loop is closed using proportional feedback. The closed-loop transfer functions are developed, and the system characteristics are derived and evaluated. The system performance is then presented and the improvements over open-loop operation are noted. The chapter concludes with a summary of the closed-loop results.

4.1. Closed-Loop Plasma Transfer Function Characteristics

The closed-loop transfer function equations are given by equations 2.13 and 2.14 with K_s and K_{T_s} not equal to zero. These are repeated below for convenience.

$$G_1(s) \equiv \frac{T(s)}{S(s)} = \frac{g_1(s - a + c/g_1)}{s^2 + (-a - d)s + (ad - cb)} \qquad 4.1$$

$$G_2(s) \equiv \frac{T(s)}{T_s(s)} = \frac{g_2(s - a)}{s^2 + (-a - d)s + (ad - cb)} \qquad 4.2$$

The supporting equations 2.12a-f remain as before.

$$a = \frac{\ell - 1}{\tau_{n_o}} - n_o\langle DT\rangle_o \qquad 4.2a$$

$$b = \frac{mn_o}{RkT_o\tau_{E_o}} - \frac{n_o^2}{2}\langle DT\rangle_\partial - K_s \qquad 4.2b$$

$$c = \left(\frac{Q_\alpha + 6kT_o}{6}\right)\langle DT\rangle_o - \frac{2}{3}b_B(kT_o)^{1/2} + (\ell - 1)\left(\frac{R - 1}{Rn_o\tau_{E_o}}\right)kT_o \qquad 4.2c$$

$$d = \left(\frac{Q_\alpha + 6kT_o}{12}\right)n_o\langle DT\rangle_\partial - \frac{b_B n_o}{6(kT_o)^{1/2}} + \frac{m(R - 1) - R}{R\tau_{E_o}} - g_1K_s - g_2K_{T_s} \qquad 4.2d$$

$$g_1 = \frac{T_{s_o} - 3kT_o}{3n_o} \qquad 4.2e$$

$$g_2 = \frac{S_o}{3n_o} \qquad 4.2f$$

Starting with the above equations, expressions for the system characteristics can be derived for the closed-loop transfer function in the same manner as previously used for the open-loop case. After some manipulation, the expressions are given by

$$g_1 = \frac{T_{s_o}/3 - kT_o}{n_o} \qquad 4.3$$

$$g_2 = \frac{S_o}{3n_o} \qquad 4.4$$

$$z_1 = -a + c/g_1 = \frac{(Q_\alpha + 2T_{s_o})}{2(T_{s_o} - 3kT_o)} n_o \langle DT \rangle_o - \frac{2b_B n_o (kT_o)^{1/2}}{T_{s_o} - 3kT_o}$$

$$- \frac{(\ell - 1)(T_{s_o} - 3RkT_o)}{R\tau_E (T_{s_o} - 3kT_o)} \qquad 4.5$$

$$z_2 = -a = n_o \langle DT \rangle_o - \frac{\ell - 1}{R\tau_{E_o}} \qquad 4.6$$

$$\omega_n^2 = \omega_{n_{\text{open loop}}}^2 + \Big[\Big(\frac{Q_\alpha + 2T_{s_o}}{6} \langle DT \rangle_o$$

$$- \frac{2}{3} b_B (kT_o)^{1/2} + \frac{(\ell - 1)(3RkT_o - T_{s_o})}{3Rn_o \tau_{E_o}} \Big] K_s$$

$$+ \Big[\frac{S_o \langle DT \rangle_o}{3} - \frac{S_o(\ell - 1)}{3n_o \tau_{n_o}} \Big] K_{T_s} \qquad 4.7$$

$$\xi = \xi_{\text{open loop}} + \frac{g_1}{2\omega_n} K_s + \frac{g_2}{2\omega_n} K_{T_s} \qquad 4.8$$

Comparing the closed-loop equations 4.3 through 4.8 with the open-loop equations 3.4 through 3.9, it can be seen that only the natural frequency and damping ratio, and therefore the poles of the system have changed by the addition of terms proportional to the feedback coefficients K_s and K_{T_s}. These additional terms can be used to effect limited control over the system performance. The effect of the new terms on the plasma thermal balance characteristics is discussed below. The closed-loop system performance is presented in Section 4.2.

The characteristic of the plasma thermal balance which is of primary importance is its stability. As previously discussed, the stability of the present system is determined by the position of the closed-loop poles. Using equations 4.1 and 4.2, and the supporting equations 4.2a through 4.2d, the closed-loop poles can be determined as a function of the feedback fractions. Alternately, using the same equations, the feedback fractions required to guarantee stable performance can be determined for any given plasma temperature. This latter approach was adopted for presentation and the results of the analysis are presented in Figures 4-1 through 4-4. These figures graphically portray the temperature range which can be stabilized with the use of proportional feedrate and/or injection energy feedback.

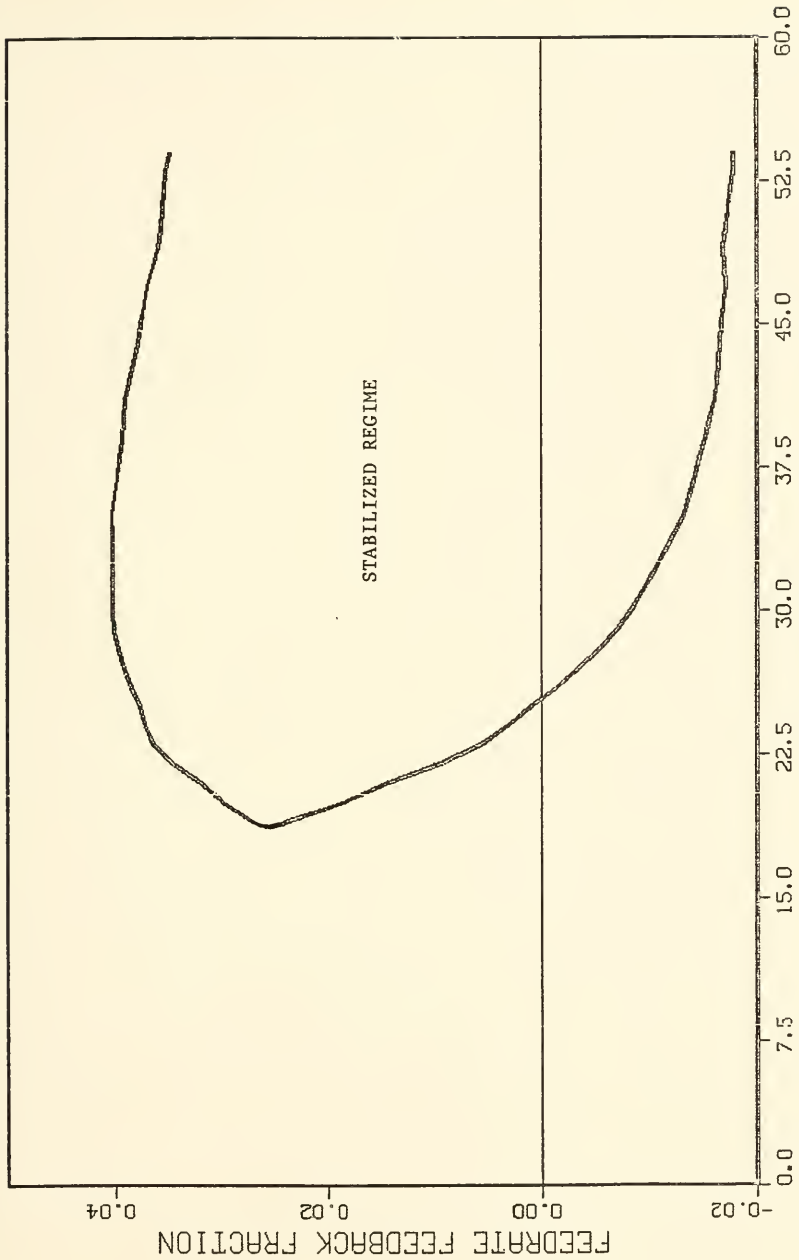

Figure 4-1. Stabilized temperature range using feedrate feedback only. No injection energy, constant confinement.

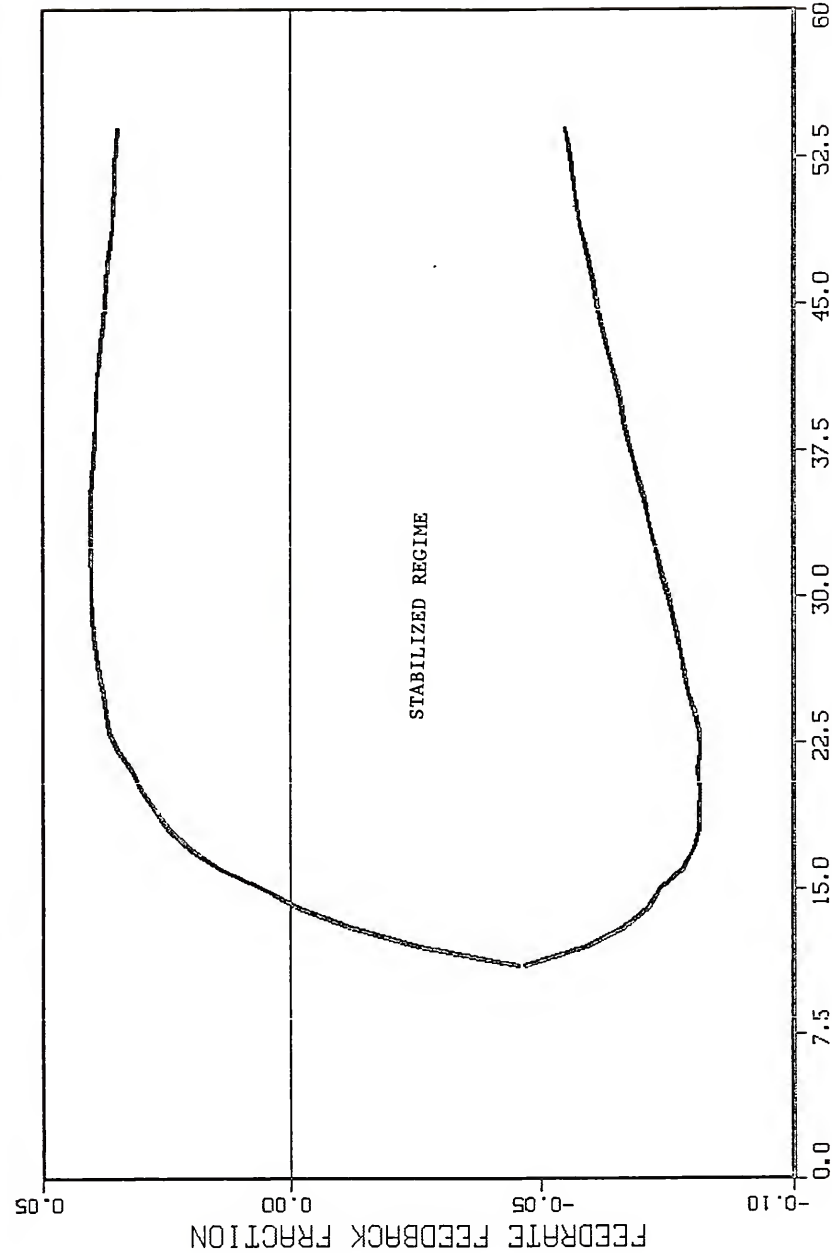

Figure 4-2. Stabilized temperature range using feedrate feedback only. No injection energy, Bohm confinement.

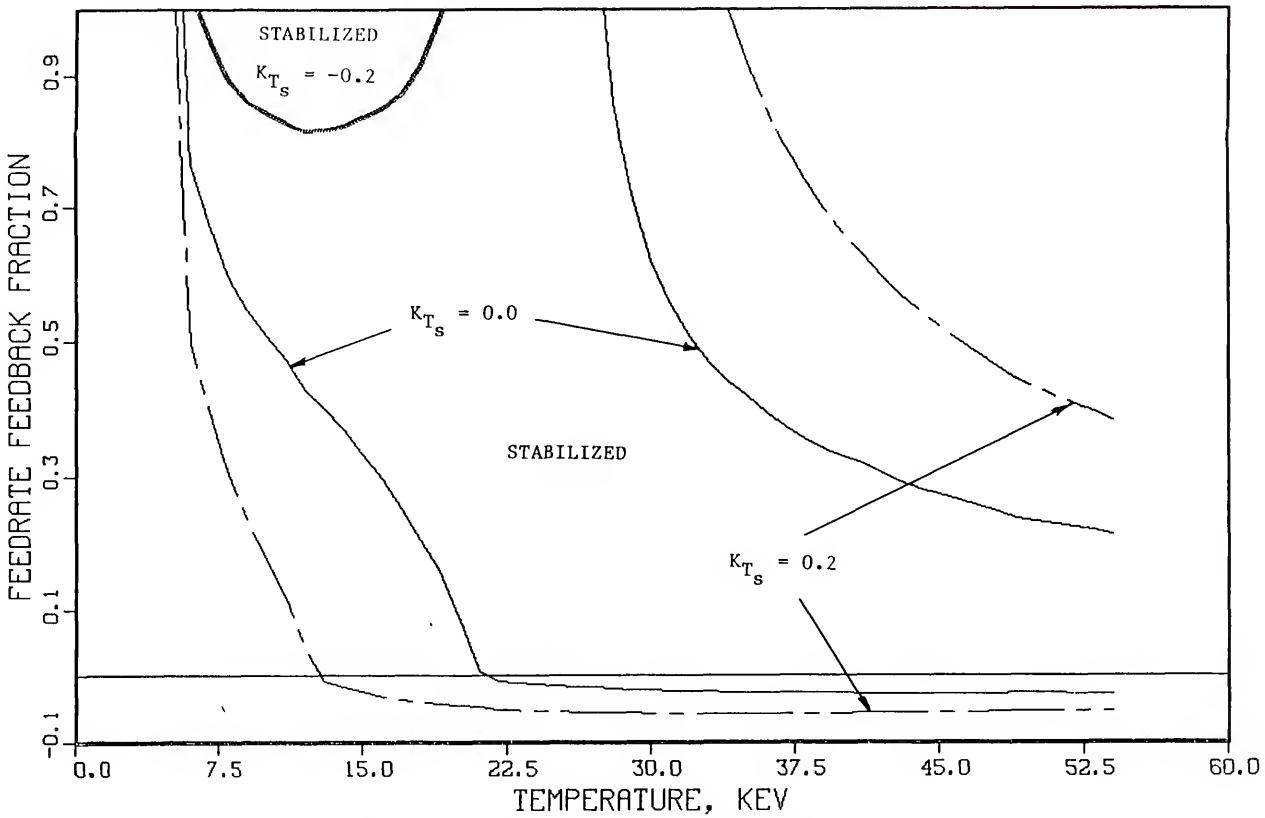

Figure 4-3. Stabilized temperature range using feedrate and injection energy feedback. T_{s_o} = 75 keV, constant confinement.

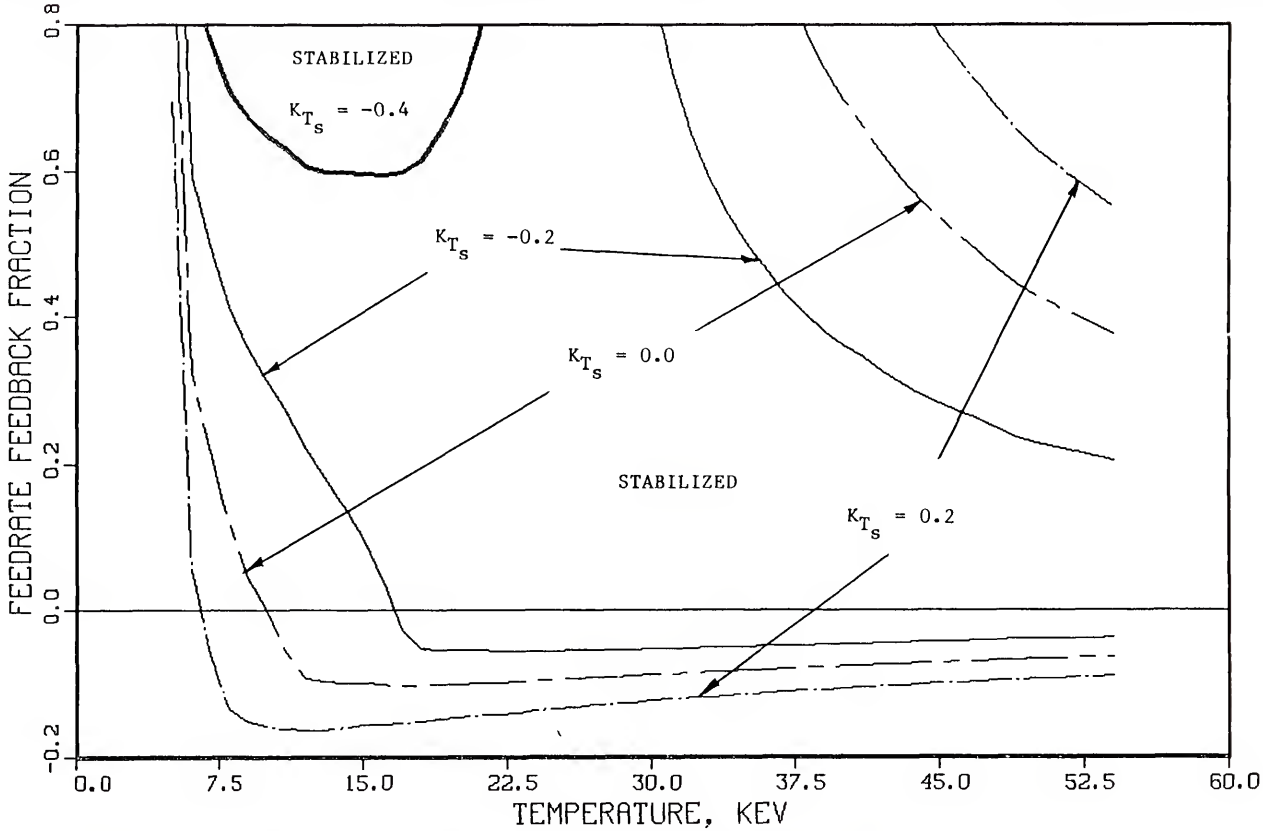

Figure 4-4. Stabilized temperature range using feedrate and injection energy feedback. T_{s_o} = 75 keV, Bohm confinement.

Figure 4-1 shows that with zero injection energy, the minimum stable temperature can be lowered to 18 keV from the minimum open-loop temperature of 25 keV using only 2 to 3% feedrate feedback fraction, assuming constant confinement. With the Bohm confinement law and no injection energy, Figure 4-2 shows that the minimum stable temperature can be lowered to 11 keV from the open-loop value of 14 keV using a -5% feedrate feedback fraction. Figures 4-1 and 4-2 further show that there is a broad range of feedback fraction that can be used, even at temperatures that are open-loop stable, to modify and improve the system performance. The selection of the operating feedback fractions is discussed below and in subsequent sections.

With 75 keV injection energy, both the feedrate and injection energy feedback fractions can be selected so as to establish stability. The stabilized regimes for constant and Bohm confinement are plotted in Figures 4-3 and 4-4, parametrically with the injection energy feedback fraction. The figures show that for either confinement scheme, with proper selection of the feedback fractions, stable operation is possible to as low as 5 keV (the ideal ignition temperature at which the fusion yield begins to exceed the minimum ideal radiative losses). This temperature can be compared to the open-loop critical temperatures of 21 keV and 10 keV for constant and Bohm confinement, respectively. Again, the figures show that a broad selection of feedback fractions is available with which to adjust the system performance. The factor of 10 change in the ordinate scale is to be noted in comparing Figures 4-1 and 4-2 with 4-3 and 4-4.

An interesting characteristic of the stability range observed in Figure 4-1 through 4-4 is that at temperatures above the critical temperature with no injection energy and above temperatures greater than approximately 25 keV with 75 keV injection energy, there is an upper limit to the feedrate feedback fraction above which unstable behavior is again encountered. This limit can be explained with the use of equation 4.8 for the system damping, and the plots of the gains g_1 and g_2 presented in Figure 3-1 of the previous section. For stability, both ω_n and ξ must be greater than zero. However, for zero injection energy, Figure 3-1 shows g_1 to be less than zero for all temperatures. With 75 keV injection energy, Figure 3-1 shows that the gain g_1 becomes negative above 25 kev and will therefore result in a decrease in the system damping with increasing feedrate feedback fraction. For a sufficiently high fraction, i.e., the limit prescribed in Figures 4-1 through 4-4, the damping ratio falls below zero and thus destabilizes the system. Additional discussion of the effect of feedback on the damping ratio is presented below.

Given the range of feedback that can stabilize the thermal balance, the selection of the feedback fraction is guided by the choice of system performance specifications. As developed in Appendix C, these specifications are determined by the system characteristics of gain, the zero, natural frequency, and the damping ratio. Of these, only the natural frequency and the damping ratio are affected by closed-loop feedback as given by equations 4.7 and 4.8. Thus, the natural frequency and damping ratio (and the system specifications) are functions of both the temperature of the plasma and the feedback

representative temperatures in the following operating scenarios:

1. Zero injection energy, constant confinement - 20, 25, and 30 keV.
2. Zero injection energy, Bohm confinement - 15, 20, and 25 keV.
3. 75 keV injection energy, constant confinement - 10, 20, and 30 keV.
4. 75 keV injection energy, Bohm confinement - 10, 20, and 30 keV.

The square of the natural frequency of the closed-loop thermal balance is given by equation 4.7. Examination of the new terms in equation 4.7 reveals that the three physical processes of fusion gain, bremsstrahlung, and confinement losses, all contribute to the effect of feedrate feedback on the undamped natural frequency, while only fusion terms and confinement losses contribute to the effect of injection energy feedback. The three terms contributing to the effect of feedrate feedback are plotted in Figure 4-5, while the two terms contributing to the effect of injection energy feedback are plotted in Figure 4-6. Figure 4-5 applies for zero and 75 keV injection energy, for both constant and Bohm confinement. Figure 4-6 applies for both confinement types, but only for the case of 75 keV injection energy. The five terms in the two figures are normalized by the value of the input control variable. The net effect of feedback on the square of the natural frequency is the product of the multiplier shown in the figures and the feedback coefficient. As in the open-loop case, bremsstrahlung is a weak contributor to the natural frequency, while the burnup and confinement terms are the primary contributors.

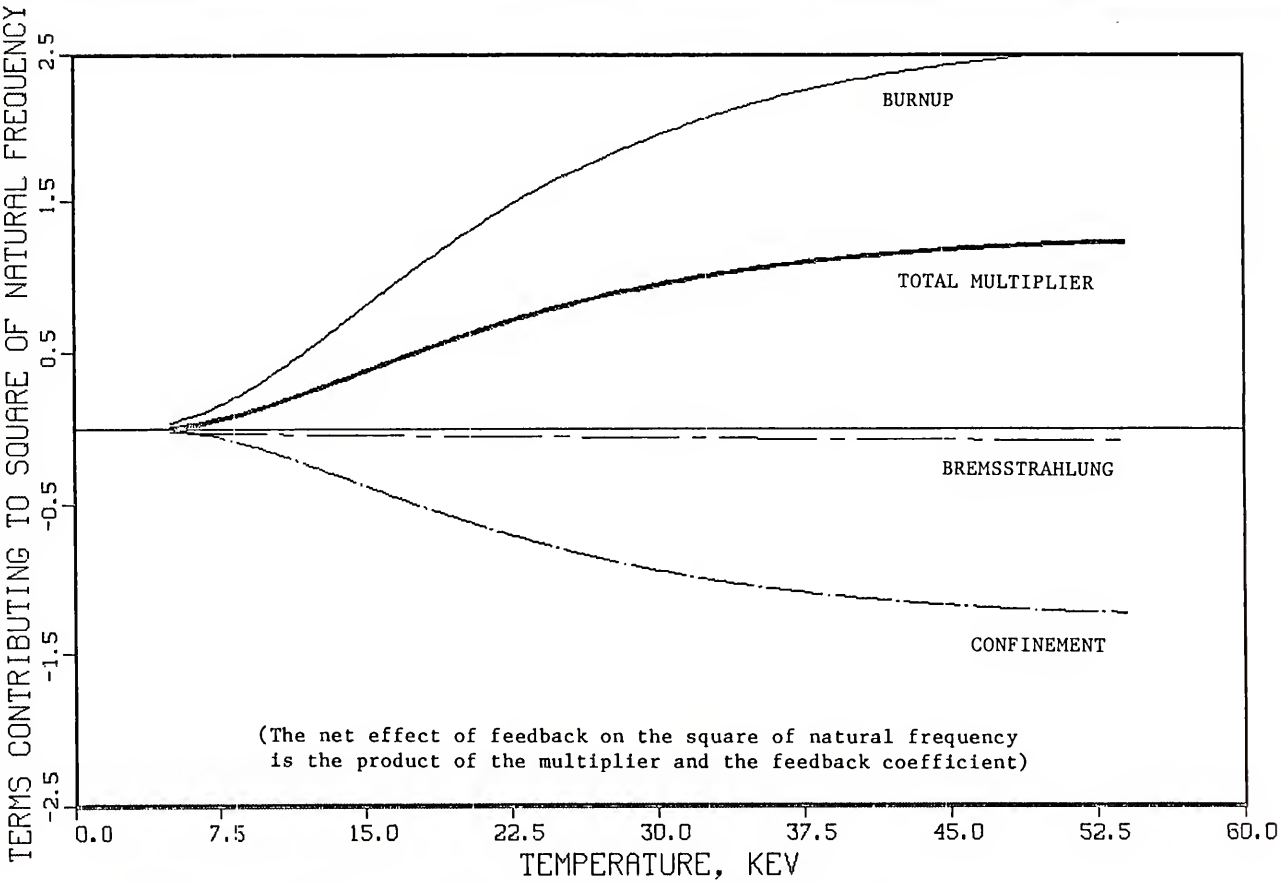

Figure 4-5. Temperature dependence of the natural frequency terms contributing to the multiplier of the feedrate feedback fraction. T_{s_o} = 0 and 75 keV, constant or Bohm confinement.

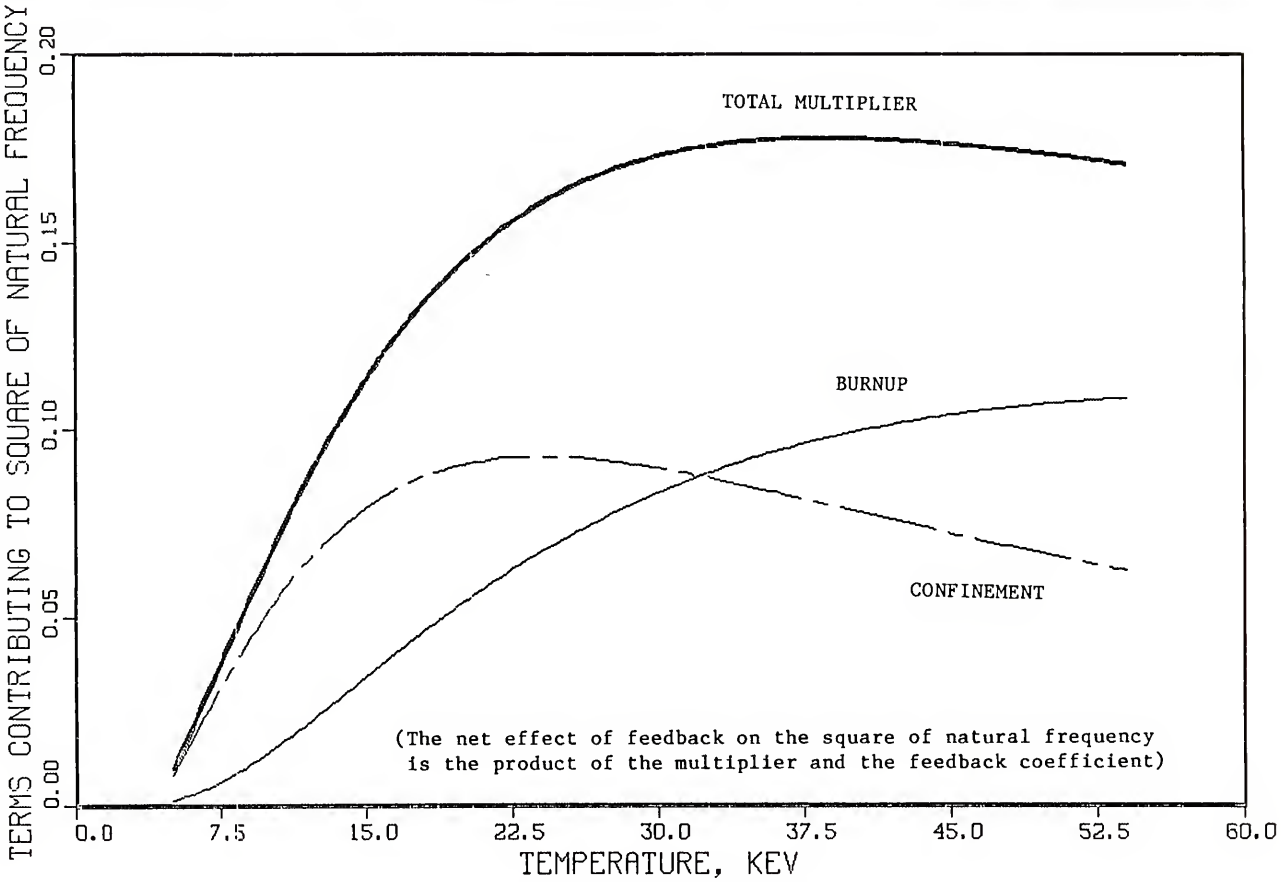

Figure 4-6. Temperature dependence of the natural frequency terms contributing to the multiplier of the injection energy feedback fraction. T_{s_o} = 75 keV, constant or Bohm confinement.

Inspection of Figures 4-5 and 4-6 shows that the net effect of feedback on the natural frequency is weaker at the lower temperatures of interest (<10 keV) but increases to appreciable levels at higher temperatures (>20 keV). The figures also show that feedrate feedback has a stronger effect on the natural frequency than injection energy feedback, by factors of 2 to 5, in the temperature range of 5 to 30 keV. These considerations are quantitatively demonstrated in the plots of the closed-loop natural frequency versus feedback fraction shown in Figures 4-7 through 4-13.

For the cases of no injection energy, Figure 4-7 shows that the natural frequency is in the range of 0.02 to 0.2 sec^{-1}. In each case, the curve drawn in the figure spans the stable feedrate feedback range. The general trend is seen to be a rapid increase of the natural frequency in the vicinity of the minimum feedrate feedback fractions necessary for stability, followed by a slowing down to a more moderate rate of increase at the higher feedrate feedback fractions. At temperatures for which stability can only be provided by a very narrow band of feedrate feedback fractions, e.g., 20 keV and constant confinement, the natural frequency shows high sensitivity to the feedrate feedback fraction and does not reach a plateau region. As the band for stabilizing feedrate feedback increases, e.g., 20 to 25 keV and Bohm confinement, the sensitivity decreases at the higher feedrate feedback fractions.

With 75 keV injection energy, the natural frequency is further increased to the 0.1 to 1.0 sec^{-1} range (Figures 4-8 through 4-13). This is due to the combination of both increased permissible feedrate feedback resulting from the lower system gain and the additional

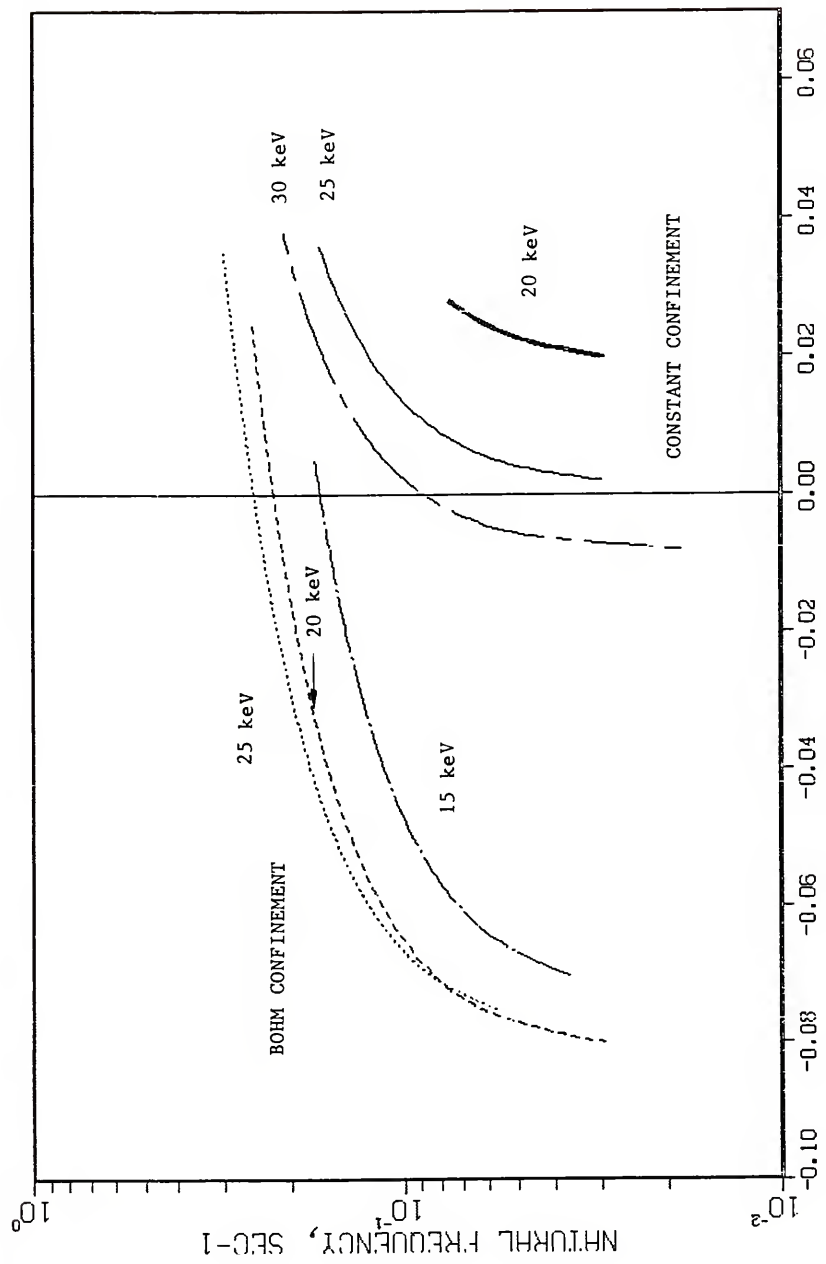

Figure 4-7. Closed-loop natural frequency versus feedback fraction. T_{s_o} = 0, constant and Bohm confinement.

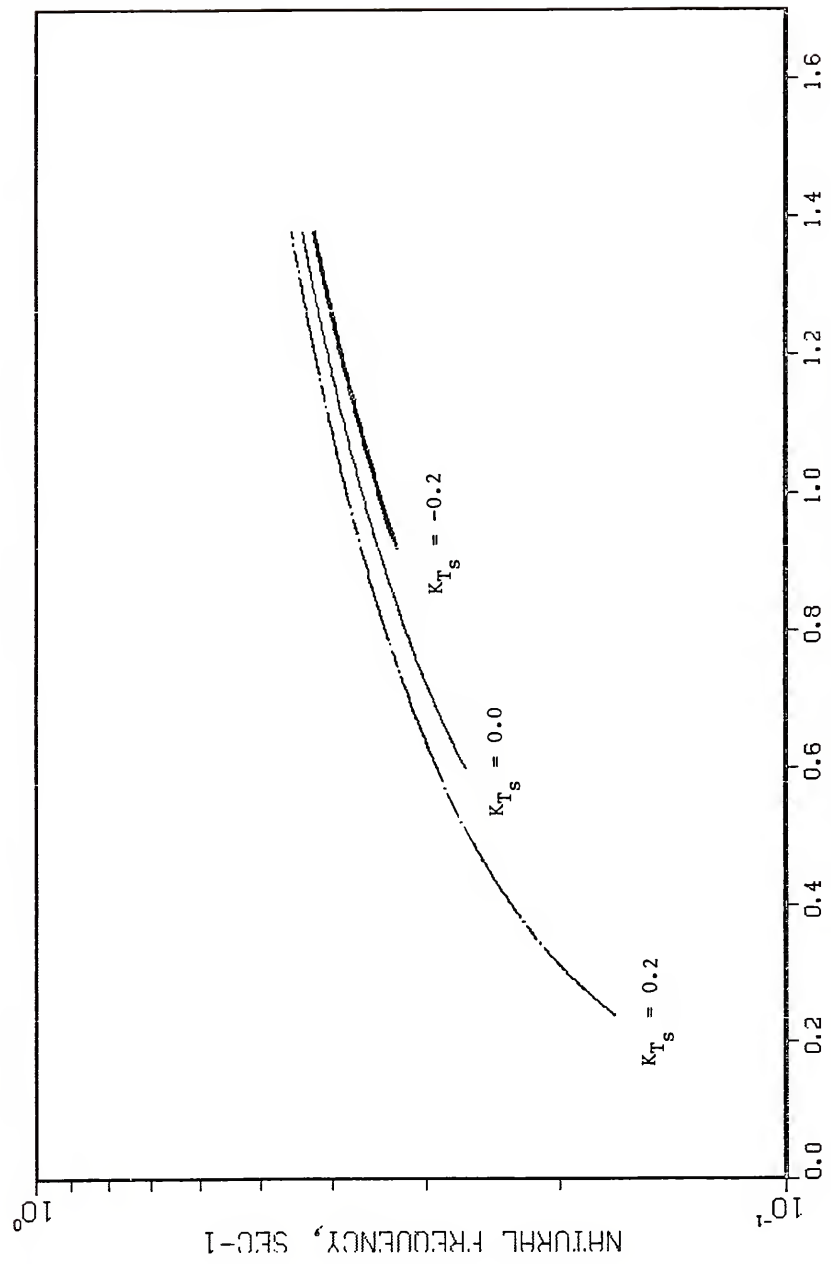

Figure 4-8. Closed-loop natural frequency versus feedback fraction. T_{s_o} = 75 keV, constant confinement, kT = 10 keV.

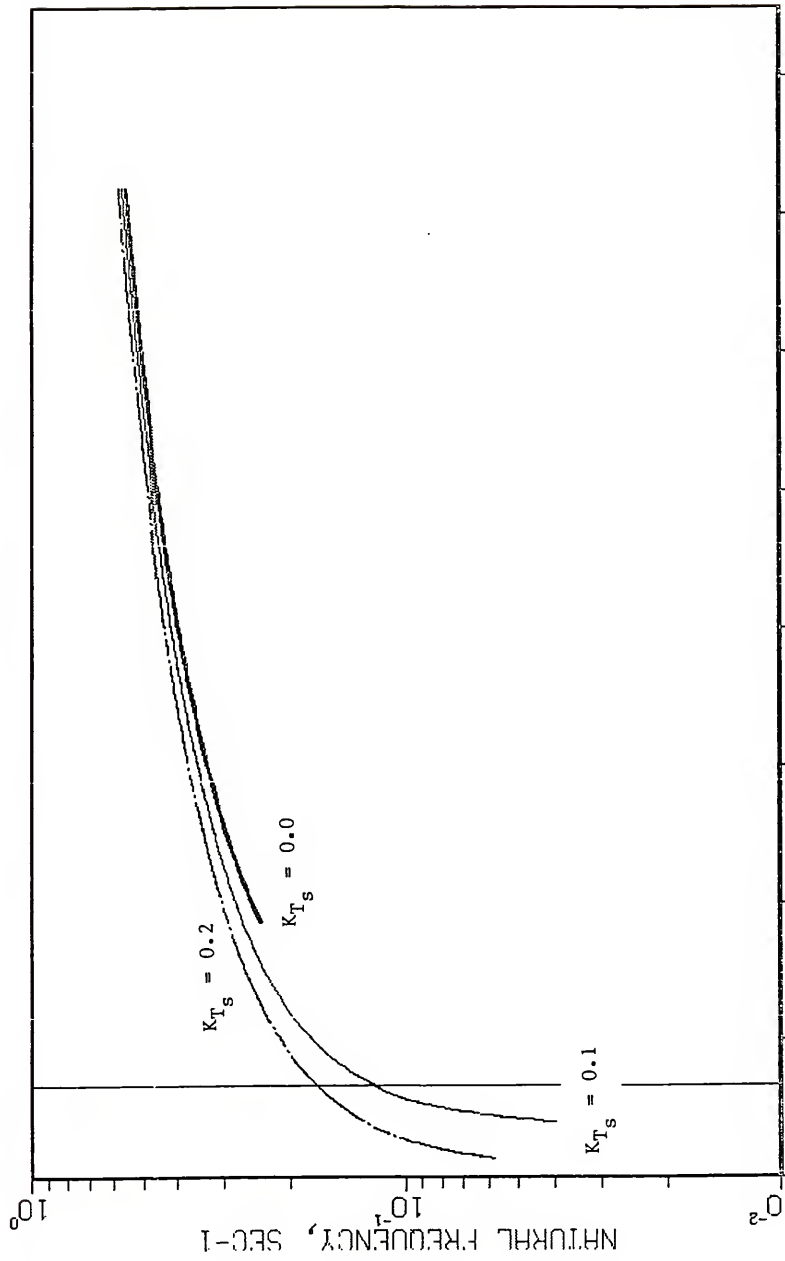

Figure 4-9. Closed-loop natural frequency versus feedback fraction. T_{s_o} = 75 keV, constant confinement, kT = 20 keV.

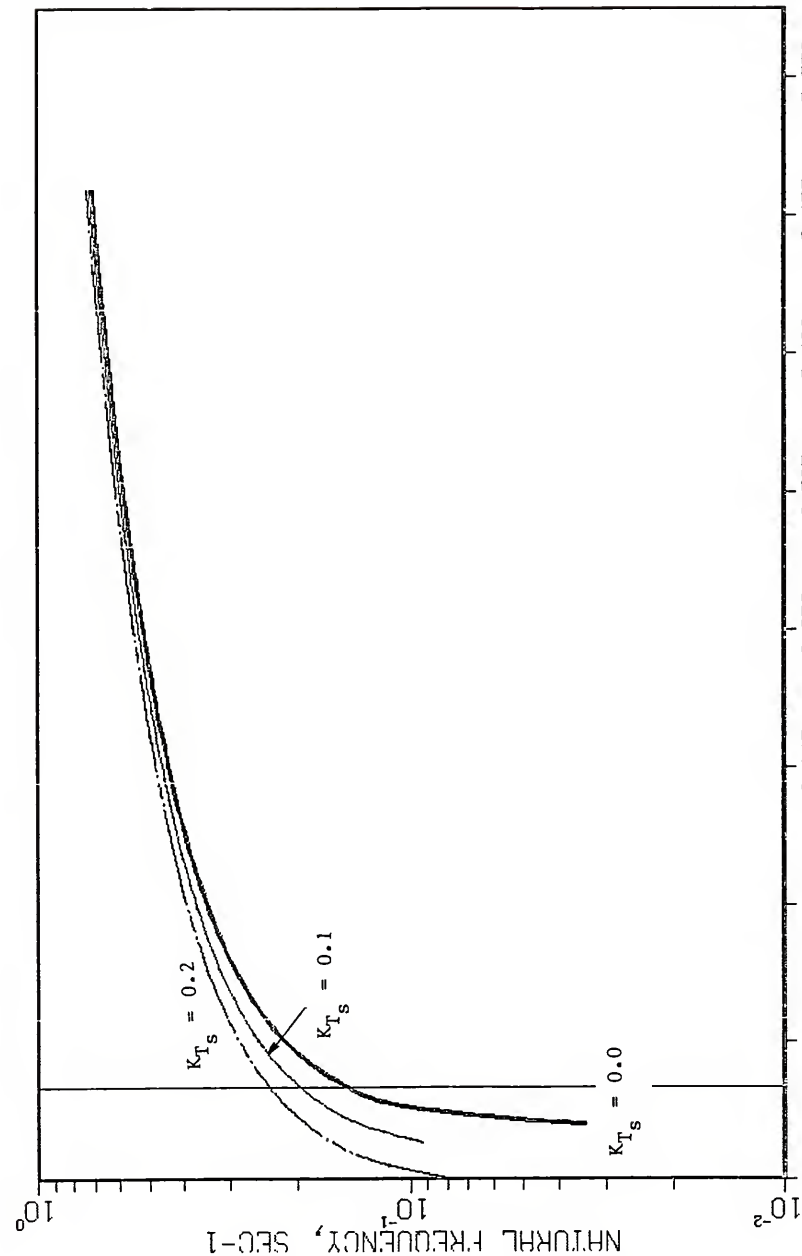

Figure 4-10. Closed-loop natural frequency versus feedback fraction. T_{s_o} = 75 keV, constant confinement, kT = 30 keV.

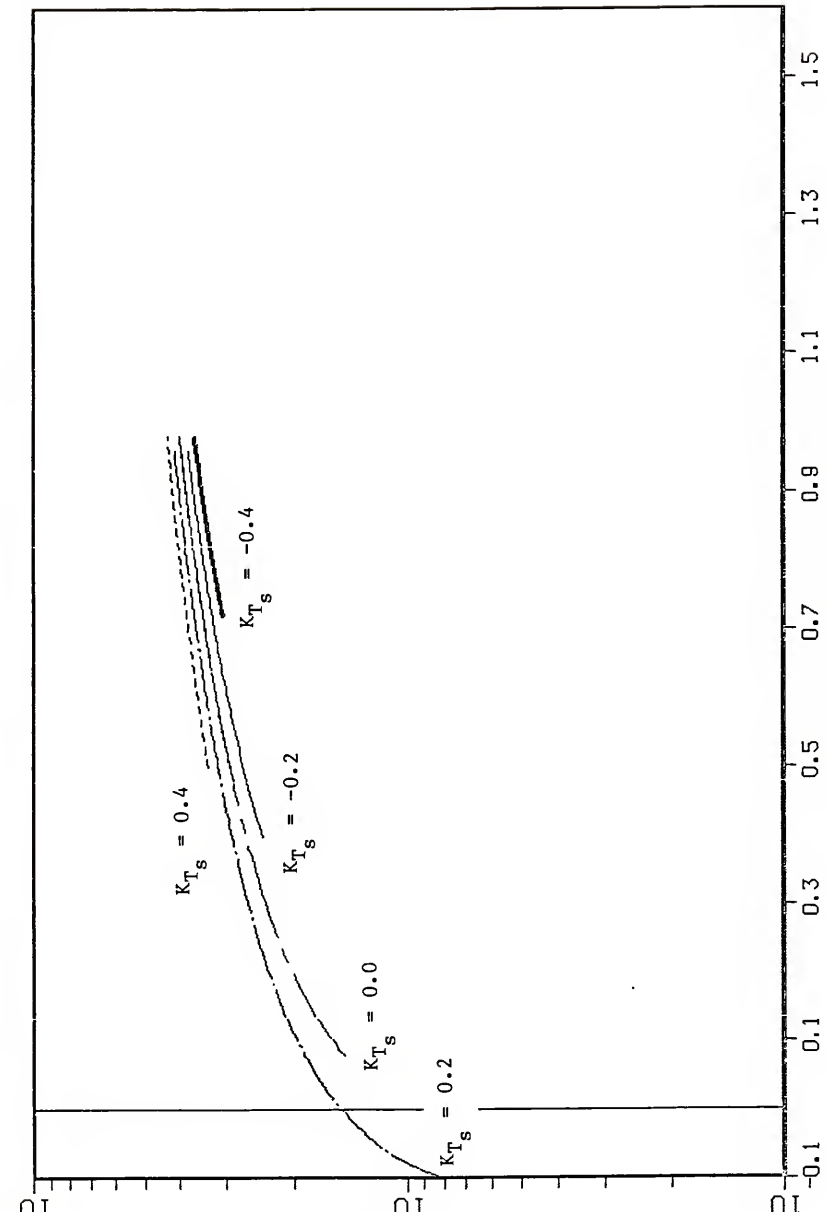

Figure 4-11. Closed-loop natural frequency versus feedback fraction. T_{s_o} = 75 keV, Bohm confinement, kT = 10 keV.

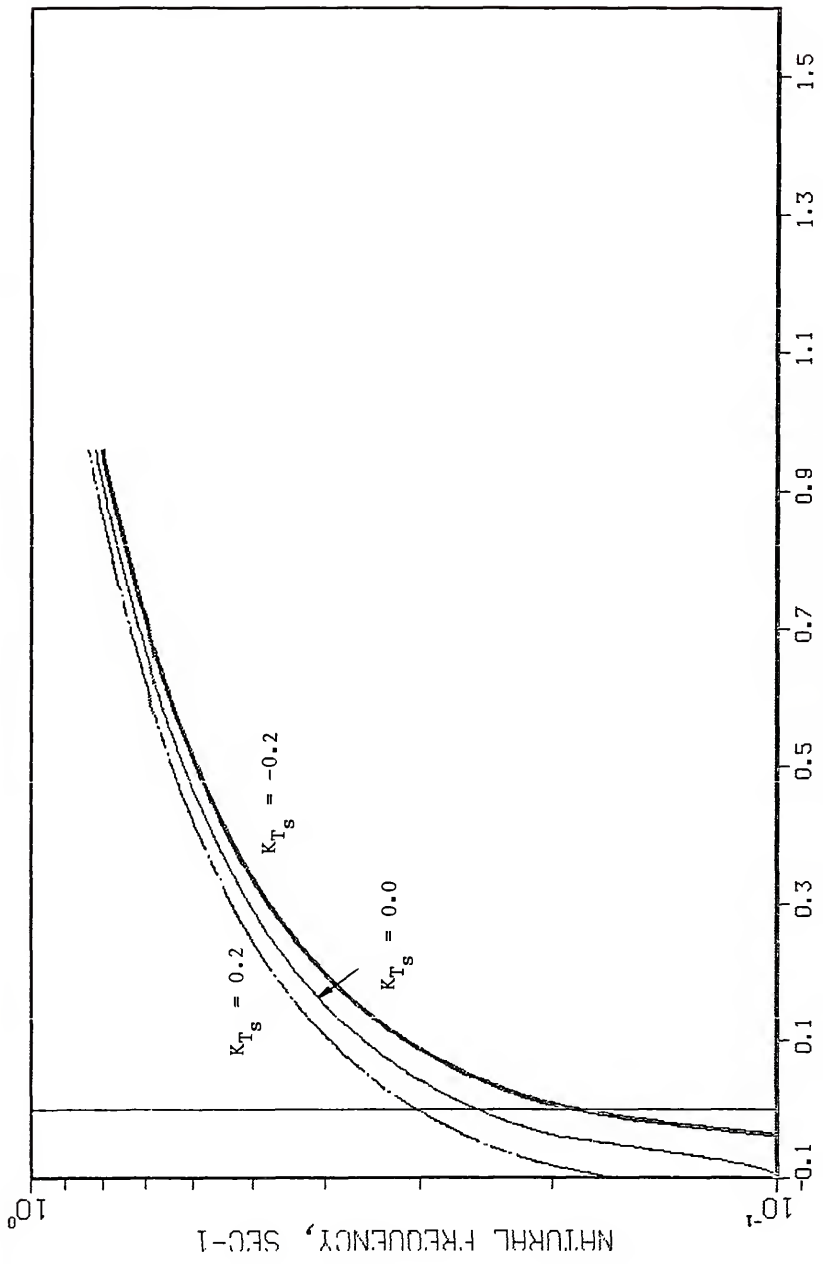

Figure 4-12. Closed-loop natural frequency versus feedback fraction. T_{s_o} = 75 keV, Bohm confinement, kT = 20 keV.

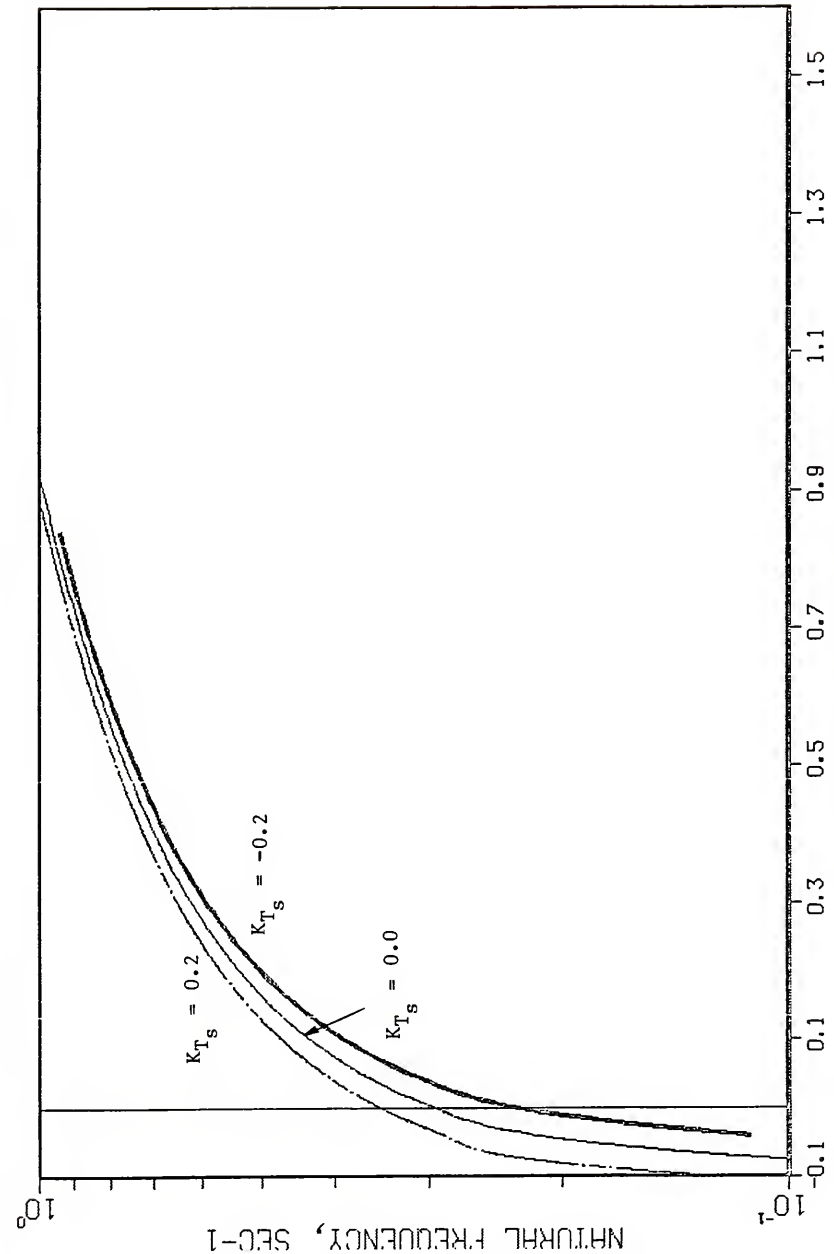

Figure 4-13. Closed-loop natural frequency versus feedback fraction. T_{s_o} = 75 keV, Bohm confinement, kT = 30 keV.

contribution of the injection energy feedback fraction. The trend of the variation of the natural frequency with feedrate feedback fraction is otherwise very similar to that discussed above for zero injection energy. Inspection of Figures 4-8 to 4-13 shows that the effect of injection energy on the natural frequency is small. This can be seen from equation 4.7 and the plots of Figures 4-5 and 4-6. The figures show that terms multiplying the feedrate feedback fractions are 5 to 10 times greater than the terms multiplying the injection energy feedback. Equation 4.7 shows this advantage to be due mainly to the burnup term multiplying K_S.

The damping ratio of the closed-loop thermal balance is given by equation 4.8. The new terms in the expression for damping essentially consist of the system gains divided by twice the natural frequency. Since the gains are not changed by the addition of feedback, the causes of the change in damping are related to those causes effecting the changes in the natural frequency, as discussed above. The effect of feedback on the system damping is displayed in Figures 4-14 and 4-15. These are plots of the two new terms in equation 4.8, normalized by the value of the input variable.

The two new terms in equation 4.8 contain the natural frequency as a factor in the denominator. Since the application of feedback alters the natural frequency, Figures 4-14 and 4-15 are plotted using the open-loop natural frequency. In order to isolate the contribution of feedback to the system damping, the data in these figures must be combined with the open-loop natural frequency curves of Figures 3-6 through 3-9. Thus, the singular points in Figures 4-14 and 4-15 can be associated with the crossover temperatures of Figures 3-6 through 3-9

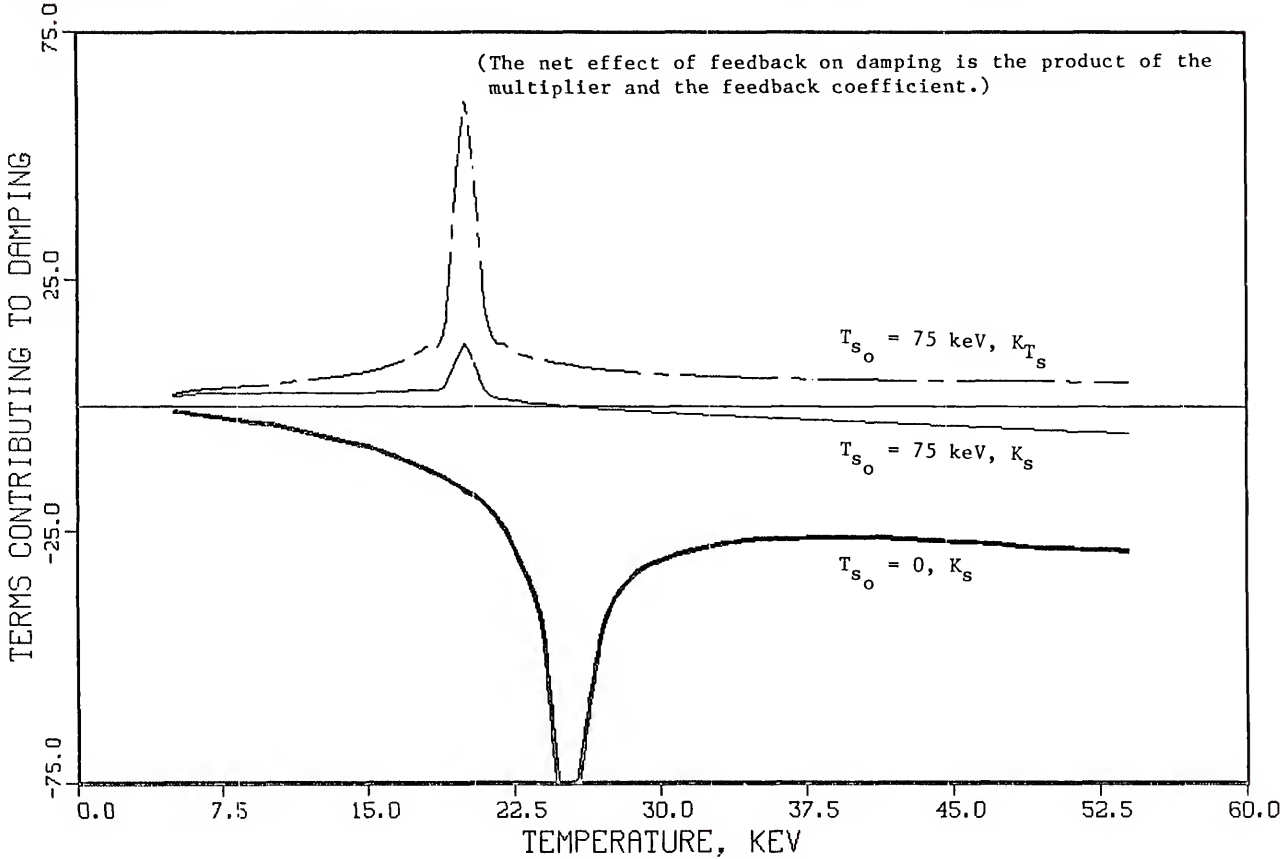

Figure 4-14. Temperature dependence of the damping terms multiplying the feedback fraction. Constant confinement.

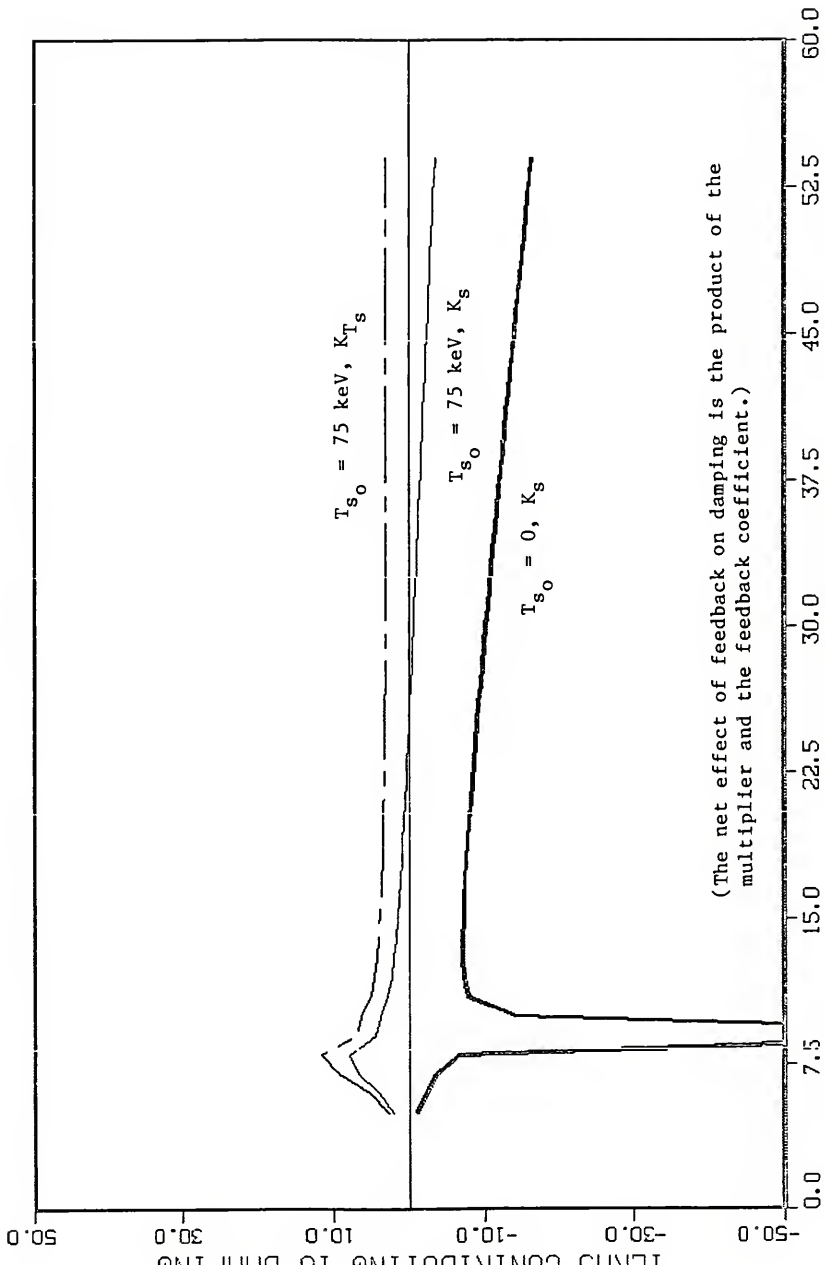

Figure 4-15. Temperature dependence of the damping terms multiplying the feedback fraction. Bohm confinement.

at which the natural frequency is identically zero. At temperatures away from the singular point, since the natural frequency is generally slowly varying with temperature, the damping multiplier follows the slope of the gain function (shown in Figure 3-1).

The net effect of feedback on the damping ratio is summarized in Figures 4-16 through 4-22. With zero injection energy, Figure 4-16 shows that at all temperatures, the system is overdamped at low feedrate feedback fraction. The damping ratio decreases with increasing feedrate feedback fraction until unstable behavior results at sufficiently high feedrate feedback. With 75 kev injection energy, Figures 4-17 through 4-22 show that damping always increases with increasing injection energy feedback. Using equation 4.8, this can be attributed to the gain g_2 being greater than zero for all temperatures, and the small effect of injection energy feedback on the natural frequency. Physically, with increasing injection energy feedback fraction, the system energy balance is more strongly dominated by the input control function and thus less sensitive to plasma parameter perturbations. At temperatures below which the system gain g_1 becomes negative, the system is initially underdamped, and the damping ratio monotonically increases with feedrate feedback for constant confinement (see e.g., Figure 4-17). At intermediate temperatures and low injection energy feedback fraction, the system damping with constant confinement is similarly behaved (see e.g., Figure 4-18). As the injection energy feedback is increased, stability is achieved at lower feedrate fractions and the K_{T_s} term in equation 4.8 initially dominates. In these constant confinement cases, the system is initially overdamped, passes through a minimum in the system damping,

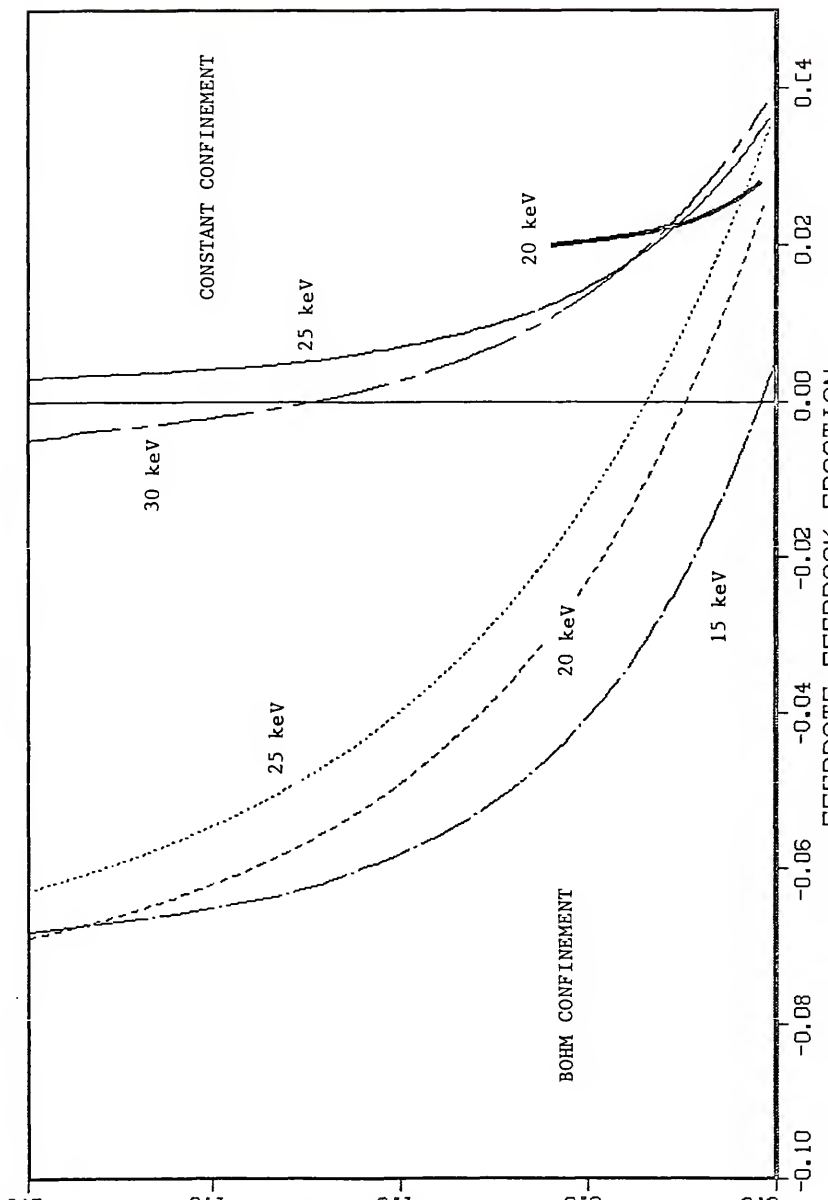

Figure 4-16. Closed-loop damping ratio versus feedback fraction. T_{s_o} = 0, constant and Bohm confinement.

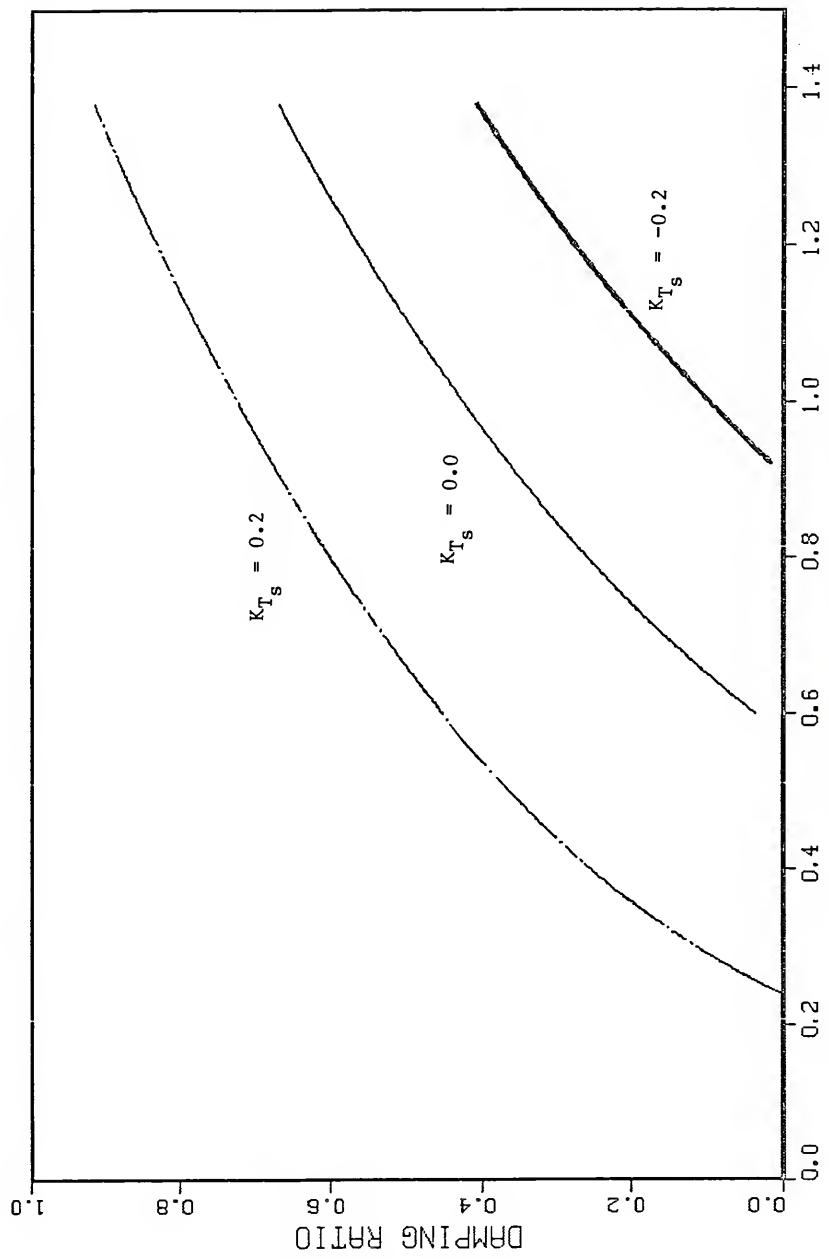

Figure 4-17. Closed-loop damping ratio versus feedback fraction. T_{s_o} = 75 keV, constant confinement, kT = 10 keV.

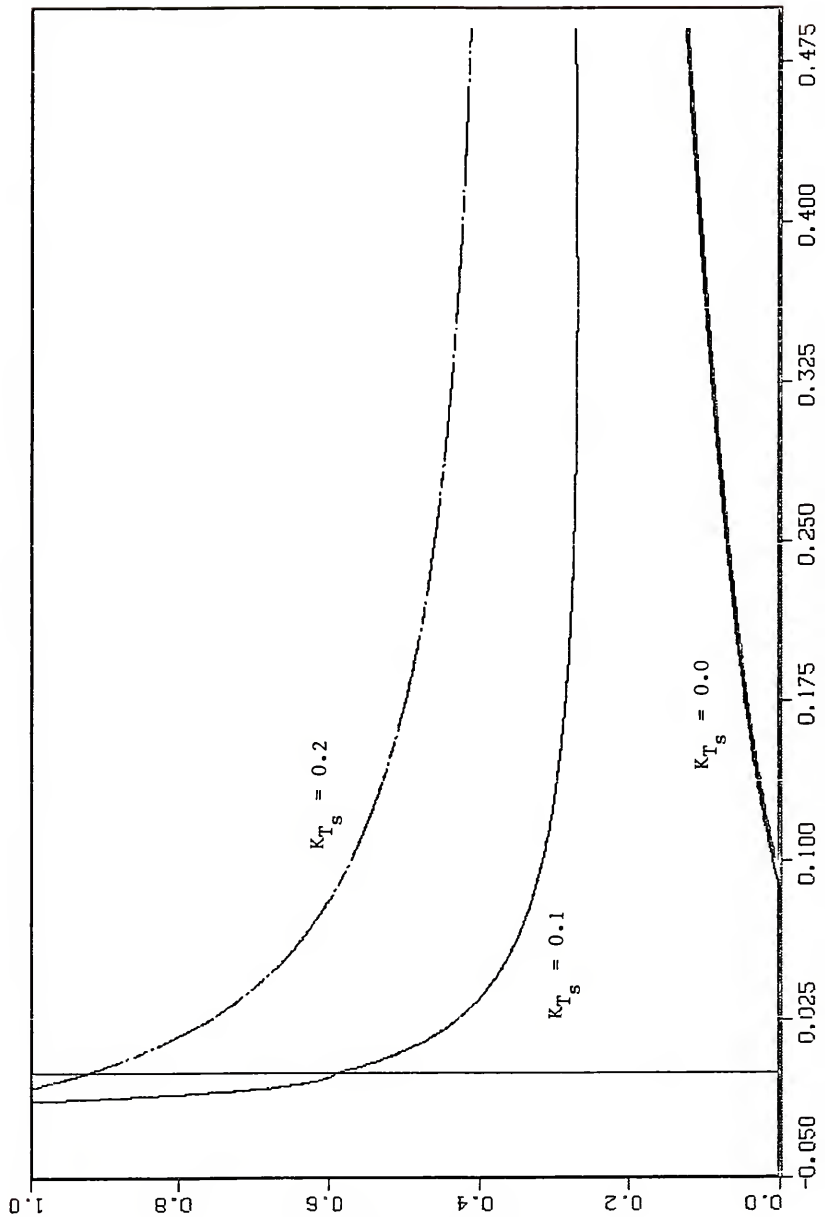

Figure 4-18. Closed-loop damping ratio versus feedback fraction. T_{s_o} = 75 keV, constant confinement, kT = 20 keV.

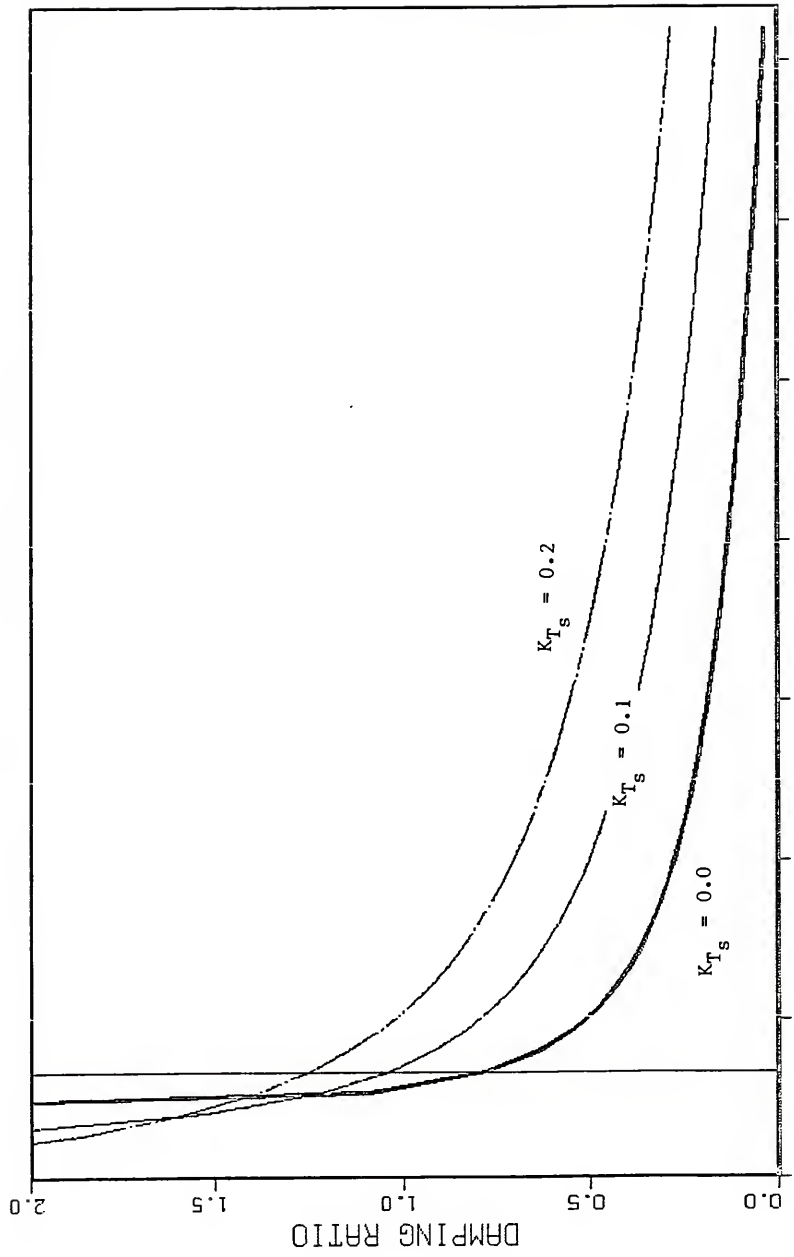

Figure 4-19. Closed-loop damping ratio versus feedback fraction. T_{s_o} = 75 keV, constant confinement, kT = 30 keV.

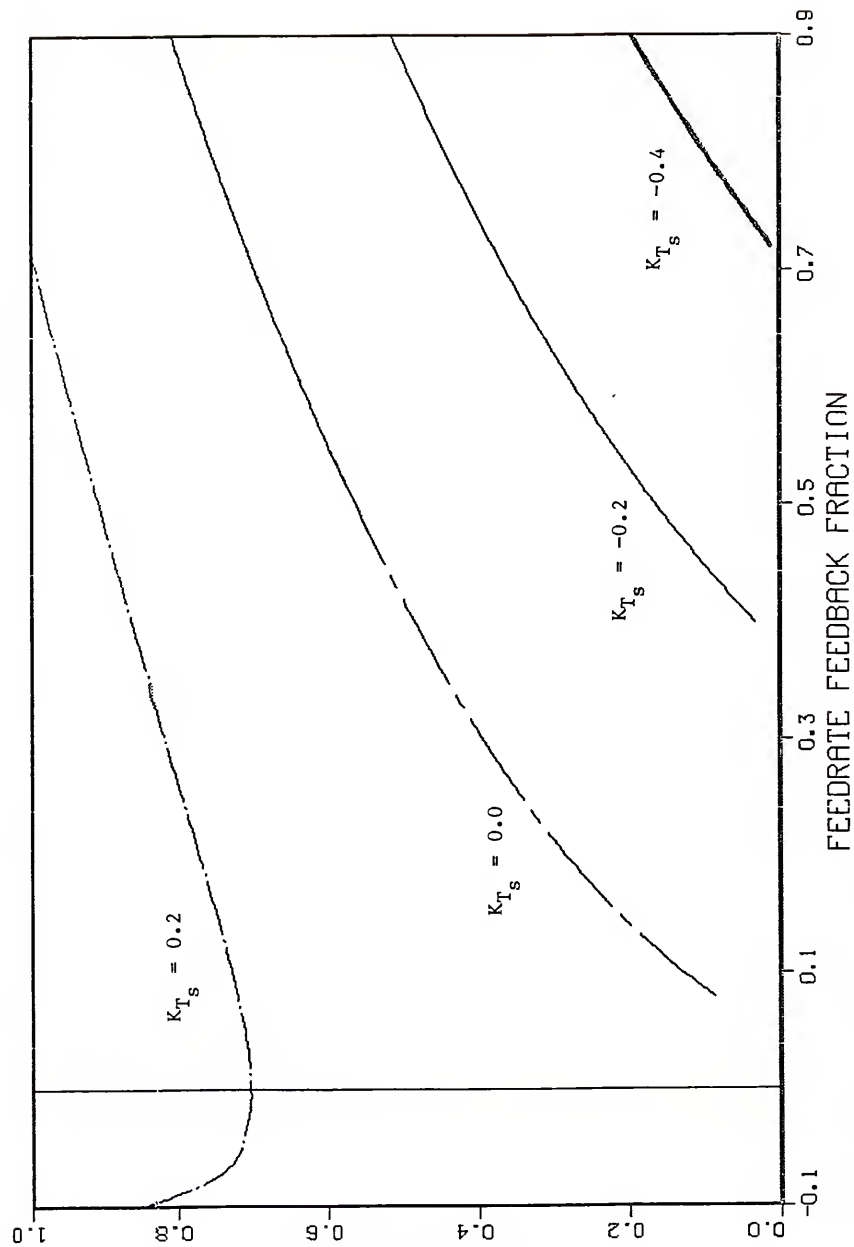

Figure 4-20. Closed-loop damping ratio versus feedback fraction. T_{s_o} = 75 keV, Bohm confinement, kT = 10 keV.

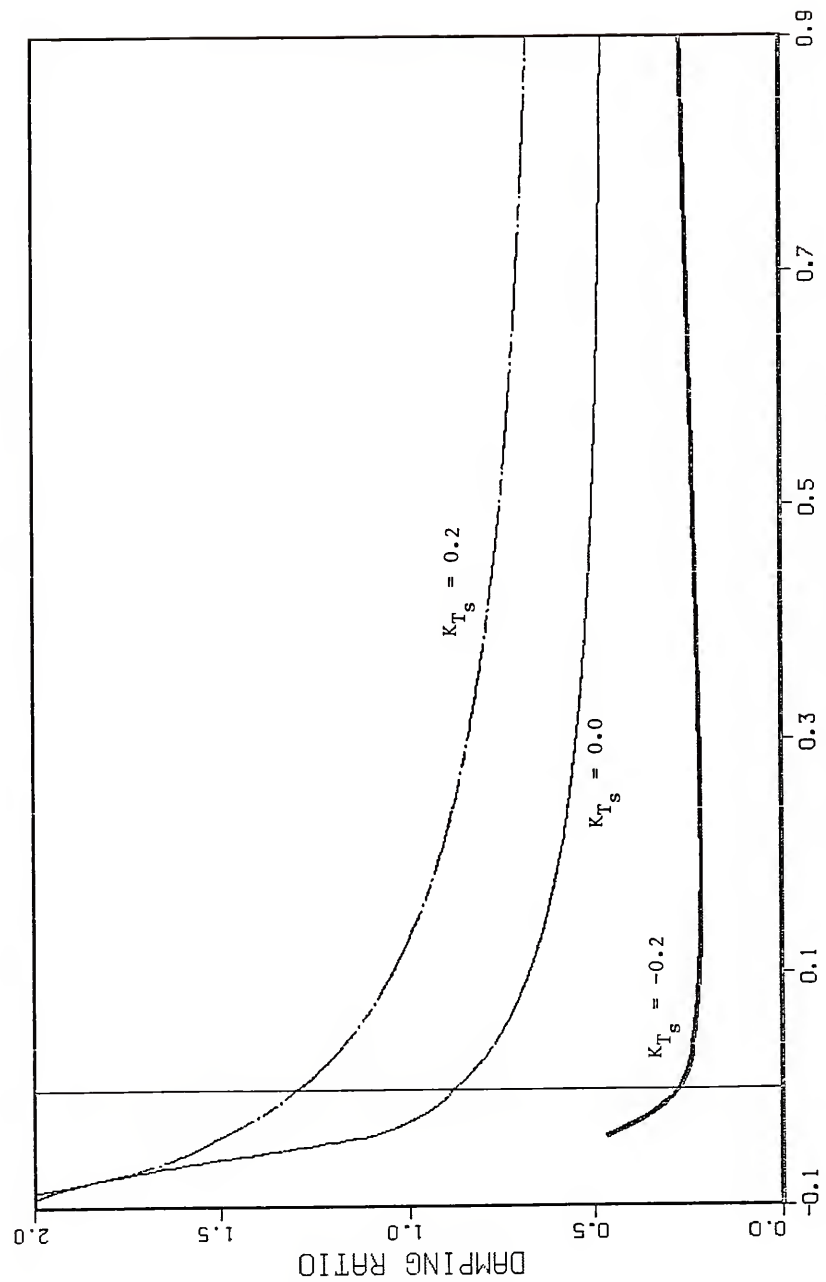

Figure 4-21. Closed-loop damping ratio versus feedback fraction. T_{s_o} = 75 keV, Bohm confinement, kT = 20 keV.

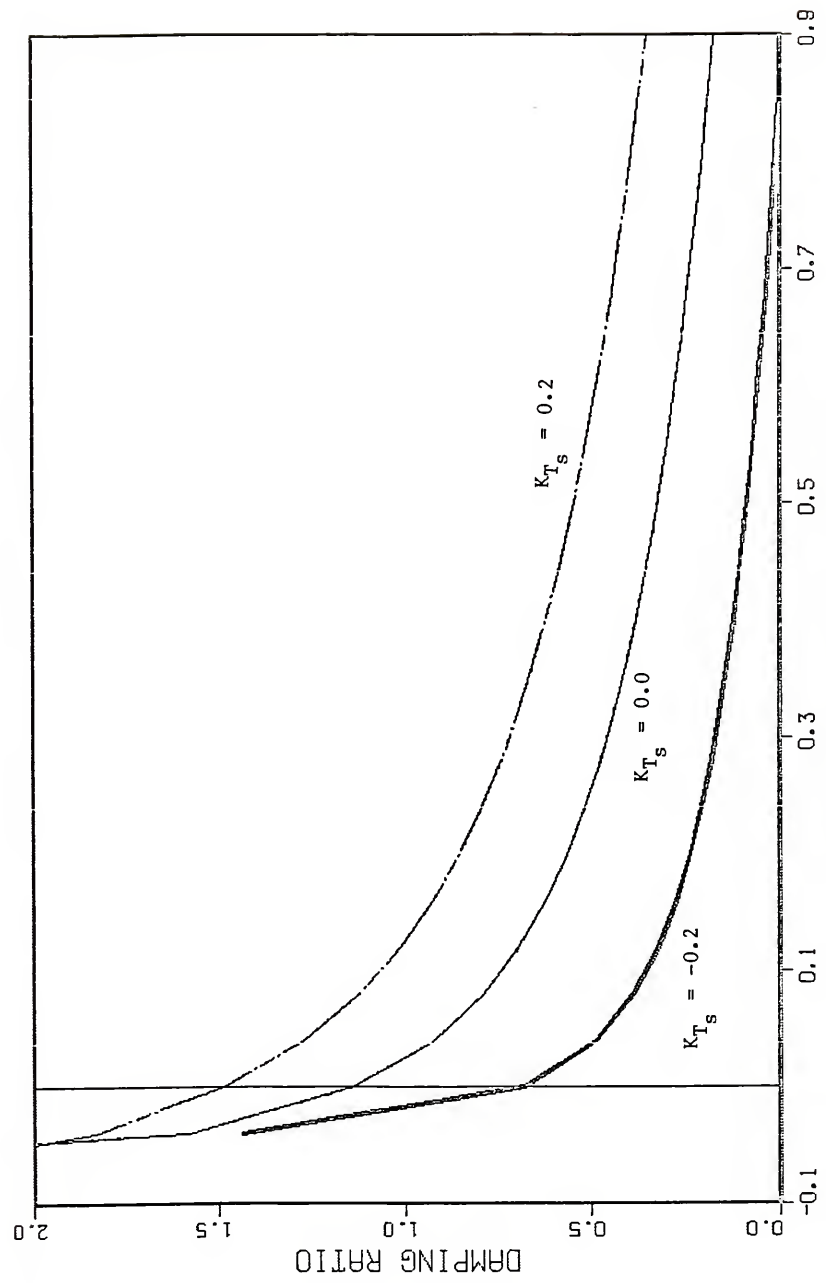

Figure 4-22. Closed-loop damping ratio versus feedback fraction. T_{s_o} = 75 keV, Bohm confinement, kT = 30 keV.

and subsequently increases with increasing feedrate feedback fraction. The behavior of the system with constant confinement at intermediate temperatures is also observed with Bohm confinement at low and intermediate temperatures because stability is again achieved at lower temperatures and feedrate feedback fractions. At high temperatures (above 25 keV), the system is overdamped at low feedrate feedback fractions with both constant and Bohm confinement, and the damping ratio monotonically decreases with increasing feedrate feedback until the onset of system instability (see Figures 4-19 and 4-22).

The present formulation of the problem of thermal stability permits the investigation of the full range of applicability of feedback. Past works have been able to assure thermally stable operation only by observing the position of the closed-loop poles for very specific plasma conditions. The general applicability of the present method in determining the pole positions and the necessary feedback fractions is displayed in Figures 4-23 through 4-29. These figures present the variation in the pole positions with feedback for the cases presented previously in this section. The methodology can be used to establish the stability range of any other injection energy and/or confinement scheme. In past works, no statements have been nor could have been made as to the preferability of one set of feedback conditions over another. By correlating the feedback fractions with the position of the closed loop poles and the system characteristics of natural frequency and the damping ratio, control can conceptually be exercised over the temporal response of the system in a systematic and predictable fashion.

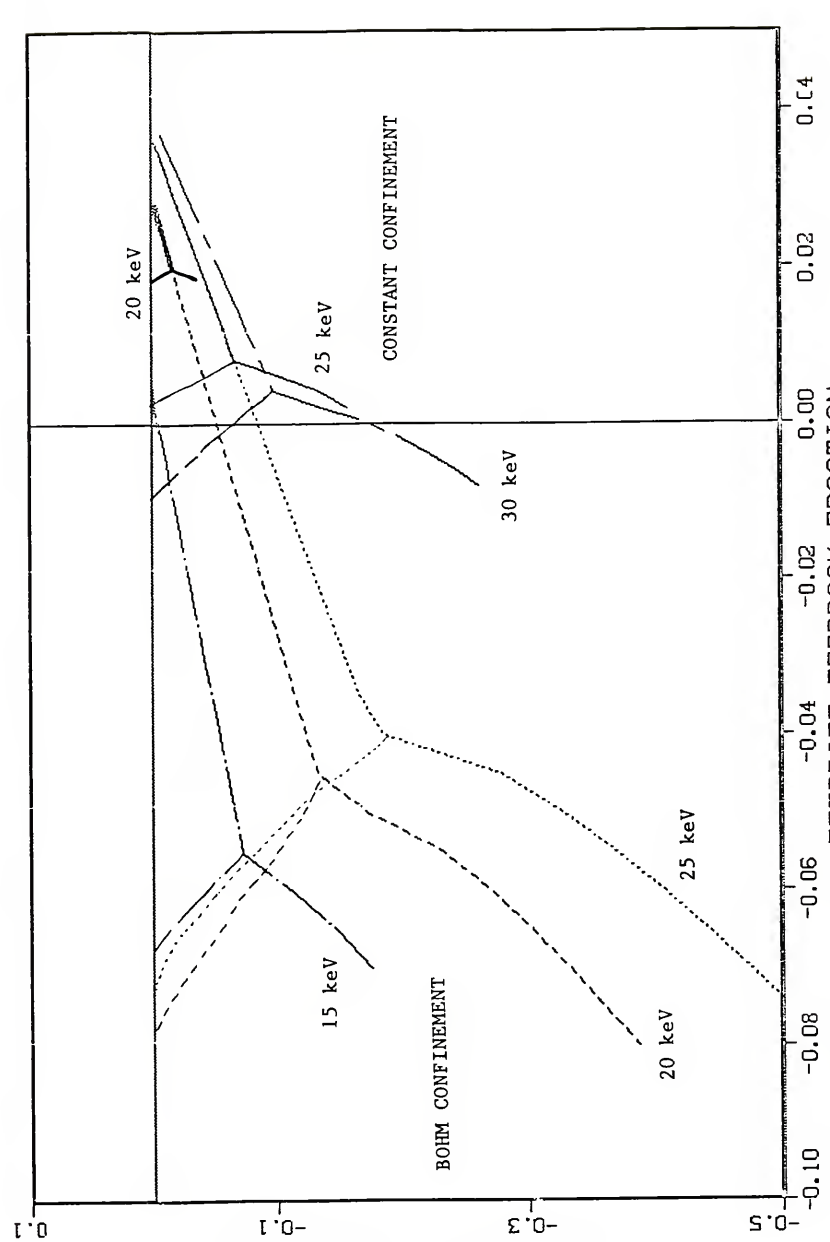

Figure 4-23. Closed-loop pole variation with feedback fraction. T_{s_o} = 0, constant and Bohm confinement.

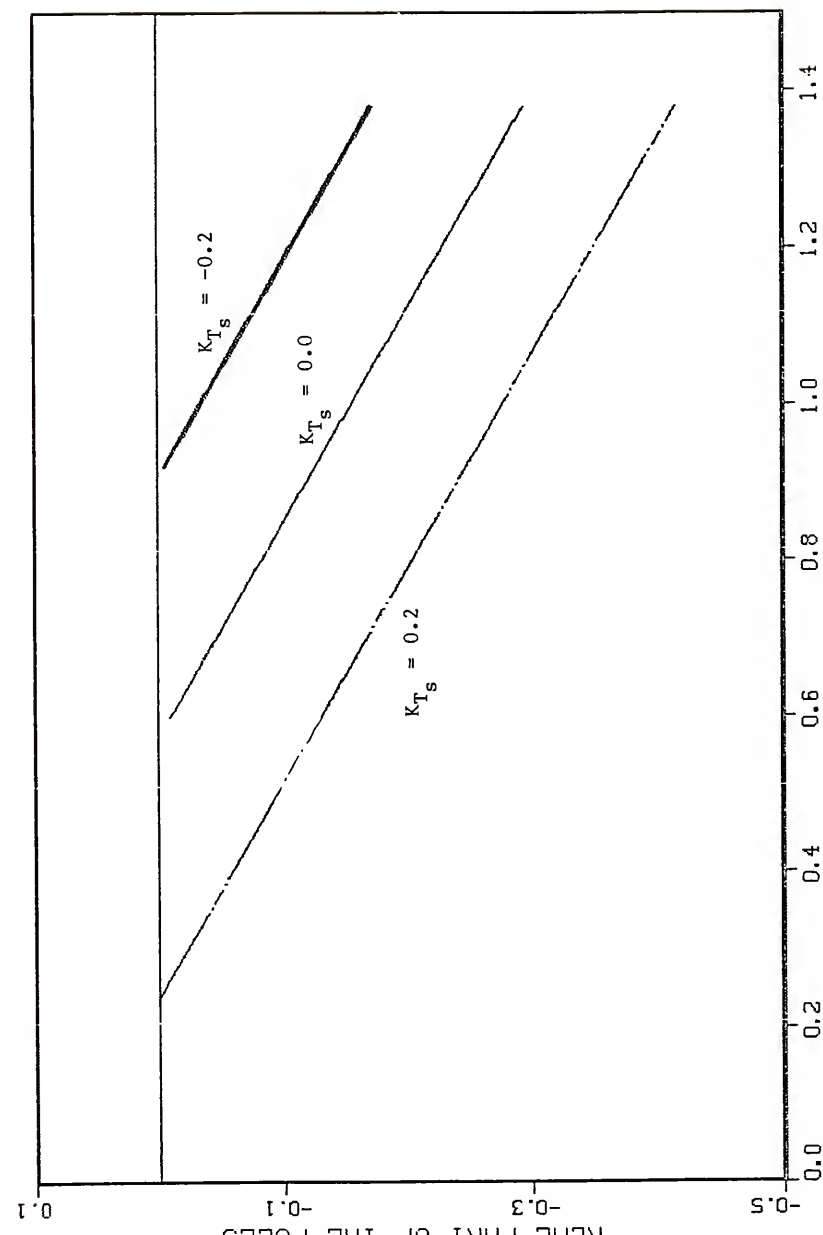

Figure 4-24. Closed-loop pole variation with feedback fraction. T_{s_o} = 75 keV, constant confinement, kT = 10 keV.

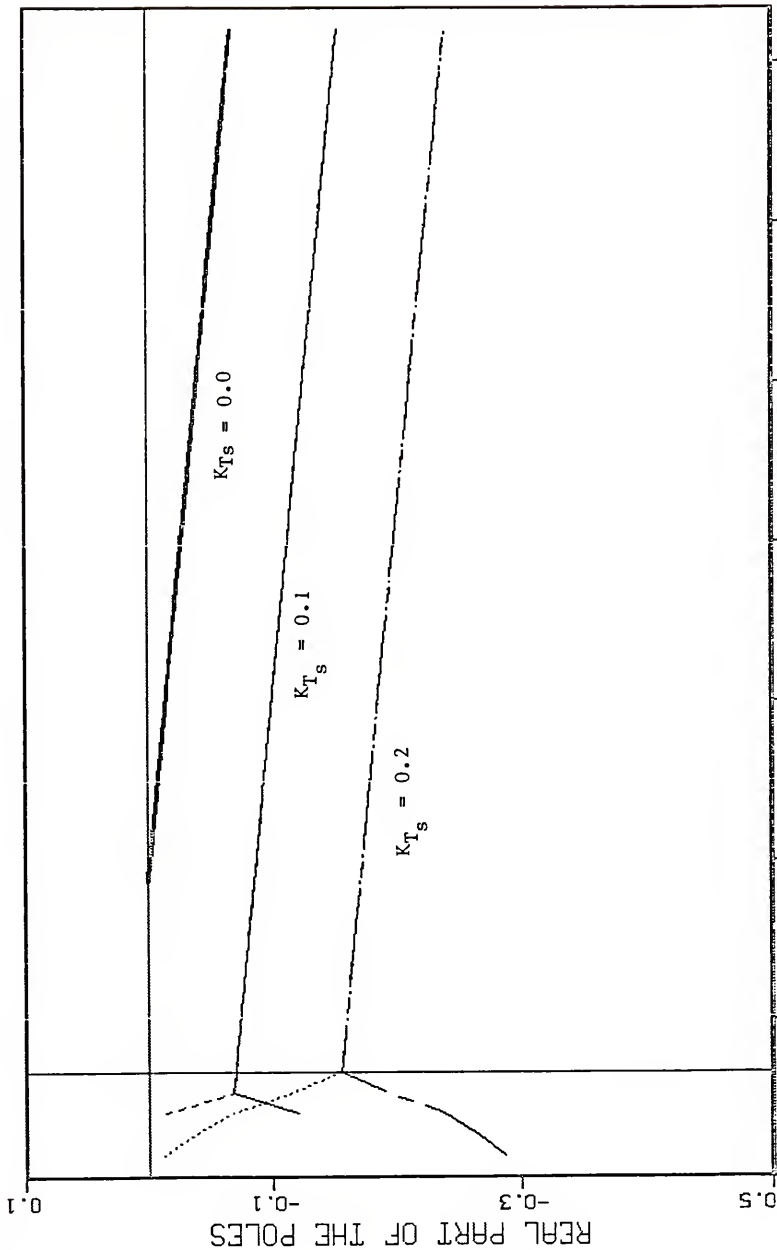

Figure 4-25. Closed-loop pole variation with feedback fraction. T_{s_o} = 75 keV, constant confinement, kT = 20 keV.

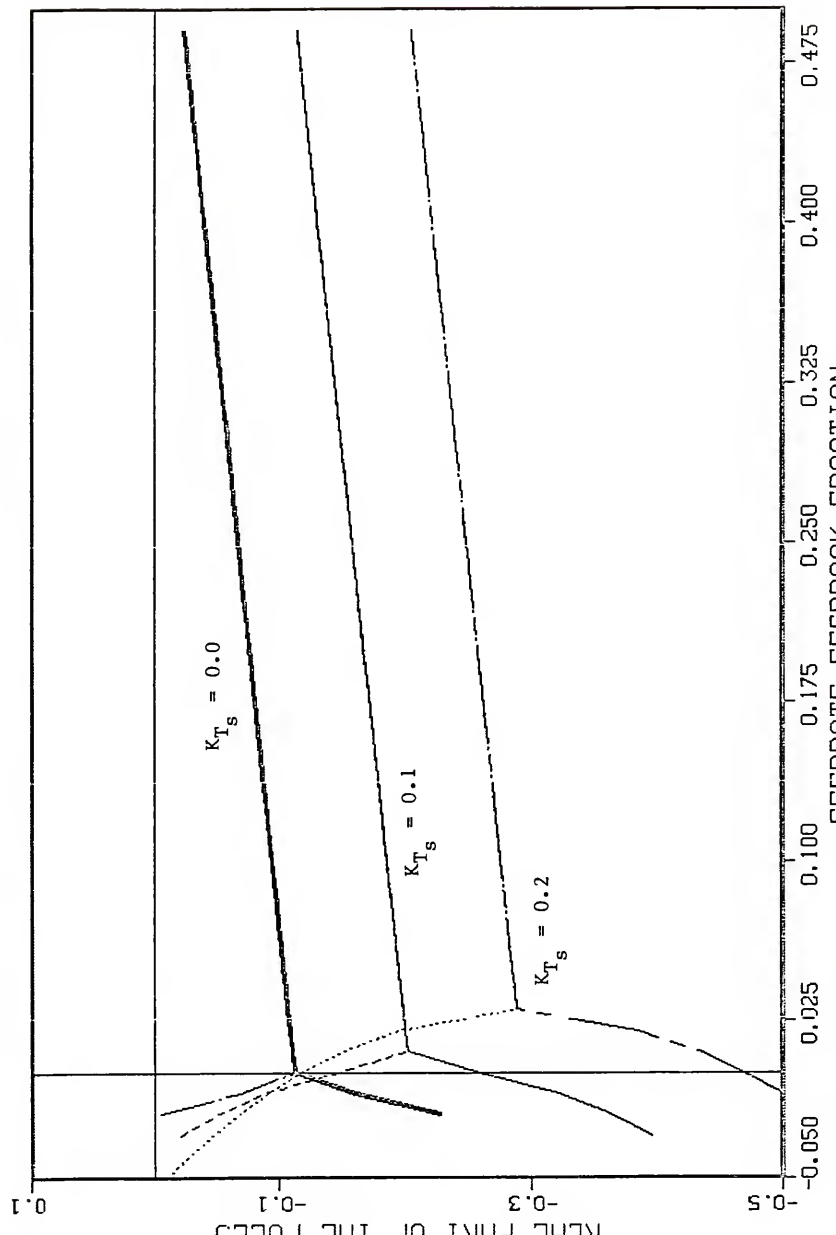

Figure 4-26. Closed-loop pole variation with feedback fraction. T_{s_o} = 75 keV, constant confinement, kT = 30 keV.

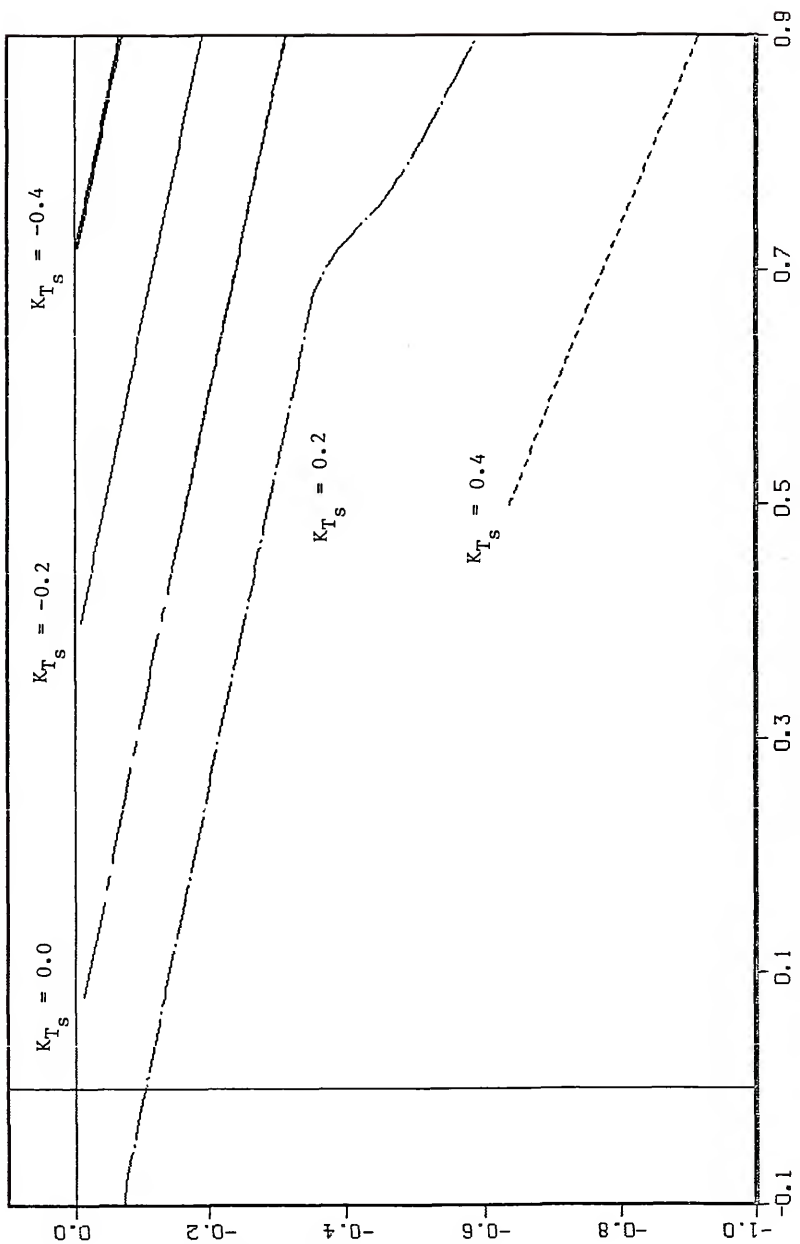

Figure 4-27. Closed-loop pole variation with feedback fraction. T_{s_o} = 75 keV, Bohm confinement, kT = 10 keV.

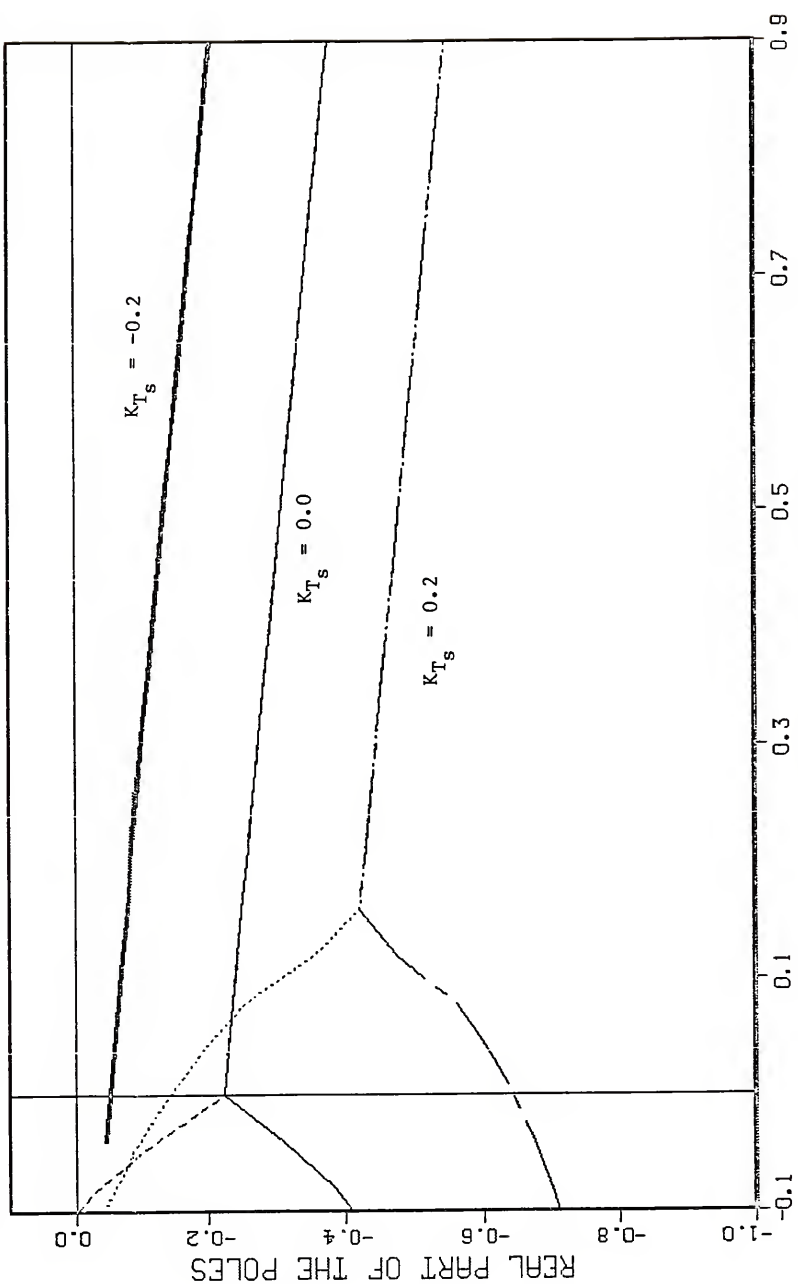

Figure 4-28. Closed-loop pole variation with feedback fraction. T_{s_o} = 75 keV, Bohm confinement, kT = 20 keV.

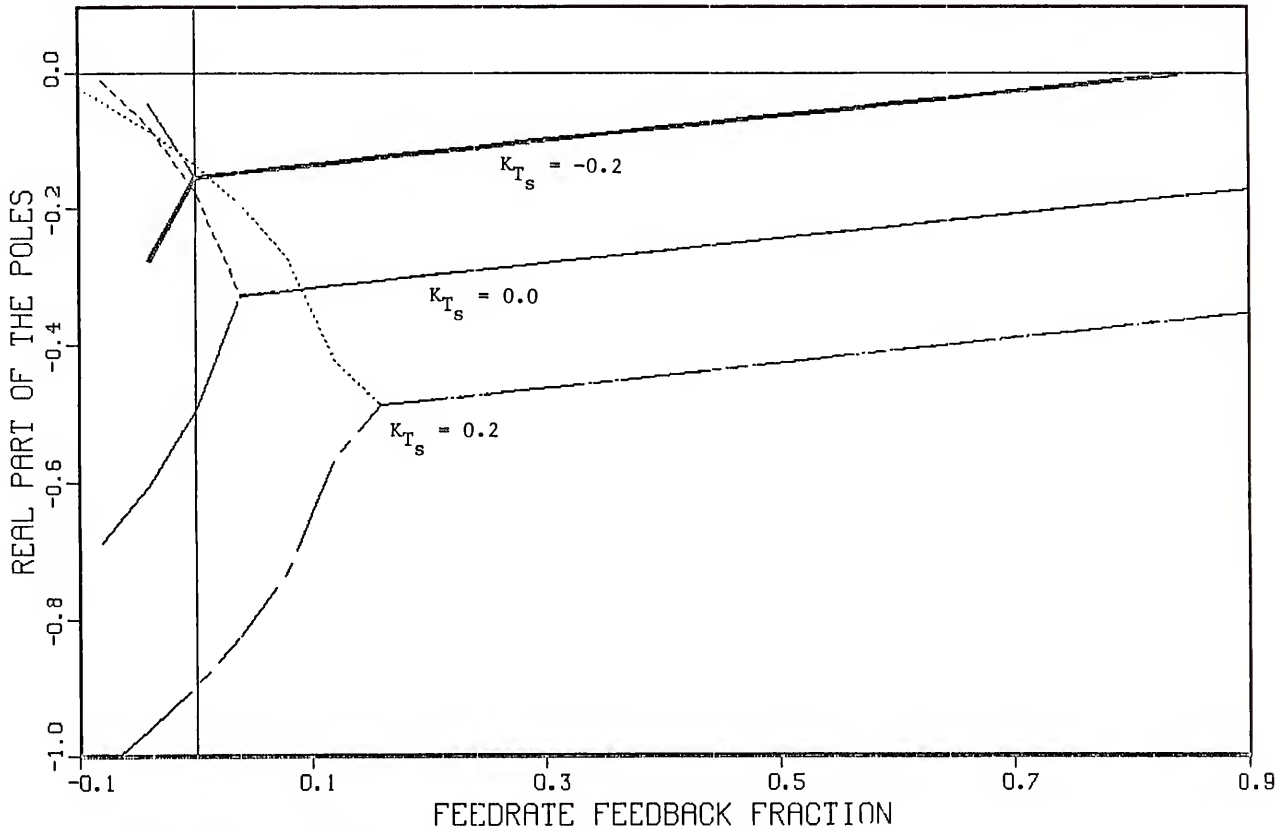

Figure 4-29. Closed-loop pole variation with feedback fraction. T_{s_o} = 75 keV, Bohm confinement, kT = 30 keV.

The next section presents the system performance for operation within the stabilized regime. The information presented provides the basis for choosing the feedback coefficients so as to achieve the desired system response.

4.2. Closed-Loop System Performance

The thermal behavior of a fusioning plasma has been shown to be unstable below the critical temperature. Section 3.1 presented a method of determining critical temperatures for a wide variety of operating parameters. In the majority of cases, even in the stable regime, the characteristics and classical control specifications of the open-loop system were shown to be unacceptable in Section 3.2. The previous section has shown how feedrate and injection energy feedback can be used to stabilize the plasma burn below the critical temperature. This was accomplished by controlling the position of the closed-loop poles. Stable system performance was found for a broad range of the feedback fraction. This section presents the variation in system performance with feedback fraction. The results can be used to choose the feedback coefficients so as to produce the desired plasma temporal response in the stabilized region and to improve the system response above the critical temperature. The time domain specifications are presented first and are shown in Figures 4-30 to 4-61. These are followed by the frequency domain specifications in Figures 4-62 to 4-85.

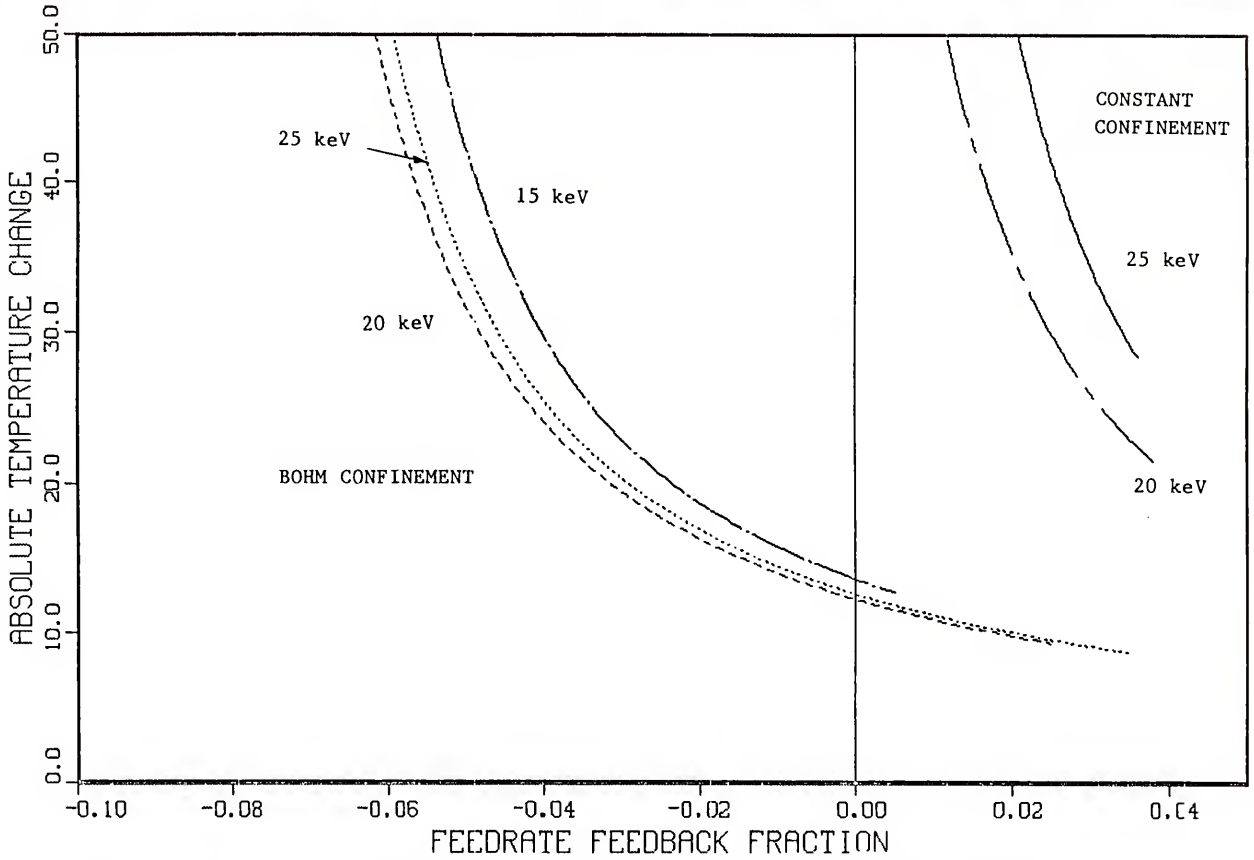

Figure 4-30. Absolute temperature change of the closed-loop transfer function versus feedback fraction, following a step input. T_{s_o} = 0, constant and Bohm confinement.

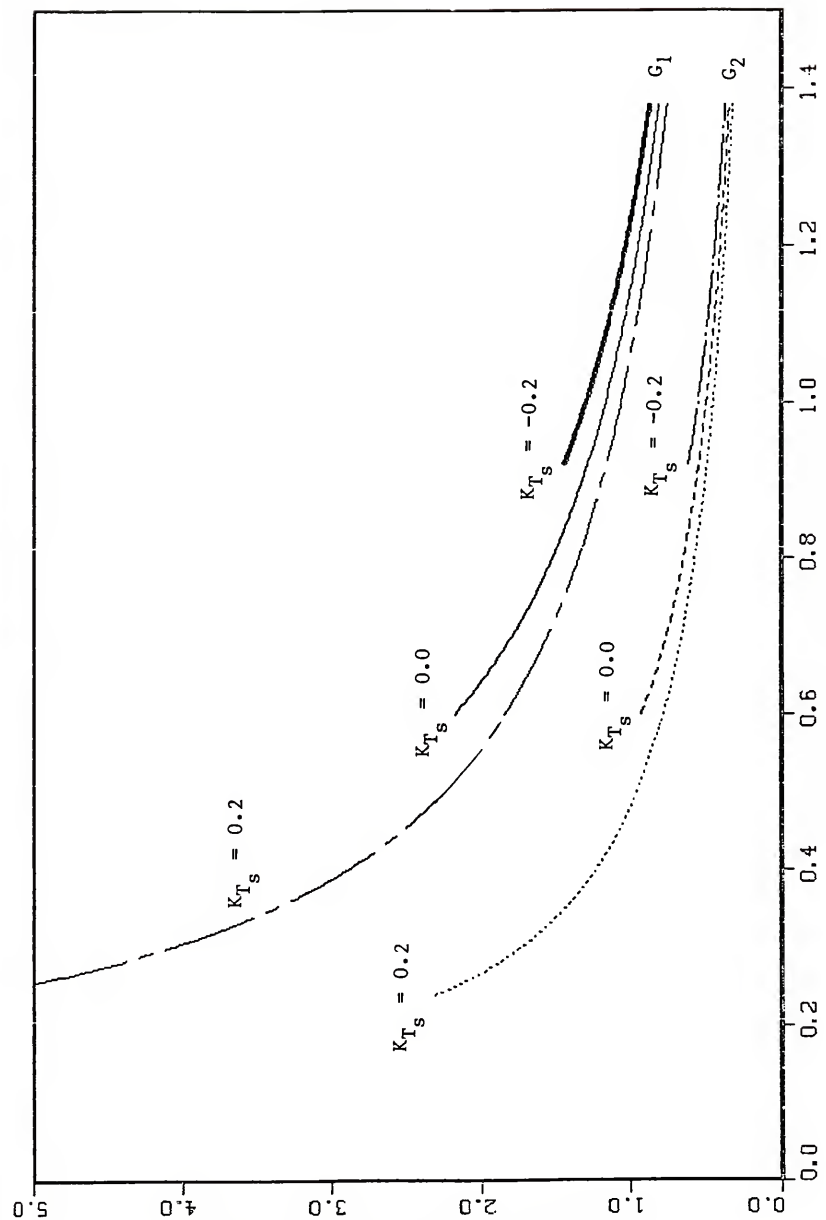

Figure 4-31. Absolute temperature change of the closed-loop transfer function versus feedback fraction, following a step input. T_{s_o} = 75 keV, constant confinement, kT = 10 keV.

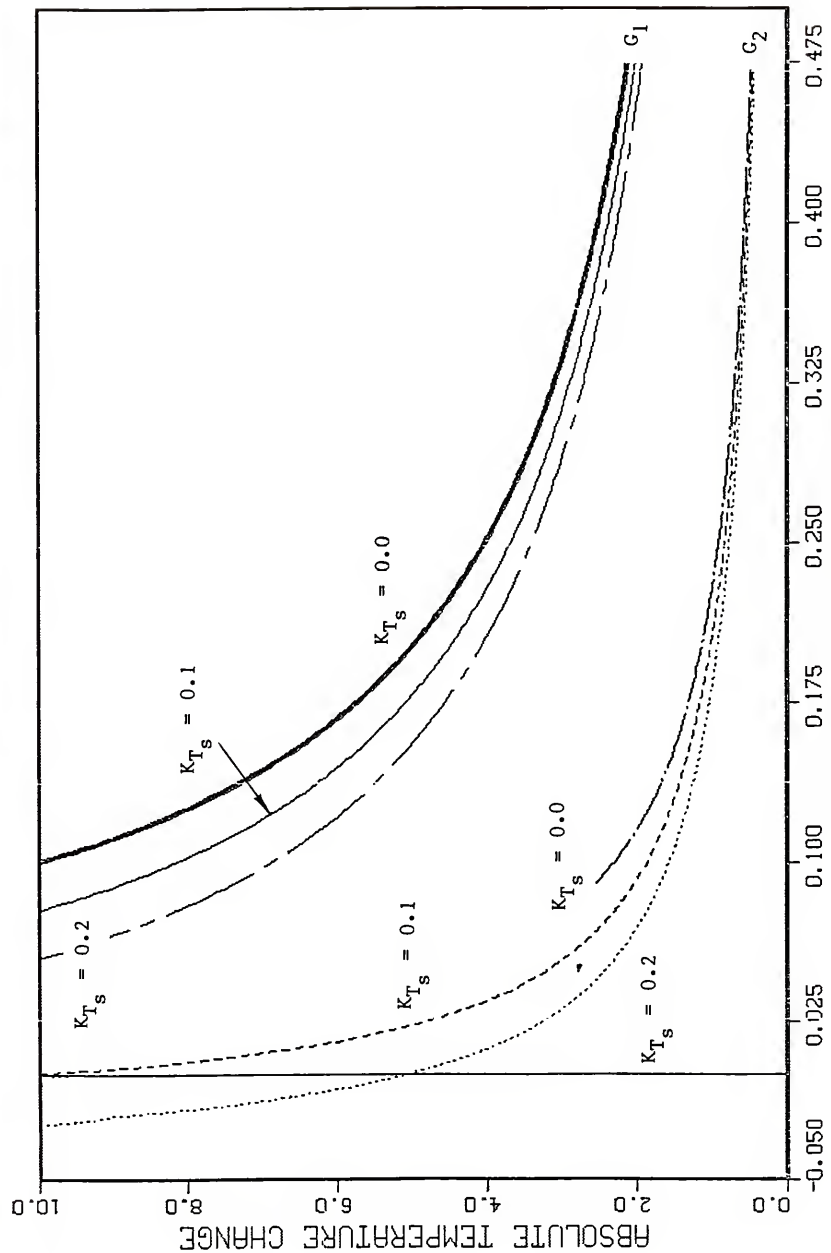

Figure 4-32. Absolute temperature change of the closed-loop transfer function versus feedback fraction, following a step input. T_{s_o} = 75 keV, constant confinement, kT = 20 keV.

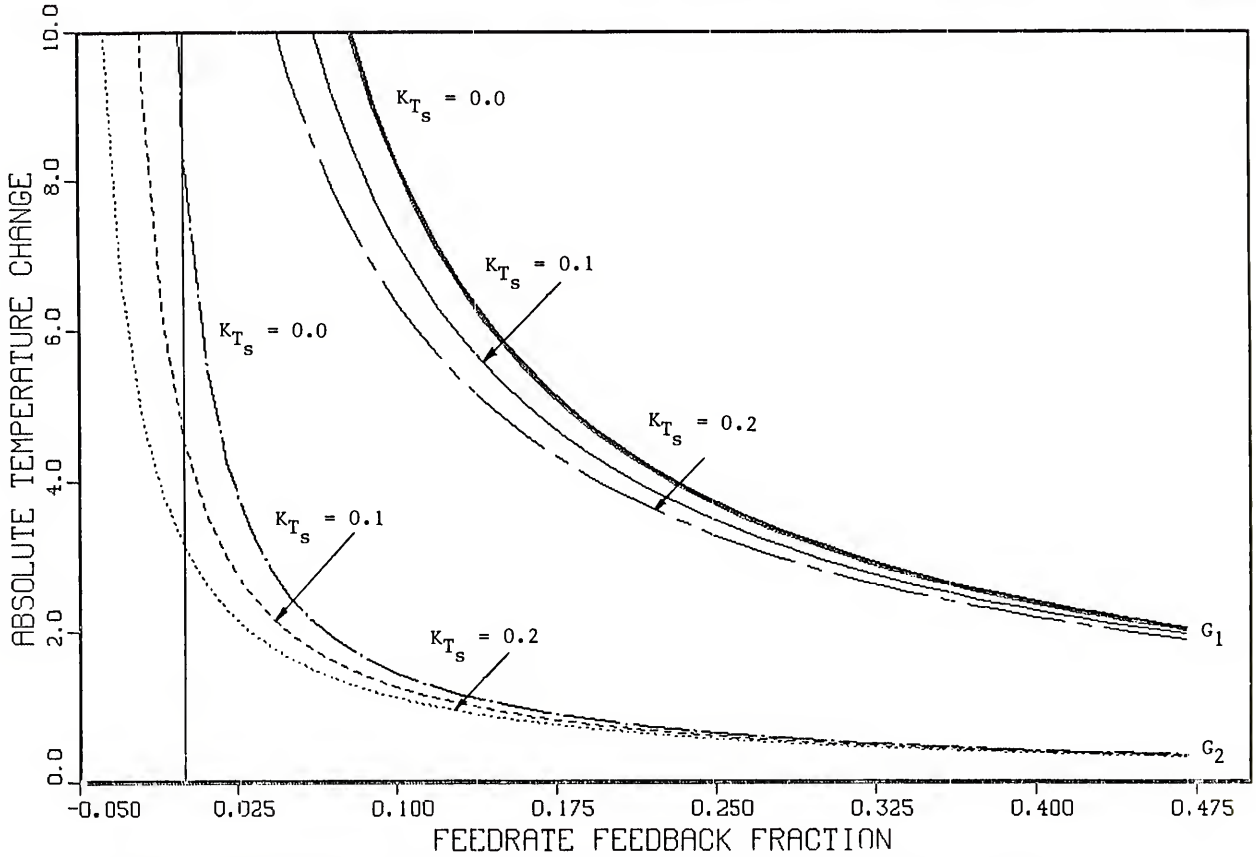

Figure 4-33. Absolute temperature change of the closed-loop transfer function versus feedback fraction, following a step input. T_{s_o} = 75 keV, constant confinement, kT = 30 keV.

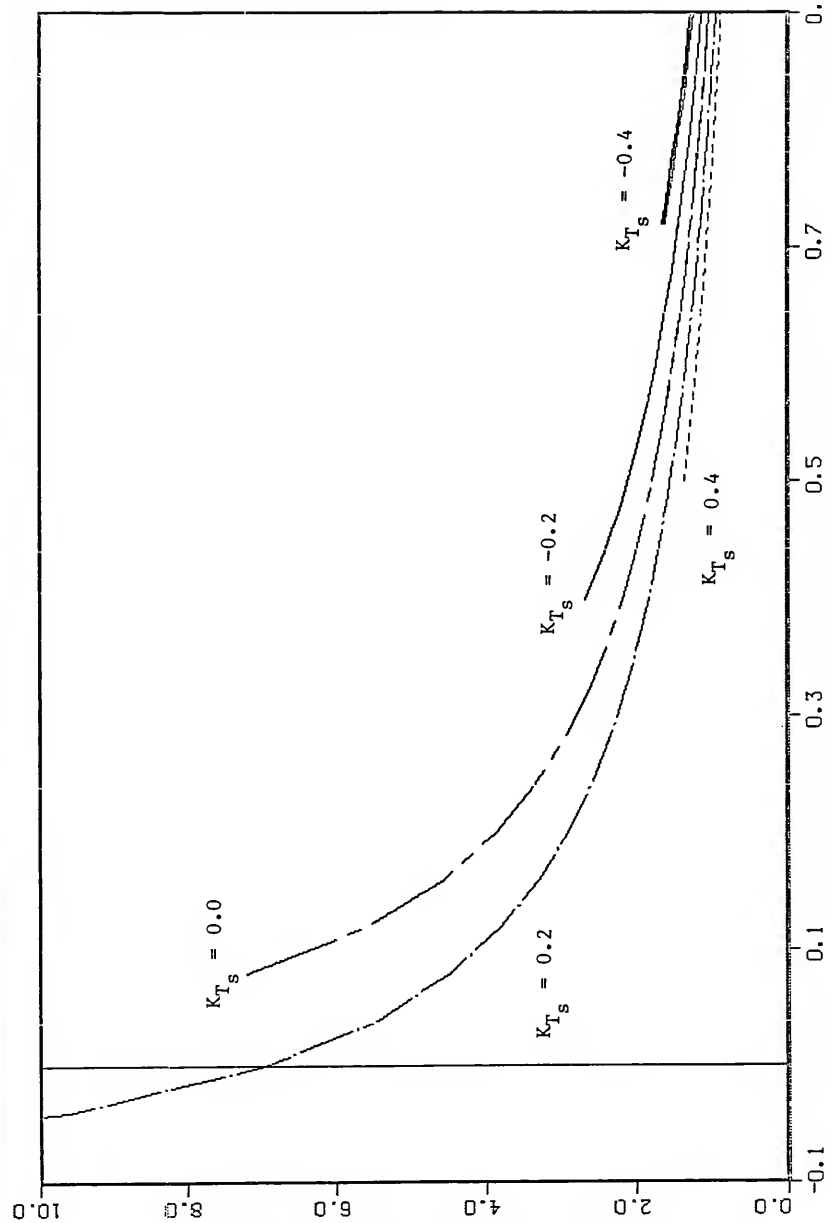

Figure 4-34. Absolute temperature change of the closed-loop transfer function G_1 versus feedback fraction, following a step input. T_{s_o} = 75 keV, Bohm confinement, kT = 10 keV.

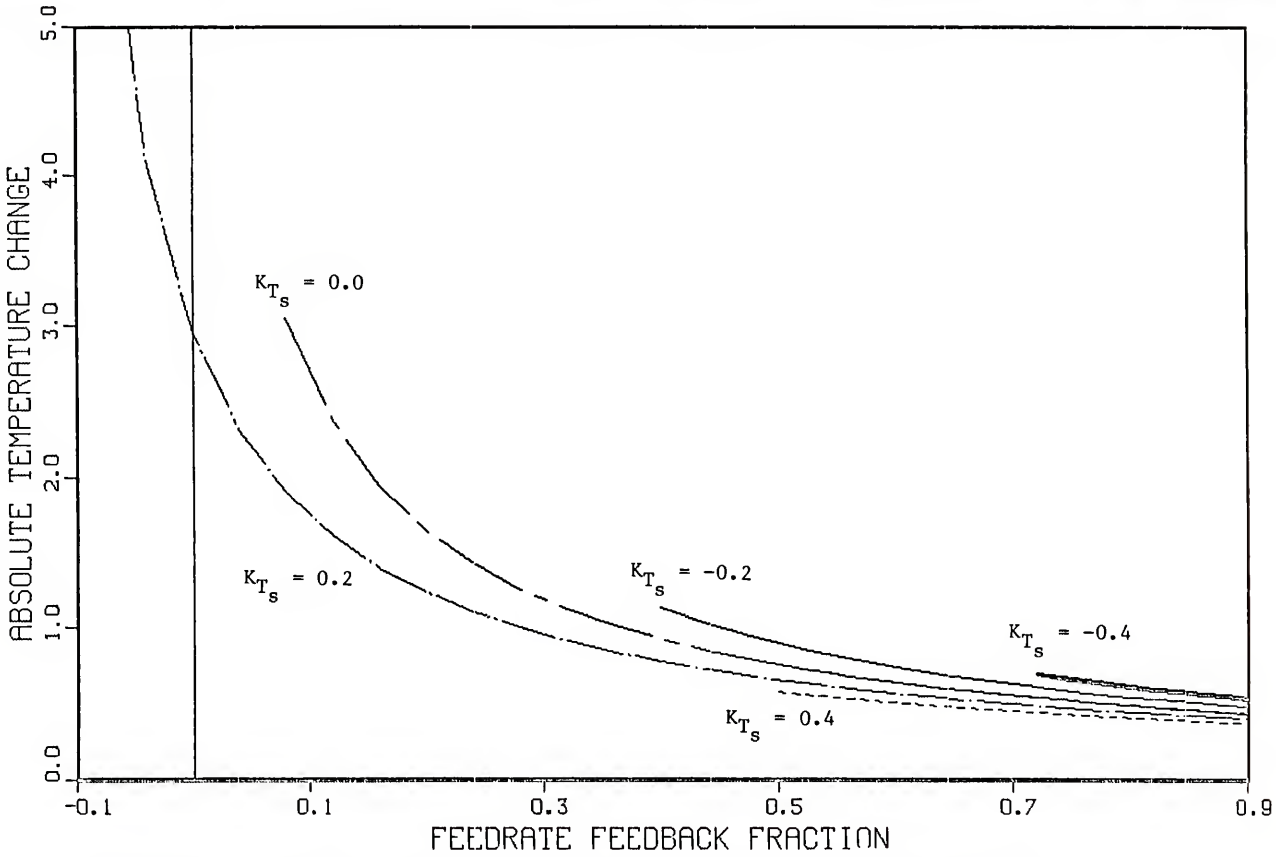

Figure 4-35. Absolute temperature change of the closed-loop transfer function G_2 versus feedback fraction, following a step input. T_{s_o} = 75 keV, Bohm confinement, kT = 10 keV.

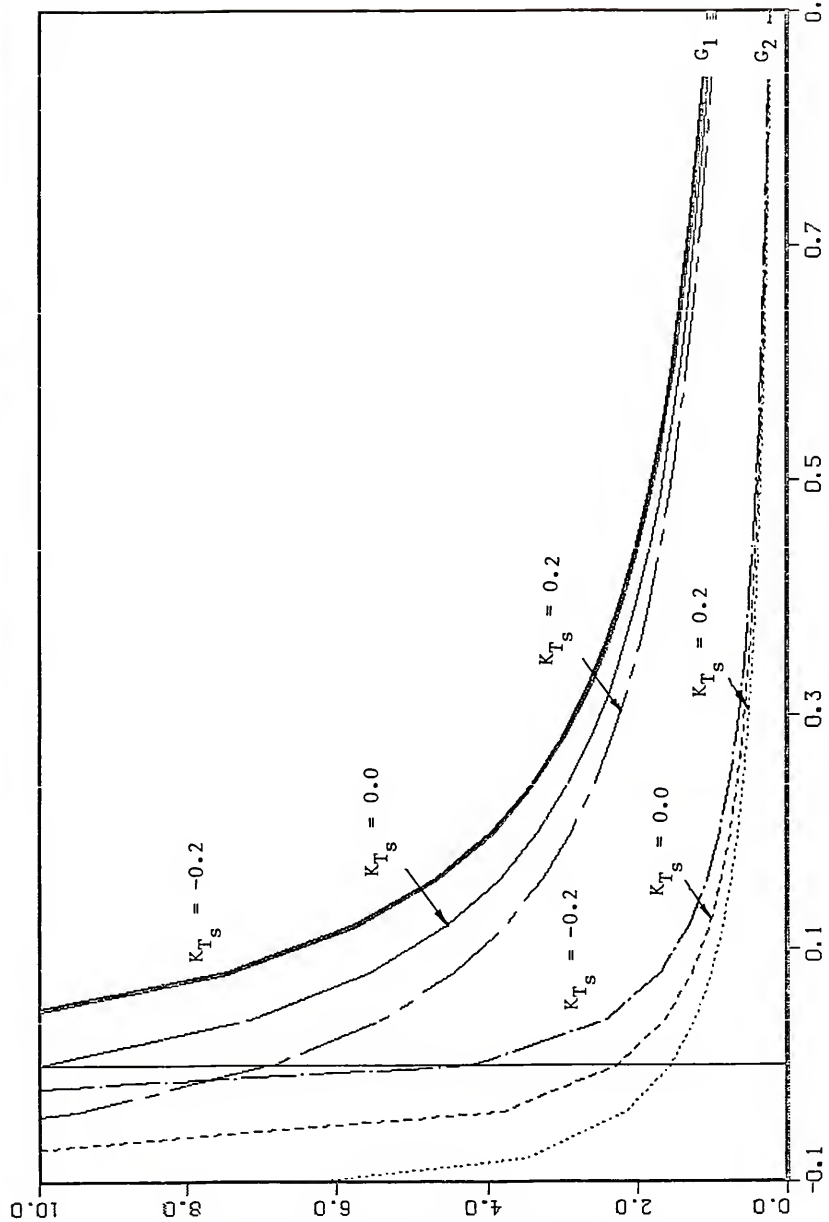

Figure 4-36. Absolute temperature change of the closed-loop transfer function versus feedback fraction, following a step input. T_{s_o} = 75 keV, Bohm confinement, kT = 20 keV.

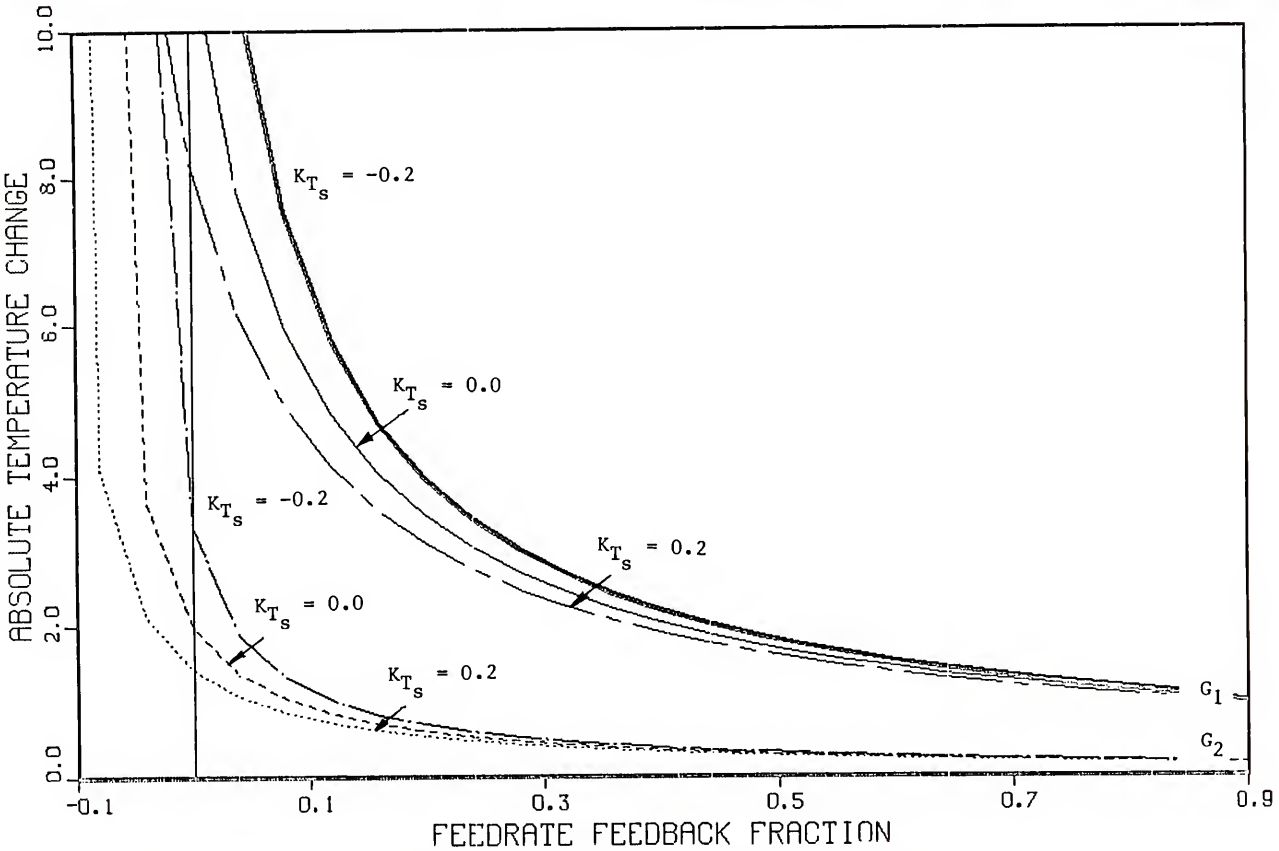

Figure 4-37. Absolute temperature change of the closed-loop transfer function versus feedback fraction, following a step input. T_{s_o} = 75 keV, Bohm confinement, kT = 30 keV.

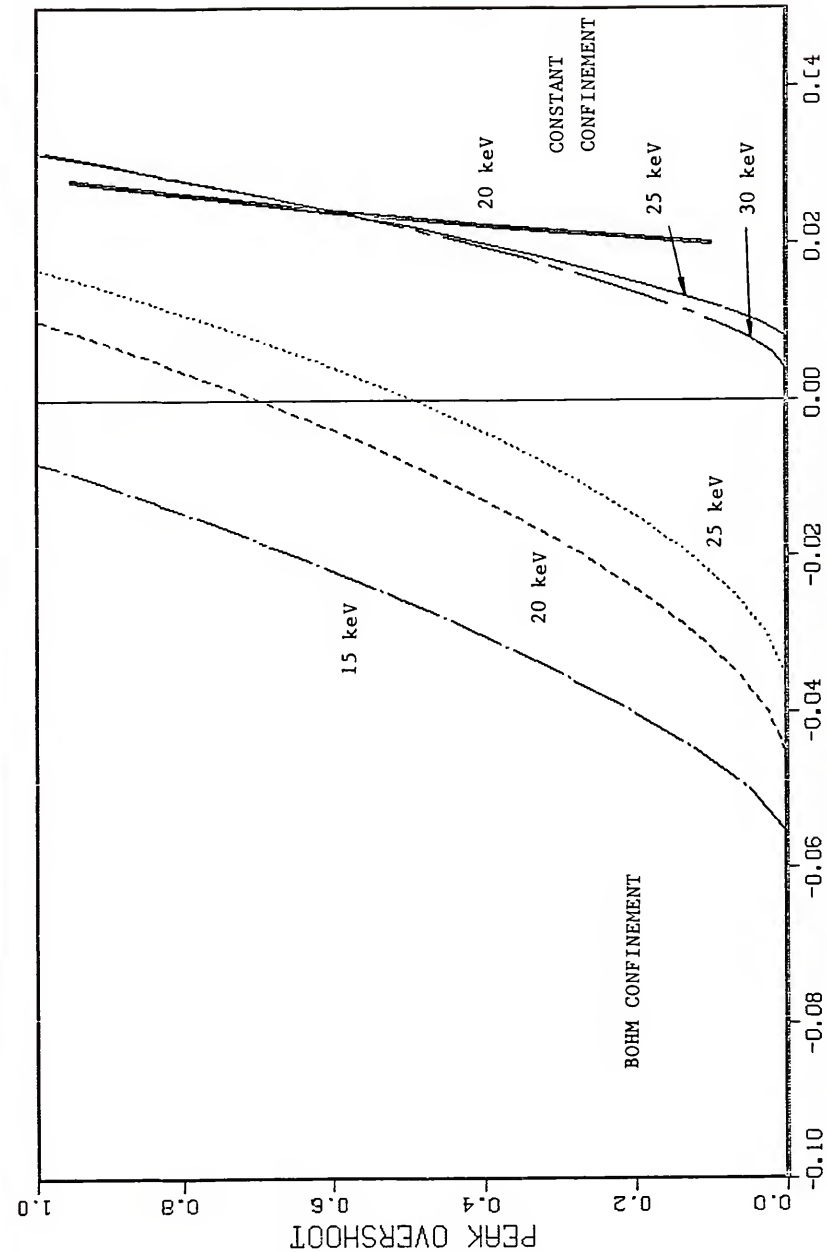

Figure 4-38. Peak overshoot of the closed-loop transfer function versus feedback fraction, following a step input. T_{s_o} = 0, constant and Bohm confinement.

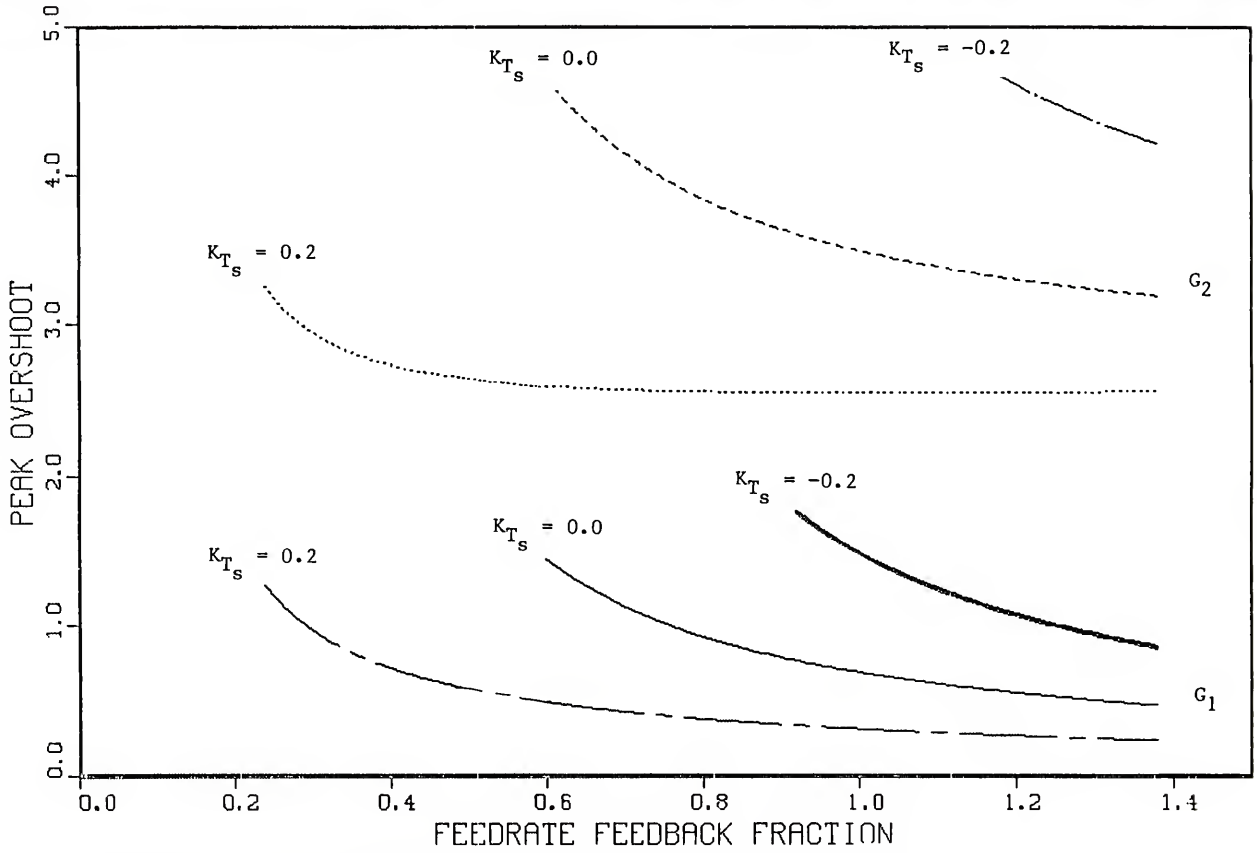

Figure 4-39. Peak overshoot of the closed-loop transfer function versus feedback fraction, following a step input. T_{s_o} = 75 keV, constant confinement, kT = 10 keV.

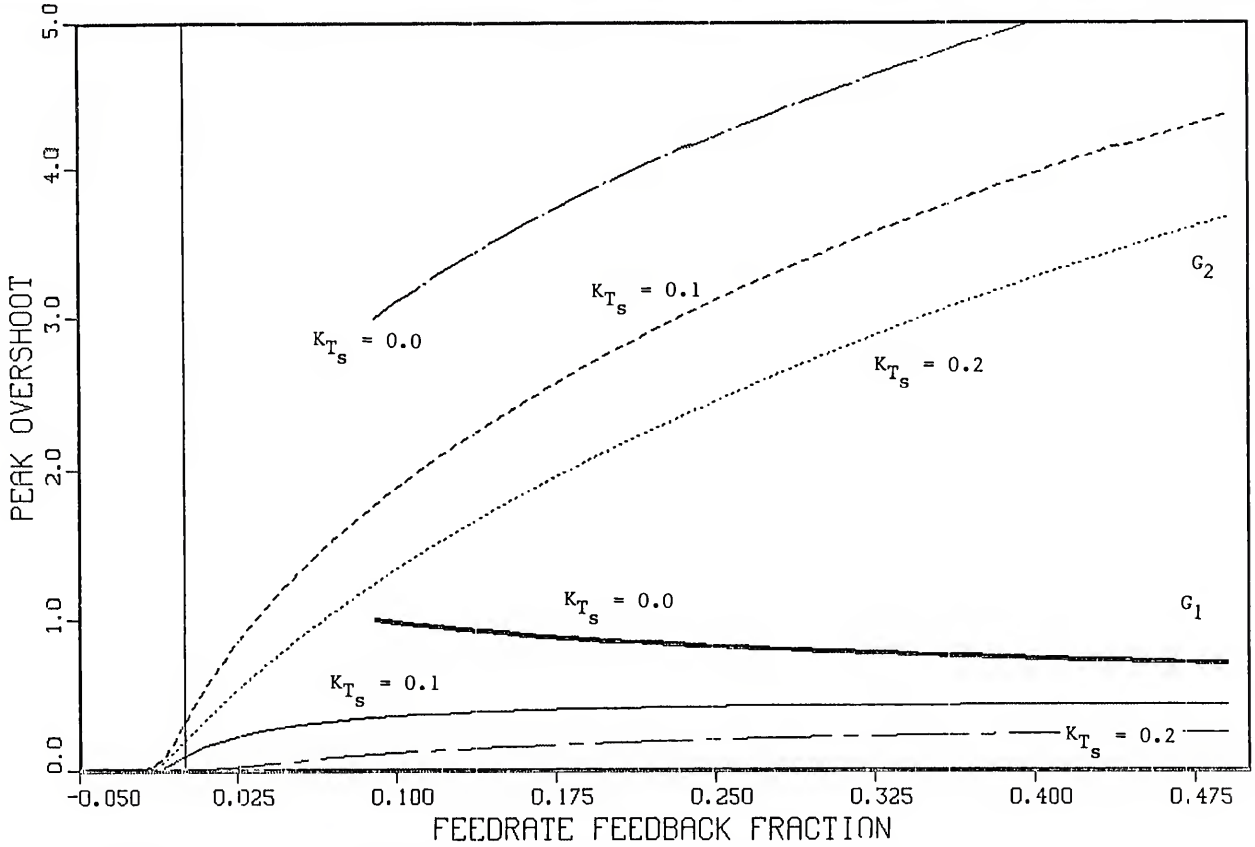

Figure 4-40. Peak overshoot of the closed-loop transfer function versus feedback fraction, following a step input. T_{s_o} = 75 keV, constant confinement, kT = 20 keV.

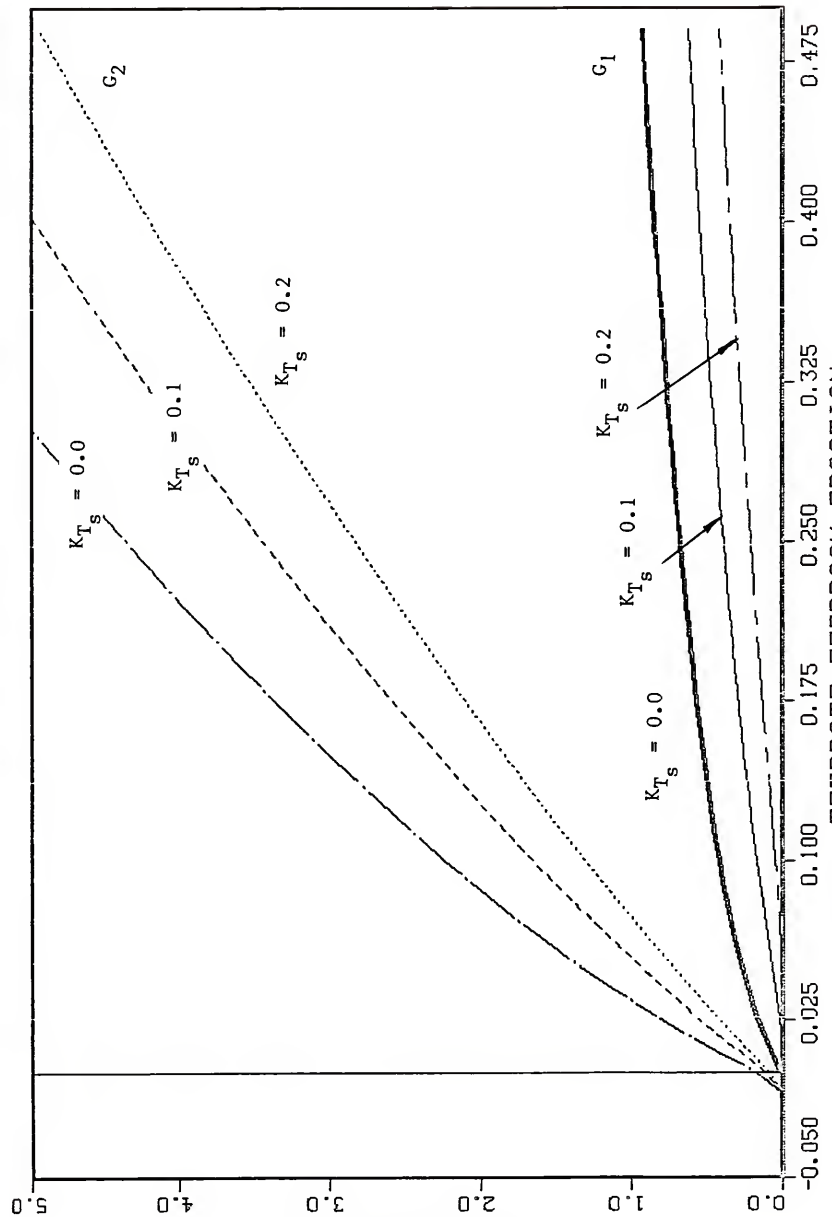

Figure 4-41. Peak overshoot of the closed-loop transfer function versus feedback fraction, following a step input. T_{s_o} = 75 keV, constant confinement, kT = 30 keV.

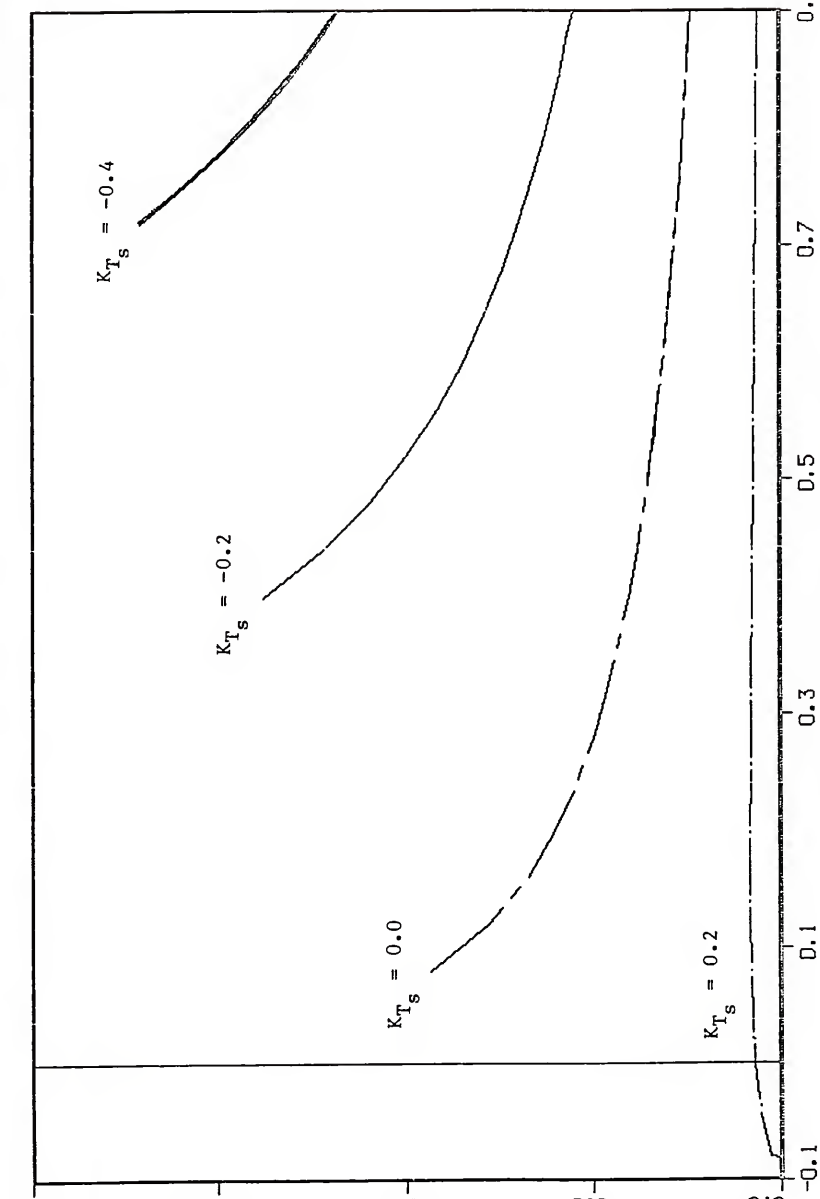

Figure 4-42. Peak overshoot of the closed-loop transfer function G_1 versus feedback fraction, following a step input. T_{s_o} = 75 keV, Bohm confinement, kT = 10 keV.

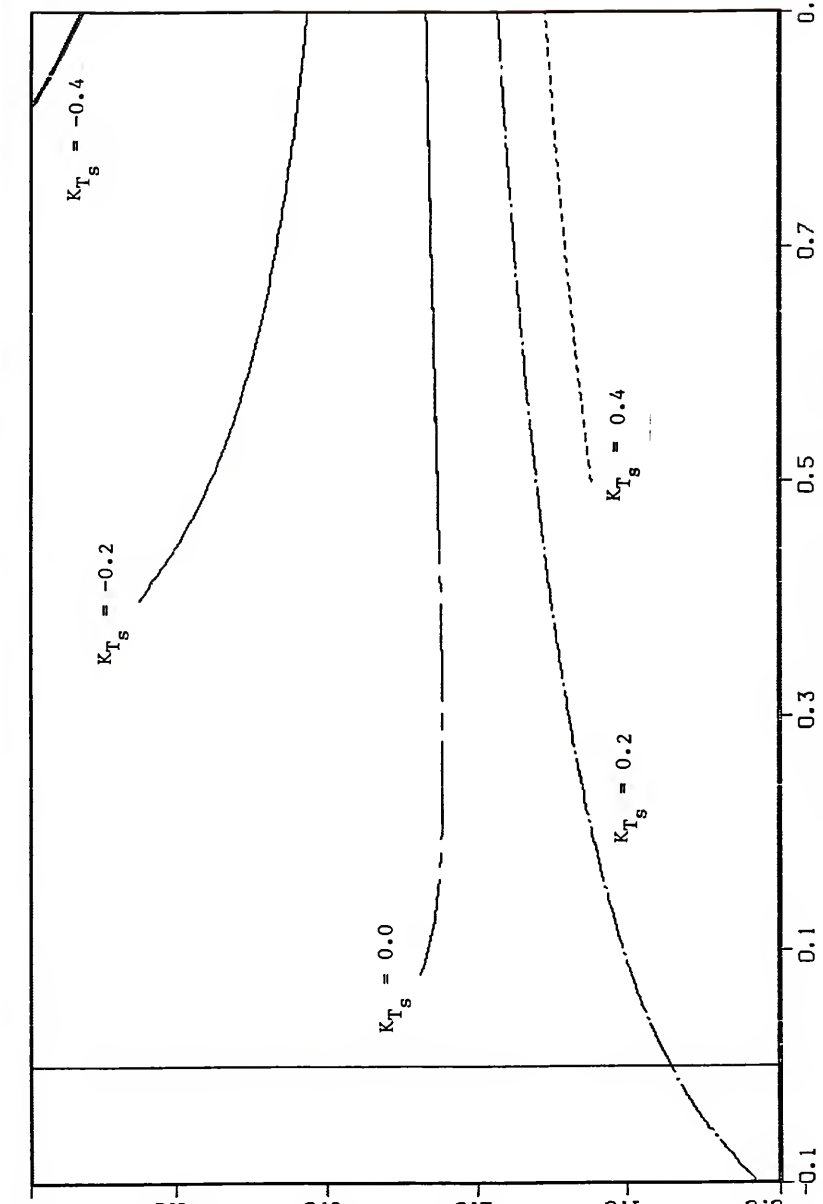

Figure 4-43. Peak overshoot of the closed-loop transfer function G_2 versus feedback fraction, following a step input. T_{s_o} = 75 keV, Bohm confinement, kT = 10 keV.

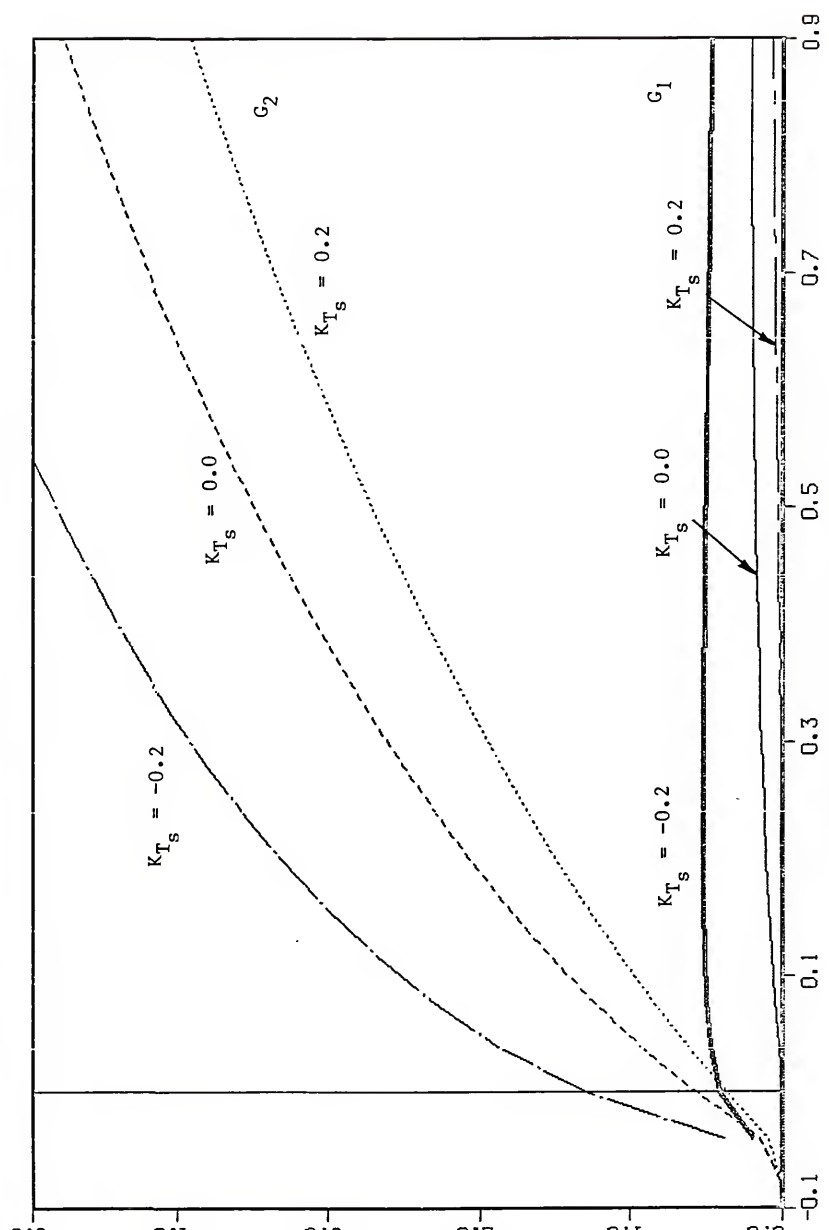

Figure 4-44. Peak overshoot of the closed-loop transfer function versus feedback fraction, following a step input. T_{s_o} = 75 keV, Bohm confinement, kT = 20 keV.

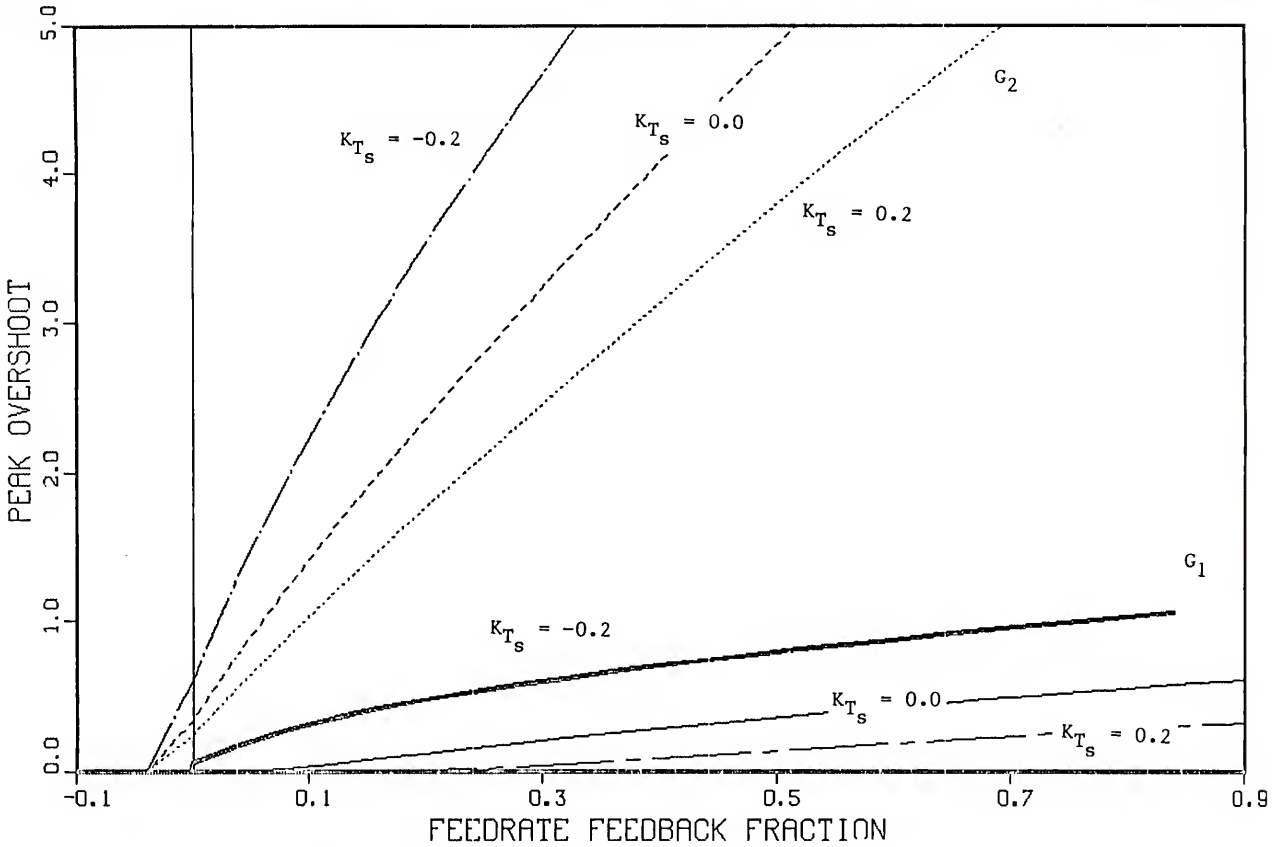

Figure 4-45. Peak overshoot of the closed-loop transfer function versus feedback fraction, following a step input. T_{s_o} = 75 keV, Bohm confinement, kT = 30 keV.

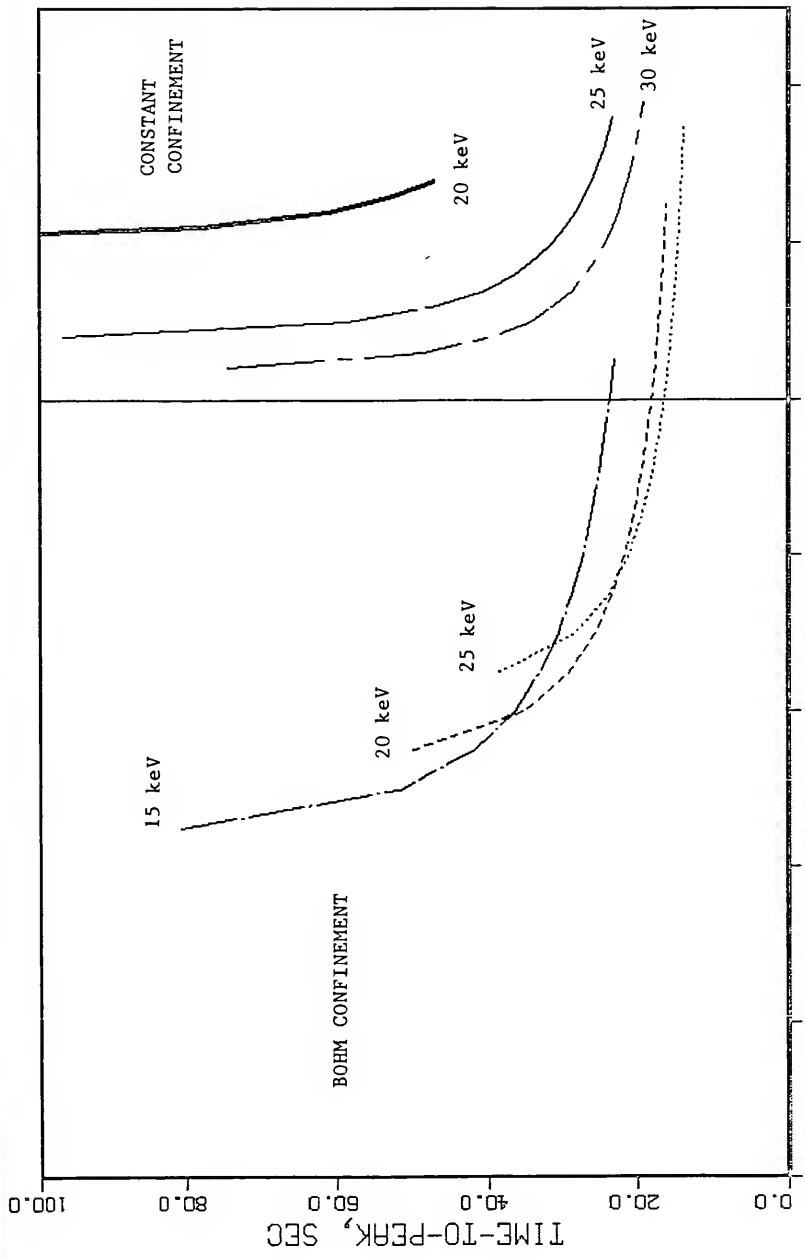

Figure 4-46. Time-to-peak of the closed-loop transfer function versus feedback fraction, following a step input. T_{s_o} = 0, constant and Bohm confinement.

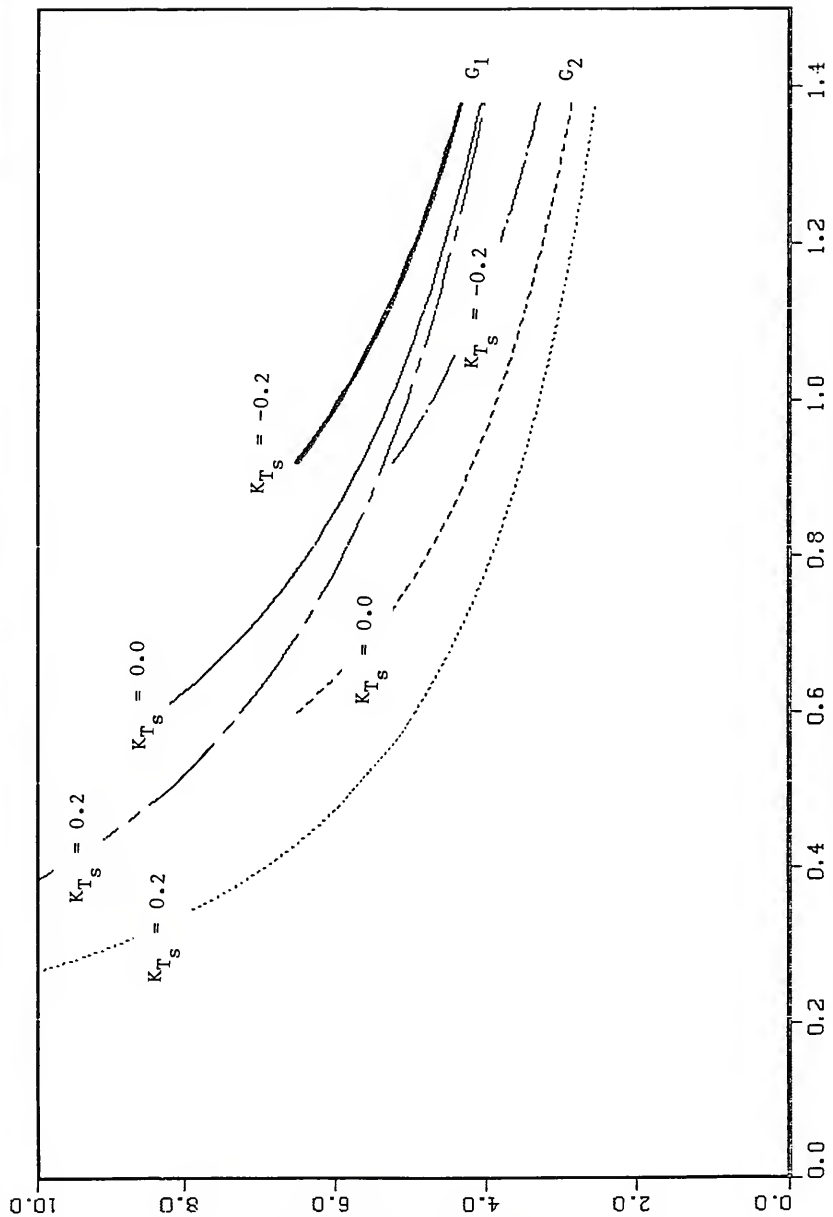

Figure 4-47. Time-to-peak of the closed-loop transfer function versus feedback fraction, following a step input. T_{s_o} = 75 keV, constant confinement, kT = 10 keV.

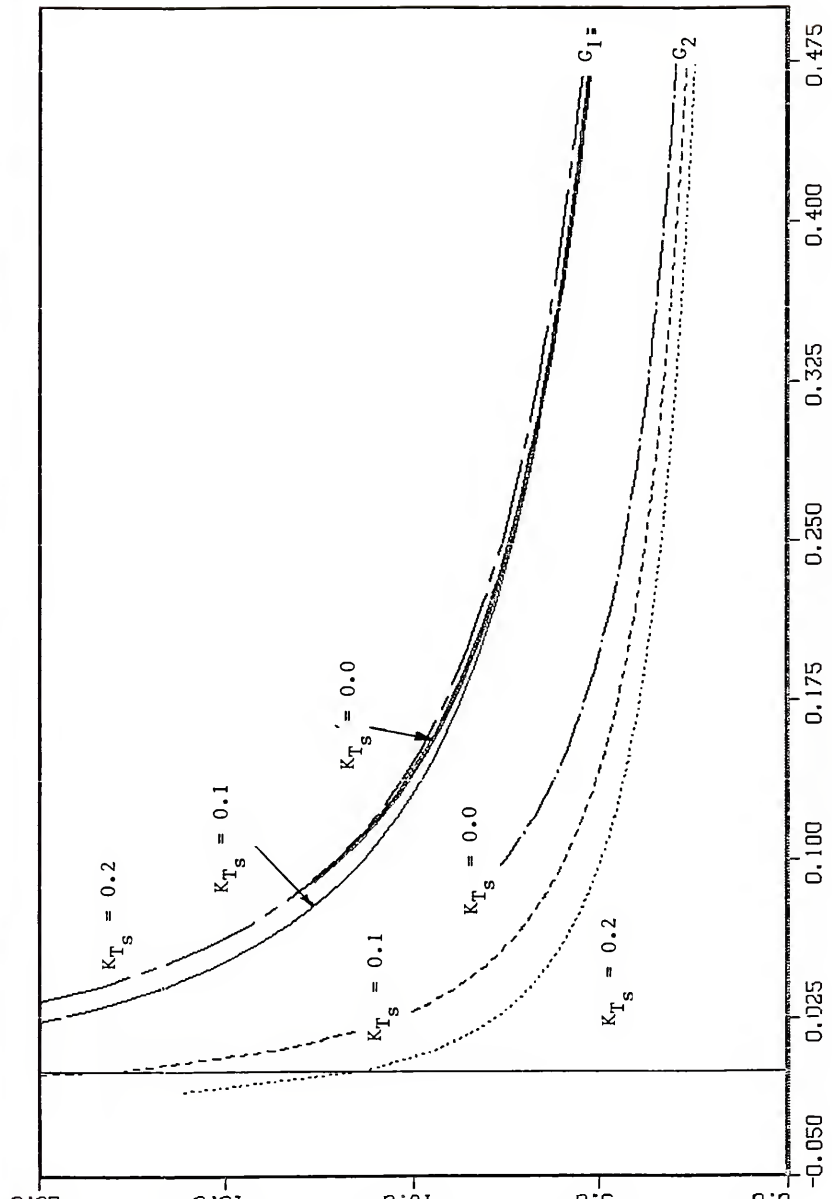

Figure 4-48. Time-to-peak of the closed-loop transfer function versus feedback fraction, following a step input. T_{s_o} = 75 keV, constant confinement, kT = 20 keV.

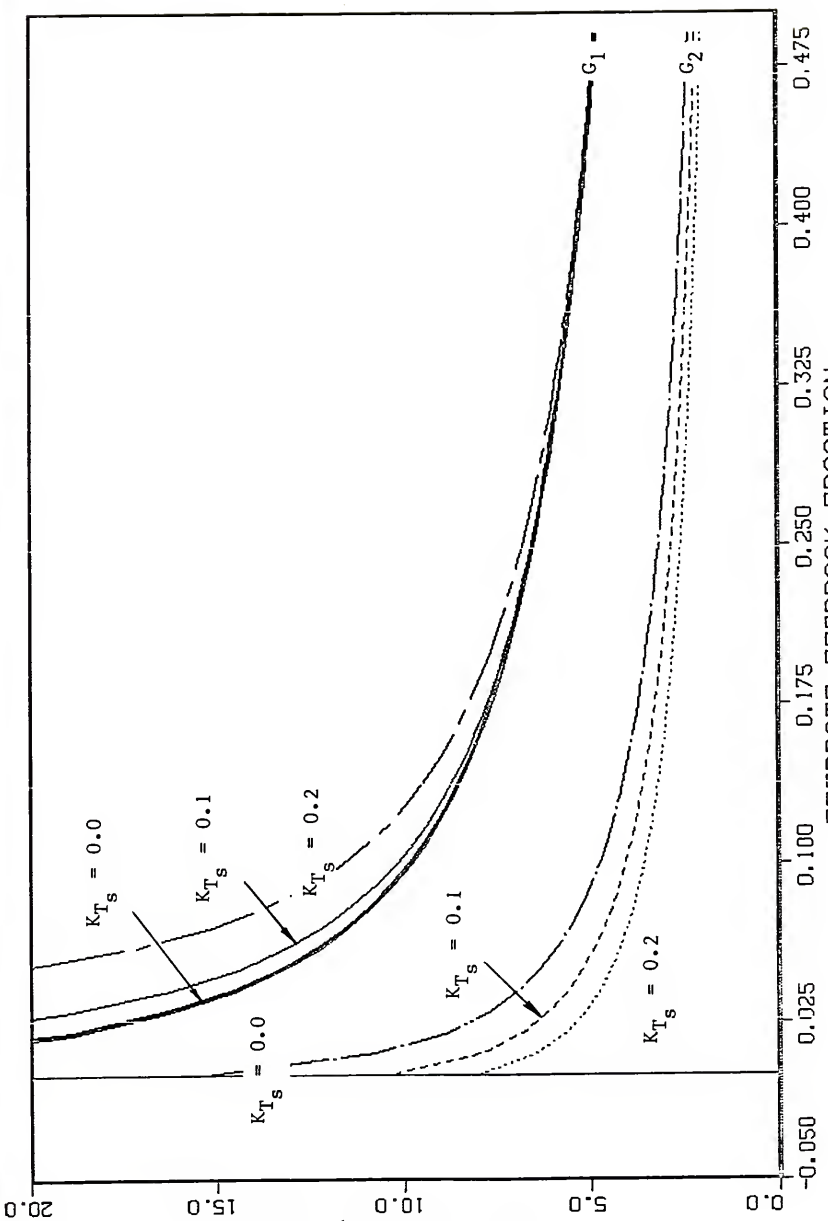

Figure 4-49. Time-to-peak of the closed-loop transfer function versus feedback fraction, following a step input. T_{s_o} = 75 keV, constant confinement, kT = 30 keV.

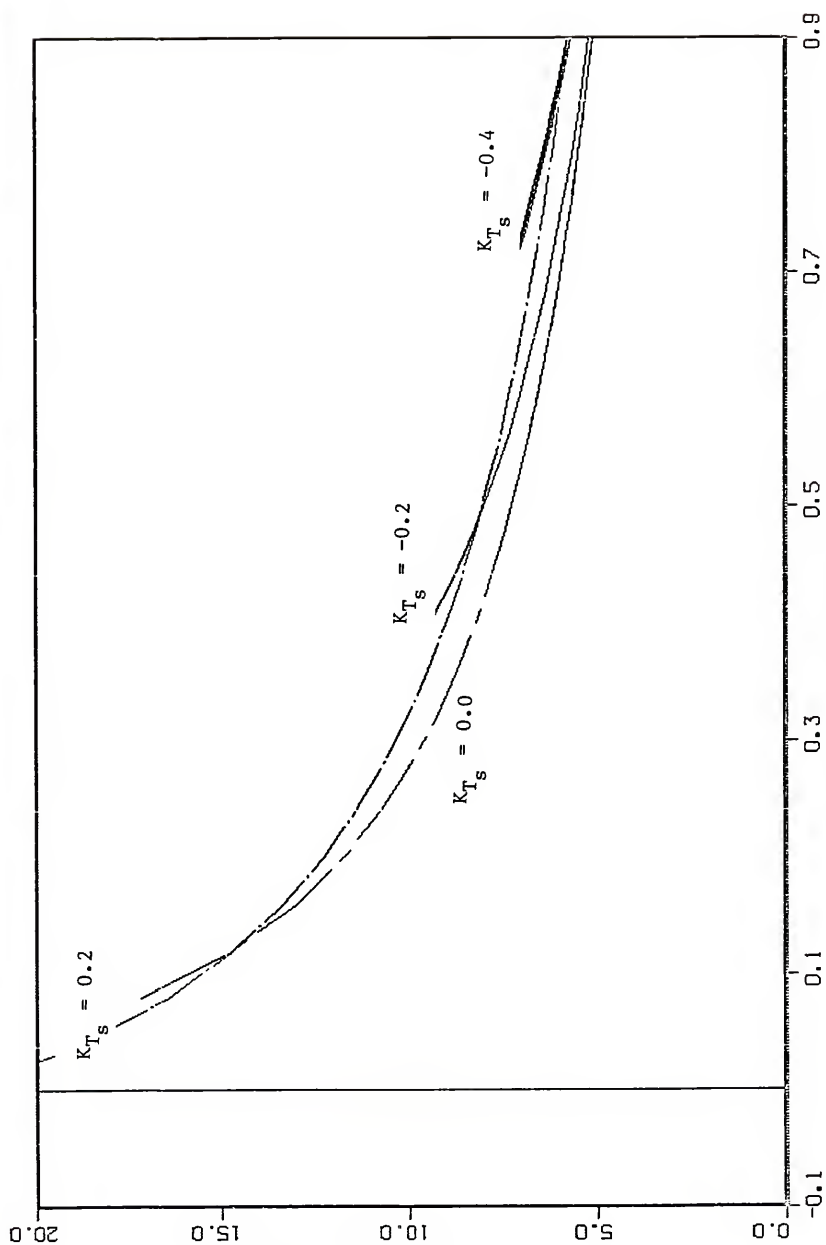

Figure 4-50. Time-to-peak of the closed-loop transfer function G_1 versus feedback fraction, following a step input. T_{s_o} = 75 keV, Bohm confinement, kT = 10 keV.

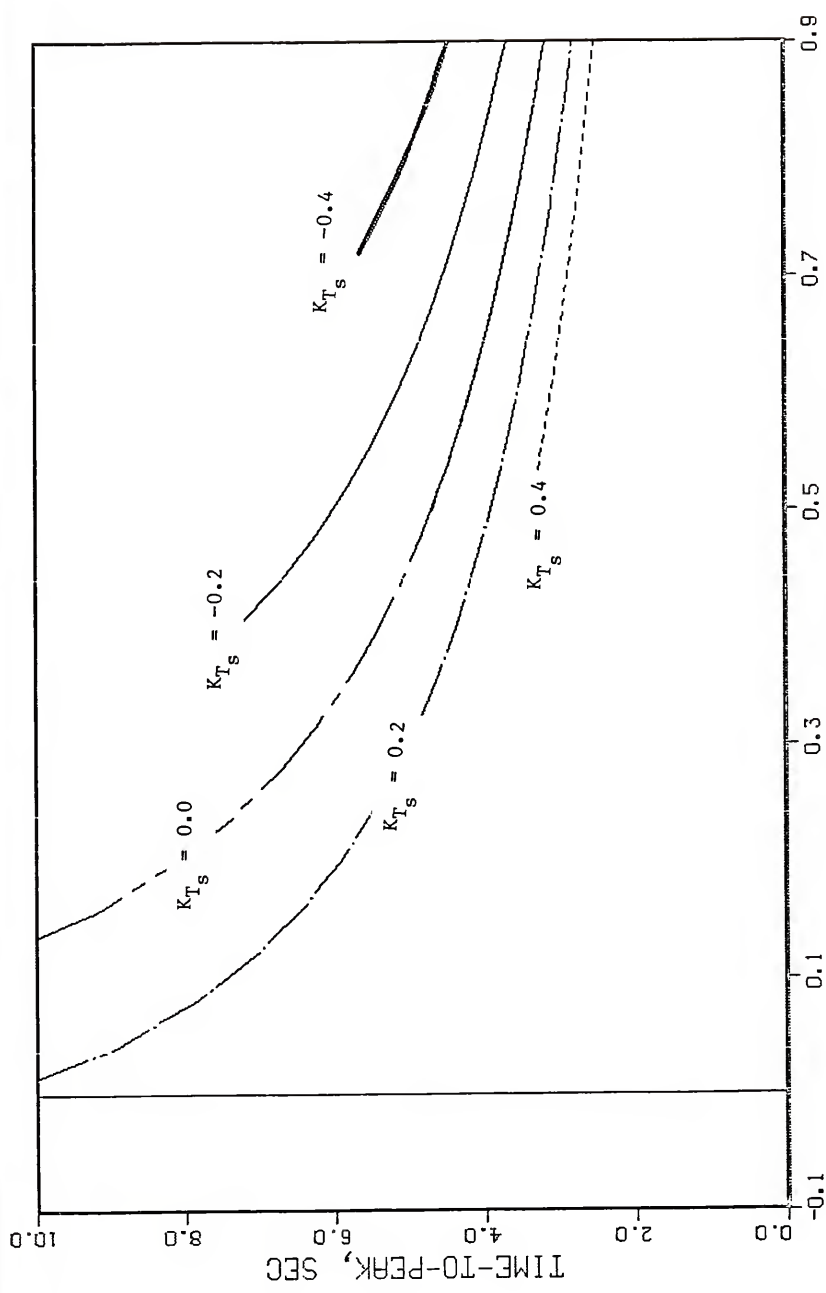

Figure 4-51. Time-to-peak of the closed-loop transfer function G_2 versus feedback fraction, following a step input. T_{s_o} = 75 keV, Bohm confinement, kT = 10 keV.

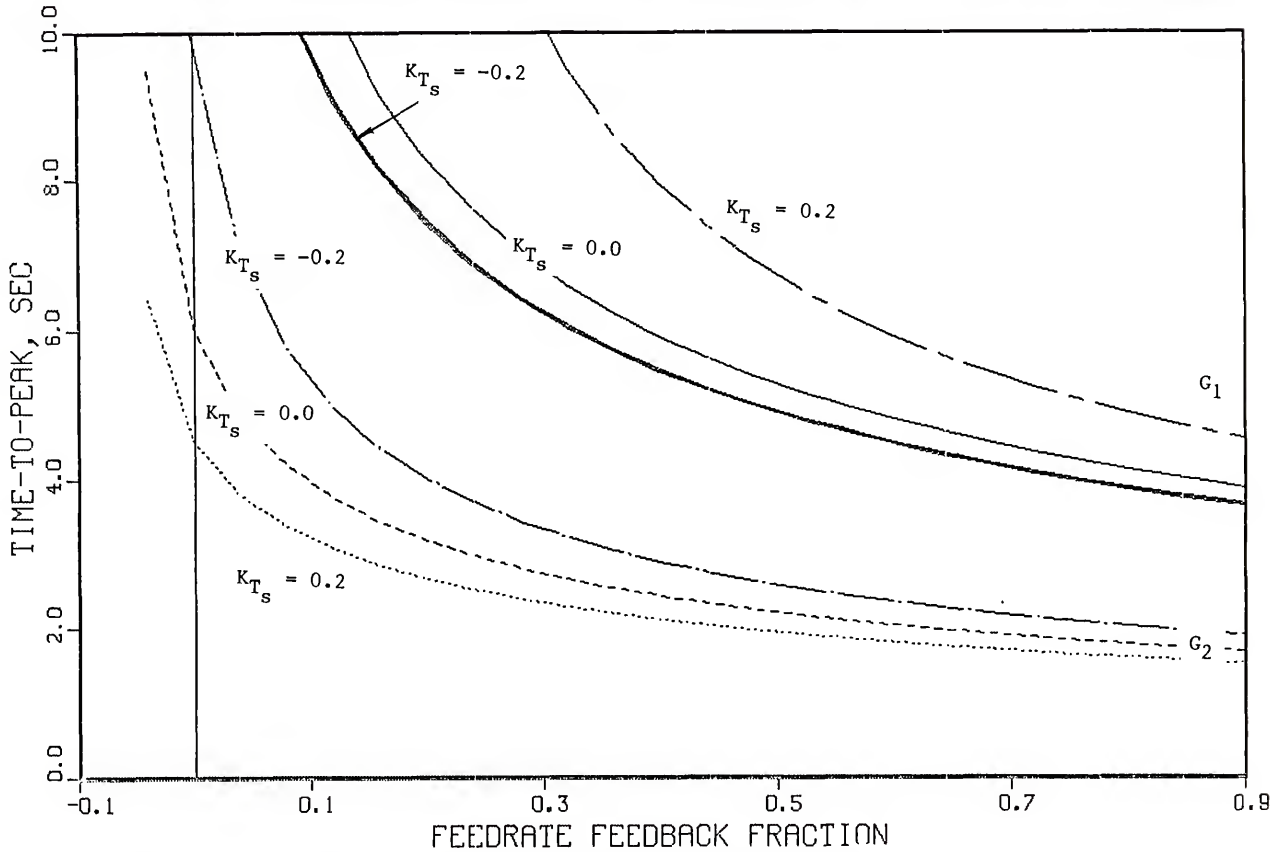

Figure 4-52. Time-to-peak of the closed-loop transfer function versus feedback fraction, following a step input. T_{s_o} = 75 keV, Bohm confinement, kT = 20 keV.

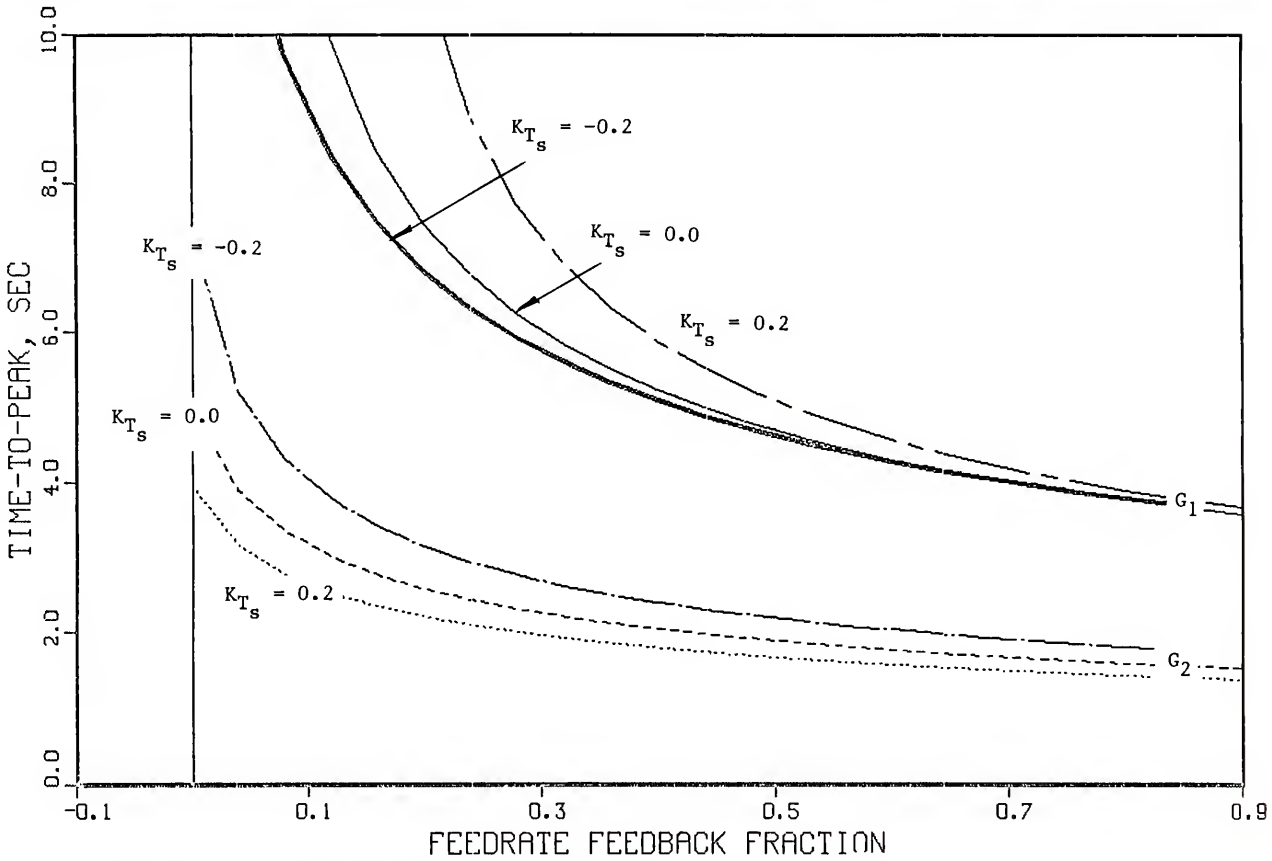

Figure 4-53. Time-to-peak of the closed-loop transfer function versus feedback fraction, following a step input. T_{s_o} = 75 keV, Bohm confinement, kT = 30 keV.

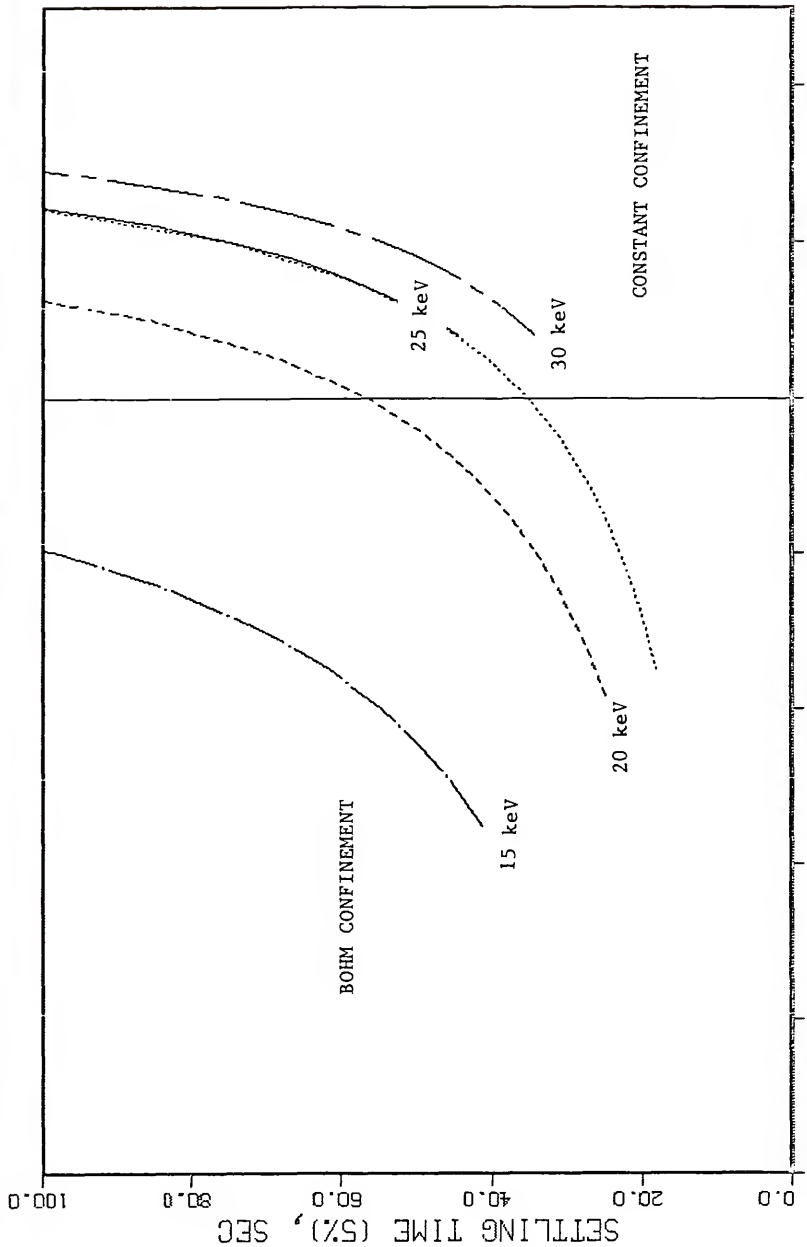

Figure 4-54. Settling time of the closed-loop transfer function versus feedback fraction, following a step input. T_{s_o} = 0, constant and Bohm confinement.

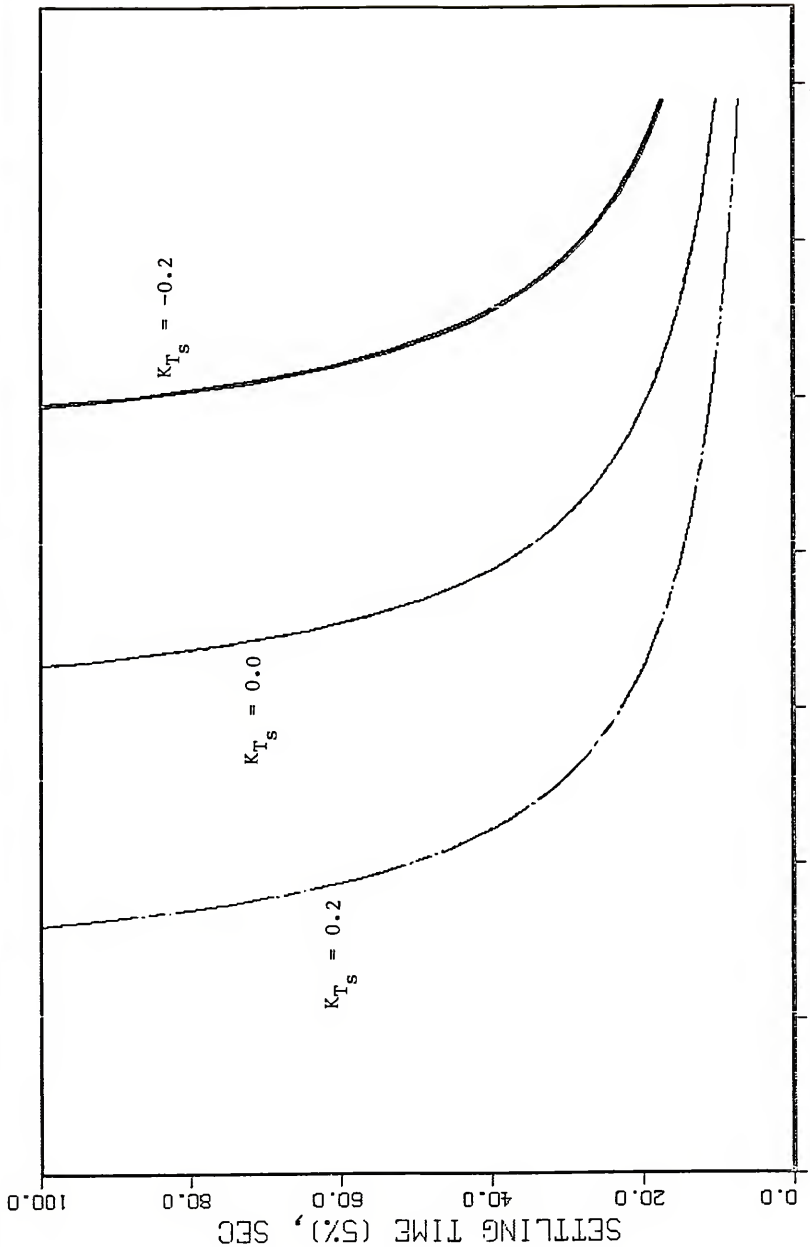

Figure 4-55. Settling time of the closed-loop transfer function versus feedback fraction, following a step input. T_{s_o} = 75 keV, constant confinement, kT = 10 keV.

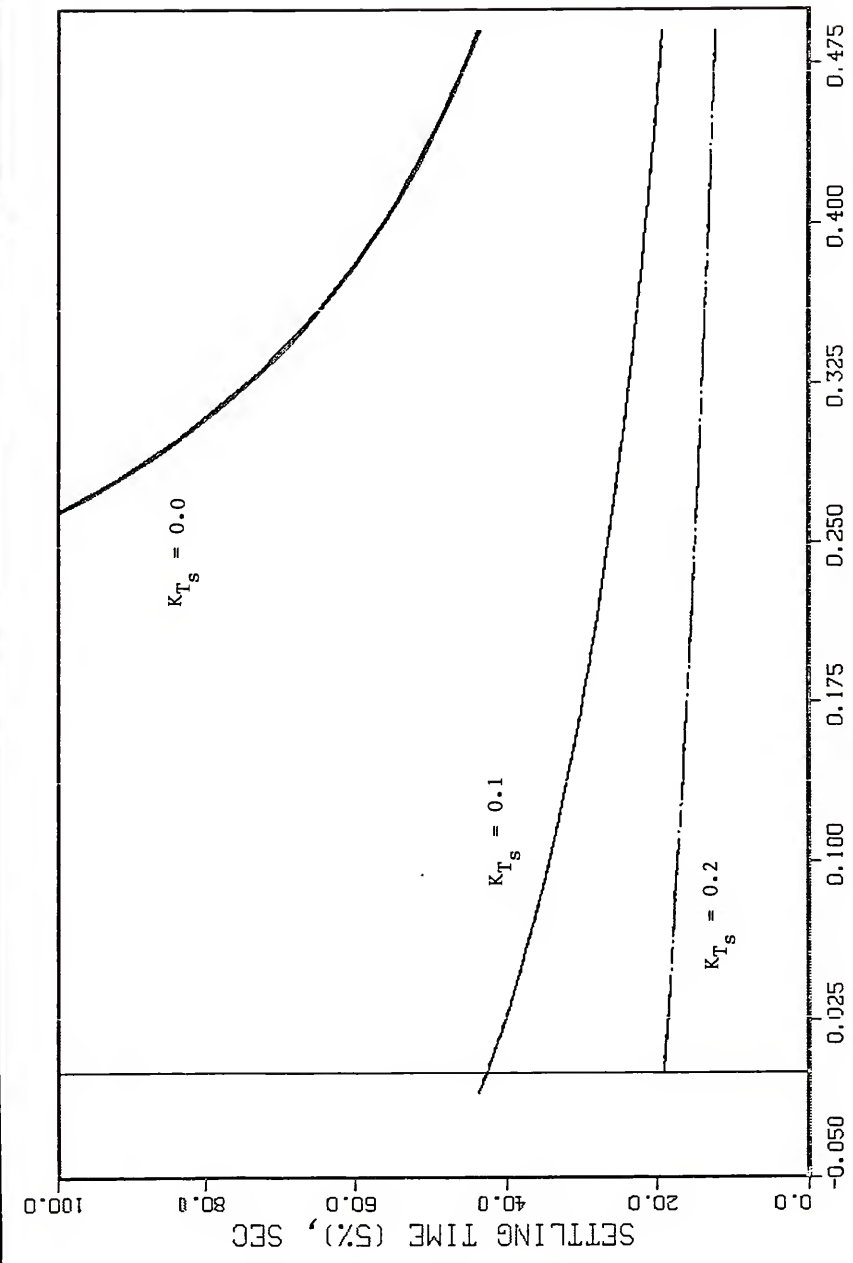

Figure 4-56. Settling time of the closed-loop transfer function versus feedback fraction, following a step input. T_{s_o} = 75 keV, constant confinement, kT = 20 keV.

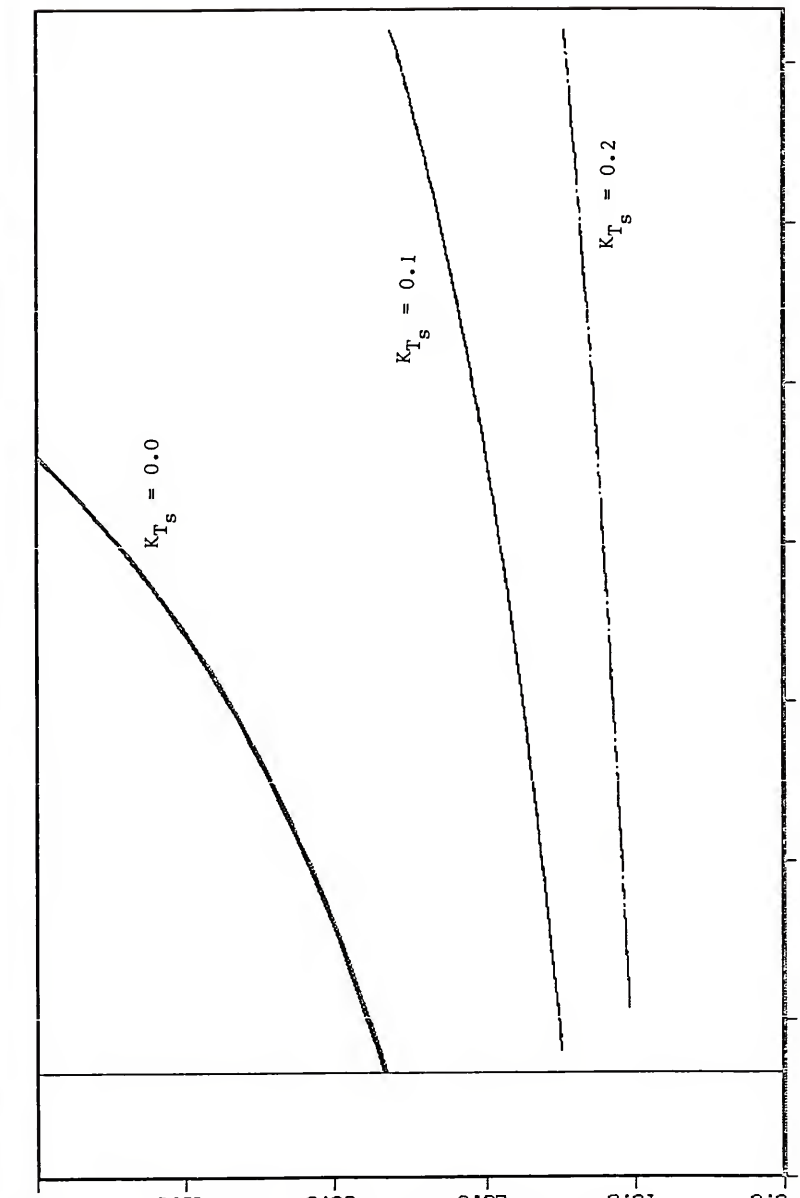

Figure 4-57. Settling time of the closed-loop transfer function versus feedback fraction, following a step input. T_{s_o} = 75 keV, constant confinement, kT = 30 keV.

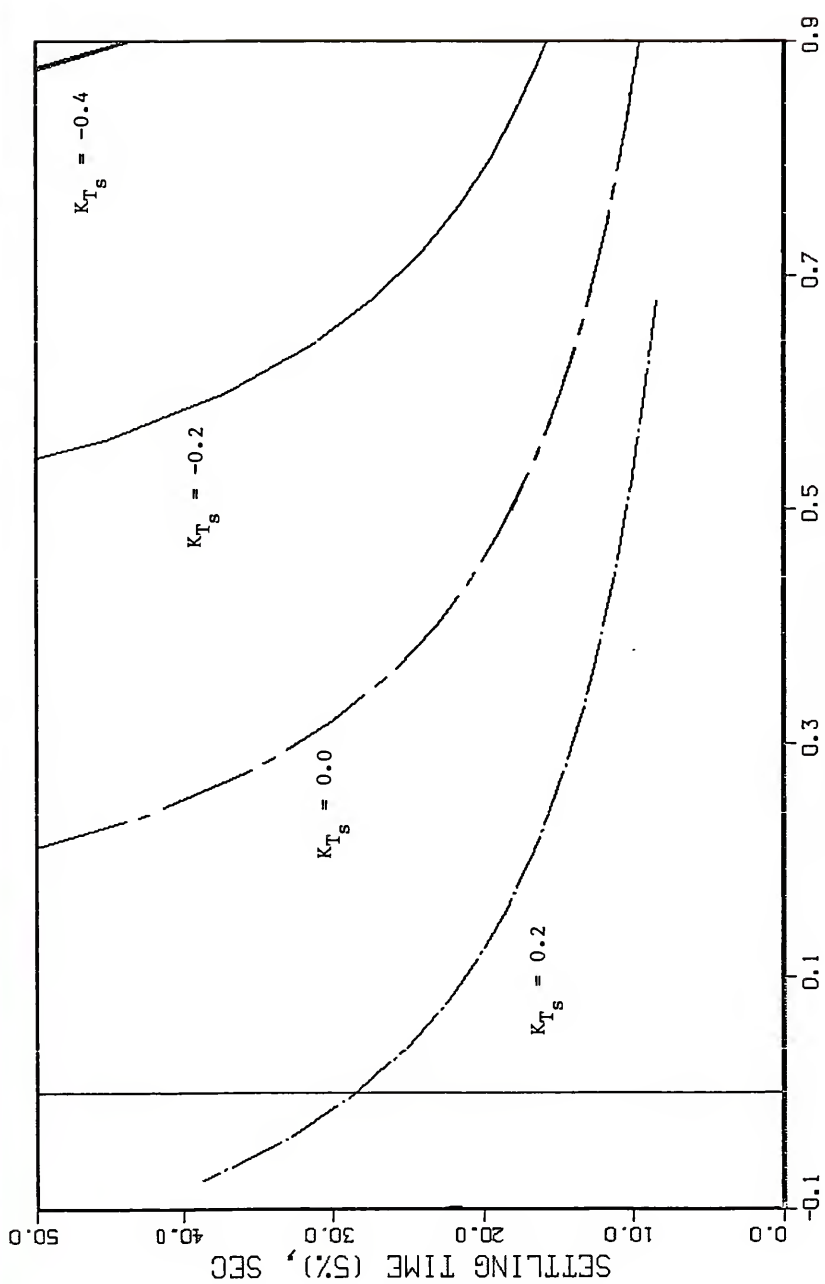

Figure 4-58. Settling time of the closed-loop transfer function G_1 versus feedback fraction, following a step input. T_{s_o} = 75 keV, Bohm confinement, kT = 10 keV.

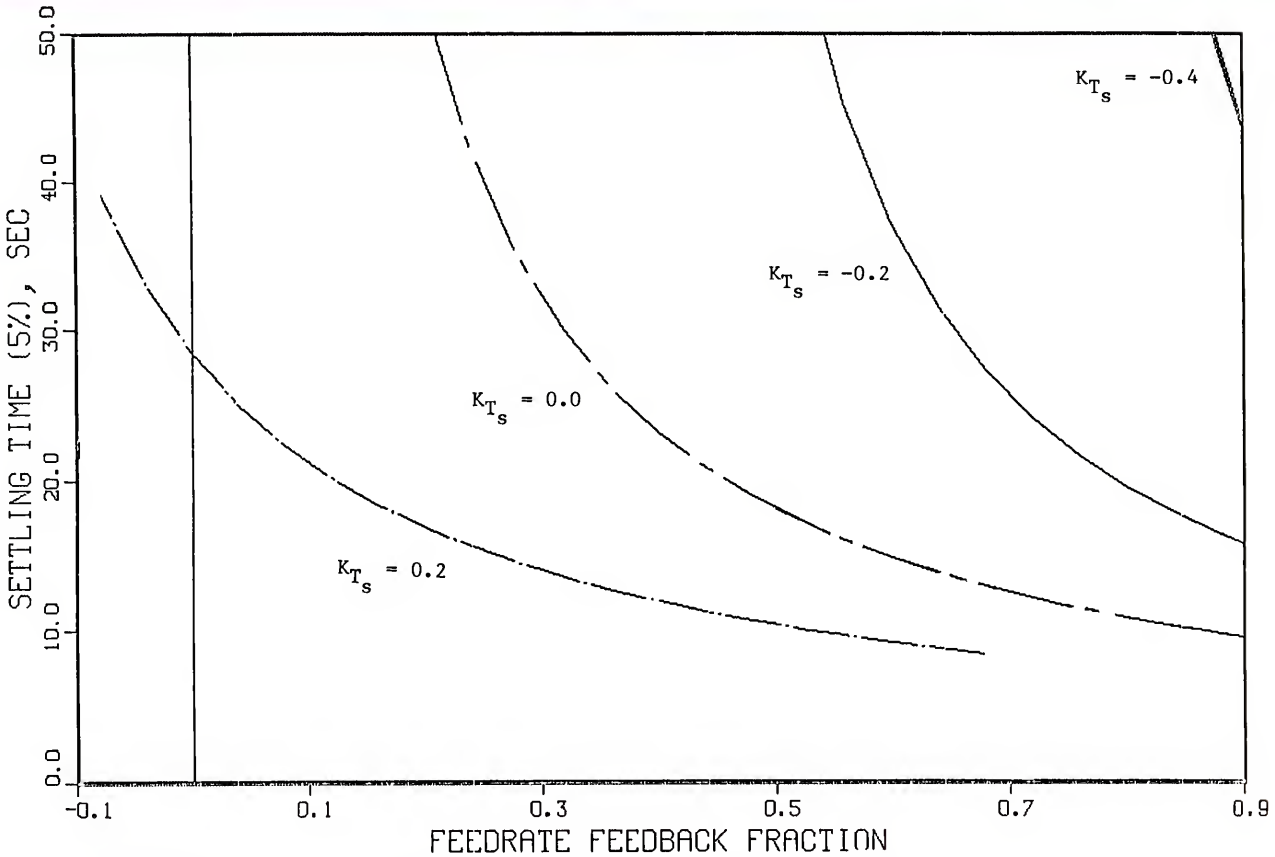

Figure 4-59. Settling time of the closed-loop transfer function G_2 versus feedback fraction, following a step input. T_{s_o} = 75 keV, Bohm confinement, kT = 10 keV.

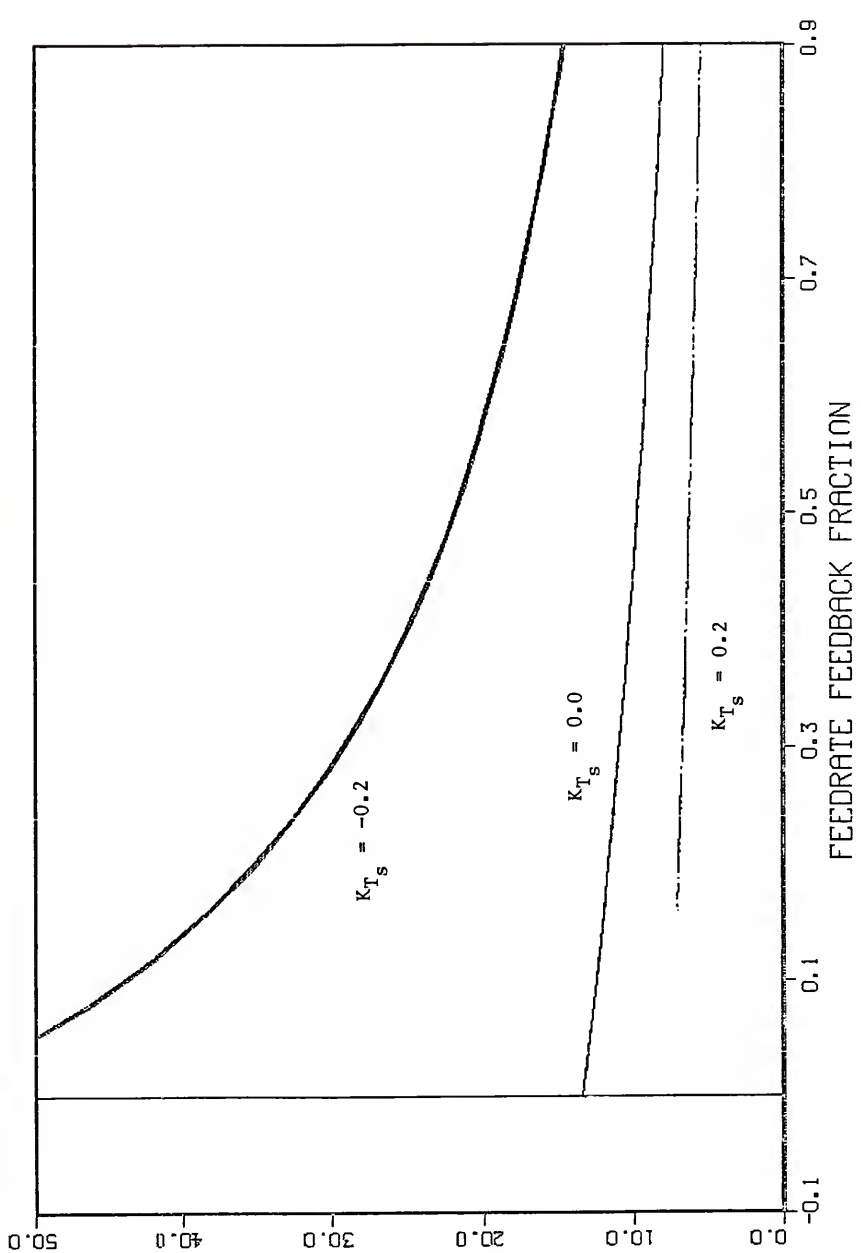

Figure 4-60. Settling time of the closed-loop transfer function versus feedback fraction, following a step input. T_{s_o} = 75 keV, Bohm confinement, kT = 20 keV.

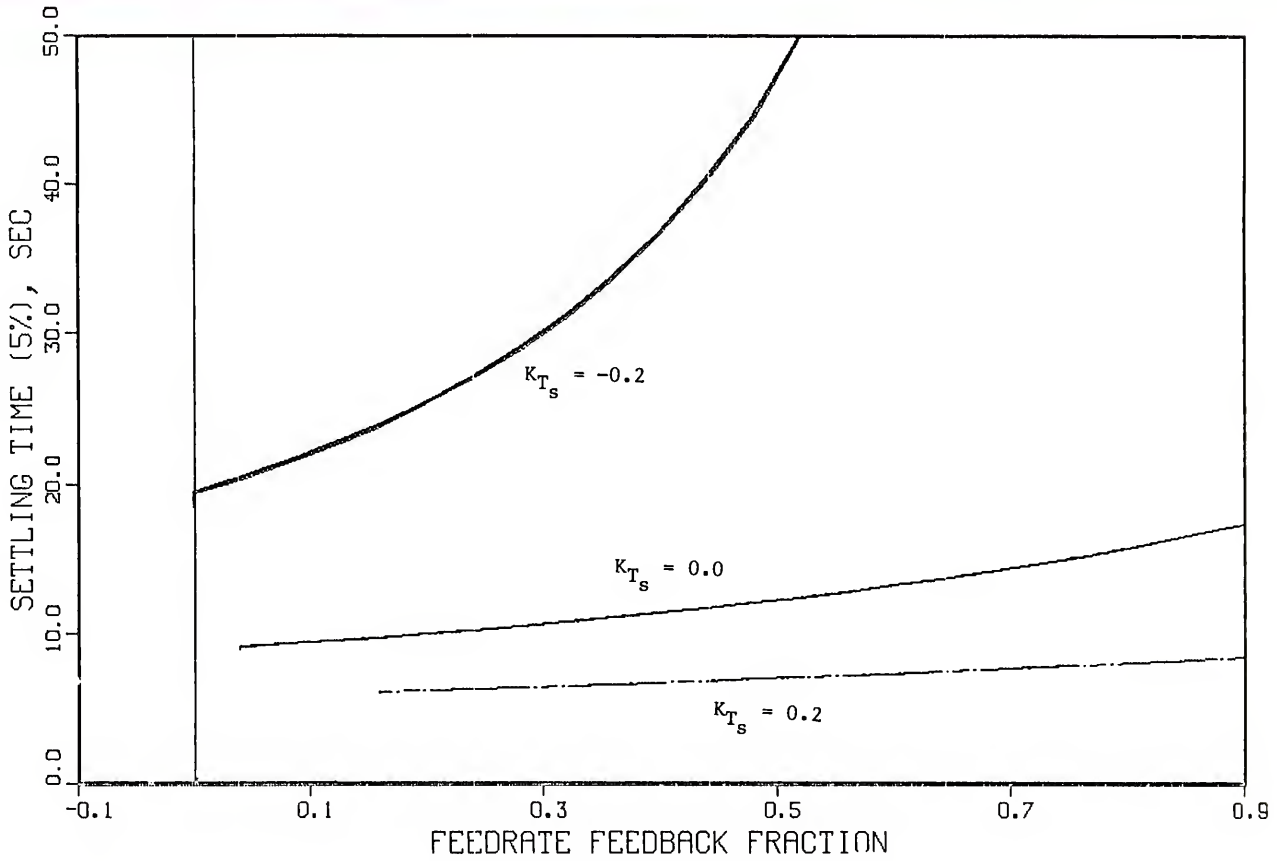

Figure 4-61. Settling time of the closed-loop transfer function versus feedback fraction, following a step input. T_{s_o} = 75 keV, Bohm confinement, kT = 30 keV.

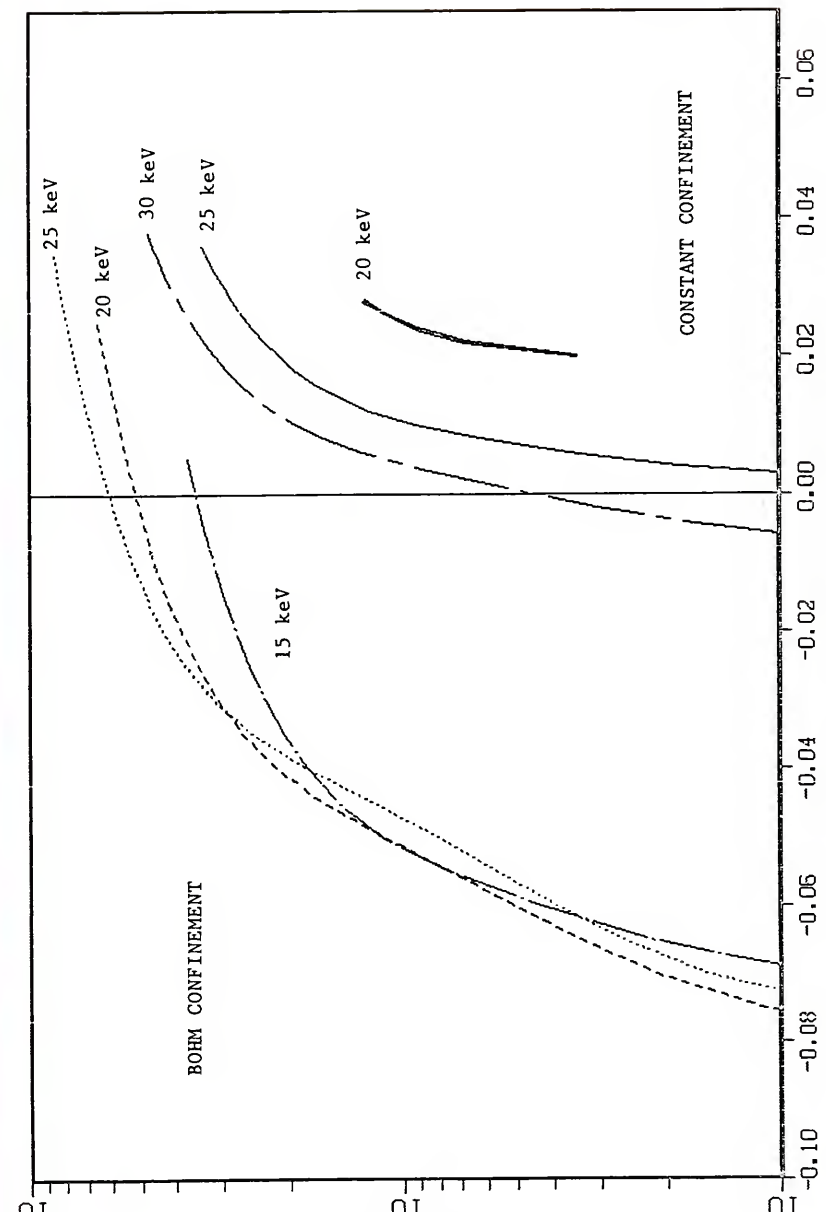

Figure 4-62. Bandwidth of the closed-loop transfer function versus feedback fraction, following a step input. T_{s_o} = 0, constant and Bohm confinement.

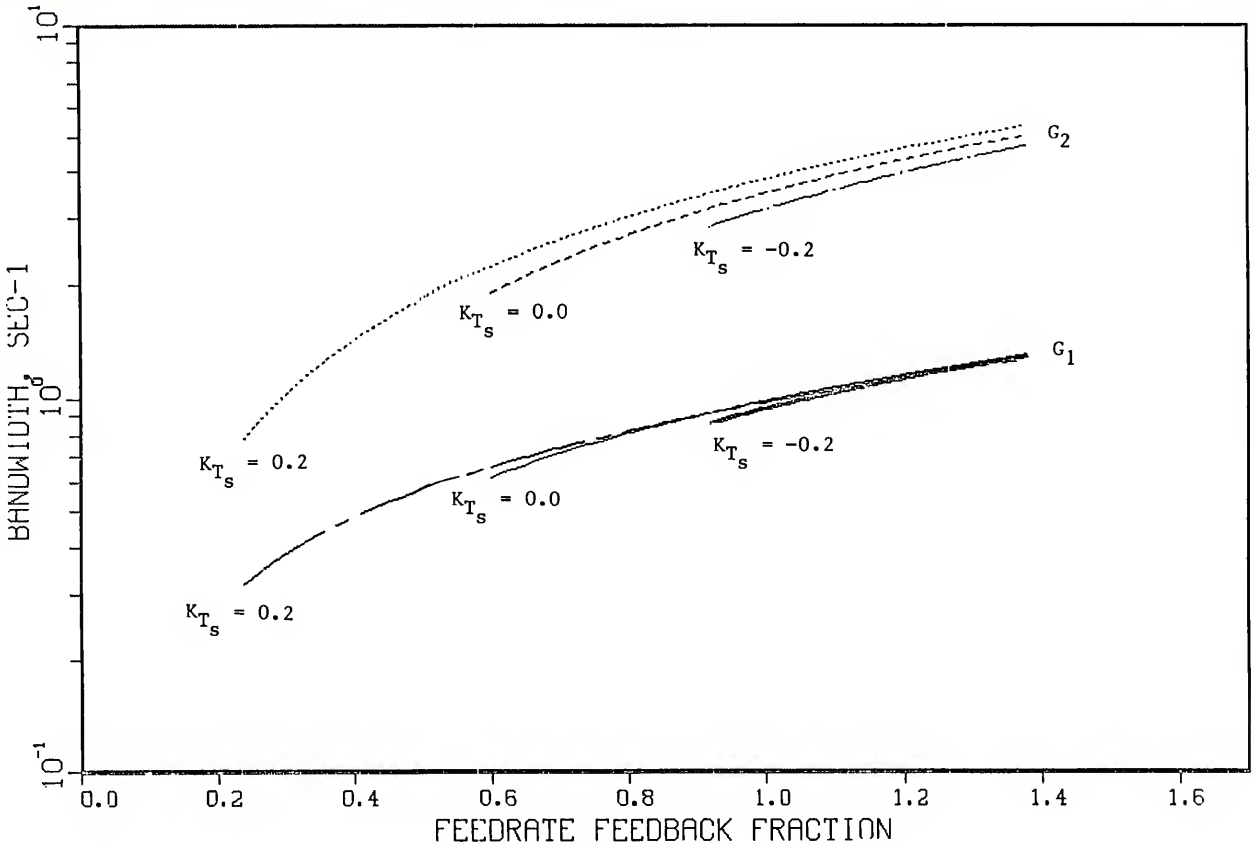

Figure 4-63. Bandwidth of the closed-loop transfer function versus feedback fraction, following a step input. T_{s_o} = 75 keV, constant confinement, kT = 10 keV.

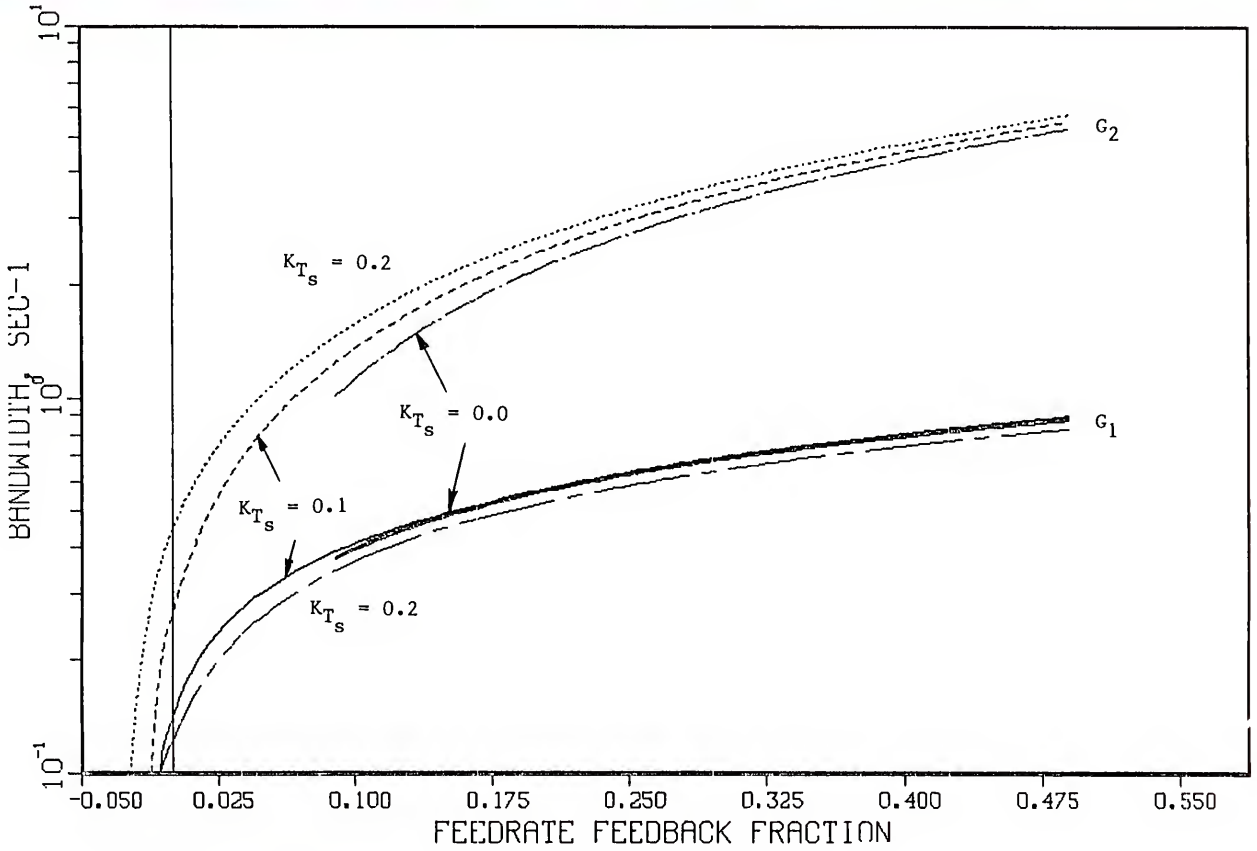

Figure 4-64. Bandwidth of the closed-loop transfer function versus feedback fraction, following a step input. T_{s_o} = 75 keV, constant confinement, kT = 20 keV.

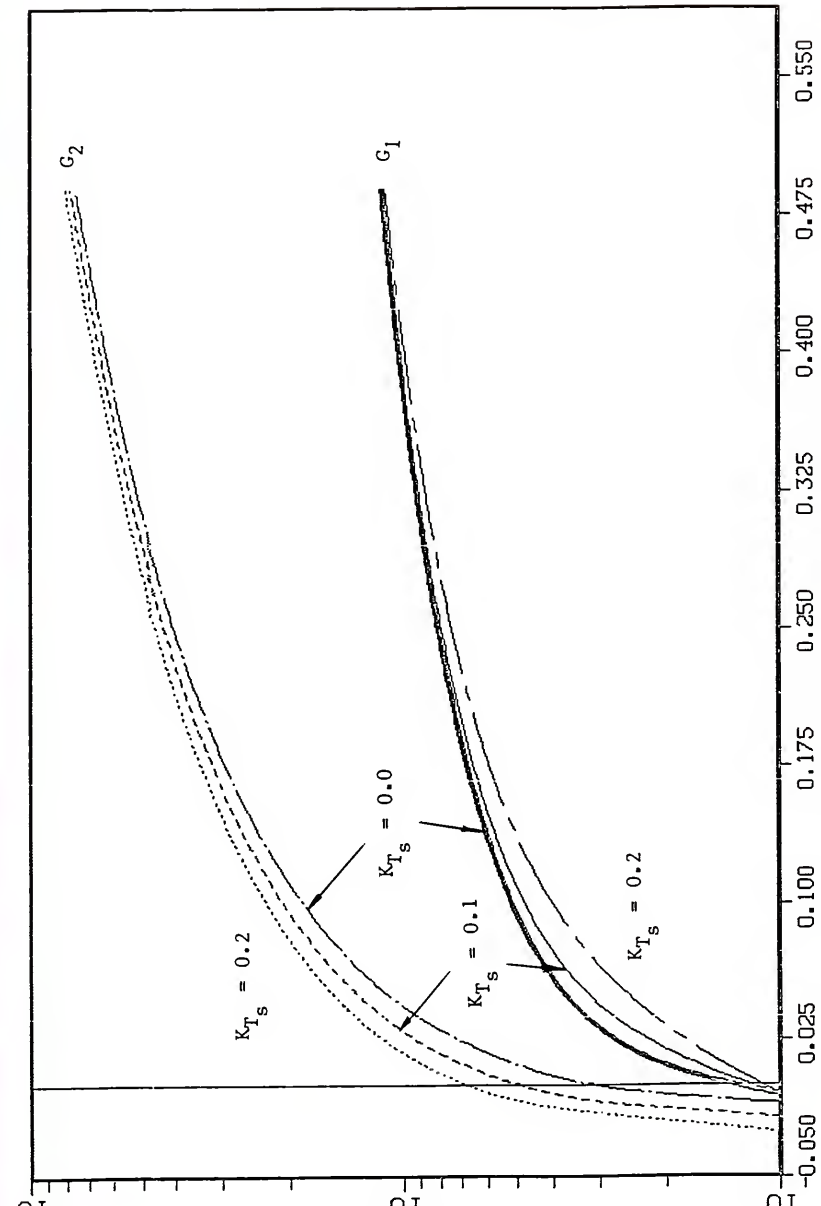

Figure 4-65. Bandwidth of the closed-loop transfer function versus feedback fraction, following a step input. T_{s_o} = 75 keV, constant confinement, kT = 30 keV.

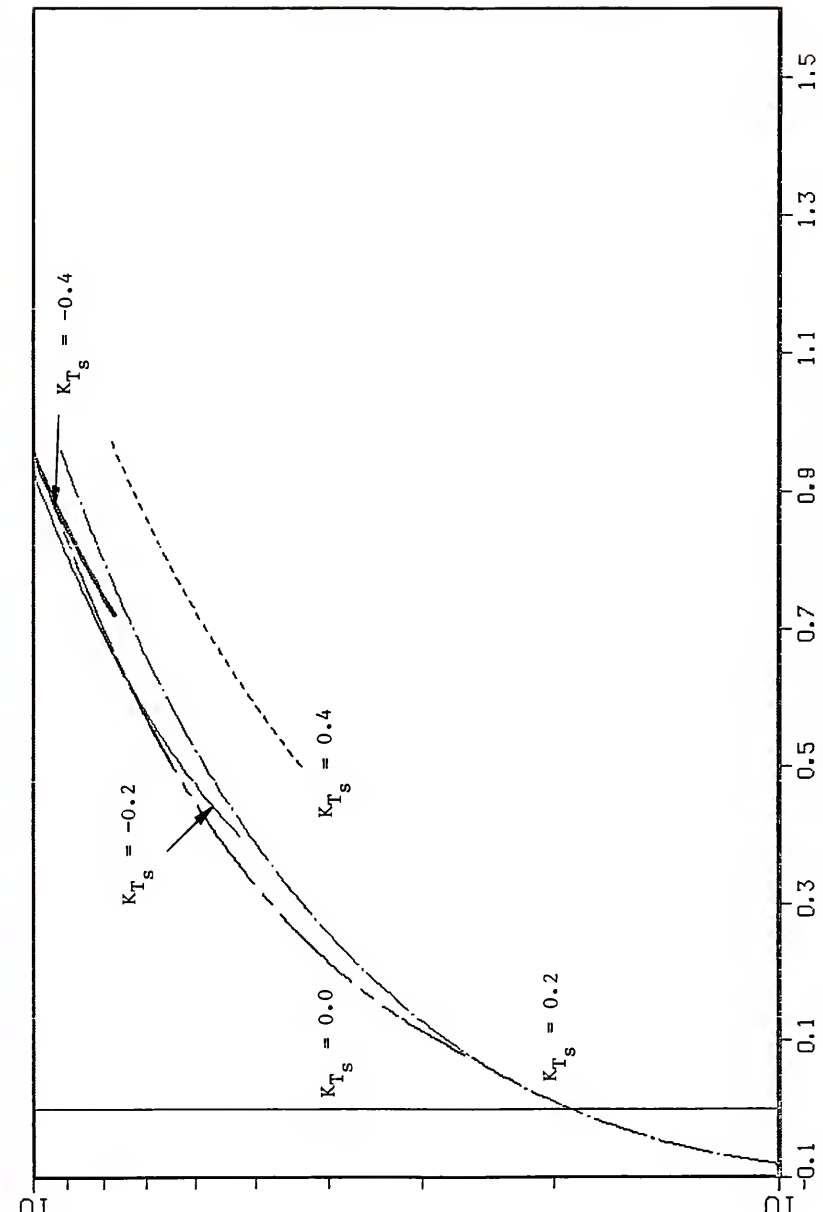

Figure 4-66. Bandwidth of the closed-loop transfer function G_1 versus feedback fraction, following a step input. T_{s_o} = 75 keV, Bohm confinement, kT = 10 keV.

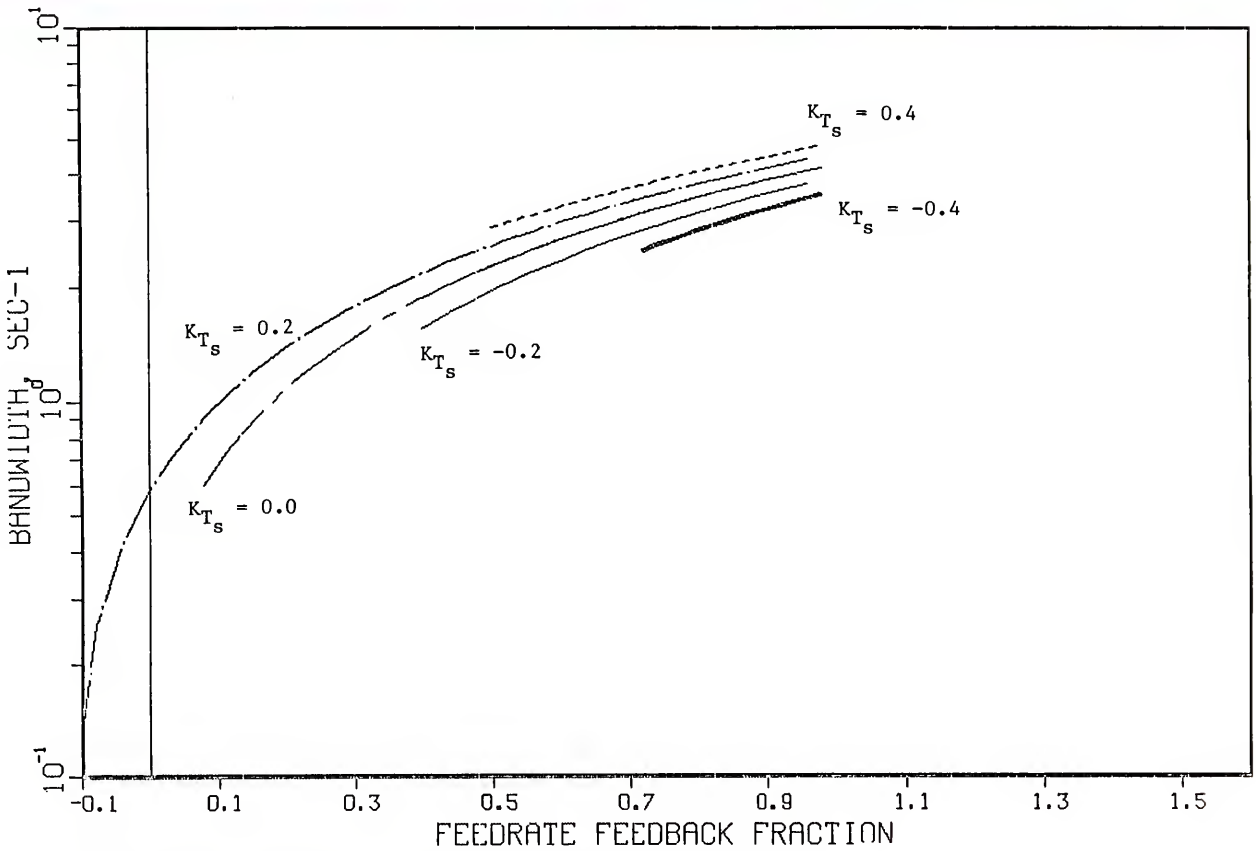

Figure 4-67. Bandwidth of the closed-loop transfer function G_2 versus feedback fraction, following a step input. T_{s_o} = 75 keV, Bohm confinement, kT = 10 keV.

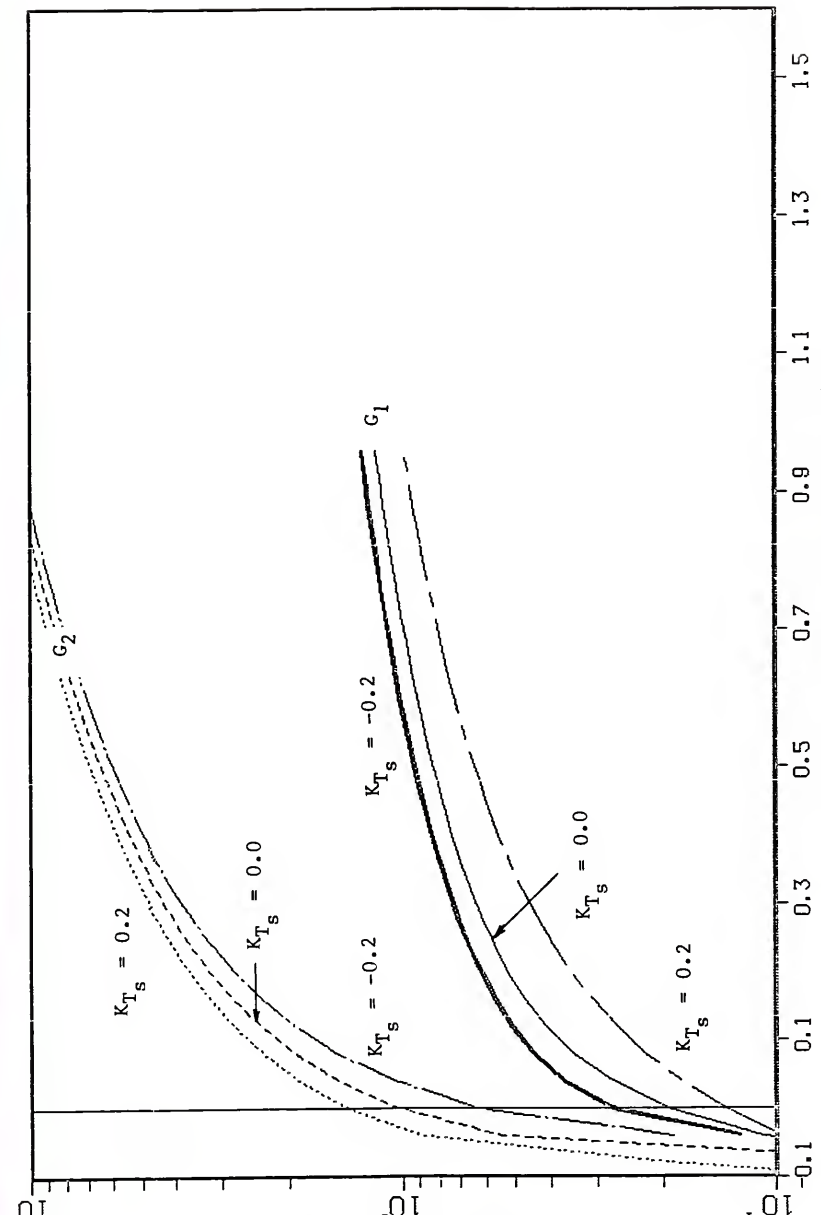

Figure 4-68. Bandwidth of the closed-loop transfer function versus feedback fraction, following a step input. T_{s_o} = 75 keV, Bohm confinement, kT = 20 keV.

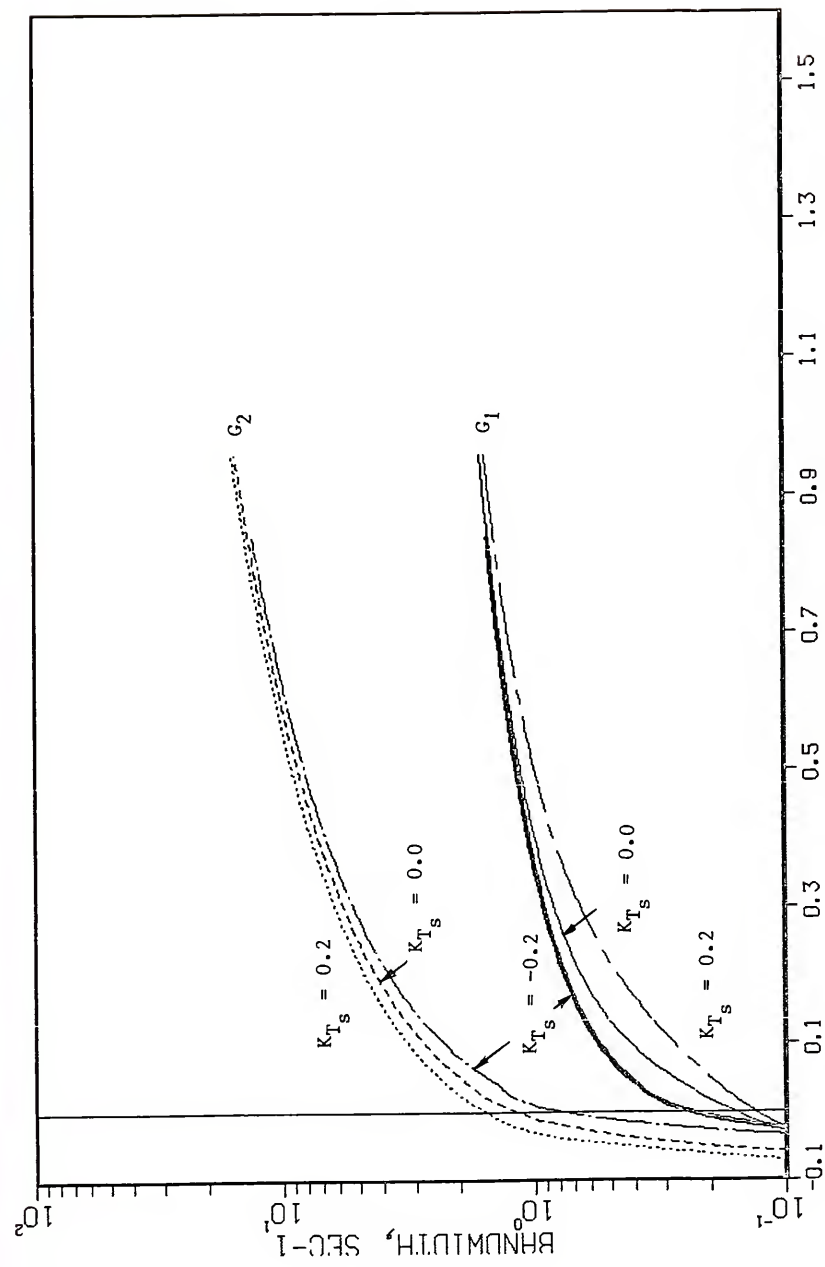

Figure 4-69. Bandwidth of the closed-loop transfer function versus feedback fraction, following a step input. T_{s_o} = 75 keV, Bohm confinement, kT = 30 keV.

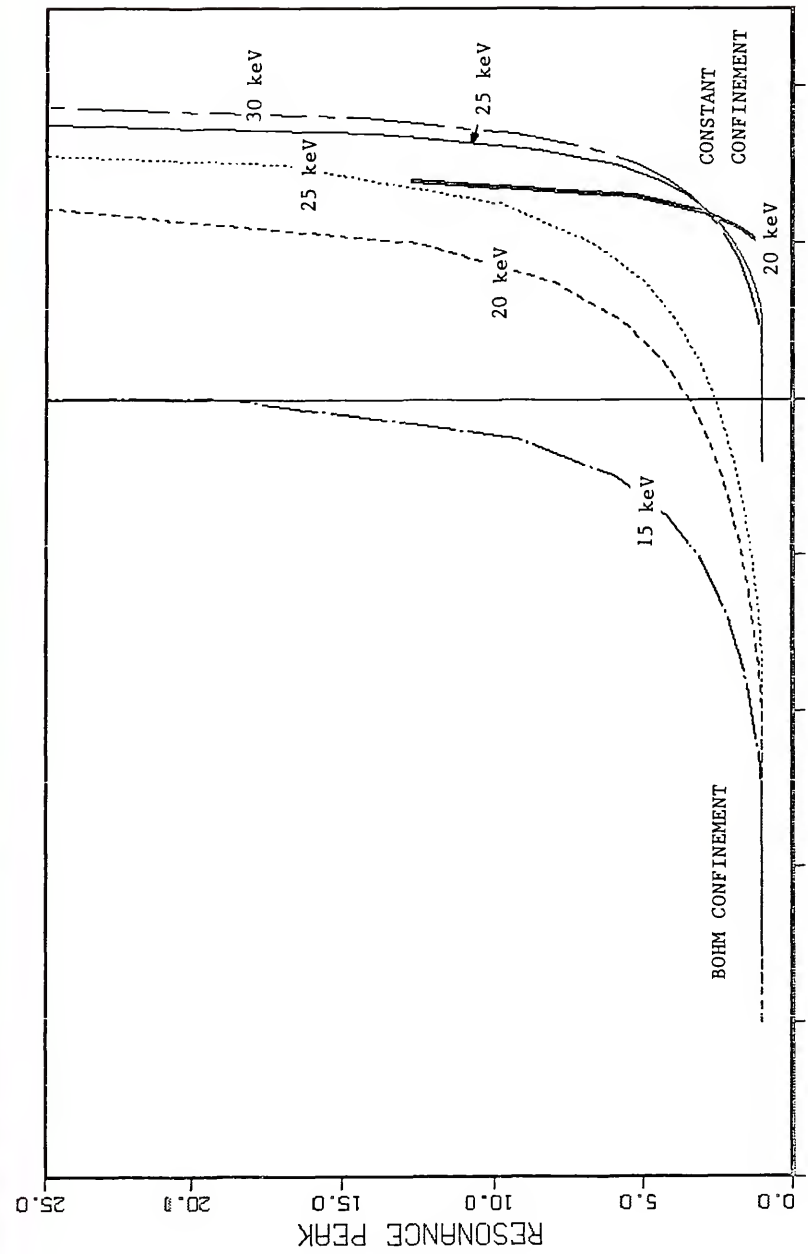

Figure 4-70. Resonance Peak of the closed-loop transfer function versus feedback fraction, following a step input. T_{s_o} = 0, constant and Bohm confinement.

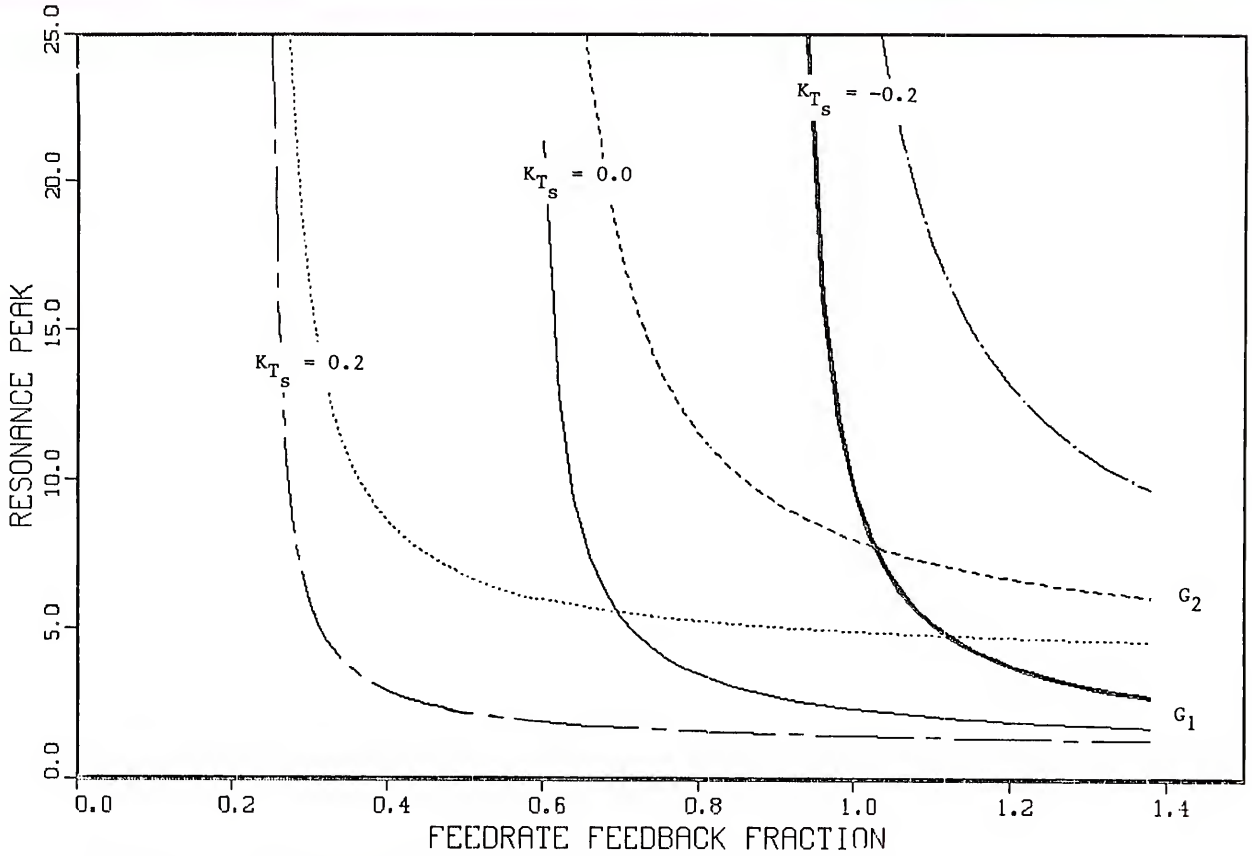

Figure 4-71. Resonance Peak of the closed-loop transfer function versus feedback fraction, following a step input. T_{s_o} = 75 keV, constant confinement, kT = 10 keV.

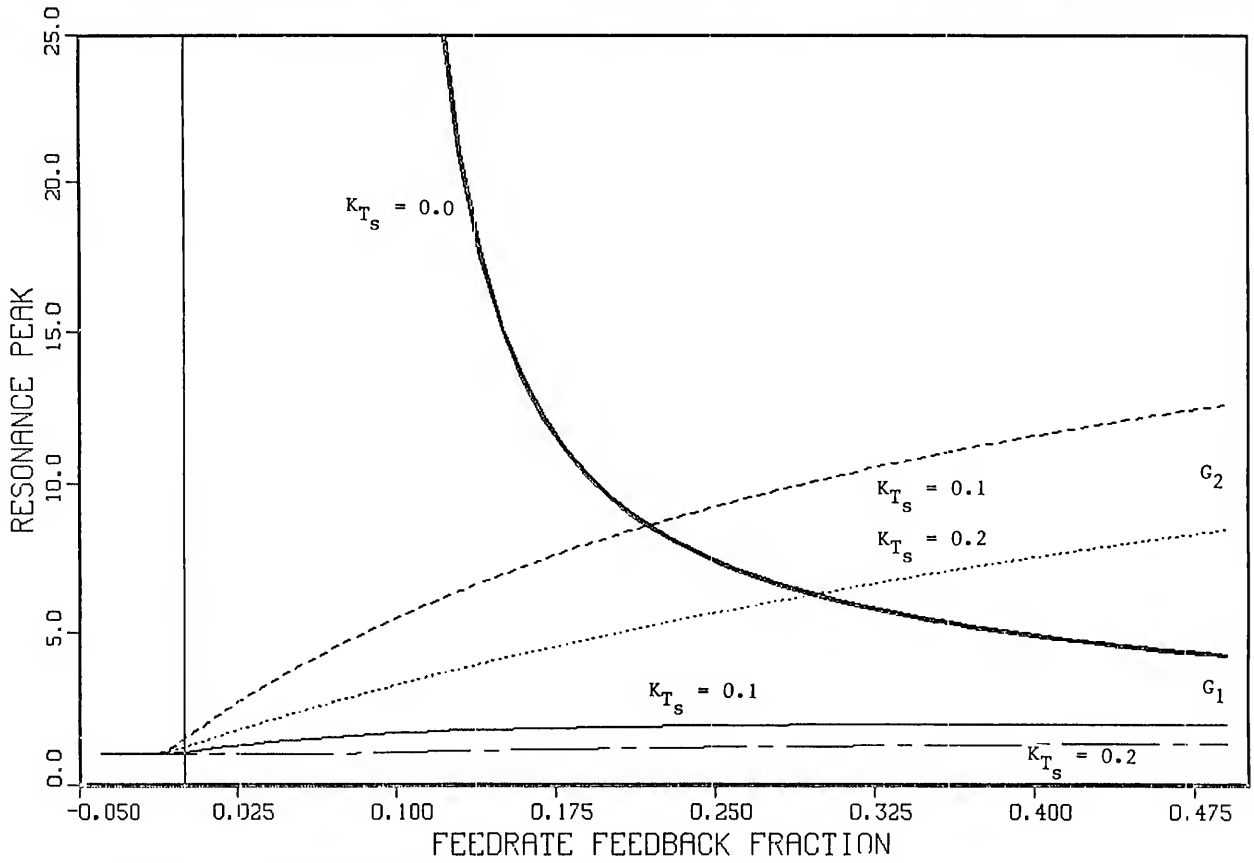

Figure 4-72. Resonance Peak of the closed-loop transfer function versus feedback fraction, following a step input. T_{s_o} = 75 keV, constant confinement, kT = 20 keV.

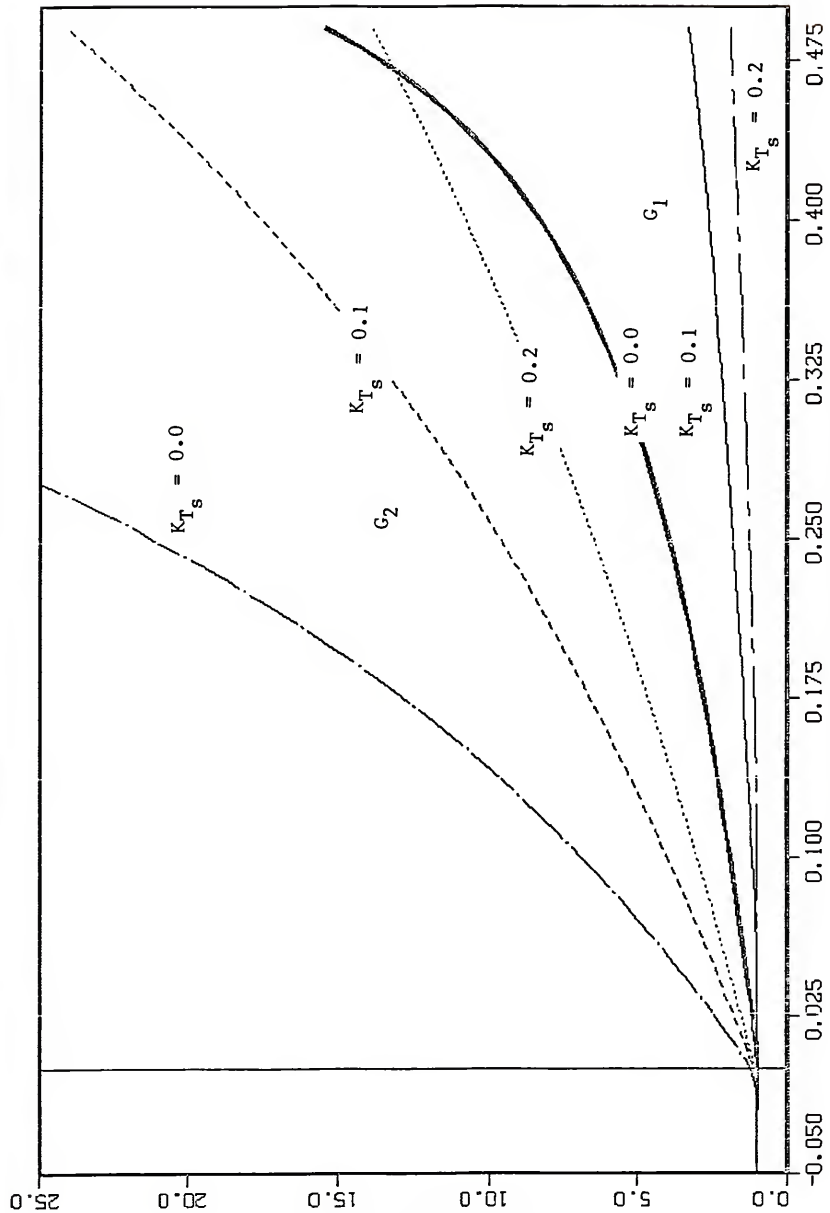

Figure 4-73. Resonance Peak of the closed-loop transfer function versus feedback fraction, following a step input. T_{s_o} = 75 keV, constant confinement, kT = 30 keV.

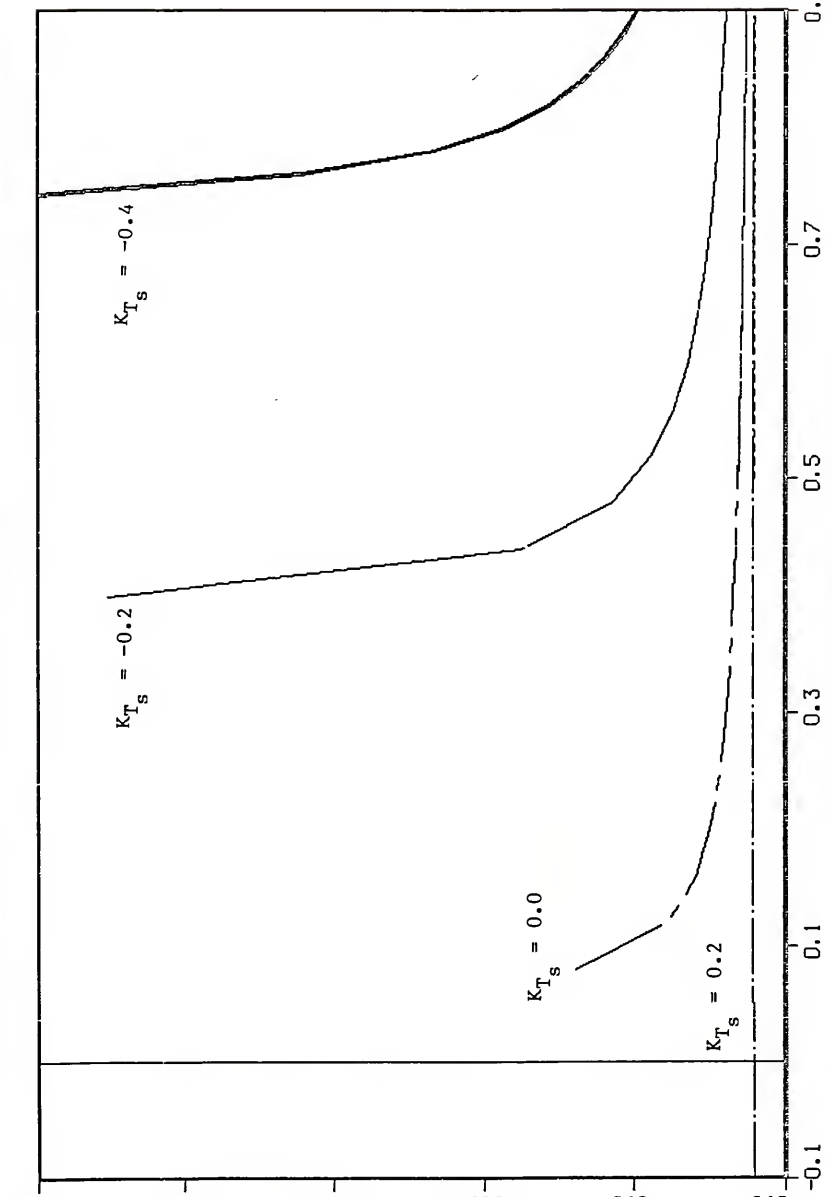

Figure 4-74. Resonance Peak of the closed-loop transfer function G_1 versus feedback fraction, following a step input. T_{s_o} = 75 keV, Bohm confinement, kT = 10 keV.

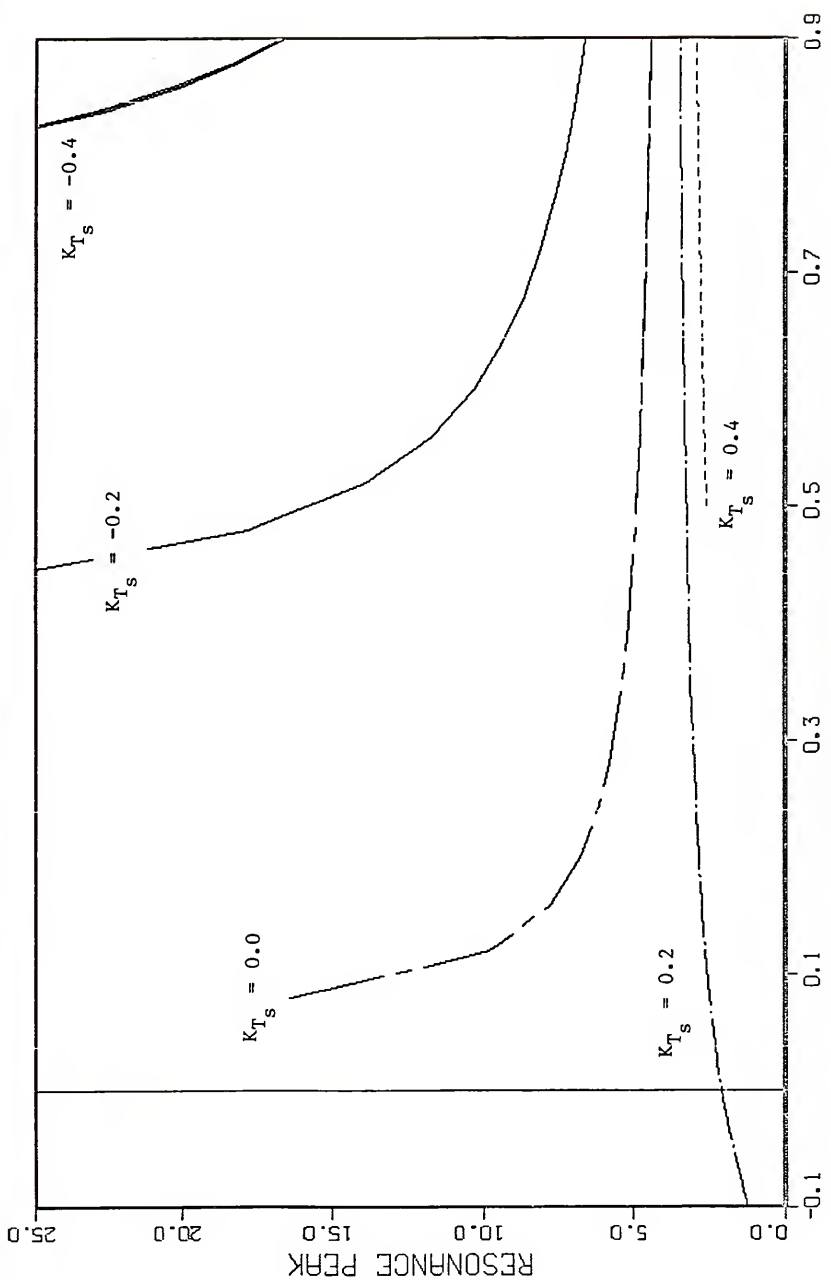

Figure 4-75. Resonance Peak of the closed-loop transfer function G_2 versus feedback fraction, following a step input. T_{s_o} = 75 keV, Bohm confinement, kT = 10 keV.

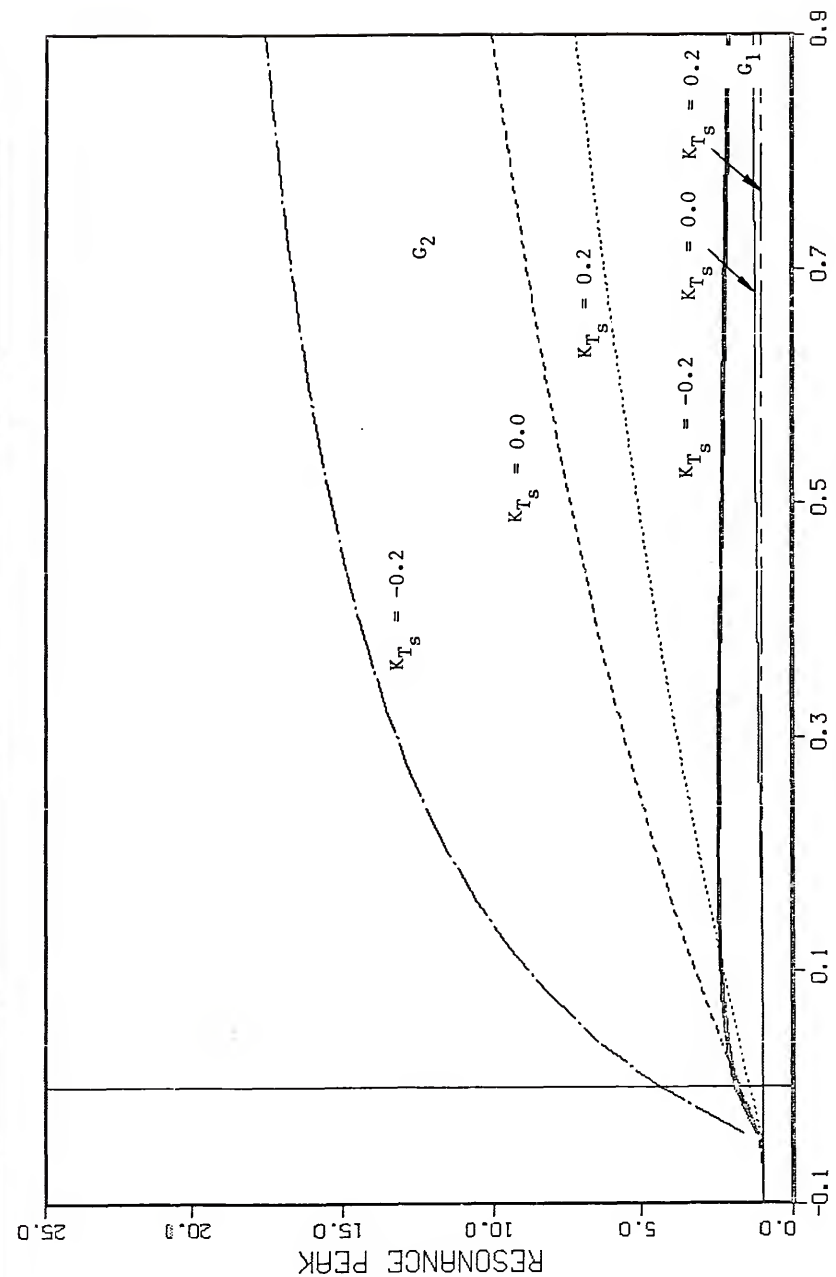

Figure 4-76. Resonance Peak of the closed-loop transfer function versus feedback fraction, following a step input. T_{s_o} = 75 keV, Bohm confinement, kT = 20 keV.

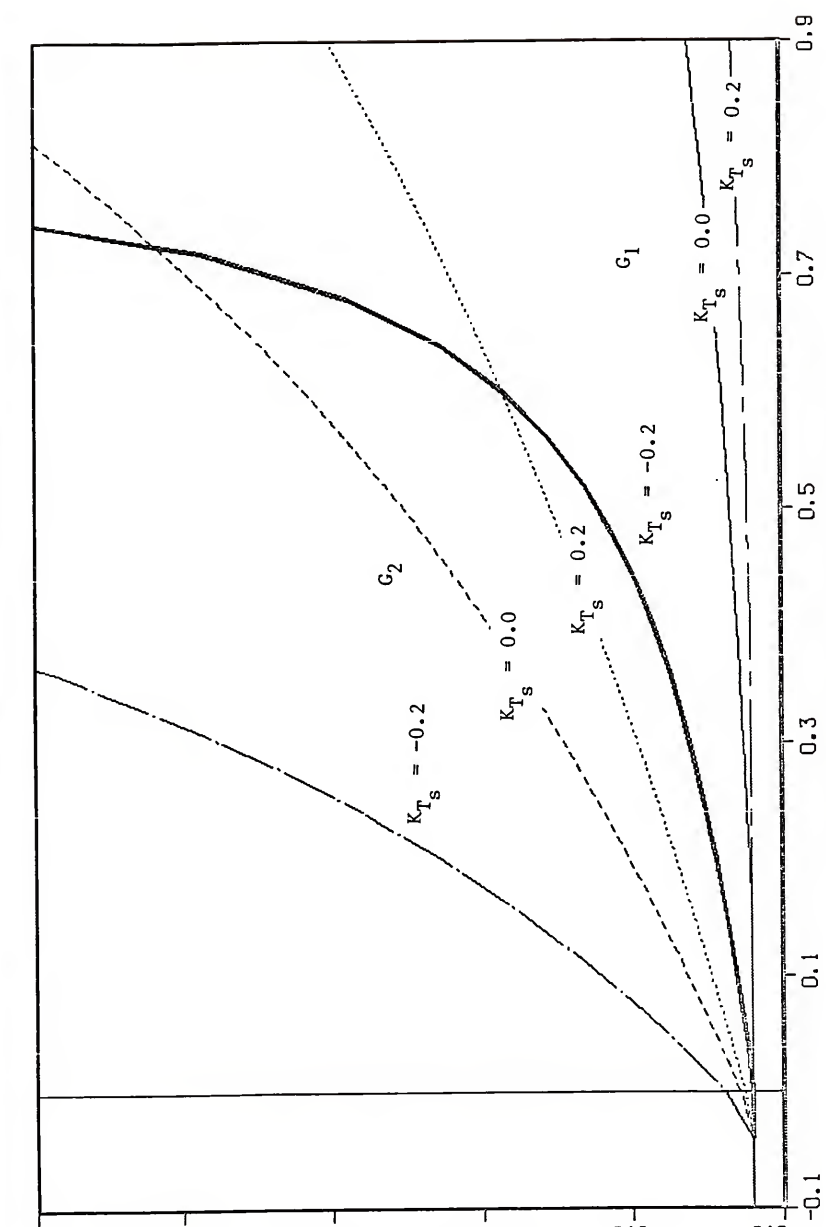

Figure 4-77. Resonance Peak of the closed-loop transfer function versus feedback fraction, following a step input. T_{s_o} = 75 keV, Bohm confinement, kT = 30 keV.

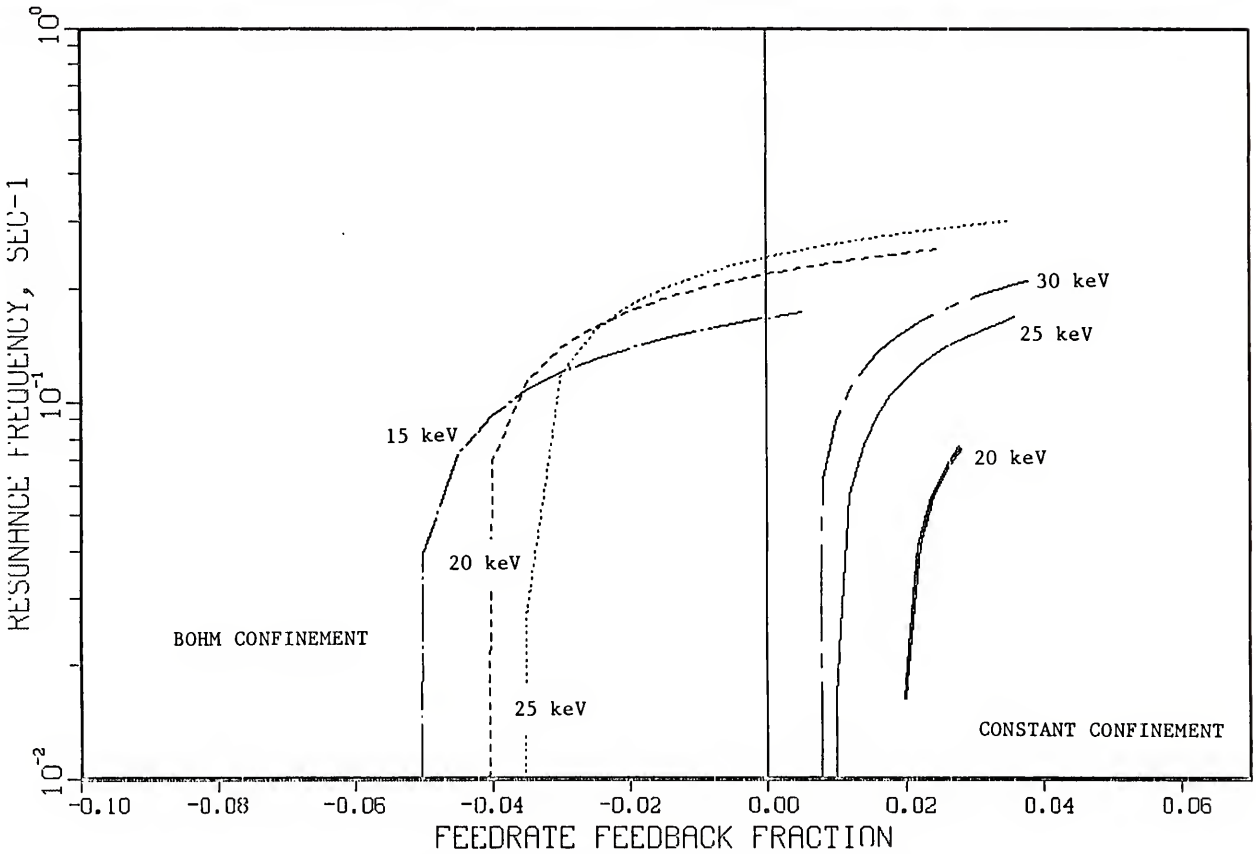

Figure 4-78. Resonance frequency of the closed-loop transfer function versus feedback fraction, following a step input. T_{s_o} = 0, constant and Bohm confinement.

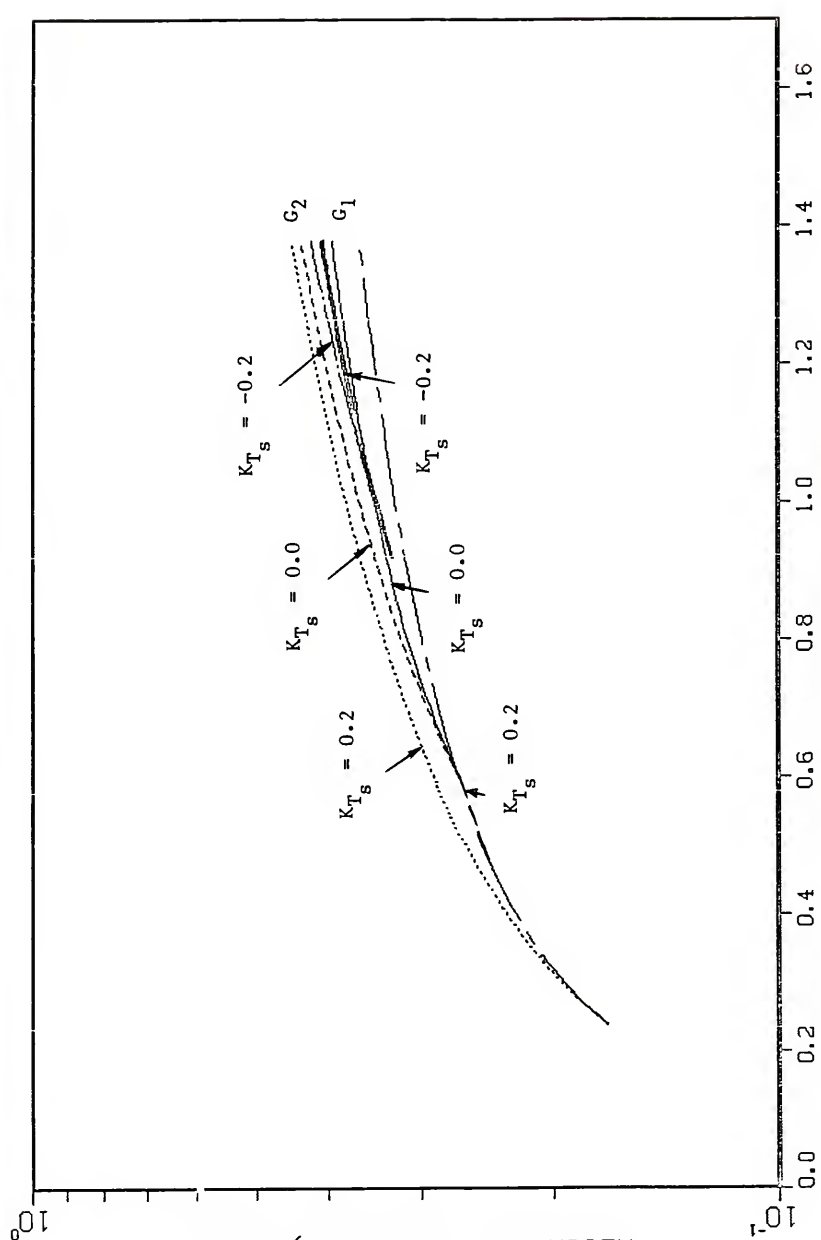

Figure 4-79. Resonance frequency of the closed-loop transfer function versus feedback fraction, following a step input. T_{s_o} = 75 keV, constant confinement, kT = 10 keV.

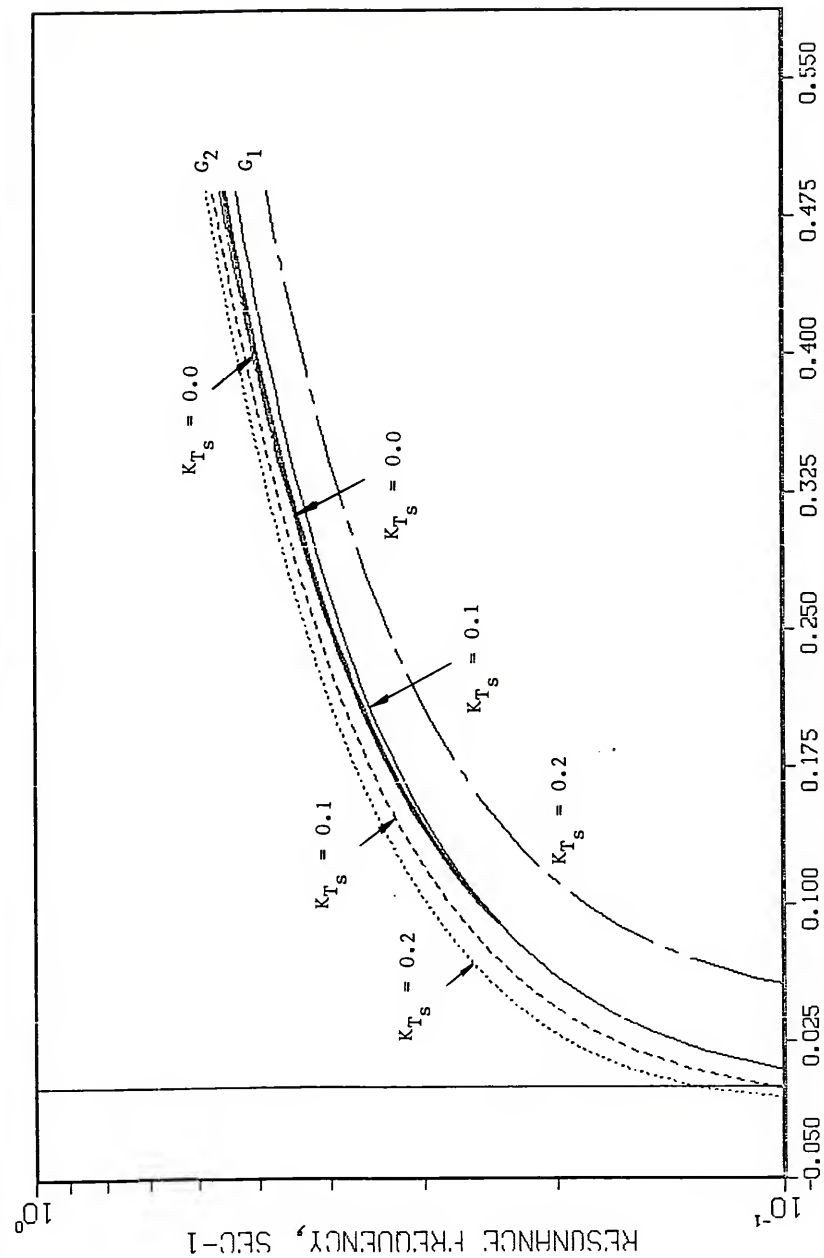

Figure 4-80. Resonance frequency of the closed-loop transfer function versus feedback fraction, following a step input. T_{s_o} = 75 keV, constant confinement, kT = 20 keV.

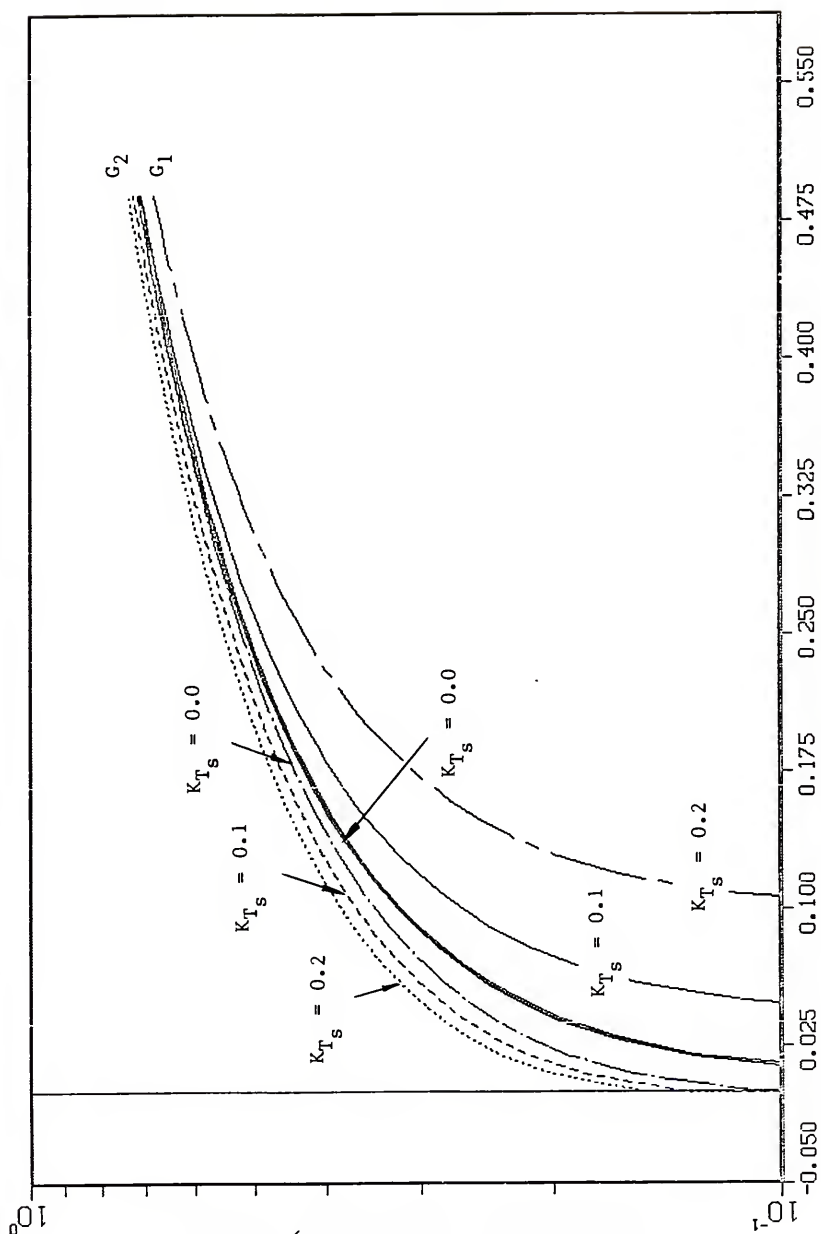

Figure 4-81. Resonance frequency of the closed-loop transfer function versus feedback fraction, following a step input. T_{s_o} = 75 keV, constant confinement, kT = 30 keV.

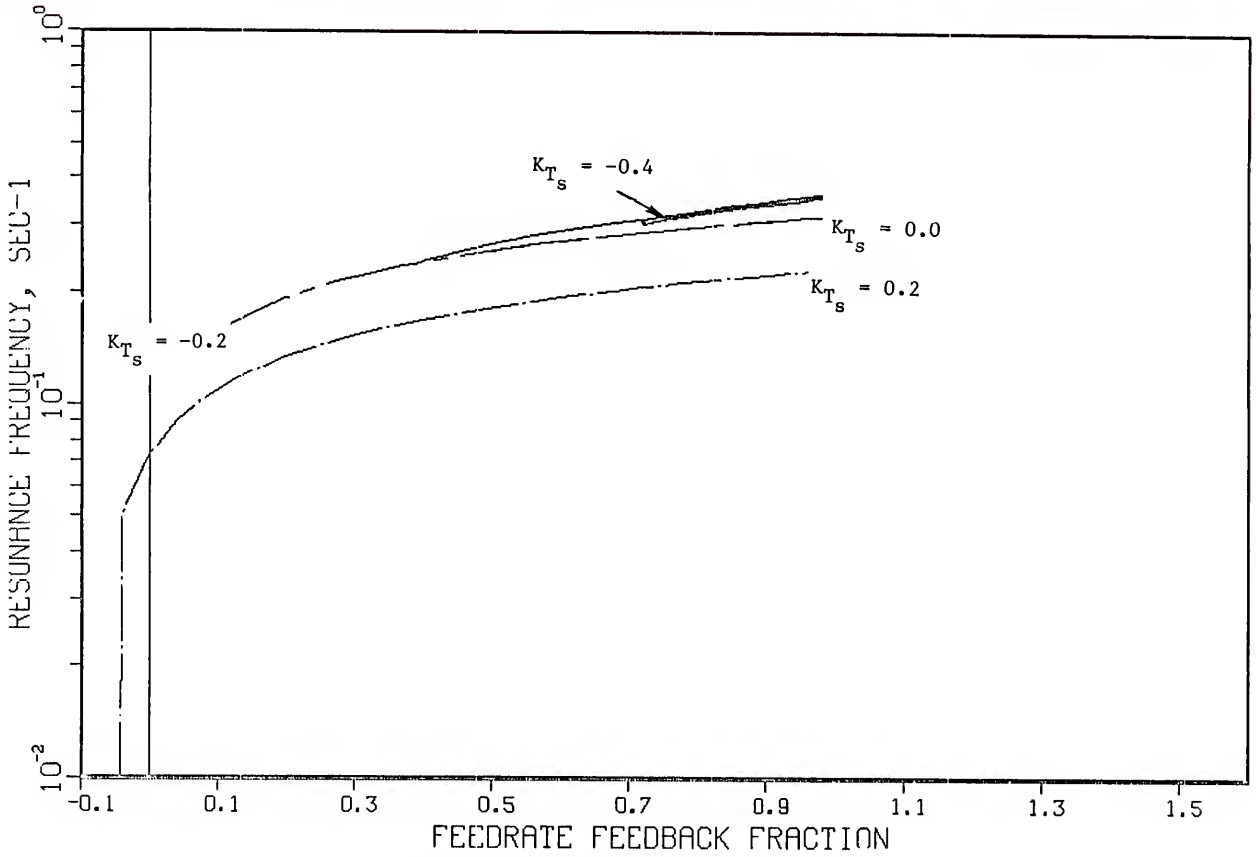

Figure 4-82. Resonance frequency of the closed-loop transfer function G_1 versus feedback fraction, following a step input. T_{s_o} = 75 keV, Bohm confinement, kT = 10 keV.

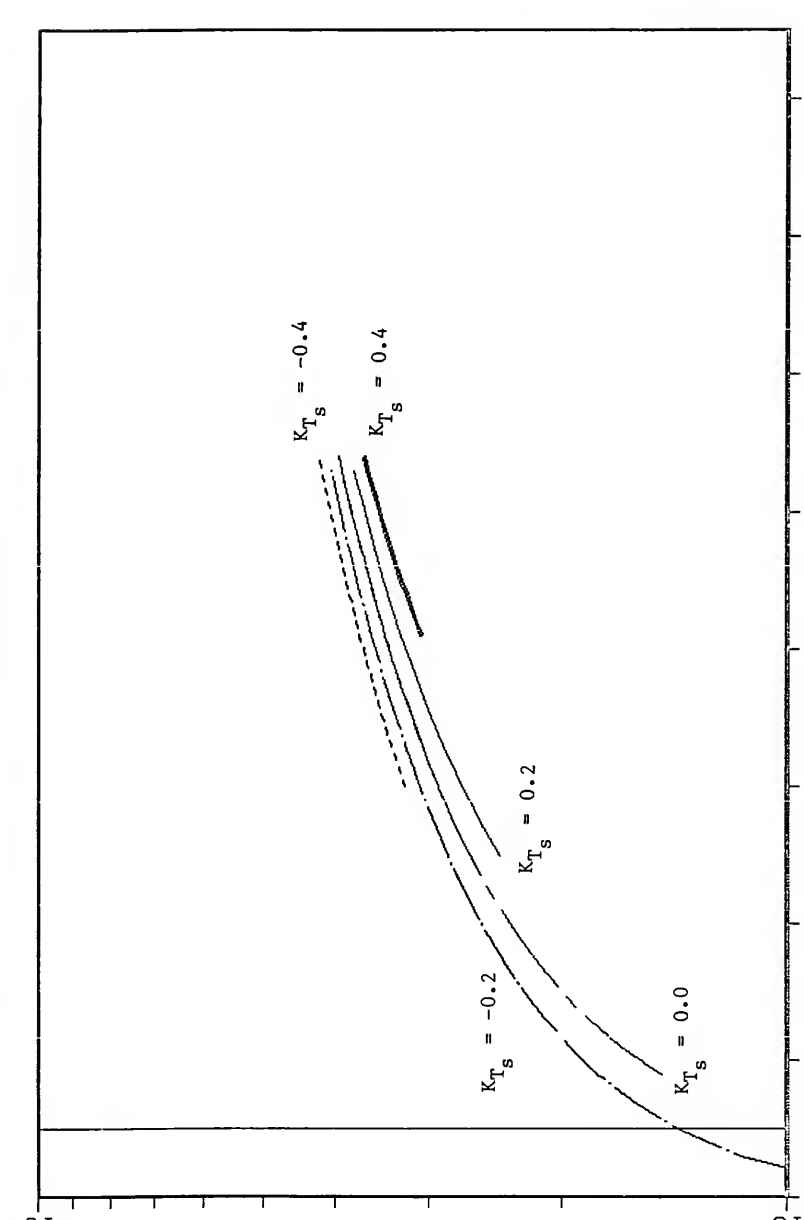

Figure 4-83. Resonance frequency of the closed-loop transfer function G_2 versus feedback fraction, following a step input. T_{s_o} = 75 keV, Bohm confinement, kT = 10 keV.

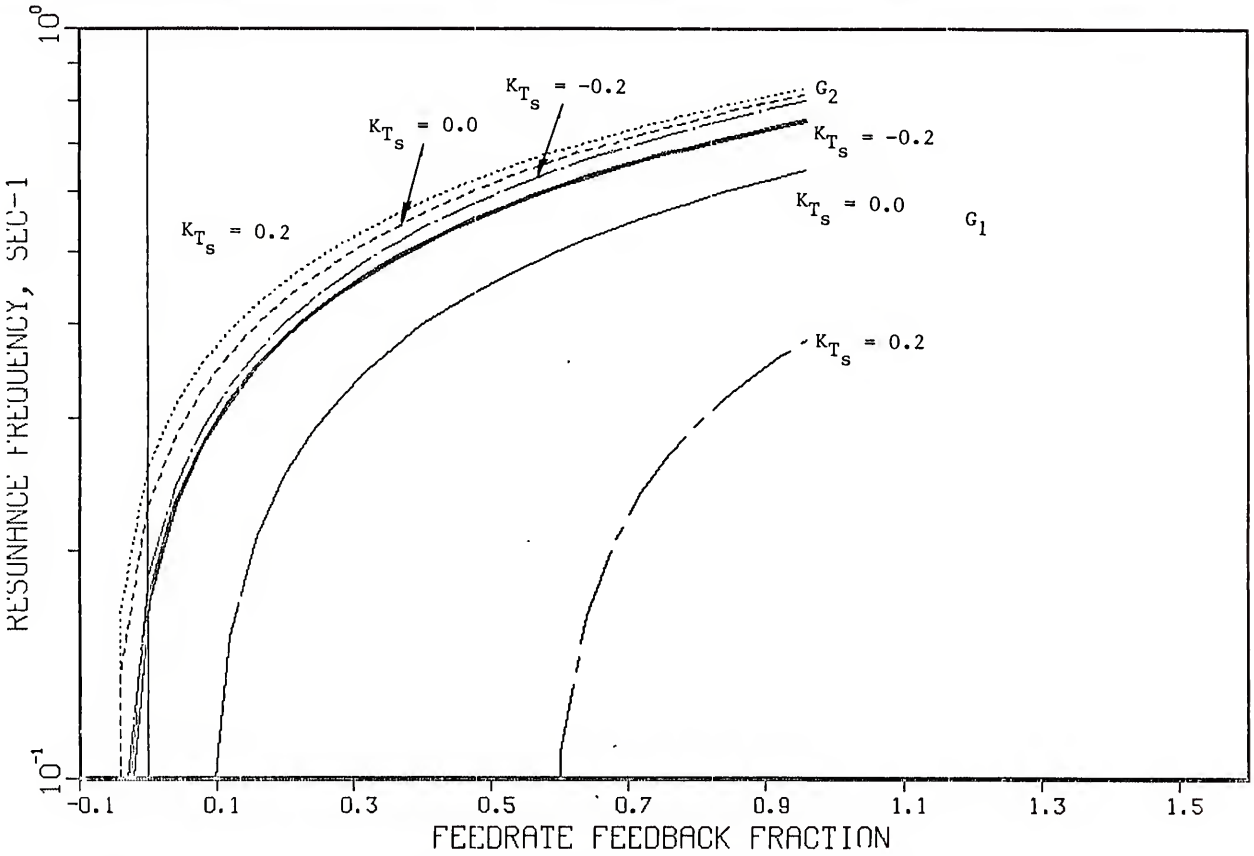

Figure 4-84. Resonance frequency of the closed-loop transfer function versus feedback fraction, following a step input. T_{s_o} = 75 keV, Bohm confinement, kT = 20 keV.

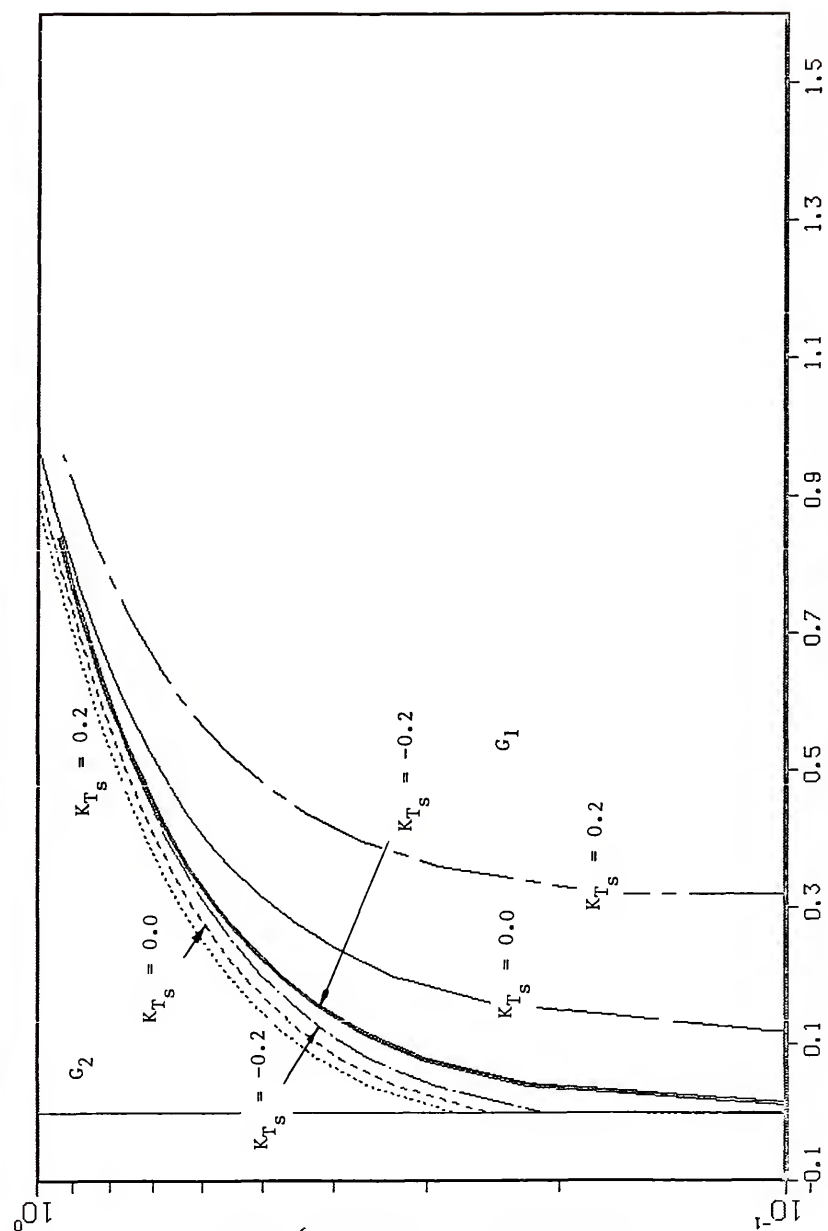

Figure 4-85. Resonance frequency of the closed-loop transfer function versus feedback fraction, following a step input. T_{s_o} = 75 keV, Bohm confinement, kT = 30 keV.

To systematically investigate the system specifications over the range through which feedback will stabilize the operating point, reference is made to Figures 4-1 through 4-4. The presentation in this section proceeds by selecting several operating temperatures of interest for each case of zero and 75 keV injection, with constant and Bohm confinement, and then examining the system response following step changes in the input over the range of feedback fractions through which the system is stable. Thus a parametric analysis is presented for each specification as a function of operating temperature, injection energy, confinement scheme, and feedrate and injection energy feedback fraction. The representation of such a broad spectrum of results is facilitated by the method of analysis chosen for this study.

As in the open-loop analysis, the final value theorem was used to compare the step responses of transfer functions involving a broad range of equilibrium conditions, inputs, and feedback coefficients. Results are shown in Figures 4-30 to 4-37 and are presented in terms of the absolute temperature change that would be brought about by a step change of a magnitude equal to the full steady state value of the input. The figures show that the trend in absolute temperature change is similar for all the conditions investigated. That is, temperature changes induced by changes in feedrate are larger than changes induced by corresponding changes in injection energy. Also, as the feedback fraction is increased, the temperature change brought about by a step input decreases. This latter trend is observed for both feedrate and injection energy feedback. In effect, this states that the feedback is serving its purpose and is attempting to minimize changes in the operating temperature. Since a perturbation analysis was used to

obtain these results, the figures are actually applicable for step changes that result in less than a 10% change in the steady state values. As in the open-loop analysis, the closed-loop results are in good agreement with time development runs.

The first time domain specification presented, in Figures 4-38 through 4-45, is peak overshoot. Feedback has a pronounced effect on peak overshoot. Whereas peak overshoot is unacceptable at most temperatures of interest in open-loop operation, closed-loop proportional feedback now yields overshoots which can be limited to less than 20% by proper selection of the feedback coefficients.

With zero injection energy and Bohm confinement, feedback fractions of -4% at 15 keV, -3% at 20 keV, and -2% at 25 keV are sufficient to provide acceptable overshoot (see Figure 4-38). With constant confinement, the problem is obtaining acceptable conditions for overshoot, time-to-peak, and settling time simultaneously. In this case, the overshoot is very sensitive to the feedback fraction. Therefore, control which may be desirable to improve the speed of response may result in unacceptable overshoot.

With 75 kev injection energy, both feedrate and injection energy can be used to control the overshoot. As shown in Figures 4-39 through 4-45, increasing the injection energy feedback fraction can always be used to lower the overshoot. This follows from the fact that the system damping increases with the injection energy feedback, whereas overshoot decreases with increasing damping ratio. As discussed previously, the system damping increases with feedrate feedback at low temperatures (<20 keV) for constant confinement. At these temperatures, overshoot decreases with increasing feedrate feedback

fraction (see Figure 4-39). As the temperature increases to approximately 20 keV, overshoot decreases with increasing feedrate feedback at low injection energy feedback fractions, and increases at high fractions (see Figure 4-40). At still higher temperatures (above 25 keV), the overshoot increases with increasing feedrate feedback (see Figure 4-41). The general trends with Bohm confinement are similar except that they they appear at approximately 5 keV lower temperatures than with constant confinement.

Inspection of the overshoot present under certain operating conditions, in particular those represented in Figures 4-38, 4-41, 4-44, and 4-45, shows that the permissible feedback range for acceptable overshoot can be quite narrow and exhibit high sensitivity. This implies that although operation with only proportional feedback is possible, only limited flexibility is available in specifying the feedback necessary to minimize overshoot. The reason for the highly sensitive behavior can be seen as follows. Referring to equation C.11 in Appendix C, it can be seen that peak overshoot is dependent on the location of the zero, the pole-zero separation, and exponentially on the system damping. It was shown in the last section that the location of the zero is not affected by feedback. It was also shown in the last section that, in general, the poles are slowly-vaying functions of the feedback fractions (see, e.g., Figures 4-23 to 4-29). Thus the main contributor to the variation in peak overshoot is its exponential dependence on the system damping. The strong variation in peak overshoot thus follows directly from the strong variation of the system damping with feedback fraction as shown previously in Figures 4-16 to 4-22.

The application of proportional feedback results in marked improvements in the speed of response. As evidenced by Figures 4-46 to 4-53, the time-to-peak can be reduced to the seconds and tens of seconds range, from the open-loop values of tens and hundreds of seconds which are shown or can be extrapolated from Figure 3-26. Except at low temperatures, this can be achieved with values of feedback fractions below 10 to 20%.

The variation of the time-to-peak with feedback fraction is rather straightforward and similar for all the cases investigated. That is, t_p decreases monotonically with both feedrate and injection energy feedback at all temperatures, with zero or 75 keV injection energy, for constant or Bohm confinement. With no injection energy and constant confinement, the time-to-peak is reduced from hundreds of seconds to the tens of seconds range (see Figure 4-46), although as mentioned previously, the reduction comes at the expense of increased overshoot. With no injection energy and Bohm confinement, the generally limited decrease in t_p obtained with the use of positive feedrate feedback fractions would not be sufficient to warrant the increased overshoot. Alternately, if increased t_p is permissible, decreased overshoot is possible with negative feedrate feedback fractions (see the discussion on p.61). With 75 keV injection energy, very modest values of the feedback fraction are sufficient to reduce the time-to-peak below 10 seconds except at low temperatures (see Figures 4-47 to 4-53). Note that the time-to-peak with 75 keV injection energy is dictated by the response of G_2, since its overshoot is many times greater than that of G_1.

As in the case of the time-to-peak, the behavior of the system settling time is similarly improved for operation with closed-loop feedrate and injection energy feedback. Thus, settling times obtained during open-loop operation of tens and hundreds of seconds are reduced to seconds and tens of seconds as shown in Figures 4-54 through 4-61. The strong effect of feedback on the settling time can be traced with the help of equations 4.8 and C.13. From equation C.13, it can be seen that the settling time is inversely proportional to the damping factor, σ. Equation 4.8 can be solved in terms of the damping factor by multiplying by ω_n to yield

$$\sigma = \omega_n \xi = \omega_n \xi_{\text{open loop}} + \frac{g_1}{2} K_s + \frac{g_2}{2} K T_s \qquad 4.9$$

The effect of the feedback fraction on σ for various injection energies and plasma temperatures can then be explained with equation 4.9 and the aid of the plots of the system gains given in Figure 3-1.

With zero injection energy, g_1 is negative for all temperatures. Thus with constant confinement, since K_s must be greater than zero for stability above 25 keV (as shown in Figure 4-1), the settling time cannot be decreased below some minimum which is in the hundreds of seconds. At temperatures above 25 keV, as the range of stabilizing feedrate feedback fraction increases, the settling time can be reduced to the tens of seconds range. With Bohm confinement, the settling time can be lowered to 20 - 40 seconds with a negative feedback fraction, while simultaneously decreasing the peak overshoot, but increasing the time-to-peak.

With 75 keV injection energy, g_1 becomes negative above 25 kev. Below this temperature, increased feedback fraction can always be used to decrease the settling time (see e.g., Figures 4-55, 56, 59, and 60). This is a beneficial trend, since as discussed previously, overshoot is similarly decreased with increased feedback fraction, for both constant and Bohm confinement. Above 25 keV, the negative sign of g_1 reverses the above trend, and at sufficiently high feedrate feedback fraction, the settling time increases with increased feedrate feedback (see Figures 4-57 and 4-61). At all temperatures, increased injection energy feedback can always be used to simultaneously reduce the settling time and peak overshoot. This can again be attributed to the gain g_2 being greater than zero at all temperatures. The last term in equation 4.9 thus decreases with K_{T_s}, increasing the damping factor and decreasing the settling time.

In the frequency domain, the specifications of bandwidth, resonance peak and resonance frequency are shown in Figures 4-62 to 4-85. The system bandwidth can be increased significantly, from one to two orders of magnitude above the open-loop values, to values from 1 to 10 sec^{-1} and higher in some cases, with the use of proportional feedback (see Figures 4-62 to 4-69). This is consistent with the improved speed of response discussed previously, but also indicates that the plasma will exhibit increased sensitivity to noise and fluctuations in the input parameters. As shown in Figures 4-78 to 4-85, the resonance frequency is similarly affected by feedback and increases by one to two orders of magnitude to the 0.1 to 1.0 sec^{-1} range. The plots of resonance peak versus feedback fraction, Figures 4-70 through 4-77, are similar in nature to the curves presented

earlier for peak overshoot. This might have been expected given the close relationship between overshoot and the resonance peak for a classical second order system. Although improvements over the open-loop values of the resonance peak are potentially available in certain feedback ranges, the large magnitude of the resonance peak is still of major concern in the event that the system stimulates frequencies in the vicinity of the resonance frequency. At low injection energy feedback fractions, the resonance peak can be maintained below 1.5 only within a very narrow range of feedrate feedback. The range, however, can always be increased by increasing the injection energy feedback fraction.

The next section summarizes the results and observations of this chapter, and offers conclusions on the effect of proportional feedback. Chapter 5 discusses the additional effect of additionally applying derivative and integral control.

4.3. Summary

To investigate the improvement in stability and system performance obtained by using feedback control, expressions for the system characteristics were derived for the closed-loop transfer function in the same manner as for the open-loop case. The loop was closed using proportional feedback because this basic type of control is very effective, has wide applicability, is appropriate for an initial investigation such as the present, and is often used in more advanced control applications in combination with additional types of control.

The relative contributions of the fusion processes to the effect of feedback on the system characteristics were evaluated. As in the open-loop case, bremsstrahlung is a weak contributor, and burnup and confinement terms are the primary contributors. The natural frequency and the damping ratio, and thus the poles of the system are affected by terms proportional to the feedback coefficients.

The poles of the closed-loop transfer function determine the stability of the system. By proper selection of the feedback fractions, and through the combined effects of feedback on the natural frequency and the damping ratio, the real part of the system poles can be forced into the negative real plane and thus closed-loop stability can be achieved. The novel formulation of the problem as presented in this study permitted the feedback fractions required to achieve stabilization to be graphically depicted in a simple form, dependent only on the input parameters, the confinement law, and temperature. Thus, given the input parameters as determined from power level or plasma physics requirements, and the confinement law, the stabilized temperature range and the required feedback can be quickly obtained.

With zero injection energy and constant confinement, proportional feedrate feedback control lowers the critical temperature to 18 keV from the previous value of 25 keV without feedback control. With Bohm confinement, the critical temperature is lowered to 11 keV from the previous 14 keV. With 75 keV injection energy, the effect of proportional feedrate feedback control in lowering the critical temperature is dependent on the injection energy feedback fraction. By appropriate choice of these two parameters, the critical temperature can be effectively lowered to the ignition temperature, 5 keV. The

selection of the feedback fractions is then motivated not just from a requirement to operate in a stable mode, but also by a desire to obtain good system response.

Good system response is obtained by proper selection of the natural frequency and system damping. For feedrate feedback, burnup serves to increase the natural frequency, while diffusion decreases it. For injection energy feedback, both processes can be used to increase the natural frequency. The combined application of both feedrate and injection energy feedback can be used to increase the natural frequency by factors of 3 to 5 over the open-loop values at most temperatures of interest.

The most dramatic display of the effect of feedback is the broad range of damping ratio which is attainable with the combination of both feedrate and injection energy feedback. The entire range from zero damping to overdamping is possible at nearly all temperatures of interest by proper selection of the feedback coefficient. In some ranges of feedback fraction, however, the system damping shows great sensitivity to the feedback coefficients. This implies that small variations in the feedback fractions will have a pronounced effect on the damping ratio.

The broad range of control available with proportional feedrate and injection energy feedback can be used to attain a broad range of system performance. The performance specifications of the plasma thermal balance with closed-loop proportional feedback are summarized in Tables 4-1 and 4-2. These are described below in the same format used for the open-loop specifications.

TABLE 4-1
SUMMARY OF CLOSED-LOOP SYSTEM RESPONSE, TIME DOMAIN SPECIFICATIONS

	Temperature (keV)	Injection Energy Feedback Fraction	Range of Feedrate Feedback Fraction for Stability	M_p	t_p (sec)	t_s (sec)
Zero injection energy, constant confinement kT_c = 18 keV	20	0.0	0.02 to 0.03	0.1 to 0.9	100 to 50	>200
	25	0.0	0.001 to 0.04	0 to >1.0	∞ to 25	40 to >100
	30	0.0	-0.01 to 0.04	0 to >1.0	∞ to 20	30 to >100
Zero injection energy, Bohm confinement kT_c = 11 keV	25	0.0	-0.07 to 0.005	0 to >1.0	80 to 30	40 to >100
	20	0.0	-0.08 to 0.003	0 to >1.0	50 to 20	20 to >100
	25	0.0	-0.08 to 0.04	0 to >1.0	40 to 20	20 to >100
75 keV injection energy, constant confinement kT_c = 5 keV	20	-0.2	>0.9	>1.0	<6	>100 to 20
		5.0	>0.6	>1.0	<8	>100 to 10
		5.2	>0.2	>1.0	<10	>100 to 7
	20	0.0	>0.09	>1.0	5 to 10	>100 to 50
		0.1	>-0.02	0 to 0.8	>20 to 5	40 to 30
		0.2	>-0.05	0 to <1.0	>10 to 5	20 to 15
	30	0.0	-0.02 to 0.6	0 to >1.0	>20 to 5	25 to >100
		0.1	-0.04 to 1.1	0 to 0.8	>20 to 5	15 to 30
		0.2	-0.06 to 1.6	0 to 0.6	>20 to 5	10 to 15
75 keV injection energy, Bohm confinement kT_c = 5 keV	20	-0.4	>0.7	>1.0	7 to 6	>50 to 40
		-0.2	>0.4	>1.0	10 to 5	>0 to 20
		5.0	>0.04	>1.0 to 0.8	15 to 5	>50 to 15
		0.2	>-0.1	0.4 to 0	>20 to 4	50 to 10
		0.4	>-0.2	0.3 to 0	>20	30 to 10
	20	-0.2	>-0.05	0 to >1.0	>10 to 5	>50 to 20
		0.0	>-0.1	0 to 0.9	>10 to 4	15 to 10
		0.2	>-0.1	0 to 0.8	>10 to 4	7 to 5
	30	-0.2	-0.05 to 0.9	0 to >1.0	>10 to 3	20 to >50
		0.0	-0.09 to 1.9	0 to >1.0	>10 to 3	10 to 20
		0.2	-0.1 to 2.9	0 to >1.0	>10 to 3	5 to 10

TABLE 4-2
SUMMARY OF CLOSED-LOOP SYSTEM RESPONSE, FREQUENCY DOMAIN SPECIFICATIONS

	Temperature (keV)	Injection Energy Feedback Fraction	Range of Feedrate Feedback Fraction for Stability	ω_B (sec^{-1})	M_m	ω_m (sec^{-1})
Zero injection energy, constant confinement kT_c = 18 keV	20	0.0	0.02 to 0.03	0.03 to 0.1	1 to >10	0.02 to 0.08
	25	0.0	0.001 to 0.04	0.01 to 0.3	1 to >10	0.01 to 0.2
	30	0.0	-0.01 to 0.04	0.01 to 0.4	1 to >10	0.01 to 0.2
Zero injection energy, Bohm confinement kT_c = 11 keV	25	0.0	-0.07 to 0.005	0.01 to 0.3	1 to >10	0.01 to 0.2
	20	0.0	-0.08 to 0.003	0.01 to 0.6	1 to >10	0.01 to 0.3
	25	0.0	-0.08 to 0.04	0.01 to 0.8	1 to >10	0.01 to 0.3
75 keV injection energy, constant confinement kT_c = 5 keV	20	-0.2	>0.9	1 to 2	>10 to 5	0.3
		-0.0	>0.6	0.9 to 2	>10 to 4	0.3
		-0.2	>0.2	0.5 to 2	>10 to 3	0.2 to 0.3
		0.0	>0.09	0.5 to 2	>10 to 4	0.2 to 0.5
		0.1	>-0.02	0.1 to 2	1 to 5	0.1 to 0.5
		0.2	>-0.05	0.1 to 2	1 to >10	0.1 to 0.5
	30	0.0	-0.02 to 0.6	0.1 to 2	1 to >10	0.1 to 0.7
		0.1	-0.04 to 1.1	0.1 to 2	1 to >10	0.1 to 0.7
		0.2	-0.06 to 1.6	0.1 to 2	1 to >10	0.1 to 0.7
75 keV injection energy, Bohm confinement kT_c = 5 keV	20	-0.4	>0.7	0.9 to 2	>10	0.3
		-0.2	>0.4	0.8 to 2	>10 to 5	0.2 to 0.3
		0.0	>0.04	0.3 to 2	5 to 3	0.2 to 0.3
		0.2	>-0.1	0.1 to 2	1 to 3	0.1 to 0.3
		0.4	>-0.2	0.1 to 2	1 to 3	0.01 to 0.2
	20	-0.2	>-0.05	0.1 to 3	1 to 7	0.1 to 0.8
		0.0	>-0.1	0.1 to 3	1 to 4	0.1 to 0.7
		0.2	>-0.1	0.1 to 3	1 to 3	0.1 to 0.5
	30	-0.2	-0.05 to 0.9	0.1 to 4	1 to >10	0.1 to 1.0
		0.0	-0.09 to 1.9	0.1 to 4	1 to >10	0.1 to 1.0
		0.2	-0.1 to 2.9	0.1 to 4	1 to >10	0.1 to 1.0

• Zero injection energy, constant confinement. Whereas the open-loop system exhibits no overshoot up to temperatures in the 40 to 50 keV range, the closed-loop overshoot can be controlled to values less than 0.25 with feedrate feedback fractions less than 0.02 at temperatures as low as 20 keV. At the low overshoot values and a temperature of 20 keV, the time-to-peak remains rather high at greater than 100 seconds, though the settling time is improved to times below 1 minute. At these conditions the system bandwidth remains below 0.3 to 0.4 sec^{-1}. At high feedrate feedback fractions, a resonance peak which can attain values greater than 10 is now also present at a frequency in the range of 0.01 to 0.2 sec^{-1}. Its magnitude decreases to less than 2 at low feedrate feedback fractions.

• Zero injection energy, Bohm confinement. The high overshoot present in the open-loop system can be reduced to an acceptable level by proper selection of the feedrate feedback fraction. The associated effect on the speed of response is that the time-to-peak can increase into the one-minute range at 15 keV with large negative feedrate feedback fractions. The settling time to within 5% of the final value improves, decreasing at these conditions to under 40 seconds. The bandwidth can be varied by two orders of magnitude with feedrate feedback, and a resonance peak of significant magnitude (greater than 5) is located in the 0.01 to 0.1 sec^{-1} frequency range for high feedback fractions.

• 75 keV injection energy, constant confinement. This set of operating condition still presents difficulties in achieving acceptable overshoot at temperatures below 20 keV. However, improvement is possible with sufficiently high injection energy feedback fractions and low feedrate

feedback fractions at temperatures above 20 keV. For these latter conditions, a time-to-peak of 5 to 10 seconds is attained, with settling times less than ~30 seconds. The bandwidth is increased by nearly an order of magnitude, up to ~2 sec^{-1}, and the resonance peak can be significantly reduced (into the 0.2 to 0.3 range, at frequencies in the range of 0.2 to 0.6 sec^{-1}) by appropriate selection of the feedback coefficients.

- 75 keV injection energy, Bohm confinement. As in the case of the open-loop system, this operating condition exhibits the most desirable performance specifications. Even at temperatures as low as 10 keV, peak overshoot can be maintained below 25%, the time-to-peak below 20 seconds, and the settling time less than 30 seconds. Bandwidth is increased to the range of 2 to 10 sec^{-1}, and the resonance peak remains approximately the same as in the open-loop case.

The results presented in this chapter show that a significant improvement in system performance can be attained using only proportional feedback. The improvement is adequate for many conditions of interest, for example, 10 to 20 keV with 75 keV injection and Bohm confinement. However some conditions still encounter difficulties at low temperatures, such as the case of constant confinement with or without injection energy. The next chapter continues to explore methods of improving the system performance by investigating the proportional-integral-derivative controller.

CHAPTER 5
PROPORTIONAL-INTEGRAL-DERIVATIVE CONTROL

The classical control theory analysis of the preceding chapters has shown how the unacceptable temporal behavior of the thermal balance of a fusioning plasma can be improved. The improvement was accomplished using only proportional feedback with the fuel feedrate and injection energy as the controlling mechanisms and the plasma temperature as the control variable. The improvement in system response with proportional feedback was shown to be sufficient for many operating conditions of interest but inadequate for others.

The selection of the proper control system for a given application is usually determined by a compromise between the quality of the control desired and the admissible cost of the control system. For a capital intensive energy source such as fusion is expected to be, the value of highly reliable and precise plasma operation will probably allow for a large initial capital expenditure for the control system so as to ensure high quality control. It is thus desirable to investigate other control schemes that may further improve system response characteristics, extend the stable plasma temperature regime, allow greater operational flexibility, and/or provide more precise control of the thermal balance. This chapter presents extensions of the work of the previous chapters to indicate how these improvements might be

accomplished with the use of the proportional-integral-derivative (PID) controller.

The major advantage of proportional control is its powerful stabilizing action, simplicity, and wide range of adjustment. As discussed in Appendix B, its major disadvantage is that proportional control is subject to an inherent steady-state error under changing load conditions. This error can be eliminated with integral control, in which the magnitude of the control action is proportional to the time integral of the error. This type of control can thus provide a permanent change in the input variables so as to eventually eliminate any deviations of the controlled variable from its desired or setpoint value. The response with proportional control can also be improved by supplementing it with derivative control, in which the magnitude of the control action is proportional to the derivative of the error function and opposite in sign. Thus, since derivative control is such so as to oppose all change in the controlled variable, this control provides an additional stabilizing influence on the system. Derivative control is also characterized by rapid response, since it functions by anticipating system response. The combined effect of these three control modes are obtained from the proportional-integral-derivative (PID) controller.

Proportional control was modeled in the formulation of the plasma particle and energy conservation equations of Chapter 2 by terms of the form

$$C_{Sp} = K_s(kT_o - kT) \tag{5.1}$$

$$C_{T_sp} = K_{T_s}(kT_o - kT) \tag{5.2}$$

in equations 2.1 and 2.2, where C_{Sp} and C_{T_sp} represent the proportional control contributions from feedrate and injection energy feedback, respectively, K_s and K_{T_s} are the feedback coefficients used previously, kT_o is the desired or setpoint operating temperature, and kT is the actual operating temperature. Similarly, integral and derivative control can be implemented by introducing the following terms into equations 2.1 and 2.2,

$$C_{Si} = K_{si} \int_t (kT_o - kT)dt \qquad 5.3$$

$$C_{T_si} = K_{T_si} \int_t (kT_o - kT)dt \qquad 5.4$$

$$C_{Sd} = K_{sd} \frac{d\ kT}{dt} \qquad 5.5$$

$$C_{T_sd} = K_{T_sd} \frac{d\ kT}{dt} \qquad 5.6$$

where,

C_{Si} = integral control contribution using fuel feedrate with feedback coefficient K_{si}

C_{T_si} = integral control contribution using injection energy with feedback coefficient K_{T_si}

C_{Sd} = derivative control contribution using fuel feedrate with feedback coefficient K_{sd}

C_{T_sd} = derivative control contribution using injection energy with feedback coefficient K_{T_sd}

and the integrals are taken over all time t.

The derivation of the new system transfer functions can now proceed as in Section 2.2. Thus, a perturbation expansion can be used to linearize equations 2.1 and 2.2 including the new terms. The linearized equations can then be Laplace transformed, and the resultant expressions solved for the system transfer functions. Alternately, new expressions for the feedback transfer functions H_1 and H_2 can be derived by taking the Laplace transforms of equations 5.1 to 5.6 to give

$$H_1 = K_s + \frac{K_{si}}{s} + K_{sd}s \qquad 5.7$$

$$H_2 = K_{T_s} + \frac{K_{T_si}}{s} + K_{T_sd}s \qquad 5.8$$

Following the sign conventions established in Figure 2-2, these expressions can be substituted into equations 2.15 and 2.16, together with the expressions for G_1 and G_2 given by equations 2.13 and 2.14 to yield the closed-loop transfer functions directly.

Following either approach, the system transfer functions are given by

$$J_1 \equiv \frac{T}{S} = \frac{g_1 s(s - a + c/g_1)}{\{s^3(1 + g_1K_{sd} + g_2K_{T_sd}) +} \qquad 5.9$$

$$s^2[-a - d^* + g_1K_s + g_2K_{T_s} + (c - ag_1)K_{sd} - g_2aK_{T_{sd}}] +$$

$$s[ad^* - cb^* + (c - ag_1)K_s - g_2aK_{T_s} + g_1K_{si} + g_2K_{T_si}] +$$

$$[(c - ag_1)K_{si} - g_2aK_{T_si}]\}$$

and

$$J_2 \equiv \frac{T}{T_s} = \frac{g_2 s(s - a)}{\{s^3(1 + g_1 K_{sd} + g_2 K_{T_s d}) + \quad 5.10}$$

$$s^2[-a - d^* + g_1 K_s + g_2 K_{T_s} + (c - a g_1) K_{sd} - g_2 a K_{T_{sd}}] +$$

$$s[ad^* - cb^* + (c - a g_1) K_s - g_2 a K_{T_s} + g_1 K_{si} + g_2 K_{T_s i}] +$$

$$[(c - a g_1) K_{si} - g_2 a K_{T_s i}]\}$$

These expressions can be used to determine the system characteristics and response performance in terms of the six individual feedback gains by following procedures similar to those presented in the previous chapters. For the present work, it suffices to provide numerical examples of plasma performance that display the general trends of the PID controller; the presented results would thereby serve as guidance for future efforts.

The main features of the PID controller that are demonstrated below are elimination of offset error by integral action and improved system response and stability from derivative action. These effects are illustrated at the optimum plasma operating temperature, 15 keV, for the case of 75 keV neutral beam injection and constant confinement. To minimize the number of variable input parameters and still demonstrate the power and versatility of PID control, only the effect of injection energy feedback will be employed, i.e., it will be assumed that $K_s = K_{si} = K_{sd} = 0.0$. The effect of PID control is then developed by successively adding integral and derivative control to the proportional component of injection energy feedback.

To observe the temporal plasma behavior, the nonlinear differential equations 2.1 and 2.2, including the control functions of equations 5.1 to 5.6, were numerically solved in time. At 15 keV, the result of a +10% temperature perturbation is shown in Figure 5-1 for three values of the injection energy proportional feedback coefficient only. The equilibrium is seen to be unstable at the desired temperature of 15 keV with $K_{T_s} = 0.0$ and 0.1 (the plasma finds a new equilibrium at 28 keV or extinguishes), and stable with $K_{T_s} = 0.2$. Note that the system response with $K_{T_s} = 0.2$ compares favorably with the predicted response obtained by studying the stability diagram of Figure 4-3, and interpolating Figures 4-39 and 4-40, 4-47 and 4-48, and 4-55 and 4-56 for the expected overshoot, time-to-peak, and settling time.

A series of dynamic simulations of the plasma equilibrium with parametric variation of the feedback coefficients $K_{T_{si}}$ and $K_{T_{sd}}$ can thus be used to demonstrate the main features of the PID controller. The results are presented in Figures 5-2 to 5-7 and discussed below.

The effect of varying the integral control feedback coefficient, $K_{T_{si}}$, on the plasma temperature temporal response is shown in Figure 5-2. For a 10% step change in the operating temperature, from 15 to 16.5 keV, proportional feedback of magnitude $K_{T_{sp}} = 0.2$ alone is unable to achieve the desired final temperature. By adding the effect of integral control, the 16.5 keV final temperature can be achieved. At low values of $K_{T_{si}}$ the behavior is overdamped and slow to respond, and at high feedback fractions it is underdamped and exhibits overshoot and oscillatory behavior. The value of $K_{T_{si}} = 0.2$ would be a reasonable compromise between acceptable overshoot and adequate speed of response.

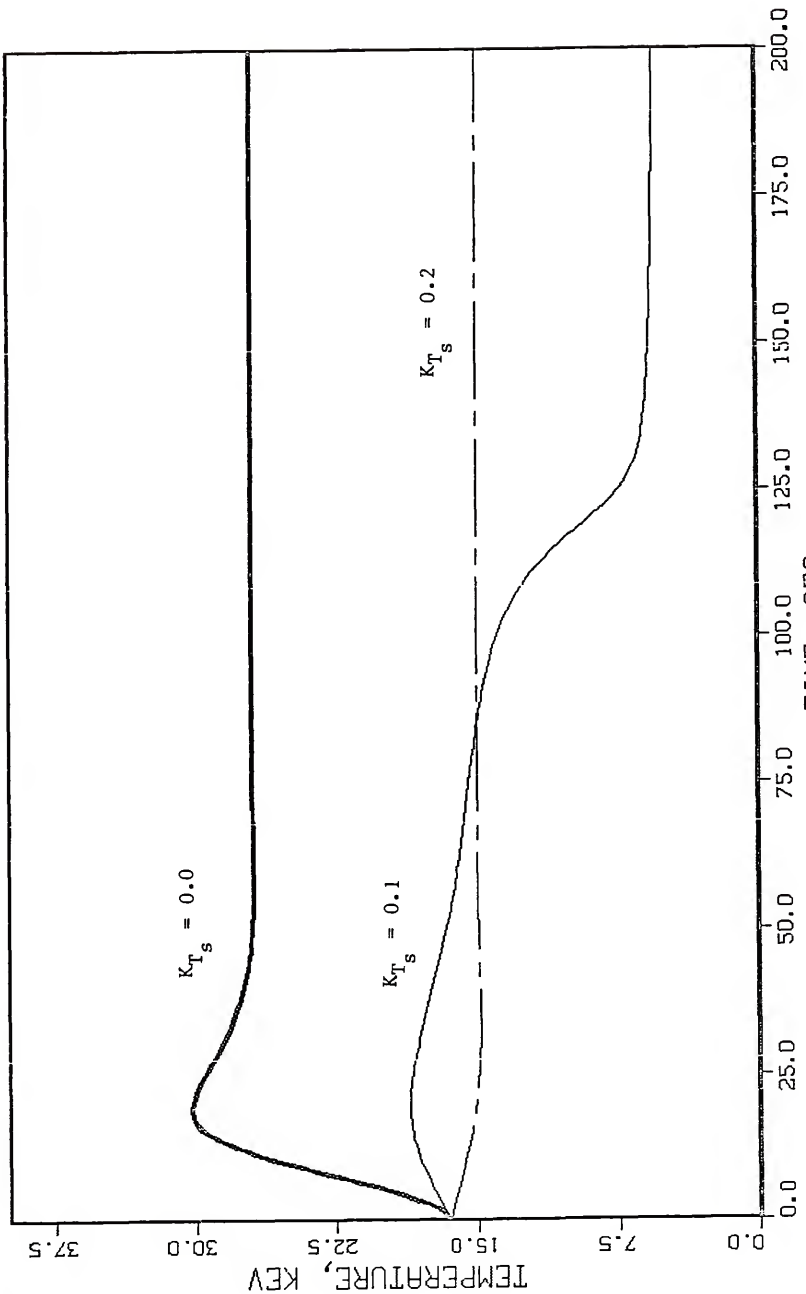

Figure 5-1. Effect of a +10% perturbation on the plasma temperature for three values of the injection energy proportional feedback coefficient, K_{T_s}. $K_{T_{s_I}} = K_{T_{s_D}} = 0.0$.

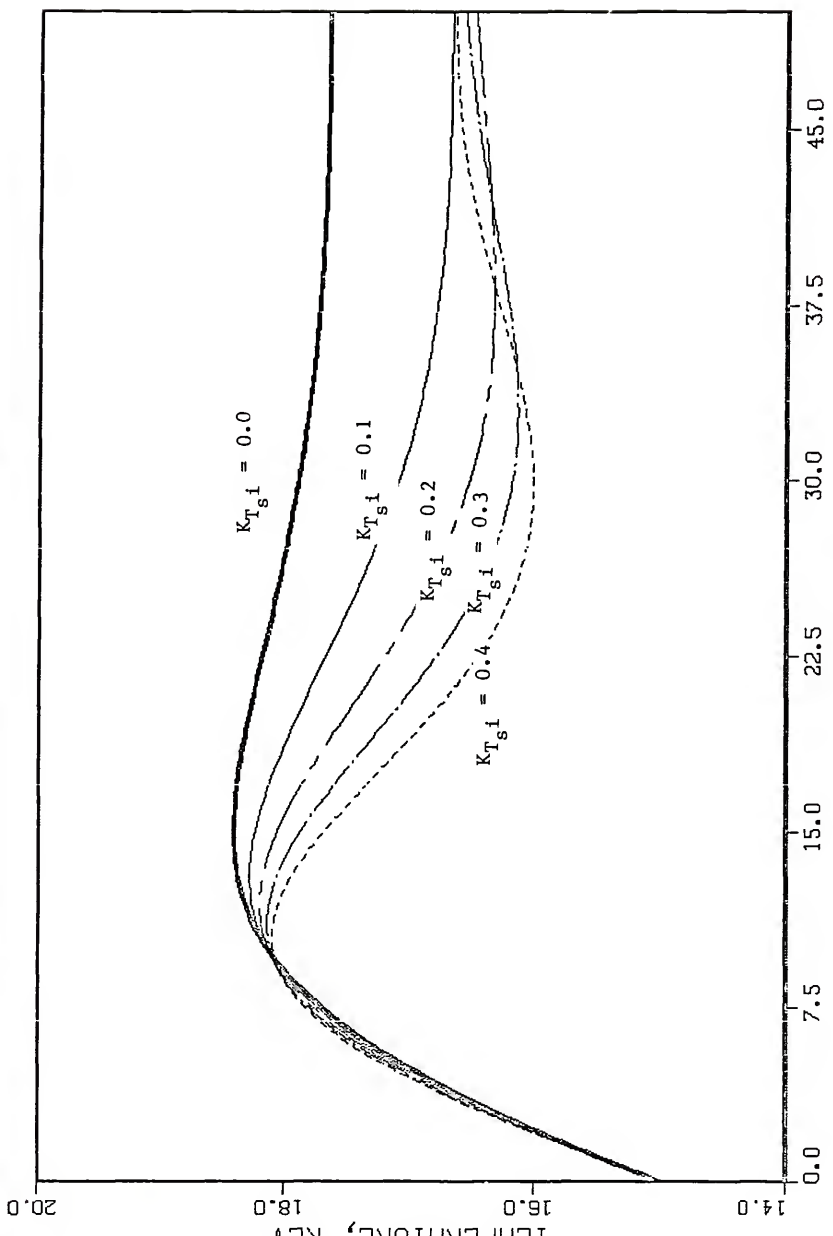

Figure 5-2. Effect on the system response of varying the value of the injection energy integral feedback coefficient. Step change in operating temperature from 15 to 16.5 keV. K_{T_s} = 0.2, $K_{T_s d}$ = 0.0.

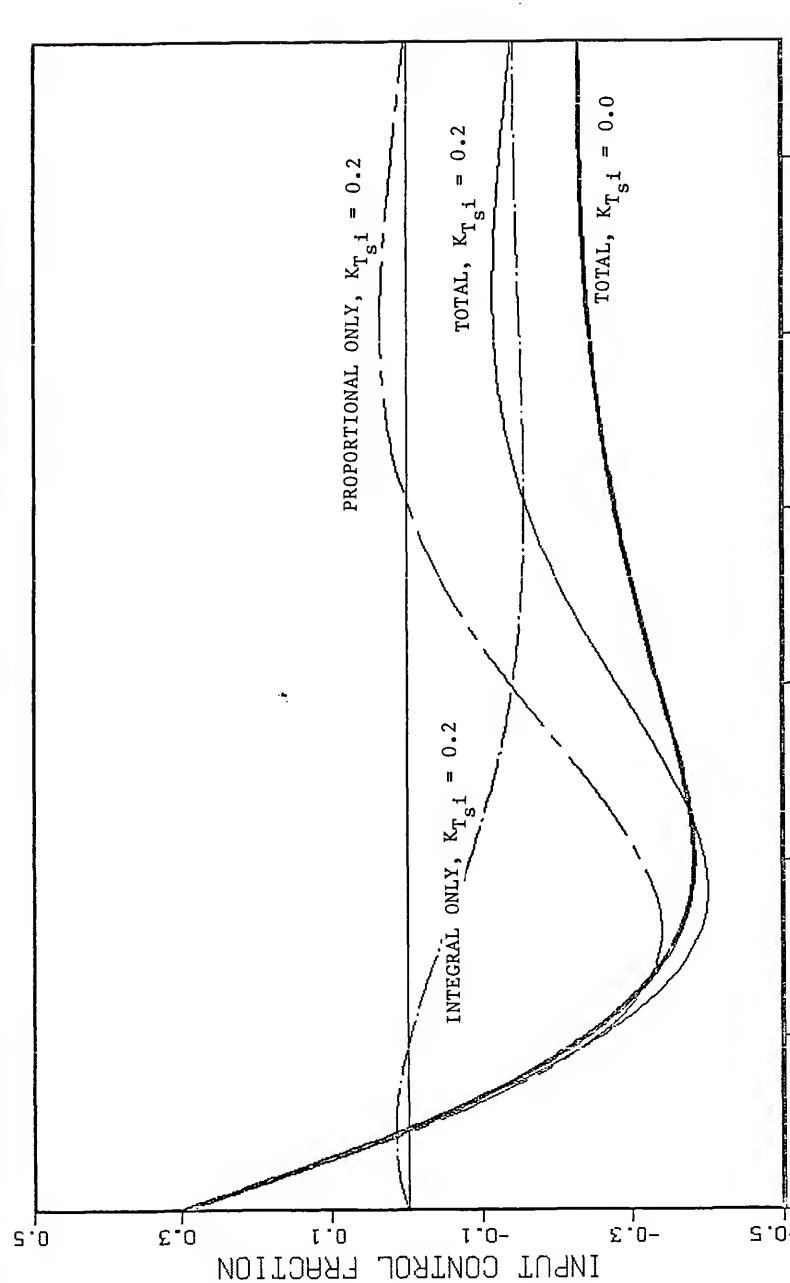

Figure 5-3. Relative contributions of the individual control modes to the total injection energy feedback fraction. Step change in operating temperature from 15 to 16.5 keV. $K_{T_s} = 0.2$, $K_{T_s d} = 0.0$.

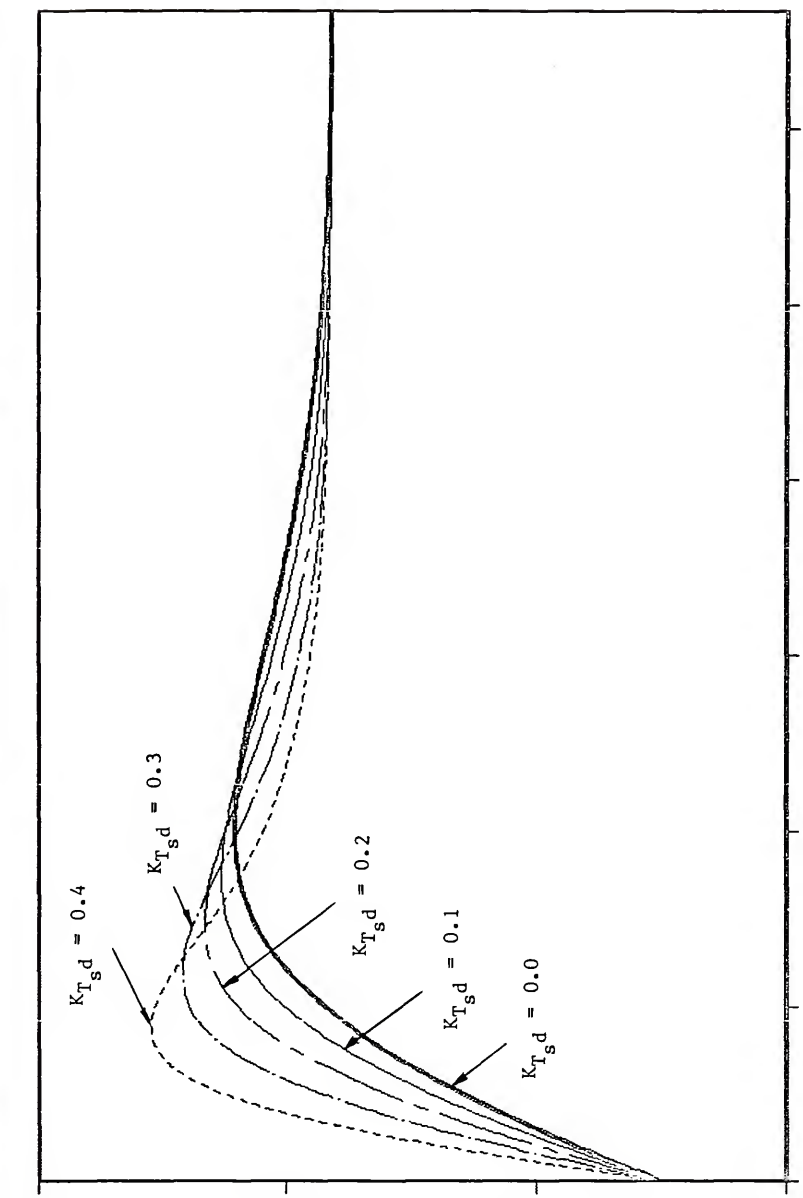

Figure 5-4. Effect on the system response of varying the value of the injection energy derivative feedback coefficient. Step change in operating temperature from 15 to 16.5 keV. $K_{T_s} = 0.2$, $K_{T_s i} = 0.0$.

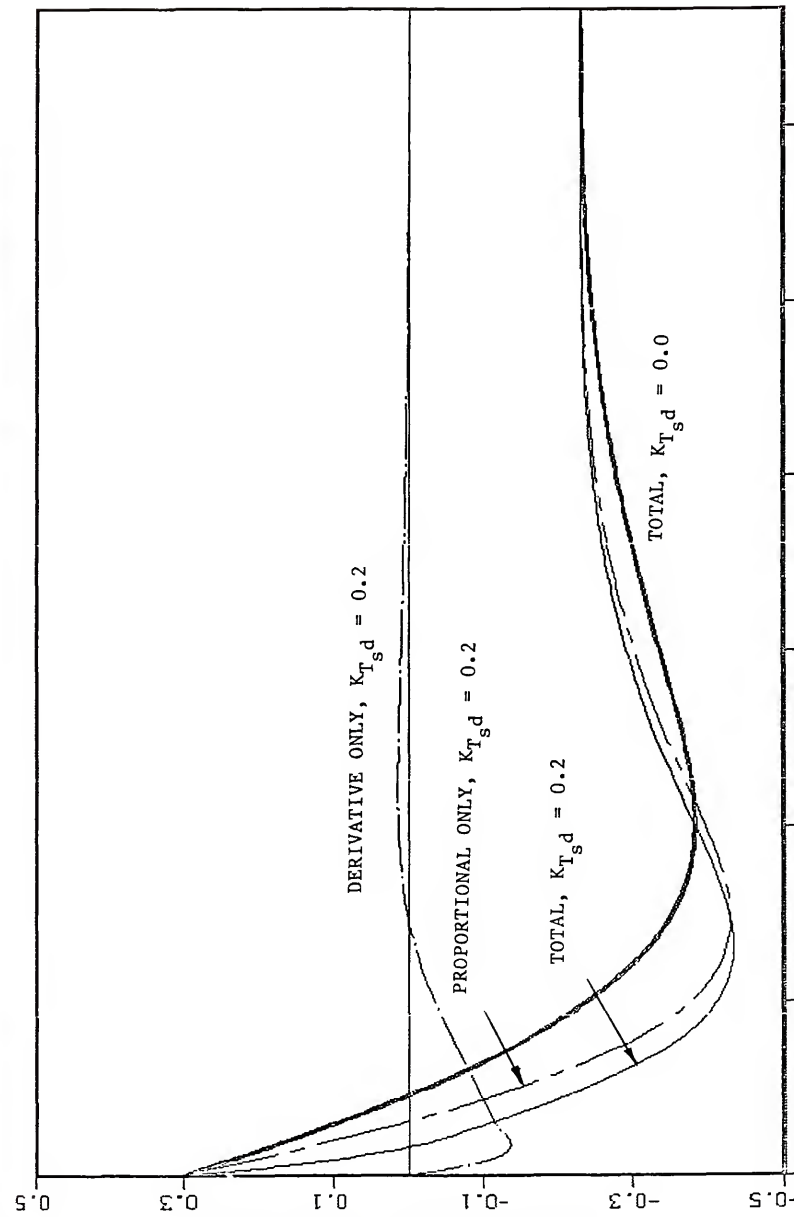

Figure 5-5. Relative contributions of the individual control modes to the total injection energy feedback fraction. Step change in operating temperature from 15 to 16.5 keV. K_{T_s} = 0.2, $K_{T_s I}$ = 0.0.

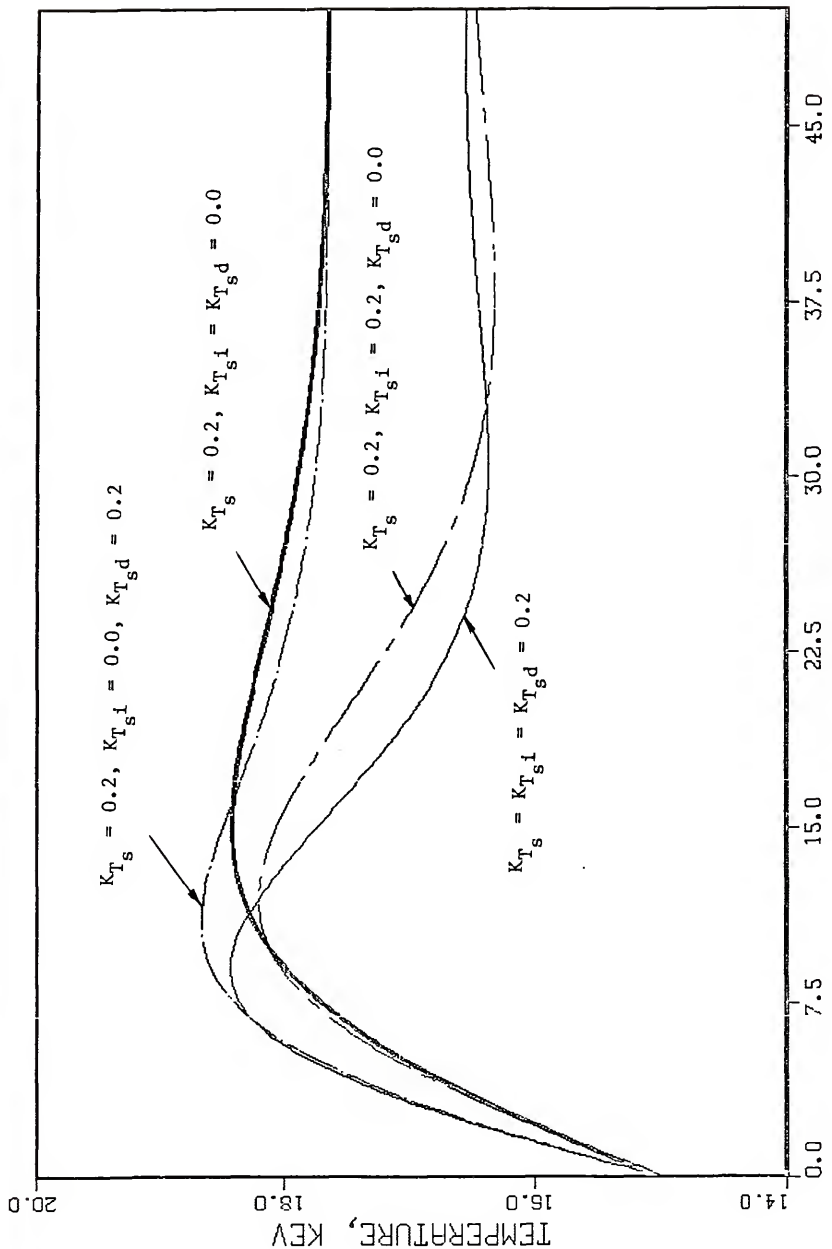

Figure 5-6. Effect on the system response of varying the value of both the injection energy integral and derivative feedback coefficients. Step change in operating temperature from 15 to 16.5 keV.

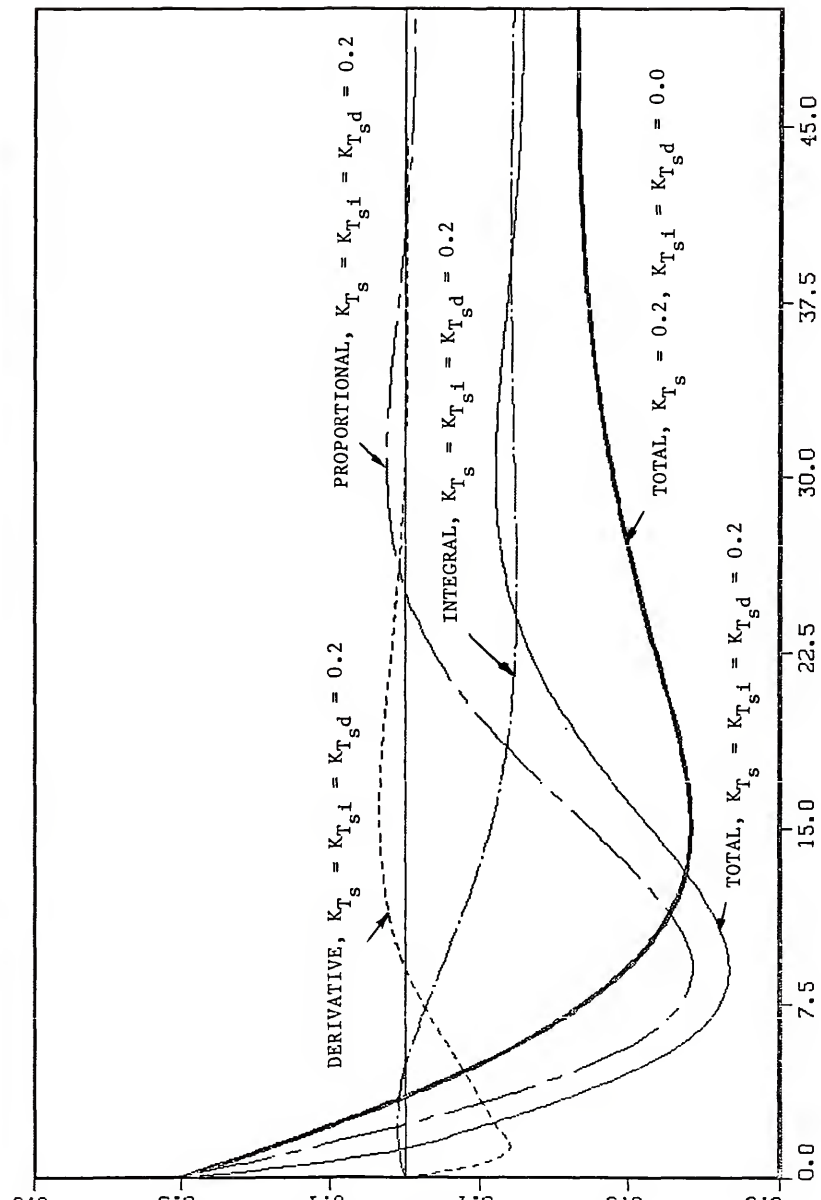

Figure 5-7. Relative contributions of the individual control modes to the total injection energy feedback fractions. Step change in operating temperature from 15 to 16.5 keV.

With $K_{T_sp} = 0.2$ and $K_{T_si} = 0.2$, the fractional contribution of the two control modes to the total effect of injection energy feedback are displayed in Figure 5-3. The case of $K_{T_si} = 0.0$ is shown for comparison. There are two important features shown in the figure. The first is that at steady state, the only active control element is that arising from the integral action. Thus, integral action is totally responsible for achieving the desired final temperature. The second feature is that since the area underneath the curves serves as a measure of the energy requirements of the control, it can be concluded that proportional-integral control is more energy-efficient than proportional control alone.

The effect of derivative control on the response of the plasma temperature is shown in Figure 5-4, again for a 10% step change in temperature at 15 keV with $K_{T_s} = 0.2$. The figure shows that derivative control attains a faster speed of response at the expense of increased overshoot. Subsequent to its first peak, however, the response does not oscillate, and attains its final temperature at times up to one-half of the no-derivative-control case. It can also be noted from Figure 5-4 that derivative action does not aid in eliminating offset error.

Using the values of $K_{T_sp} = K_{T_si} = K_{T_sd} = 0.2$, Figure 5-5 shows the fractional contributions to the total feedback of the individual proportional and derivative control modes. This figure shows that derivative control makes its contributions at the early times, when the temperature is changing most rapidly. Its effect diminishes as the temperature levels off. The figure also shows that the increased speed

of response is obtained at a cost of an increase in the injection energy requirement from the neutral beams.

Finally, the effect of the PID controller is demonstrated in Figures 5-6 and 5-7. Thus, it can be seen that with $K_{T_s} = K_{T_s i} = K_{T_s d} = 0.2$, the plasma attains the desired final temperature of 16.5 keV with a noticeably improved speed of response, and with a negligible increase in the overshoot. The price is an increased power requirement during early times, but a lower overall energy requirement is achieved.

The PID controller gains chosen for this example may not necessarily be the optimum selections. Simultaneous variation of the feedback coefficients either experimentally or analytically using equations 5.9 and 5.10 could potentially improve the effectiveness of the controller. Still, Figures 5-6 and 5-7 serve to indicate the improvements achievable with PID control.

In addition, displays similar to Figures 5-6 and 5-7 could be used in conjunction with optimal control methods in establishing the relative weighting criteria that would be assigned to deviations from desired or setpoint conditions and input control requirements. These would be used in establishing a quantitative definition of optimality. The general approach of using modern control methods in the control of the plasma thermal balance is presented in Appendix B.

CHAPTER 6
CONCLUSIONS

A review of the literature on the problem of fusion thermal stability has shown that many control mechanisms have been proposed, implemented and analyzed which permit operation of the plasma power balance in otherwise unstable temperature regimes. Though these control mechanisms can achieve the goal of stabilizing the thermal balance, the issues of overall system performance have not been addressed. Certainly stability is a necessary condition for operation, but perturbations and disturbances associated with real-world systems additionally require that the system possess desirable response characteristics, such as acceptable overshoot and adequate speed of response.

This work represents an analysis of the thermal balance of a fusioning plasma from a control system perspective. By applying the techniques of classical control theory, in addition to determining the requirements for stability, the response characteristics of the thermal balance have been evaluated. Thus, where previous studies were directed at determining the critical temperature for stability, the present methods were additionally directed at obtaining the system response in the stable regime.

The response of the thermal balance was evaluated using standard inputs to permit comparison of the system behavior to accepted control system guidelines. The results show that the stable regimes and

response characteristics of open-loop equilibria are highly dependent on the governing transport law and the injection energy of the incoming fuel. With constant confinement, operation without control would be limited to undesirably high temperatures. Even at the elevated temperatures, the open-loop response would be either exceedingly sluggish with no injection energy, or would exhibit high overshoots with only 75 keV injection energy. With Bohm confinement, stable operation is possible in a broader temperature range with or without injection energy, but overshoot is unacceptable at all temperatures without injection energy, and also at temperatures below nearly 20 keV with 75 keV injection.

Although it may be possible to obtain acceptable system response through the selection of the proper injection energy, this mode of operation would place additional and unnecessary constraints on plasma physics considerations and reactor operations. Restrictions on the injection energy are unnecessary because the system response can be improved via a dedicated control system employing closed-loop feedback. This work has shown that closed-loop proportional feedback using the feedrate and injection energy can be used to extend the stable operating temperature range. The results also show that significant improvements in system response are possible using only proportional feedback.

The stabilized temperature regime is a function of the confinement law, injection energy, and feedback coefficients. A range of feedrate and injection energy feedback fractions is available with which to stabilize the fusion power balance. Using only proportional feedback and no injection energy, the critical temperature decreases to 18 keV

and 11 keV with constant and Bohm confinement respectively, in contrast to the corresponding open-loop values of 25 and 14 keV. With injection energy, stable operation is available to as low as 5 keV, the ideal ignition temperature, by proper selection of the feedback coefficients.

The flexibility in selecting the feedback coefficients provides a broad range of control over the system performance. With constant confinement, the sluggish open-loop performance with no injection energy can be moderately improved, and the high overshoots with injection energy can be significantly reduced. However, these improvements are possible only at temperatures above 20 keV and require high feedback fractions. With Bohm confinement, the high overshoots present in open-loop operation with zero injection can be reduced to acceptable levels at temperatures as low as 20 keV, with a simultaneous decrease in the settling time to under 30 seconds. With 75 keV injection, acceptable overshoot can be obtained at temperatures as low as 10 keV, with the time-to-peak below 20 seconds and settling times less than 30 seconds. Even with Bohm confinement, it is still difficult to simultaneously satisfy overshoot and speed of response requirements at low temperatures and low feedback fractions.

The present techniques are of sufficient accuracy to provide an adequate representation of the actual system response without requiring dynamic simulation of the thermal balance. Thus, the techniques can be used in investigations of the control potential of other mechanisms such as the radiation-enhanced control of Reference 17, and the promising ripple-transport control mechanism of Reference 30. The control methodology presented here can be then used to ensure acceptable temporal behavior of the plasma output power.

Though the system response is significantly improved with only proportional feedback, additional improvement is available with the control mechanisms studied in this work by employing proportional-integral-derivative (PID) control. This work provides some preliminary indications of the potential benefits of PID control, and the indications are that more efficient control is possible while simultaneously improving the system response. Either an analytical or parametric analysis would be suitable for further examining plasma behavior with PID control.

It is expected that the complex interrelationships and large number of variables that are potentially available to effect control of the thermal balance of a fusioning plasma will require the use of modern control theory and optimization techniques. The plasma equations used in this work are well suited for adapting to state variable form, and the state variable representation can expand to accommodate additional control mechanisms and system variables.

If fusion achieves its ultimate potential as a viable energy source, the control of the power balance is a technical area which will have been satisfactorily addressed. This work has shown how only two control variables, the feedrate and injection energy proportional feedback fractions (and variations including integral and derivative control) can significantly change plasma performance. It is hoped that this work serves as a framework on which other control schemes can be analyzed and evaluated, using increasingly sophisticated techniques, which lead to achieving satisfactory control for fusion thermal stability.

APPENDIX A
INTRODUCTION TO FUSION
AND
REVIEW OF THE LITERATURE ON THERMAL STABILITY

A.1. Introduction

The fusion reaction receiving the majority of attention at the present time is the reaction of deuterium and tritium to yield a neutron, helium, and energy as follows:

$$ {}_{1}^{2}D + {}_{1}^{3}T \rightarrow {}_{2}^{4}He + {}_{0}^{1}n + 17.6 \text{ MeV} $$

The energy production rate per unit volume, or power density, P_f, of a plasma sustaining this fusion reaction can be expressed as

$$ P_f = n_D n_T \langle \sigma v \rangle E \qquad \text{A.1} $$

where n_D and n_T are the deuterium and tritium fuel ion densities, $\langle \sigma v \rangle$ is the reaction rate, i.e., the probability of fuel ions with a given velocity distribution of undergoing fusion per unit time, and E is the energy given off per reaction, 17.6 MeV. The temperature of the plasma enters the determination of fusion power density via the reaction rate and the relationship between the plasma temperature and the particle velocity distribution. Typical values of the reaction rate for a

Maxwellian velocity distribution are 10^{-16} to 10^{-15} cm^3/sec for temperatures in the range of 10 to 100 keV. Thus, from equation A.1, in order to obtain plasma power densities comparable to present day alternative energy sources such as fission power or coal, e.g., in the 10 to 100 watts/cm^3 range, fuel ion densities on the order of 10^{14} to $10^{15}/cm^3$ are required.

The leading approaches to achieving such densities and temperatures are the magnetic confinement schemes. In general, these schemes preferentially direct ions along magnetic field lines and/or suppress cross flow so that by sufficiently compressing the field lines, or sufficiently suppressing cross flows, high ion densities can be achieved. A figure of merit often used to evaluate the magnetic confinement schemes is the ratio of the particle kinetic pressure to the magnetic energy density (magnetic pressure). This ratio is denoted by β and is expressed as

$$\beta = \frac{nkT}{\frac{B^2}{2\mu_o}} \qquad \text{A.2}$$

where n is the total particle density, kT is the kinetic temperature, B is the magnetic field strength, and μ_o is the magnetic permeability constant in vacuum. The constant β is a characteristic of the confinement method effected by the particular machine configuration and hardware. For example, the Tokamak type of machine has a typical β of 5%, and the mirror type has a typical β of 50%.

Using equations A.1 and A.2, and assuming that the plasma has equal densities of deuterium and tritium ions in a fully ionized state, i.e., $n_D = n_T = \frac{n_{electrons}}{2} = \frac{n}{4}$, the densities can be eliminated from the equations, resulting in an expression for the power density in terms of machine characteristics and temperature only. This expression is given by

$$P = \frac{E\beta^2 B^4}{\mu_0^2} \frac{\langle\sigma v\rangle}{(kT)^2} \qquad A.3$$

For a given fuel cycle, the energy released per fusion event, E, is a known constant, and for a given machine, β is approximately a constant. Therefore, for a given maximum, technologically-limited magnetic field strength, the power density is optimized by optimizing the quantity $\frac{\langle\sigma v\rangle}{(kT)^2}$. The optimum occurs in the vicinity of 12 to 16 keV and, as described in the next section of this Appendix, this temperature range has been found to be thermally unstable.

An appreciation for the reasons for operating at the temperatures determined from peak $\frac{\langle\sigma v\rangle}{(kT)^2}$ considerations can be obtained as follows. The most comprehensive description of a commercial fusion reactor design to date is contained in the STARFIRE report[16]. The STARFIRE reactor operates at an average fuel ion temperature of 24 keV, has a fusion power density of 6.75 W/cm^3, and its nuclear fusion island cost is estimated at $1.2 billion. This latter figure includes only those systems necessary to confine and heat the plasma, and convert the neutron energy into the currently useful form of heat. The net cost of electricity was estimated to be 35 mills/kWh. If the temperature were

increased to 40 keV, for example, and assuming that magnetohydrodynamic (MHD) plasma stability requirements can be satisfied without additional penalty, the power output of the plant would decrease by 45%, resulting in a simultaneous increase in the cost of electricity to 53 mills/kWh. This increase includes credit for a decrease in the power production equipment cost. Alternately, the net power output can be maintained by increasing the reactor size - at an additional cost of $326 million for the reactor equipment only. By comparison, the entire instrumentation and control system for the STARFIRE complex was estimated to cost $29 million, or approximately 2% of the original nuclear equipment cost. Control to permit operation at the desired optimum condition is thus economically justified.

An alternative to operating at lower power density is to operate at higher magnetic field. In the STARFIRE reactor, the superconducting toroidal field coils are designed to produce an on-axis magnetic field of 5.8 Tesla, and a maximum field of 11.1 Tesla. If the operating point of the thermal balance were increased to 40 keV, the power density can be maintained at the previous 6.75 W/cm^3 by increasing the magnetic field strength. If the reactor maintains the same value of β, according to equation A.3 a new field strength of 12.9 Tesla is required to retain the previous power density. This is beyond the capability of anticipated fabrication and metallurgical advances in superconducting magnet technology during the next two to three decades. Thus, the rationale has been established for desiring to operate fusion reactors at temperatures approaching the 12 to 16 keV range, and for exploring methods of effecting effective control.

A.2. Literature Review

As presented in Chapter 1, the first consideration of thermal stability and its control was provided by Mills [2]. In Reference 2, Mills formulated the following particle and energy equations,

$$\frac{dn_i}{dt} = S - \frac{n_i}{\tau}$$

$$n_i \frac{d}{dt}\frac{3}{2}k(T_i + T_e) = n_i^2 p(1 - p)\langle\sigma v\rangle_{DT} c E^* - \frac{3}{2}Sk(T_i + T_e)$$

where p is the ratio n_T/n_i, E^* is the energy of the alpha particle, c is the fraction of the charged particle energy retained in the plasma, and S is the particle feedrate. Setting temporal derivatives to zero, Mills obtained the conditions for steady state. To study the stability of the equilibrium, he solved his steady state conditions for an expression mathematically equal to a constant and proceeded to find its logarithmic variation. Examination of the behavior of the resultant equation indicated that the equilibrium was stable against temperature fluctuations when the plasma temperature was above 28 keV. He suggested several methods, including feedrate, fuel mixture, radiation loss, and confinement time, by which control might be exercised for operation below 28 keV. He demonstrated the method which he deemed best, confinement time control inversely proportional to the temperature (Bohm-type confinement), to achieve stability to as low as 7 keV.

This work was performed using a very simple model. Only the D-T reaction was included and the ion species were assumed to be either tritium or "everything else". Only cold fuel was injected, fuel burnup was neglected, and radiative losses were artificially lumped and evaluated as a constant fraction of the fusion energy output. The fusion energy was assumed to thermalize instantaneously, and the differences in the electron and ion temperatures were determined in a simple fashion. Still, the analysis was very useful in obtaining results. In his second paper [3], Mills extended and improved this model by including three ion species - deuterium, tritium, and the product alpha, two types of radiative losses - bremsstrahlung and synchrotron, and explicit energy transfer between all particles.

Using this second model Mills repeated his Bohm confinement control and found that the stabilizing influence of this type of control depended on the confinement constant assumed. He concluded that mixture control was a better control method and presented time-dependent behavior demonstrating stable operation with a relay-type (on-off) application of mixture control. Nonetheless, some confinement time control was necessary to prevent unreasonable temperature overshoot. This was the first work to be performed on fusion thermal stability.

Ohta *et al.* [4] approached the problem using a similar model but with a different control methodology. The equations this time were

$$\frac{dn}{dt} = -\frac{n}{\tau_n} + S$$

$$\frac{dnT}{dt} = n^2 f(T) - \frac{nT}{\tau_E} + ST_s$$

$$f(T) = \frac{Q_c \langle \sigma v \rangle}{12} - 1.12 \times 10^{-15} T^{1/2}$$

where n (cm^{-3}) and T (keV) are the density and temperature of the plasma. Ions and electrons were assumed to be at the same temperature. The particle and energy confinement times are distinguished as τ_n and τ_E. The fuel injection rate is S ($cm^{-3} sec^{-1}$) and the injection energy is $3T_s$ (keV). The fuel cycle was D-T, and the ion species were assumed to be 50-50 deuterium-tritium. Bremstrahlung was explicitly included. The confinement time was assumed to be proportional to $n^{\ell} T^m$, with ℓ and m as constants defining the diffusion type. Different constants of proportionality were used for particle and energy confinement. Synchrotron radiation was neglected. High energy injection of the incoming fuel was included.

The nonlinear particle and energy equations were linearized by a perturbation expansion about an equilibrium condition, i.e., $n = n_o + n'$, $T = T_o + T'$, etc. The results were linear differential equations in the perturbed quantities. The following equations were explicitly solved

$$\frac{1}{n_o} \frac{dn'}{dt} = -\left(\frac{1}{\tau_{no}} + \frac{1}{\tau_{n1}}\right)\frac{n'}{n_o} - \frac{1}{\tau_{T1}} \frac{T'}{T_o}$$

$$\frac{1}{n_o} \frac{dn'}{dt} + \frac{1}{T_o} \frac{dT'}{dt} = \left(\frac{1}{\tau_1} - \frac{1}{\tau_{Eo}}\right)\frac{n'}{n_o} + \left(\frac{1}{\tau_2} - \frac{1}{\tau_{Eo}}\right)\frac{T'}{T_o}$$

$$\frac{1}{\tau_{n1}} = n_o \frac{\partial \tau_n^{-1}}{\partial n}\Big]_o$$

$$\frac{1}{\tau_{T1}} = T_o \frac{\partial \tau_n^{-1}}{\partial T}\Big]_o$$

$$\frac{1}{\tau_1} = \frac{1}{T_o}\Big[2nf(T) - nT\frac{\partial \tau_E^{-1}}{\partial n}\Big]_o$$

$$\frac{1}{\tau_2} = \frac{1}{n_o}\Big[n^2\frac{\partial f(T)}{\partial T} - nT\frac{\partial \tau_E^{-1}}{\partial T}\Big]_o$$

This yielded the conditions necessary to insure that perturbations decay in time, thus indicating the stability of the equilibrium. The conditions are presented in Table A-1, along with the resultant critical temperatures. For operation in the unstable regime, Ohta et al. [4] suggested feedback stabilization. Confinement time, bremsstrahlung, feedrate, and injection energy were suggested, and the latter two were deemed preferable. Feedback proportional to the density perturbation was ineffective and feedback proportional to the temperature perturbation was investigated in detail. The feedback term, incorporating a delay time, was added to the above perturbation equations and a generalized set of conditions necessary for feedback stabilization was obtained. The conditions are given by

$$A\gamma^2 + B\gamma + C = 0$$

TABLE A-1
STABILITY CRITERIA AND CRITICAL TEMPERATURE (Ref. 4)

Confinement Scheme	Stability Criteria[a]	Critical Temperature (keV)	
		Charged Particle Heating[b]	150 keV Neutral Beam Injection[c]
τ_E = constant	$\frac{T_o}{F_o}\frac{\partial F_o}{\partial T_o} > 0$	28	21
$\tau_E \propto T^{-1}$ (Bohm)	$\frac{T_o}{F_o}\frac{\partial F_o}{\partial T_o} > -2$ and $-\frac{1}{\zeta_2}$	14	5
$\tau_E \propto n^{-1}T^{1/2}$ (Classical)	$\frac{T_o}{F_o}\frac{\partial F_o}{\partial T_o} > \frac{1}{2}$ and $\frac{1}{2\zeta_2}\left(1 - \frac{5}{R}\right)$	42	33

(a) $F(T) = \frac{\zeta_2 T}{f(T)}$

(b) $T_s = 0$, $R = 1$

(c) $T_s = 50$ keV, $R = 10$

with

$$A = 1 + (T_s/T_o - 1)\alpha\Delta t$$

$$B = \frac{1}{\tau_{no}} - \frac{1}{\tau_2} + \frac{1}{\tau_{Eo}} - (T_s/T_o - 1)\alpha + \frac{\alpha\Gamma t\xi_2}{\tau_{Eo}}$$

$$C = \frac{1}{\tau_{no}}\left(\frac{1}{\tau_{Eo}} - \frac{1}{\tau_2}\right) - \frac{\alpha\xi_2}{\tau_{Eo}}$$

where

$$\xi_2 = 1 - \frac{T_s}{RT_o}$$

The system is stable if $A>0$, $B>0$, $C>0$, or $A<0$, $B<0$, $C<0$. Note that the conditions for stability migrate as the equilibrium conditions change.

The dynamic behavior of a fusioning plasma was then studied by Horton and Kammash [18] using a model similar to Mills' second model. The strength of this model stemmed from its refined treatment of the confinement laws (three Tokamak reactor-type scaling laws were included), and charged particle heating (energy transfer) mechanisms. Fuel burnup was included. Stable operating regimes for a range of reactor parameters were obtained by observing the time dependent behavior of the system. The three confinement schemes investigated demonstrated differing characteristic behavior- negligible overshoot with Bohm diffusion, damped oscillation with anomalous diffusion, and quasi-steady (no true steady state) with neoclassical diffusion.

Powell and Hahn [19] added a novel feature to the previous models - the interaction of the plasma with the confining magnetic field. Their contention was that results obtained previously were too pessimistic. They contended that as the temperature of a plasma increases due to a runaway (unstable) condition, the plasma would tend to expand, thereby doing work on the magnetic field. A reverse situation would exist if the temperature were decreasing. This exchange of energy in the form of work might serve as a stabilizing influence on the energy balance, leading to lower critical temperatures.

The plasma model assumed both pure deuterium or D-T fuel injection, allowance for the four dominant fusion reactions, equal electron and ion temperatures, quasistatic expansion of the plasma, and a sharp plasma-magnetic field boundary. Power input to the magnetic coils was included but its effect was investigated in a subsequent study. Volume was introduced in the equations, as was the magnetic field strength (implicitly, through the sharp boundary assumption). Results were presented for the deuterium injection case only. A stable energy balance was obtained for temperatures above 100 keV and the effect of including the magnetic field was estimated as a 20 keV reduction in the critical temperature.

In the subsequent paper [20], Powell significantly extended the results and conclusions of the previous model, including the effect of including the input power to the magnetic field coils. He first established the association of the input control triplet (B, S_2, τ), with a unique equilibrium point in n-T-V space. The unique association so ascertained, the conclusion was drawn that field strength, feedrate,

and confinement time constituded a satisfactory set of control variables. He introduced the following control functions:

$$\frac{dB^2}{dt} = C(B_f{}^2 - B^2)$$

$$\frac{ds_2}{dt} = C(S_{2f} - S_2)$$

$$\frac{d\tau}{dt} = C(\tau_f - \tau)$$

where C is a constant, and B_f, S_{2f}, and τ_f are the desired values of the magnetic field strength, deuterium feedrate, and confinement time. These control functions were employed to transfer the plasma from one equilibrium state to another without instabilities or other misbehavior. Overshoot was minor. Other conclusions of this study were that scores of dynamic simulations would be required to give a complete picture of the system response, that the control functions may have difficulties at low temperatures, and that optimization of the control is an important area deserving study.

The first explicit eigenvalue analysis of the thermal balance was presented by Stacey [21]. The plasma model included the D-T fuel cycle only, two ionic species, instantaneous particle slowing down and energy equilibration, explicit energy transfer between particles, and separate ion and electron temperatures. Confinement time and radiation losses were modeled in great detail. The equations were linearized about an equilibrium point, Laplace transformed, and the eigenvalue dependence on temperature was observed. The largest eigenvalue of the system was shown to be positive at low temperatures, becoming negative and

indicating stability at temperatures consistent with previous results. The results were confirmed by dynamic simulation. For control of the plasma at an unstable point, Stacey investigated both feedrate and fuel mixture. He used three relay-type algorithms responding to the electron temperature. Delay time in control application was included. The results depicted a reactor operating in an oscilltory mode, with the inability to restrict the oscillations to a narrow band unless the delay was reduced to zero.

The same type of eigenvalue analysis performed by Stacey was performed by Fujisawa [22], who included a separate energy equation for the fast alpha group. Energetic injection of the fuel was included in the model, but confinement expressions were simpler and synchrotron radiation was ignored. Fujisawa linearized his equations and cast them into the form $\frac{d\vec{x}}{dt} = A\vec{x} + B\vec{u}$, where A and B are the system matrices, $\vec{x}$ is the state vector representing particle densities and energies, and $\vec{u}$ is the input vector (used as a scalar in this study). The system stability was examined by observing the eigenvalues of A. For operation in the unstable region, Fujisawa investigated the effect of external feedback control. The control mechanism investigated was a pure capacitive delay of the fuel injection flow rate. The effect of this control on the dominant eigenvalue resulted in stabilized behavior in a limited temperature range. Additional calculations indicated improved temporal behavior of the stabilized plasma by the use of a phase advance compensation network.

Bassioni and Husseiny [23] reverted to the earlier model of Ohta et al. [4] and examined the controllability of the linearized system. Fuel burnup was included as the only revision of the earlier model.

Casting the linearized system into the form of Fujisawa, the earlier stability criteria of Ohta et al. [4] shown in Table A-1 were rederived with good agreement. In addition, the matrix $G = [B \mid AB]$ was found to be non-singular. This indicated the controllability of the system with the input vector $\vec{u}$. This vector consisted of particle injection, external heating, and bremsstrahlung radiation loss control. Invoking a constant feedback law including time delay, the characteristic equation of the system was then obtained. Using the Pontryagin criterion, the domain of linear stability was found. More general results were derived using the Mikhailov criterion.

The results obtained in Reference 23 are very general. Due to their generality, it is difficult to translate their conditions into critical temperatures. On the other hand, Usher and Campbell [24,25], using essentially the model of Ohta et al. [4], and including burnup, reaction product accumulation, and beam-plasma interactions, clearly delineated the critical temperatures for various fuel cycles and confinement models. Their findings are presented in Table A-2. The differences from Table A-1 are due to improvements in the plasma modeling. For operation below the critical temperature, delayed feedback control was employed. The results permitted the characterization of the confinement schemes as to ease of control, required magnitude of the feedback, and the allowable delay times. Maya [14] then quantitatively demonstrated that the use of the type of feedback of Ohta et al. [4] was limited as to how far below the critical temperature stabilized operation was possible. O'Farrill and Campbell [11] then presented critical temperatures for two component plasmas. They used an extensive model for the beam-plasma interaction

TABLE A-2

CRITICAL TEMPERATURES (keV) FOR
DIFFERENT FUEL CYCLES (Ref. 24)

Fuel Cycle	Diffusion Model			Maximum Temperatures
	BOHM	Constant	Classical	
D-T	14	24	38	200
D-He^3	68	98	140	660
D-D	40	82	260	>1000

and extended previous results by including non-Maxwellian fusion reactions. Table A-3 summarizes the extended ranges of operation resulting from the beam-plasma interaction.

Nonlinear techniques were applied to the analysis of thermal stability by Ferrell and Kastenberg [27]. Using the model of Ohta et al. [4], the Mean Value Theorem was used to cast the system into a form readily analyzed by comparison theorems. Upper and lower bounds of stability, as well as the domain of allowable perturbations were thus obtained.

A multigroup formulation of the slowing down of the alpha particles was included in the work of Ohnishi and Wakabayashi [28]. The energy transfer of the product alphas and energetic injected ions to the thermal background plasma was treated in great detail. The linearized state equation was obtained as before and the eigenvalues of the system were obtained. The effect of the instantaneous slowing down approximation could thus be evaluated. The results showed that in the unstable regions, the multigroup approximation resulted in nearly a 30% reduction in the magnitude of the largest eigenvalue over that obtained assuming instantaneous slowing down. These results demonstrated the stabilizing influence of the finite time required by the fusion alphas to transfer their energy to the bulk background plasma.

The use of toroidal field ripple as a control mechanism of the thermal balance was proposed by Petrie and Rawls [29]. Magnetic field ripple is the non-axisymmetric component of the toroidal magnetic field created by the finite number of coils used to generate the confining magnetic field. The resultant ripple-enhanced thermal conductivity, with its $T^{7/2}$ dependence, was proposed as an effective method of

TABLE A-3
EFFECT OF THE ENERGETIC DEUTERON FRACTION
ON THE STABLE OPERATING BULK TEMPERATURES
OF THE TCT FOR THREE CONFINEMENT MODELS (Ref. 11)

Diffusion Model	w	Stability Range[a] (keV)
$\tau_E \alpha$ Constant	0.0	27 to 30
$\ell = 0$, $m = 0$	0.1	1 to 5 and 25 to 30
	0.2	1 to 7 and 23 to 30
	0.3	1 to 11 and 18 to 30
	0.4 to 1.0	1 to 30 all stable
Bohm		
$\tau_E \alpha T^{-1}$	0.0	15 to 30
$\ell = 0$, $m = -1$	0.1	1 to 30 all stable
Classical		
$\tau_E \alpha n^{-1}T^{1/2}$	0.0	All unstable
$\ell = -1$, $m = 1/2$	0.1	1 to 3
	0.2	1 to 4
	0.3	1 to 6
	0.4	1 to 7 and 29 to 30
	0.5	1 to 9 and 26 to 30
	0.6	1 to 15 and 19 to 30
	0.7 to 1.0	1 to 30 all stable

Deuteron injection energy = 150 keV

$nT = \frac{1}{2} n_e$, $w = \frac{n_B}{(n_B + n_D)}$, $R = 0.016$

[a] 1 keV to 30 keV was the range of temperatures studied.

inhibiting the runaway growth of the plasma temperature by increasing energy loss faster than the energy gain from the increase in reactivity. A set of conditions determined from physics and engineering considerations were derived in Reference 29 specifying the range of ripple required to provide satisfactory burn control. The conditions were specified in order to ensure that the ripple-enhanced transport does not appreciably increase the difficulty of reaching ignition, that it is the primary loss mechanism during burn, and that the increased loss of fast alphas does not degrade the reactor performance. The work was performed using a 0-D model, and one-dimensional transport analysis results were shown to be in good agreement.

The use of ripple-enhanced transport to effect thermal stability was also investigated by Bromberg and Cohn [30]. As in Reference 29, since stability is achieved by enhancing an energy loss mechanism, a higher $n\tau$ condition is necessary to achieve ignition. In Reference 30, thermal stability by radial motion of the plasma as determined by MHD constraints was also investigated. Physically, the radial motion accompanying a runaway temperature condition reduces the plasma density and thus the alpha heating power, minimizing the thermal excursion. A critical temperature as low as 25 keV was obtained without resorting to any anomalous ion loss mechanism.

The use of low energy neutral fuel injection at the plasma edge ("gas puffing") as a thermal control mechanism was investigated in Reference 31. This type of control enjoys the advantage of requiring negligible auxiliary power in that some form of gas injection for refueling of the reactor during operation is postulated for many

reactor designs. It effects control of the thermal instability by controlling the plasma ion density via diffusion of the injected neutrals into the central reactor region. Though the oscillations in reactor power ranged as high as 20% in the numerical examples presented in the articles, the authors presented arguments stating that the excursions could, in principle, be reduced to zero amplitude.

The literature review presented herein describes all the mechanisms which have been proposed for the control of the thermal instability. Emphasis has been placed on 0-D models since even most of the analyses reported in the literature which began with 1-D models averaged the plasma parameters over the appropriate dimension in order to be able to obtain manageable mathematics and quantifiable results. Illustrative examples have been presented where appropriate. However, this review is not exhaustive in numerical examples since the applications to specific reactor conditions do not provide any additional insights. The view that has been presented of the thermal stability problem is one in which many mechanisms have been proposed that provide varying degrees of control. However, no formal method of specifing, evaluating, and selecting the preferred choice has been put forth. This issue is addressed in the main body of this report.

APPENDIX B
CONTROL THEORY REVIEW

B.1. Introduction

The most fundamental function of a control system is to adjust the operating state of a process, as determined by the measured values of a set of variables, to match a set of desired values for the same set of variables. This can be accomplished by using either open- or closed-loop control. An open-loop system is one in which the controller action is not dependent on the actual response of the controlled system. A closed-loop control system is one in which the deviation of the actual operating condition from the desired operating condition determines the course of action taken by the controller to return the system to the desired state.

The thermal balance of a fusioning plasma can be viewed as an open-loop control system as follows. The values of the input parameters required to maintain a prescribed level of energy production in the plasma can be obtained by solving the appropriate governing equations of mass and energy balance. In theory, the steady state value of the system variables is dictated by the choice of input parameters. In practice, however, external disturbances are quite likely to cause deviations from the nominal operating conditions. In this open-loop system, the input parameters would not be automatically

adjusted to offset the deviations, since the input controller is not affected by the system response. Chapter 3 and the previous Appendix have shown how the open-loop plasma thermal balance is unstable to such disturbances in the temperature range of 12 - 16 keV, although stability could subsequently be achieved at higher temperatures. Even at the higher, stable temperatures the thermal balance was shown to have poor system response.

This open-loop system can be transformed into a closed-loop system through the addition of feedback, i.e., by modifying the input (control) variables in accordance with the behavior of the system variables. The closed-loop plasma system may then be able to sustain stable performance at temperatures which were previously unstable. The closed-loop system may also be able to improve the system response at temperatures which were previously stable, but had poor response characteristics.

Other desirable features of a control system are that it can increase the ability of the overall system to tolerate spurious signals and noise, i.e., it can decrease the system sensitivity to perturbations, and that it can return perturbations of the system variables to their nominal values in a reasonable time, i.e., that it result in acceptable overall system response. A review of representative system specifications of these and other desirable features, in both the time and frequency domain, which are used to evaluate system performance are presented in this Appendix. Many of these desirable characteristics can be achieved with closed-loop control systems.

The analysis and design of control systems can be divided into two general categories, classical and modern control. Whether classical or modern, the analysis phase consists of certain basic steps which include gaining a thorough understanding of the physical processes involved, describing the system with a sequence of functional block diagrams and/or differential equations, the application of the analysis technique (whether classical or modern), and the comparison of the results of the analysis with intuition, past experience, and the physical understanding of the system.

In the classical control system design method, if the results of the analysis reveal inadequacies in system performance, equipment or components can be added to the system in order to improve the responce and obtain the desired specifications. The process is iterative in that the analysis phase is reentered and the response of the plant is reevaluated, including the effect of the added compensation elements. The latter elements are then readjusted in light of the updated analysis results. The iteration is terminated and the control system design considered complete when acceptable behavior is obtained as measured by the set of performance specifications.

In the modern control system design method, a performance index is first defined for the system. Then the necessary structure to obtain or minimize the specified performance index is determined by following a logical mathematical formulation which completely and uniquely satisfies the constraints. These methods are described in this Appendix, beginning with the classical methods.

B.2. Classical Methods

Consider the linear open-loop system of Figure B-1, and the closed-loop system of Figure B-2. The functions r(t) and c(t) represent the system input (control) and output functions. The system feedforward transfer function, defined as the Laplace transform of the system impulse response for zero initial conditions, is given by G(s). H(s) represents the feedback transfer function. The open-loop transfer function is defined as G(s)H(s), while the closed-loop transfer function is given by the expression

$$\frac{C(s)}{R(s)} = \frac{G(s)}{1 + G(s)H(s)}$$

For second order systems, the denominator of the transfer function $\frac{C(s)}{R(s)}$, called the characteristic polynomial, when set equal to zero, yields the system characteristics of natural frequency, damping ratio, and the closed-loop poles of the system. These characteristics dictate the transient response of the system.

The evaluation of system performance in the time domain involves observing the response of the system to standard inputs such as an impulse- or step-function. The specifications used to judge the analysis include:

1. Maximum overshoot, M_p- the magnitude of the system response following a step input, at the peak of the first overshoot.

2. Time-to-peak, t_p- the time required to reach the first peak (maximum overshoot)

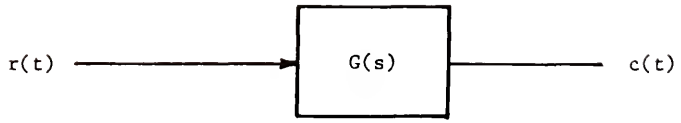

Figure B-1. Open-loop system.

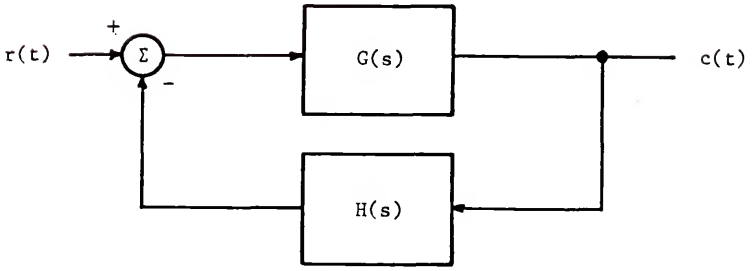

Figure B-2. Closed-loop system.

3. Time to first zero, t_o- the time required to reach the final value for the first time.

4. Settling time, t_s- time for the output response to remain within a specified percentage, usually 5%, of the final value.

In the classical second order system, the above performance specifications can be explicitly expressed in terms of the system characteristics. (The specifications for the plasma system are derived in Appendix C.) When the real parts of all the poles are less than zero, the transient response decays exponentially, i.e., the system is stable. If any of the poles have positive real parts, the response grows with time, indicating instability. To study the response of the classical second order system, it is therefore necessary to study only the system's poles.

The open loop transfer function of Figure B-1 has a constant gain, K, associated with it. If this gain is allowed to vary, the roots of the characteristic equation (1 + KGH) will vary. The root locus method provides a graphical means of evaluating the roots of the characteristic equation as the loop gain varies. Basically, a set of construction rules [32 - 34] are followed that permit the plotting of the root loci. Mechanical aids and computer programs [35] are available that provide accurate root locus plotting. An unstable linear system is stabilized by adjusting the gain such that all the roots have crossed the imaginary axis and entered the left-half plane. If stability is not attainable, additional elements or modifications are incorporated into the control system.

For the analysis and synthesis of control systems in which the specifications are specified in the time domain, the root locus technique is an able tool. However, frequency response methods are often naturally applicable due to the presence of sinusoidally varying time signals. Quite often, the desired performance of a system can be translated into frequency domain specifications such as bandwidth, resonance peak and frequency, and gain and phase margins. These are defined below for the case of second order systems.

1. Bandwidth, ω_B- the frequency where the closed loop response magnitude is $1/\sqrt{2}$ of its low frequency magnitude.

2. Resonance frequency, ω_m- the frequency at which the transfer function obtains its maximum magnitude.

3. Resonance peak, M_m- the magnitude of the transfer function at the resonance frequency.

4. Gain margin, GM- At the frequency where the phase of the open loop transfer function $G(j\omega)H(j\omega)$ passes through -180°, GM is the additional gain needed to make the system unstable if it is already stable, or the amount by which the gain must be reduced to make the system stable if it is already unstable.

5. Phase Margin, PM- At the frequency at which the magnitude of $G(j\omega)H(j\omega)$ is unity, PM is the additional phase lag needed to make the system unstable if it is already stable, or it is the additional phase gain needed to make the system stable if it is already unstable.

Three of the more common methods of plotting the frequency response of a system include polar plots, Bode plots, and gain-phase or log-modulus plots. It is convenient, in plotting frequency response, to substitute $j\omega$ for the Laplace transform variable, s. The polar plot

is useful in connection with the Nyquist stability criterion, discussed below. Both the gain-phase plot as well as the polar plot can be obtained from the Bode plot, so only the latter will be discussed.

The Bode plot is simply a graph of the magnitude and phase of the transfer function versus frequency. Also called the corner or logarithmic plot, the Bode plot applies the property of logarithms of changing multiplications into additions. Because of this simplicity, the addition of poles and zeros to the transfer function (in a design step, for instance) is quickly incorporated in the graph. A gain adjustment merely raises or lowers the magnitude plot at every point a fixed amount, while the phase plot remains the same. The construction rules for the Bode plot are quite simple and straightforward and are also available in References 32 to 35.

The Nyquist stability criterion is a graphical method of predicting the stability of the closed loop system using the frequency response of the open loop transfer function. Consider a closed (clockwise) contour Q enclosing the whole right-half plane in s-space. Consider now a polar plot of G(s)H(s), as s follows the contour Q. The Nyquist criterion states that the net number of (counterclockwise) encirclements of the point (-1,0) by the plot of GH is equal to the number of poles of GH minus the number of poles of the closed loop system inside the contour Q, i.e., in the right-half s-plane. For stability, it is required that there be no closed-loop poles in the RHP, therefore, the number of counterclockwise encirclements of (-1,0) should equal the number of poles of GH.

Whereas numerical stability techniques such as the Routh criterion tell only if a system is stable or not, Bode and Nyquist plots additionally give a measure of the relative stability of the system. Relative stability is measured by gain and phase margin.

After the specifications have been assessed for the given system, if the desired specifications have not been met, gain adjustments and additional frequency-dependent compensation is designed into the system. It is in this design phase, that all the specifications must be simultaneously satisfied, if possible. This is accomplished by the addition of physically realizable components in one of two ways- in cascade (in the feedforward path), or in the feedback loop. Two examples of compensation elements are the phase lag and the phase lead networks. Other types of compensation elements can be found by the use of Truxal's method, inverse root locus method, Chen's method, etc.[32] These methods involve trial and error procedures, experience, ingenuity, and a great deal of perseverance. The satisfactory system design is by no means unique.

The number of techniques available with which to effect control of a system is large. Table B-1 presents a partial list of generic control types. Each control type has certain advantages and disadvantages, and the list is structured in the order of increasing control system sophistication. These are discussed below, including examples of their applications to the control of the plasma thermal balance.

The on-off controller is the simplest type of control. The control input only has two states in this mode of operation, either fully on or fully off, depending on the value of a predetermined system

Table B-1
GENERAL MECHANISMS AVAILABLE FOR EFFECTING FEEDBACK CONTROL

On-off (Two-position control)

On-off with time delay or differential-gap

Multiposition control

Proportional

Integral

Derivative

Proportional plus integral

Proportional plus derivative

Proportional plus integral plus derivative

variable in relation to its desired value. This control is thus often called two-position control. Its advantages include its simplicity and practicality. Its disadvantages include indefinite cycling, and the inability to ever achieve an exact correction or a stable, balanced condition. Variations of the basic on-off control which attempt to reduce the cycling frequency and the magnitude of the oscillations are the multiposition control, and on-off with time delay. This type of control was attempted for control of the plasma thermal balance using the fuel ion injection ratio as the control variable in References 3 and 21, as discussed in Appendix A. Oscillatory behavior was indeed observed in dynamic simulations. In summary, cycling and overshoot are characteristics of the on-off control mode, and their effects are unacceptable in the present application.

Proportional control offers a continuous, linear relation between the adjustment of the input parameter and the deviation from the desired operating condition, i.e., the feedback fraction is proportional to the perceived error. This type of control has been used by many researchers of thermal stability with good results in terms of obtaining a stable thermal balance (see Appendix A). The advantages of proportional control are its powerful stabilizing action, and its reduction of the system sensitivity to external perturbations. Its disadvantage is that proportional control is balanced for only one set of plasma conditions. Thus, for permanent departures from this condition, whether it be planned, such as a load change, or the result of component drift, proportional control will only approach the desired condition, but will not reach it. This can be understood as follows. To reach equilibrium at the new condition, a change in the input is

required. However, with proportional control, the change in the input is proportional to the perceived deviation from the desired condition. Thus, if the system did reach the new, desired condition, the change in the input would decrease to zero. The net result is that an offset from the desired condition, or an error, will always be present with proportional control except for one reference set of conditions. This error can be eliminated by manually readjusting the input variables or the new set point. However, this manual readjustment would need to be repeated for each load change, and this procedure would not be practical in a complex application. An alternative method of eliminating offset is to use integral control.

With integral control, the magnitude of the change effected on the input parameter is proportional to the integral of the error. Thus, there is no offset error with integral control since the control input will be continuously adjusted until the error remains at zero. The disadvantage of integral control is that its initial response may be slow, since it may take some time for the integral of the error to increase to a significant value. For this reason, integral control is often combined with proportional control to improve its speed of response.

To improve the response of slow systems, derivative control is often used. Derivative control is accomplished by making the adjustments to the control input proportional to the rate of change of the error. Thus, in a sense, derivative control predicts the error and compensates accordingly, often reducing the maximum error. Since the compensation of derivative control is such so as to oppose all change, this type of control has a great stabilizing effect of the system.

However, since this type of control only affects the input during a change in the error, derivative control alone can not correct a steady state error. It is therefore usually coupled with either proportional control, to give what is known as proportional-plus-derivative control action, or with proportional and integral control, to give the proportional-integral-derivative (P-I-D) controller. This latter control scheme combines the advantages of the three previous control modes in that, following a system disturbance or load change, in addition to the temporary contribution to the change in input from the proportional control, integral control introduces the required permanent change in the input to give zero steady state error; derivative action gives good initial speed of response, decreases overshoot and cycling, and enhances system stability. Even with the current advancements in modern control theory, the P-I-D controller remains as a standard on which comparisons of control system performances are based.

The original development of classical control theory has given way since the 1960's to theoretical investigations into better approaches to control. With the aid of computers, microprocessors, and software developments, hardware limitations have been removed, and the advanced control techniques are finding widespread, practical applications. Modern control theory analysis and design methods are covered in the next section, which begins with a discussion of the notion of state space.

B.3. Modern Methods

The state of a system is defined by Kalman [36] as follows:

State. The state of a system is a mathematical structure containing a set of n variables $x_1(t)$, $x_2(t)$, $\cdots$, $x_n(t)$, called the state variables, such that the initial values $x_i(t_o)$ of this set, and the system inputs $u_j(t)$ are sufficient to uniquely describe the system's future response, for $t \geq t_o$.

From this definition, the n-dimensional state vector is formed whose components are the state variables, the state space is defined as the n-dimensional space in which the components of the state vector represent the coordinate axes, and the state trajectory is the path produced in state space by the vector with the passage of time. It is noted that there is no unique way of selecting the system variables with which to represent the state of the system.

Consider the linear dynamical system represented by

$$\dot{\underline{x}}(t) = A(t)\underline{x}(t) + B(t)\underline{u}(t) \qquad \text{B.1}$$

$$\underline{y}(t) = C(t)\underline{x}(t) + D(t)\underline{u}(t) \qquad \text{B.2}$$

where $\underline{x}$, $\underline{u}$, and $\underline{y}$ are the state, input, and output vectors of dimensions n, r, and m, respectively, and A, B, C, and D are $n \times n$, $n \times r$, and $m \times r$ matrices. Also consider the matrix differential equation

$$\dot{X} = A(t)X \qquad \text{B.3}$$

where X and A are both $n \times n$ matrices, and the i-th column of X(t) is the solution to

$$\dot{\underline{x}} = A(t)\underline{x} \qquad \text{B.4}$$

subject to the initial condition given by the i-th column of X_o. A solution of B.3, $X(t)$, subject to the initial condition $X(t_o) = X_o$, is called a fundamental matrix of B.4, provided X_o is nonsingular. The solution of B.3 subject to $X(t_o) = I$, where I is the identity matrix, is called the state transition matrix of B.4 and is denoted as $T(t,t_o)$. Thus the following holds

$$T(t,t_o) = A(t)T(t,t_o),\ T(t_o,t_o) = I$$

The state transition matrix has several interesting properties. Among these are[37]:

1. $T(t,t_o)$ is unique for all t.
2. The solution of B.4, with $\underline{x}(t_o) = x_o$ is $\underline{x}(t) = T(t,t_o)\underline{x}_o$.
3. For all t, t_o, and t_1, $T(t,t_1)T(t_1,t_o) = T(t,t_o)$.
4. $T(t,t_o)$ is nonsingular for all t, and $T^{-1}(t,t_o) = T(t_o,t)$.
5. If $X(t)$ is any fundamental matrix of B.4, then $T(t,t_o) = X(t)X^{-1}(t_o)$.

Employing the state transition matrix, the state transition function of the system represented by B.1 and B.2 is given by[37]

$$\underline{x}(t) = T(t,t_o)\underline{x}_o + \int_{t_o}^{t} T(t,t')B(t')\underline{u}(t')\,dt'$$

The output vector $y(t)$ is then given by

$$\underline{y}(t) = C(t)T(t,t_o)\underline{x}_o + C(t)\int_{t_o}^{t} T(t,t')B(t')\underline{u}(t')\,dt' + D(t)\underline{u}(t)$$

and the $\underline{x}(t)$ given above represents the unique state trajectory through the point $\underline{x}_o$. The $C(t)T(t,t_o)\underline{x}_o$ term in $\underline{y}(t)$ is known as the zero-input response, and the remainder of $\underline{y}(t)$ is the zero-state response.

Continuing with definitions, the m × r matrix whose k^{th} column represents the response of a system in the zero-state ($\underline{x}_o = \underline{0}$), to a unit impulse at time t′ at the k^{th} input, all other inputs remaining identically zero, is called the impulse response matrix. The zero state response is then given by

$$\underline{y}_{zs}(t) = \int_{t_o}^{t} H(t,t')\underline{u}(t')\, dt'$$

which then results in

$$H(t,t') = C(t)T(t,t')B(t') + \delta(t - t')D(t'), \quad t \geq t'.$$

$H(t,t')$ is assumed to be zero for $t < t'$.

Since the system studied in this work yields linear, constant coefficient differential equations, the concept of time-invariance is presented here. A system is time-invariant if its input-output relations do not change with time, i.e., the shape of the response to an input depends only on the shape of the input, and not on the time the input is applied. A system characterized by linear differential equations with constant coefficients is time-invariant[38]. The property of time-invariance allows considerable simplification in the upcoming discussions and will henceforth be assumed unless otherwise indicated.

Time invariance removes the time dependence of the matrices A, B, C, and D in equations B.1 and B.2. As a consequence, the state transition matrix is neatly given by

$$T(t,t_o) = \exp A\cdot(t - t_o)$$

Substitution of this result into the state transition function $\underline{x}(t)$ and the output $\underline{y}(t)$ provides explicit expressions for these entities. Also, the impulse response matrix now depends only on $t - t'$, and is customarily written as $H(t - t')$, or $H(t)$ when $t' = 0$.

There are several methods of computing $\exp A\cdot(t - t_o)$, including finding a similarity transformation to reduce A to its Jordan canonical form[39], as a particular case of function of a matrix, and using the Laplace transform[37,40]. The result is, taking $t' = 0$,

$$T(t,0) = \exp At = R_i \exp (\lambda_i t) \qquad B.5$$

where the R_i are the (constant) residue matrices of T(s), the Laplace transform of T(t,0), corresponding to the eigenvalues λ_i of the matrix A. This formula is valid for the case of distinct eigenvalues. If this is not the case, modifications are required and reference is made to [40].

The definition of stability for a linear, time-invariant system may now be easier to understand. The response of the system given by B.1 and B.2 to any input is the sum of a term having the form of the input plus a term containing terms of the form of B.5. If the λ_i all have real parts less than zero, then if the input is bounded, then the response will be bounded, as the $R_i \exp (\lambda_i t)$ terms will decay with

time. In the case of the zero-input response, which is of interest in the present work, a system starting with the condition $\underline{x}_o = \underline{0}$ will return to the $\underline{x}_o$ state following a perturbation, if the system is stable. If an eigenvalue is identically equal to zero (real part), an additional constraint is that it be a simple zero, i.e., it have a distinct eigenvector associated with it. Also, to prevent states from growing unbounded, any undamped modes of the system (eigenvalue with zero real part) must not be coupled directly to the input.

As in the case of classical control, if the system performance does not meet the desired specifications, compensation is employed to yield the desired transfer function. In modern control theory, the concept involves the utilization of all the system states to provide the necessary improvement in system response. In effect, the classical control theory design specifications are applied to the system, but these are satisfied by the use of state variable feedback. A summary of the design procedure is as follows [33]:

1. From the state equations, the state variable block diagram is drawn.

2. The equivalent feedback transfer function and the overall transfer function are found and written in terms of k_i, the feedback gain for each state variable.

3. The desired closed-loop transfer function is synthesized from the desired performance specifications.

4. The closed-loop transfer functions of steps 2. and 3. are equated and solved for the k_i, yielding the necessary feedback compensator.

Before proceeding to the optimal control methods, the concepts of controllability and observability for a time-invariant system are presented.

The system represented by equations B.1 and B.2 is said to be controllable if any $(\underline{x}_o, t_o)$ can be transferred to any $(\underline{x}_1, t_1)$, including zero states, by some input function applied from t_o to t_1. For the time-invariant case, the test for controllability requires that the $n \times nr$ matrix Q defined by $[B \mid AB \mid \cdots \mid A^{n-1}B]$ have rank n. A system is said to be observable if no $\underline{x}_o$ yields a null zero-input response. The test for observability requires that the $nm \times n$ matrix R $= [C', A'C', \cdots, (A^{n-1})'C']$ have rank n, where the prime denotes transpose.

B.4. Optimal Control Theory

Optimal control is a particular branch of modern control that attempts to design a system that is the "best" possible system. Many optimal control problems do not have easily obtainable solutions, but nearly all linear optimal control problems do. The results of a linear optimal control problem are often directly applicable to nonlinear systems operating on a small signal basis, and the procedures followed to obtain the linear optimal design can often be carried over to the nolinear problem. The linear optimal control design, in fact, can tolerate nonlinearities without major reduction of its properties. In the remainder of this section the linear optimal control problem will be discussed in the context of the regulator problem.

"Best," as used in the above paragraph, is defined by specifying a performance index (PI). The selection of the PI is often based on mathematical convenience. That is, the PI is chosen so that the system will have a mathematical solution. The resulting optimal control will satisfy the performance index, but certain classsical specifications may not be met. A compromise must therefore be achieved between desirable system characteristics and the tolerable computational difficulty associated with the PI.

Given a starting time and state, and a final time and state, an integral performance index to yield an optimal control is specified by

$$PI = \int_{t_i}^{t_f} L(\underline{x}, \underline{u}, t)\, dt.$$

$L(\underline{x}, \underline{u}, t)$ is selected to be positive, making PI a monotonically increasing function of t in the interval $t_i \leq t \leq t_f$. If the magnitude of PI is a minimum over the time interval, in transferring the state from $\underline{x}(t_i)$ to $\underline{x}(t_f)$, the system is said to be optimal.

Adding constraints on the amount of energy that can be spent as input (the magnitude of the control functional), and the error or deviation permitted in the system states results in the quadratic performance index (QPI), having the form

$$QPI = \int_0^{\infty} (\underline{x}'Q\underline{x} + \underline{u}'Z\underline{u})\, dt.$$

In general, Q and Z must be nonnegative and positive definite symmetric matrices. In addition, the system in question must be controllable and observable.

The resulting optimal control law $\underline{u}^*(t)$ that satisfies the QPI has a very desirable property. The minimization of the QPI turns out to be achieved by a linear feedback law of the form $\underline{u}(t) = K'\underline{x}(t)$ where K is the feedback matrix. The derivation of the optimal control can be found in the literature [41]. The basic steps can be outlined as follows. The minimum performance index is shown to exist and be of the form $\underline{x}'(t)P\underline{x}(t)$, P being a positive definite matrix (symmetric). P is shown to satisfy the matrix Riccati equation, a nonlinear differential equation of the form

$$-\dot{P} = PA + A'P - PBZ^{-1}B'P + Q.$$

And finally, the optimal control is shown to be $\underline{u}^*(t) = -Z^{-1}B'P\underline{x}(t)$.

The notion of optimality can be satisfactorily extended to accommodate classical design criteria, such as closed-loop pole placement, gain and phase margin, etc. The satisfaction of the desired system specifications is achieved by the selection of the Q and Z matrices in the QPI. Methods for choosing the elements of the Q and Z matrices can also be found [42].

APPENDIX C
DERIVATION OF SPECIFICATIONS FOR A STABLE CLASSICAL SECOND ORDER SYSTEM WITH A FINITE ZERO

Given the transfer function of a stable second order system of the form

$$G(s) = \frac{T(s)}{R(s)} = \frac{\frac{\omega_n^2}{z}(s + z)}{s^2 + 2\xi\omega_n s + \omega_n^2} = \frac{\frac{\omega_n^2}{z}(s + z)}{(s + \sigma)^2 + \omega_d^2} \qquad C.1$$

where,

$-z$ = location of the zero

ξ = damping ratio

ω_n = undamped natural frequency

$\sigma = \xi\omega_n$ = damping factor

$\omega_d = \omega_n\sqrt{1 - \xi^2}$ = damped natural frequency

analytic expressions for the following can be derived:

1. Impulse response
2. Step Response
3. Time-to-Peak, t_p

4. Peak Overshoot, M_p

5. Settling time, t_s (5%)

6. Bandwidth, ω_B

7. Resonance frequency, ω_m

8. Resonance peak, M_m

9. Phase margin, PM

Note that the restriction of stability translates into negative roots of the characteristic equation. This in turn specifies $\xi > 0$ and ω_n real and positive.

C.1. Impulse Response

For the case of a unit impulse input, R(s) = 1, the expression for G(s) can be partial fraction expanded and then inverse Laplace transformed into the time domain. The result, given in most compilations of Laplace transform pairs is given by,

$$g(t) = \frac{\omega_n^2\sqrt{(z-\sigma)^2 + \omega_d^2}}{z\omega_d} e^{-\sigma t}\sin(\omega_d t + \phi), \quad 1 > \xi > 0 \qquad C.2$$

$$= \frac{\omega_n^2}{z(\sigma_2 - \sigma_1)}[(z - \sigma_1)e^{-\sigma_1 t} - (z - \sigma_2)e^{-\sigma_2 t}], \quad \xi \geq 1 \qquad C.3$$

with

$$\phi = \tan^{-1}\frac{\omega_d}{z - \sigma}$$

$$\sigma_1 = \sigma + \omega_d^*$$

$$\sigma_2 = \sigma - \omega_d^*$$

$$\omega_d^* = \omega_n\sqrt{\xi^2 - 1}$$

C.2. Step Response

For $R(s) = \frac{1}{s}$, the expression for $G(s)$, following the same procedure as for the impulse response, transforms in the time domain to

$$g(t) = 1 - \frac{\omega_n}{z\omega_d}\,\overline{zp}\; e^{-\sigma t}\sin(\omega_d t + \phi), \quad 1 > \xi > 0 \qquad C.4$$

$$= 1 + \frac{\omega_n^2(z - \sigma_1)}{2z\sigma_1\omega_d^*}\, e^{-\sigma_1 t} + \frac{\omega_n^2(z - \sigma_2)}{2z\sigma_2\omega_d^*}\, e^{-\sigma_2 t}, \quad \xi \geq 1 \qquad C.5$$

with

$$o = \tan^{-1}\frac{\omega_d}{z - \sigma} + \tan^{-1}\frac{\omega_d}{\sigma}$$

$$\overline{zp} = \sqrt{(z - \sigma)^2 + \omega_d^2}$$ (a measure of the pole-zero separation)

and σ_1, σ_2 and ω_d^* as before.

C.3. Time-to-Peak, t_p

To determine the time to peak overshoot following a step input, take $\frac{dg(t)}{dt}$ in equations C.4 and C.5 and equate to zero. For C.4, this gives

$$\frac{dg(t)}{dt} = 0 \quad \Rightarrow \quad \omega_d e^{-(\sigma t_p)} \cos(\omega_d t_p + \phi) = \sigma e^{-(\sigma t_p)} \sin(\omega_d t_p + \phi)$$

Rearranging gives

$$\tan(\omega_d t_p + \phi) = \frac{\omega_d}{\sigma} \qquad \text{C.6}$$

Substituting the expression for ϕ given previously for a step response into C.6, and defining

$$\Psi_1 \equiv \tan^{-1}\frac{\omega_d}{-\sigma} \quad \Rightarrow \quad \frac{\omega_d}{\sigma} = \tan(k\pi - \Psi_1)$$

and

$$\Psi_2 \equiv \tan^{-1}\frac{\omega_d}{z - \sigma}$$

an expression for t_p can be extracted as

$$t_p = \frac{k\pi - \Psi_2}{\omega_d}, \quad 1 > \xi > 0 \qquad \text{C.7}$$

It can be shown that the peak overshoot occurs for k = 1 or 2.

Proceeding in the same fashion for C.5 results in

$$t_p = \frac{1}{2\omega_d^*} \ln\left(\frac{z - \sigma_1}{z - \sigma_2}\right), \quad \xi > 1 \qquad C.8$$

Since the logarithmic function exists only for positive argument, a necessary restriction for t_p to exist is that the zero not be located between the poles, i.e.,

$$z > \sigma_1 \text{ and } z > \sigma_2$$

or $$z < \sigma_1 \text{ and } z < \sigma_2.$$

C.4. Peak Overshoot, M_p

Peak overshoot, defined by

$$M_p \equiv g(t_p) - 1$$

can be obtained by substituting C.7 into C.4 or C.8 into C.5, as appropriate. For $1 > \xi > 0$, substituting C.7 into C.4 gives

$$g(t_p) = 1 + \frac{\omega_n}{z\omega_d}\sqrt{zp}\, e^{-\left[\frac{\sigma}{\omega_d}(\pi - \Psi_2)\right]}\sin\Psi_1, \quad k = 1 \qquad C.9$$

$$= 1 - \frac{\omega_n}{z\omega_d}\sqrt{zp}\, e^{-\left[\frac{\sigma}{\omega_d}(2\pi - \Psi_2)\right]}\sin\Psi_1, \quad k = 2 \qquad C.10$$

Noting that for $1 > \xi > 0$, $\sin\Psi_1 = \sqrt{1 - \xi^2} > 0$, either expression can

define the peak, depending on whether the zero is in the left ($z > 0$) or right ($z < 0$) hand plane. The resultant expression for peak overshoot is then,

$$M_p = \frac{\overline{zp}}{|z|} e^{-\left[\frac{\sigma}{\omega_d}(k\pi - \Psi_2)\right]} \qquad C.11$$

with $k = 1$ for $z > 0$, and $k = 2$ for $z < 0$.

For $\xi \geq 1$, no clarification is obtained by substituting C.8 into C.5. The expression for peak overshoot will simply be written as

$$M_p = \frac{\sigma_2(z - \sigma_1)}{z(\sigma_1 - \sigma_2)} e^{-\sigma_1 t_p} - \frac{\sigma_1(z - \sigma_2)}{z(\sigma_1 - \sigma_2)} e^{-\sigma_2 t_p} \qquad C.12$$

with t_p as given by equation C.8.

C.5. Settling Time, t_s (5%)

Since the damping factor σ, and the oscillation frequency ω_d, do not change due to the presence of the zero, the settling time for the present case remains unchanged from the case of the simple second order system with no zero. The settling time in either case is given by

$$t_s = \frac{3}{\sigma} \qquad C.13$$

C.6. Bandwidth, ω_B

The frequency function associated with G(s) is obtained by substituting $s = j\omega$ into C.1. Doing so results in

$$G(j\omega) = \frac{\frac{\omega_n^2}{z}(z + j\omega)}{\omega_n^2 - \omega^2 + 2\xi\omega_n\omega j} \qquad C.14$$

The bandwidth frequency is defined as that frequency at which the magnitude of the transfer function is -3dB, or $\frac{\sqrt{2}}{2}$ of its zero frequency value. Applying this definition to the magnitude of $G(j\omega)$ yields

$$|G(j\omega)| = \frac{\frac{\omega_n^2}{z}(z^2 + \omega^2)^{1/2}}{[(\omega_n^2 - \omega^2)^2 + (2\sigma\omega)^2]^{1/2}} = \frac{\sqrt{2}}{2} \qquad C.15$$

which results in the quartic equation

$$\omega^4 + [4\sigma^2 - 2\omega_n^2(1 + \frac{\omega_n^2}{z^2})]\omega^2 - \omega_n^4 = 0$$

Imposing physical constraints on ω_B results in there being one and only one solution for ω_B given by

$$\omega_B = (-A + \sqrt{A^2 + \omega_n^4})^{1/2} \qquad C.16$$

with

$$A = 2\sigma^2 - \omega_n^2\left(1 + \frac{\omega_n^2}{z^2}\right)$$

C.7. Resonance Frequency, ω_m

The resonance frequency can be found by taking the derivative of the magnitude of the frequency function, equation C.15, equating the result to zero and solving as follows:

$$\frac{d|G(j\omega)|}{d\omega} = 0 \quad \Rightarrow$$

$$\Rightarrow \quad \omega[(\omega_n^2 - \omega^2)^2 + (2\sigma\omega)^2]^{1/2}(z^2 + \omega^2)^{-1/2} =$$

$$[4\sigma^2\omega - 2\omega(\omega_n^2 - \omega^2)][(\omega_n^2 - \omega^2)^2 + (2\sigma\omega)^2]^{-1/2}(z^2 + \omega^2)^{1/2}$$

This reduces to the quartic

$$\omega^4 + 2z^2\omega^2 + 4\sigma^2z^2 - 2\omega_n^2z^2 - \omega_n^4 = 0$$

which physical constraints limit to at most the one solution given by

$$\omega_m = \{-z^2 + [z^4 + (2\omega_n^2 - 4\sigma^2)z^2 + \omega_n^4]^{1/2}\}^{1/2} \qquad C.17$$

C.8. Resonance Peak, M_m

No gain in clarity is obtained by substituting C.17 into C.15. Therefore M_m is presented as

$$M_m = \frac{\omega_n^2(z^2 + \omega_m^2)^{1/2}}{z[(\omega_n^2 - \omega_m^2)^2 + (2\sigma\omega_m)^2]^{1/2}} \qquad \text{C.18}$$

with ω_m given by equation C.17.

C.9. Phase Margin, PM

For a system that is stable, phase margin is defined as the excess phase gain available at the gain crossover frequency over that required for marginal stability. For a system that is initially unstable, phase margin is defined as the excess phase lag at the gain crossover frequency over that required for marginal stability. To find the gain crossover frequency, set the magnitude of the frequency function, equation C.15, equal to one to obtain

$$\omega_{gc} = \left(\frac{\omega_n^4}{z^2} + 2\omega_n^2 - 4\sigma^2\right)^{1/2}$$

The phase of the frequency function at ω_{gc} is

$$\underline{/G(j\omega_{gc})} = \tan^{-1}\frac{\omega_{gc}}{z} - \tan^{-1}\frac{2\sigma\omega_{gc}}{\omega_n^2 - \omega_{gc}^2}$$

so that the phase margin is

$$PM = 180^\circ - |\underline{/G(j\omega_{gc})}|, \quad \underline{/G(j\omega_{gc})} < 0 \qquad \text{C.19}$$

$$= \underline{/G(j\omega_{gc})} - 180^\circ, \quad \underline{/G(j\omega_{gc})} > 0 \qquad \text{C.20}$$

REFERENCES

1. J. M. Rawls, ed., "Status of Tokamak Research," U. S. Department of Energy Report DOE/ER-0034, October 1979.

2. R. G. Mills, "The Problem of Control of Thermonuclear Reactors," Proceedings of the 1969 Symposium on Engineering Problems of Controlled Thermonuclear Research, LA-4250, April 1969, BI-1 - BI-5.

3. R. G. Mills, "Time-Dependent Behavior of Fusion Reactors," B.N.E.S. Nuclear Fusion Reactor Conference at Culham Laboratory, September 1969, 322-335.

4. M. Ohta, H. Yamato, and S. Mori, "Thermal Instability and Control of Fusion Reactor," Plasma Physics and Controlled Thermonuclear Fusion Research, Vol. 3, 1971, 423-433.

5. S. O. Dean, Ed., "Status and Objectives of Tokamak Systems for Fusion Research," U. S. Atomic Energy Commission Report WASH-1295, 1973.

6. W. A. Houlberg, "A Review of Plasma Transport Theories for Tokamaks and Experimental Results," University of Wisconsin Report FDM-8, January 1975.

7. W. W. Pfeiffer, R. H. Davidson, R. L. Miller, and R. E. Waltz, "ONETWO: A computer Code for Modeling Plasma Transport in Tokamaks," GA Technologies Report GA-A16178, December 1980.

8. M. N. Rosenbluth, W. M. MacDonald, and D. L. Judd, Physical Review, Vol. 107, No. 1, 1957, 1-6.

9. S. T. Butler and M. J. Buckingham, "Energy Loss of a Fast Ion in a Plasma," Physical Review, Vol. 126, No. 1, April 1, 1962, 1-4.

10. W. A. Houlberg, "Thermalization of an Energetic Heavy Ion in a Multispecies Plasma," University of Wisconsin Report FDM-103, May 1974.

11. C. G. O'Farrill and H. D. Campbell, "Preliminary Thermal Stability Study of a Two Component Fusion Plasma," American Nuclear Society Transactions, Vol. 23, 1976, 51-53.

12. C. L. Hoxie, "Steady State and Thermal Stability Analysis of a Two-Energy-Component Fusion Plasma," University of Florida Master's Thesis, 1978.

13. L. Spitzer, Jr., Physics of Fully Ionized Gases (New York: Interscience Publishers), 1962.

14. I. Maya, "Equilibrium Conditions and Critical Temperatures of Thermonuclear Plasmas," University of Florida Master's Thesis, 1976.

15. D. L. Jassby, "Neutral-Beam-Driven Tokamak Fusion Reactors," Nuclear Fusion, Vol. 17, 1977, 309-363.

16. C. C. Baker, "STARFIRE- A Commercial Tokamak Fusion Power Plant Study," Argonne National Lab Report ANL/FPP-80-1, September 1980.

17. B. F. Gore and E. S. Murphy, "Current Fusion Power Plant Design Concepts," Battelle Report BNWL-2013, September 1976.

18. W. Horton and T. Kammash, "Model Tokamak Reactors Limited by Anomalous Diffusion and Synchrotron Radiation," Texas Symposium on the Technology of Controlled Thermonuclear Fusion Experiments and Engineering Aspects of Fusion Reactors, November 1972.

19. C. Powell and Q. J. Hahn, "Energy-Balance Instabilities in Fusion Plasmas," Nuclear Fusion, Vol. 12, 1972, 667-672.

20. C. Powell, "Control of the Energy Balance in a Fusion Reactor," Plasma Physics, Vol. 15, 1973, 1007-1017.

21. W. M. Stacey, "Operating Regimes of Controlled Thermonuclear and Stability Against Fundamental Mode Excursions in Plasma Densities and Temperature," Nuclear Fusion, Vol. 13, 1973, 843-861.

22. T. Fujisawa, "Effect of Injection Fuel Energy on Fusion-Reactor Stability and Feedback Control," Nuclear Fusion Vol. 14, 1974, 173-183.

23. A. A. Bassioni and A. A. Husseiny, "Stabilizing Control of D-T Fusion Systems," Proceedings of the First Topical Meeting on the Technology of Controlled Nuclear Fusion, April 1974, 355-363.

24. J. L. Usher and H. D. Campbell, "Thermal Instabilities for Different Fusion Fuel Cycles", Ibid., 302-308.

25. H. D. Campbell and J. L. Usher, "Thermal Instability and Control for CTR Fuel Cycles," American Nuclear Society Transactions, Vol. 21, 1975, 45-46.

26. C. G. O'Farrill, "Preliminary Study of the Thermal Stability of a Two-Component Torus," University of Florida Master's Project, 1976.

27. W. L. Ferrell and W. E. Kastenberg, "Nonlinear Temperature-Density Stability in Tokamak Reactors Operating on the D-T Cycle," American Nuclear Society Transactions, Vol. 23, 1976, 53-54.

28. M. Ohnishi and J. Wakabayashi, "Thermal Stability Considering the Slowing-Down Process of Alpha Particles," American Nuclear Society Transactions, Vol. 23, 1976, 50-51.

29. T. W. Petrie and J. M. Rawls, "Burn Control Resulting from Toroidal Field Ripple," GA Technologies Report GA-A15218, March 1979.

30. L. Bromberg and D. R. Cohn, "Effect of Impurities and Ripple Upon Power Regulation in Self-Sustained Tokamaks," M.I.T. Plasma Fusion Center Report PFC/RR-80-16, 1980.

31. D. E. T. F. Ashby and M. H. Hughes, "Dynamic Control of a Tokamak Reactor by Fuel Injection," Nuclear Fusion, Vol. 20, No. 4, 1980, 451-457.

32. J. J. D'Azzo and C. H. Houpis, Linear Control System Analysis and Design, Conventional and Modern (New York: McGraw-Hill), 1975.

33. R. Saucedo and E. E. Schiring, Introduction to Continuous and Digital Control Systems (New York: Macmillan Co.), 1968.

34. D. L. Hetrick, Dynamics of Nuclear Reactors (Chicago: University of Chicago Press), 1971.

35. J. L. Melsa, Computer Programs for Computational Assistance in the Study of Linear Control Theory (New York: McGraw-Hill), 1970.

36. R. E. Kalman, "On the General Theory of Control Systems," Proceedings IFAC First Congress, Moscow 1960, Butterworths: London, 1961.

37. C. A. Desoer, Notes for a Second Course on Linear Algebra (New York: D. Van Nostrand), 1970.

38. R. J. Schwarz and B. Friedland, Linear Systems (New York: McGraw-Hill), 1965.

39. M. C. Pease, Methods of Matrix Algebra (New York: Academic Press), 1965.

40. L. A. Zadeh and C. A. Desoer, Linear system Theory (New York: McGraw-Hill), 1963.

41. B. D. O. Anderson and J. B. Moore, Linear Optimal Control (New Jersey: Prentice-Hall), 1971.

42. T. E. Bullock and J. M. Elder, "Quadratic Performance Index Generation for Optimal Regulator Design," IEEE Conference on Decision and Control, 1971, 123-124.

BIOGRAPHICAL SKETCH

Since 1979, Isaac Maya has been working at GA Technologies, Inc. (formerly General Atomic Co.) on the engineering research and development of fusion energy. During this time he has directed his efforts at investigating fusion reactors for electrical production, fusion synfuel reactors for the production of hydrogen, and fusion breeder reactors for the production of fissile fuel. His primary areas of interest have been the nuclear blanket design, and safety and environmental issues.

He received a Master of Engineering degree in 1976, and a Bachelor of Science in Nuclear Engineering Sciences degree, with high honors, in 1973, both from the University of Florida. Isaac thoroughly enjoyed his college years at U. of F., being quite active in intramural activities, including all the major sports.

Isaac was born in the beautiful capital of Cuba, on September 9, 1952. He was expatriated in May of 1961 shortly after the advent of Communism to the Caribbean Pearl, taking refuge in the United States. He lived in Miami Beach, Fl., until 1979, moving to San Diego as a result of his employment with GA. He married the former Debbie Eichenbaum on July 8, 1979 (they met while they were both attending U.F.; she graduated with a B.S. in Accounting). They presently have one daughter, Faryn, and a Toy Poodle named Shooma.

I certify that I have read this study and that in my opinion it conforms to acceptable standards of scholarly presentation and is fully adequate, in scope and quality, as a dissertation for the degree of Doctor of Philosophy.

Hugh D. Campbell, Ph.D., Chairman
Associate Professor of Nuclear
Engineering Sciences

I certify that I have read this study and that in my opinion it conforms to acceptable standards of scholarly presentation and is fully adequate, in scope and quality, as a dissertation for the degree of Doctor of Philosophy.

Edward E. Carroll, Jr., Ph.D.
Professor of Nuclear Engineering
Sciences

I certify that I have read this study and that in my opinion it conforms to acceptable standards of scholarly presentation and is fully adequate, in scope and quality, as a dissertation for the degree of Doctor of Philosophy.

Edward T. Dugan, Ph.D.
Assistant Professor of Nuclear
Engineering Sciences

I certify that I have read this study and that in my opinion it conforms to acceptable standards of scholarly presentation and is fully adequate, in scope and quality, as a dissertation for the degree of Doctor of Philosophy.

Thomas E. Bullock, Ph.D.
Professor of Electrical Engineering

I certify that I have read this study and that in my opinion it conforms to acceptable standards of scholarly presentation and is fully adequate, in scope and quality, as a dissertation for the degree of Doctor of Philosophy.

Francis E. Dunnam, Ph.D.
Professor and Associate Dean of
Liberal Arts and Sciences

This dissertation was submitted to the Graduate Faculty of the College of Engineering and to the Graduate Council, and was accepted as partial fulfillment of the requirements for the degree of Doctor of Philosophy.

April, 1983

Dean, College of Engineering

Dean, Graduate School

UNIVERSITY OF FLORIDA
3 1262 08666 297 9